

STRAIN-SPECIFIC ALLELES OF *PHOX2B* DIFFERENTIALLY
MODIFY *SOX10*^{DOM} AGANGLIONOSIS

By

Lauren Colleen Walters

Dissertation

Submitted to the Faculty of the
Graduate School of Vanderbilt University

In partial fulfillment of the requirements

For the degree of

DOCTOR OF PHILOSOPHY

In

Human Genetics

May, 2011

Nashville, Tennessee

Approved:

Dr. E. Michelle Southard-Smith, Ph.D.

Dr. Douglas P. Mortlock, Ph.D.

Dr. Jennifer A. Kearney, Ph.D.

Dr. David C. Airey, Ph.D.

Dr. David W. Threadgill, Ph.D.

Copyright ©2011 by Lauren Colleen Walters
All Rights Reserved

To Sam, for providing his own special brand of support,

and

To Mom, for always believing in me, even when I didn't believe in myself

ACKNOWLEDGEMENTS

This work would not have been possible without the financial support of the NIH (NIDDK R01 DK60047, NINDS F31 NS064754) or the American Gastroenterological Association Foundation for Digestive Health and Nutrition. I would also like to thank the Vanderbilt University Center for Human Genetics Research (CHGR), the Vanderbilt Kennedy Center (VKC), and the Vanderbilt University Graduate School for their financial support. I would be remiss if I didn't also thank the mice, without which none of this would have been possible.

I am extremely grateful to the faculty members who have guided my scientific journey. I thank Dr. David Airey for his statistical prowess. I thank Dr. Jennifer Kearney for her quiet insights. I thank Dr. David Threadgill for his vast knowledge of mouse genetics. I thank Dr. Doug Mortlock, my committee chairman, for his ability to not only forward my scientific progress but also act as a life-coach. Lastly, I thank Dr. Michelle Southard-Smith, my mentor, for teaching me not only about the mechanics but also the politics of science and for helping me discover what kind of scientist I want to be.

I would also like to thank other members of the CHGR. I thank Maria Ritchie, our program coordinator, for keeping my life on schedule. I thank Dr. Marilyn Ritchie for proving that it's possible to have both a career and a wonderful family. I thank Dr. Jonathan Haines, the director of the CHGR, for his humor and support. I thank Dr. Jeff Canter for his love of all things Ohioan and his support of my future career plans. Lastly, I thank Dr. Scott Williams, our

Director of Graduate Studies, for dealing with my stubbornness and pushing me to do my best.

I am grateful to the lab of Dr. Jeff Smith as well. I thank Joan Breyer for her experimental assistance. I thank Kevin Bradley for his amazing skill with code and the ability to fix my computer, no matter what I've managed to do to it. I thank Dr. Jeff Smith for his scientific insight into the world of large-scale genotyping and association studies.

I appreciate the camaraderie of the students of the CHGR. Thank you all for your support and uninhibited questioning of my scientific progress-even if the majority of you only work with computers! In particular, I would like to thank Dr. Will Bush for always pushing me to understand statistics. It may actually come in handy some day! I would also like to thank Anna Cummings and Dawn Clendenning for their cheery dispositions and conscientious ways. You are the future of the program-don't let me down!

I am very grateful to all members of the Southard-Smith lab, both past and present. Dr. Sarah Owens not only laid the groundwork of my project but also provided encouragement and advice on navigating graduate school. Alex Nickle showed me not to take life too seriously, except when it comes to music. Sara Ireland taught me that everything is better with sauce and that you can be a great scientist even if you do have a round diploma. Ashley Cantrell was my lab mentor and taught me (almost) everything I know. I miss her humor and level-headed attitude every day. Jennifer Corpening was my partner in climbing the

learning curve of embryonic dissections. I admire her courage to decide what you want out of life and go for it.

Nicole Fleming and Carrie Wiese have become friends and ladies that I admire. While definitely more outdoorsy than me, we bonded over board games and cocktails. Their humor and straight-forward attitudes have made laboratory life a little easier, even when I was in the middle of a nervous breakdown. I will miss their zest for life, but I trust that I'm leaving the lab in good hands.

I thank Melissa "Mus Mus" Musser for reminding me what graduate school was like before I became bogged down in the details of finishing. Her excitement for learning is inspiring. Even though we only worked together for a short time, I feel like I gained a sister. I know she will accomplish great things in life, and I hope that we remain close friends.

I thank Dustin "D-train" Temple for being the little brother I never had. His humor made lab more bearable. The ability to relive college vicariously through him reminded me that I was glad that I graduated! I couldn't have asked for a better mentee and Mario Kart partner.

I thank Stephanie "Bizzle" Byers Skelton for being my work spouse. Over the past two years, we have become great friends. I can't thank her enough for being my level-headed sounding board and talking me off the ledge numerous times. She monitored my snack intake and always had time for a chimichanga. Hopefully we will again work together in the future in the field of medical genetics!

I am grateful for the friends I have made over the past five years in Nashville. Members of the IGP class of 2005-2006 will always hold a special

place in my memories. In particular, I would like to thank Megan Wadington and Kevin Branch. Kevin's love of the Buckeyes and cornhole abilities made us fast friends, but his love for Megan will make us lifelong ones. Megan's wisdom beyond her years and calm nature was a much-needed presence in my life. Weekly dinners with her have been a saving grace from the craziness of science. I hope to remain close over the years to come.

Lastly, I have to thank my partners in crime in Human Genetics. My life would be sad and lonely without Meaghan Neill and Becca Zuvich, my fellow MGGs. While we weren't friends IGP year, we formed an indelible bond over studying for quals. Between shopping and cocktails, preparing for talks and being cheerleaders at dissertations, we've been there through everything graduate school has to offer. I couldn't have asked for better people to make this journey with. While we may be far apart in the near future, I know we will stay close at heart throughout the years.

I am grateful for the love and support of my family through this process. While they may not have understood exactly what I was working on, they always believed that I would accomplish my goals. In particular, I would like to thank PK and Ann Sen for their encouragement. I also would like to thank my sisters, who will be relieved that I am FINALLY finished with school. Lastly, I thank my dad, for his love and undying belief that I would be a doctor someday.

I would not have made it out of graduate school alive without my partner for the better half of a decade, Dr. Soumitra Sen. His unconditional love, especially when I misplaced my rage, has been my rock. While this journey

wasn't easy, I'm proud that we made it through, stronger for the future. He may have become a doctor first, but he's not the only one now!

Finally, I cannot express my appreciation and love for my biggest fan, my mom. Her never-ending support has kept me going, even when I wasn't sure exactly what the destination was. She's the smartest person I know, as some knowledge can't be measured by degrees. I can only hope that I'll live up to her example. Thanks for everything Mom.

TABLE OF CONTENTS

	Page
DEDICATION	iii
ACKNOWLEDGEMENTS.....	iv-viii
LIST OF TABLES.....	xiii
LIST OF FIGURES.....	xiv-xv
LIST OF ABBREVIATIONS	xvi-xxi
 Chapter	
I. INTRODUCTION	1
Formation of the ENS.....	1
Hirschsprung disease etiology.....	2
Modifiers of HSCR in humans	5
Mouse models of HSCR.....	5
Modulation of HSCR in mice	8
Modifiers of <i>Sox10^{Dom}</i> aganglionosis.....	10
<i>Phox2B</i> as a modifier of <i>Sox10^{Dom}</i> aganglionosis.....	13
Summary	15
References.....	17
 II. EFFECT OF STRAIN BACKGROUND ON ENTERIC DEVELOPMENT IN THE <i>SOX10^{DOM}</i> MODEL OF HSCR	 26
Introduction	26
Results.....	29
Both the <i>Sox10^{Dom}</i> mutation and strain background in the context of the <i>Sox10^{Dom}</i> allele alter ENP migration	29
ENP proliferation is not affected by the <i>Sox10^{Dom}</i> mutation or by strain background	32
Isolation of ENPs by flow cytometry in the mouse.....	34
Effect of the <i>Sox10^{Dom}</i> mutation and strain background on developmental potential of ENPs.....	38
Effect of the <i>Sox10^{Dom}</i> mutation and strain background on <i>in vivo</i> neurogenesis in the developing fetal gut.....	45
Effect of the <i>Sox10^{Dom}</i> mutation and strain background on postnatal ganglion patterning.....	48

Discussion.....	55
Materials and Methods	67
Animals	67
Fetal mouse dissections	67
Genotyping.....	67
Analysis of migration	68
Analysis of proliferation.....	70
Identification of HNK-1 immunoreactivity on mouse ENPs	73
Flow cytometric isolation of p75 ⁺ /HNK-1 ⁺ ENPs	75
Immunocytochemical labeling of p75 ⁺ /HNK-1 ⁺ progenitors	76
Neurosphere culture of p75 ⁺ /HNK-1 ⁺ progenitors	77
Analysis of developmental potential.....	79
Analysis of <i>in vivo</i> neurogenesis.....	81
Analysis of postnatal ganglion patterning.....	83
References	84
III. DIFFERENTIAL EXPRESSION OF <i>PHOX2B</i> BETWEEN INBRED STRAINS OF MICE	91
Introduction	91
Results.....	93
Quantitative Real-Time PCR highlights variation of <i>Phox2B</i> expression between pooled RNA samples	93
B6 and C3Fe alleles of <i>Phox2B</i> are differentially expressed across the 3' UTR	98
Reverse-transcriptase PCR reveals unanticipated architecture of the <i>Phox2B</i> 3' UTR	101
Analysis of <i>Phox2B</i> expression by Northern blot suggests differential expression between strain backgrounds.....	103
Discussion.....	107
Materials and Methods	119
Animals	119
Fetal mouse dissections	119
Genotyping	119
RNA isolation.....	120
Reverse transcription.....	121
Real-Time PCR	121
Staggered primer PCR	123
Allele-specific expression	125
Northern blot generation	129
Northern probe generation.....	131
Northern probe labeling	132
Northern blot labeling analysis.....	134
References	136

IV.	SEQUENCE VARIATION IN THE <i>SOX10M3</i> INTERVAL	139
	Introduction	139
	Results	143
	B6 and C3Fe genetic backgrounds are highly divergent around <i>Phox2B</i>	143
	Focused genotyping reveals mouse strain phylogeny at sub-chromosomal level.....	148
	Reporter expression in C3Fe-Tg ^{<i>Phox2B</i>-H2BCFP} Line C points to a regulatory region 3' of <i>Phox2B</i>	152
	Haplotype at <i>Phox2B</i> is significantly associated with severity of aganglionosis	155
	Discussion.....	160
	Materials and Methods	170
	BAC selection	170
	BAC purification for STR analysis	170
	BAC STR analysis	171
	BAC purification for sequence analysis.....	173
	Cesium chloride DNA extraction	173
	CHEF gel analysis	176
	Solexa sequencing of BAC clones	176
	Illumina panel design	177
	Illumina DNA selection	178
	Illumina DNA quality analysis	179
	Illumina panel genotyping	185
	Haplotype generation	186
	Haplotype analysis	186
	References.....	188
V.	EFFECT OF STRAIN-SPECIFIC ALLELES OF <i>PHOX2B</i> ON ENS DEVELOPMENT.....	191
	Introduction	191
	Results	194
	Hemizyosity at <i>Phox2B</i> impacts the effects of the <i>Sox10^{Dom}</i> allele and strain background on ENP migration	194
	Hemizyosity at <i>Phox2B</i> has no impact on ENP proliferation	198
	Hemizyosity at <i>Phox2B</i> differentially affects foregut ENP patterning	200
	Discussion.....	203
	Materials and Methods	211
	Animals	211
	Fetal mouse dissections	211
	Genotyping	211
	Analysis of migration	212

	Analysis of proliferation.....	213
	Analysis of <i>in vivo</i> neurogenesis.....	216
	References.....	218
VI.	CONCLUSIONS AND FUTURE DIRECTIONS.....	220
	Conclusions	220
	Potential Impact	229
	Future Directions.....	232
	References.....	242

LIST OF TABLES

Table	Page
2.1 Effect of strain background and <i>Sox10^{Dom}</i> mutation on ENP migration ...	32
2.2 Effect of strain background and <i>Sox10^{Dom}</i> mutation on developmental potential.....	43
3.1 Composition of RNA sets used in expression analyses	95
3.2 Primers used for staggered primer PCR	124
3.3 Specifications for Taqman SNP Genotyping Assays.....	128
4.1 Haplotype groups identified by Illumina genotyping	151
4.2 Severity of aganglionic phenotype across F ₁ crosses with the B6. <i>Sox10^{Dom}</i> congenic strain	155
4.3 Primers used in BAC STR analysis.....	172
4.4 Mouse strains used in Illumina Panel I.....	180
4.5 Mouse strains used in Illumina Panel II.....	183
5.1 Effect of <i>Phox2B</i> hemizyosity in conjunction with the <i>Sox10^{Dom}</i> allele and strain background on ENP migration	197
5.2 Foregut patterning in <i>Sox10^{Dom};Phox2B^{LacZ}</i> embryos.....	201

LIST OF FIGURES

Figure	Page
1.1 Formation of the ENS by neural crest-derived progenitors.....	2
1.2 Variation in penetrance and severity of aganglionosis in congenic <i>Sox10^{Dom}</i> lines of mice.....	7
2.1 Effect of strain background and <i>Sox10^{Dom}</i> mutation on density and migration of ENPs.....	31
2.2 Effect of strain background and <i>Sox10^{Dom}</i> mutation on proliferation of ENPs	34
2.3 Mouse fetal gut cells express HNK-1 on neural crest-derived enteric progenitors.....	36
2.4 Generation of neurospheres from p75 ⁺ /HNK-1 ⁺ fetal gut cells	39
2.5 Effect of strain background and <i>Sox10^{Dom}</i> mutation on proportion of p75 ⁺ /HNK-1 ⁺ ENPs in fetal gut.....	41
2.6 Effect of strain background and <i>Sox10^{Dom}</i> mutation on developmental potential of <i>in vitro</i> cultures of flow-sorted ENPs	42
2.7 <i>In vivo</i> neurogenesis in <i>Sox10^{Dom}</i> embryos.....	46
2.8 Ganglion patterning in <i>Sox10^{Dom}</i> mutants	50
2.9 Gut muscle strip sections.....	51
2.10 Controls for postnatal gut muscle strip analysis	54
2.11 Gating parameters used in flow cytometric isolation of eNCSC	76
3.1 Variation of <i>Phox2B</i> expression levels with real-time PCR using the Phox2Bex1-2 assay.....	95

3.2	Relative quantification of <i>Phox2B</i> expression levels by real-time PCR using the Phox2Bex1-2 assay	98
3.3	Allele-specific expression of <i>Phox2B</i> across the 3' UTR	99
3.4	Staggered primer PCR fails to detect majority of 3' UTR	102
3.5	<i>Phox2B</i> expression across congenic <i>Sox10^{Dom}</i> lines by Northern blot analysis	105
3.6	Relative quantification of <i>Phox2B</i> expression by Northern blot analysis	106
3.7	Allele-specific expression analysis	127
4.1	Phylogenetic tree of the laboratory mouse	140
4.2	Probes used to select CHORI BACs	143
4.3	STR markers used for BAC quality analysis	144
4.4	Genomic positions of CHORI BACs	145
4.5	Solexa sequencing identified SNPs between B6 and C3H	147
4.6	Inappropriate reporter expression in C3Fe-Tg ^{<i>Phox2B</i>-H2BCFP} Line C	153
4.7	A deleted regulatory region in C3Fe-Tg ^{<i>Phox2B</i>-H2BCFP} Line C	154
4.8	Association of candidate gene haplotypes with aganglionic severity	156
4.9	Sliding window haplotype analysis in the <i>Phox2B</i> genomic region	159
5.1	Effect of <i>Phox2B</i> hemizyosity in conjunction with the <i>Sox10^{Dom}</i> mutation and strain background on ENP migration	195
5.2	Effect of <i>Phox2B</i> hemizyosity in conjunction with the <i>Sox10^{Dom}</i> mutation and strain background on ENP proliferation	199
5.3	Foregut patterning in <i>Sox10^{Dom};Phox2B^{LacZ}</i> embryos	201

LIST OF ABBREVIATIONS

7-AAD	7-Amino-Actinomycin
B6	C57BL/6J mouse strain
B6D2	B6 X DBA/J F ₁ mouse strain
BAC	Bacterial artificial chromosome
bFGF	Basic human fibroblast growth factor
BSA	Bovine serum albumin
C3Fe	C3HeB/FeJ mouse strain
C3H	C3H/HeJ mouse strain
CAM	Chloramphenicol
CCHS	Central congenital hypoventilation syndrome
CEE	Chick embryo extract
CFP	H2BCerulean fluorescent protein
CHEF	Contour-clamped homogenous electrical field
CHORI	Children's Hospital Oakland Research Institute
DAPI	4',6-diamidino-2-phenylindole
DMEM	Dulbecco's modified Eagle's medium
DMSO	Dimethyl sulfoxide
DPBS	Dulbecco's phosphate buffered saline
dpc	Days post-coitus (fetus age)
EGC	Enteroglial cell
ENP	Enteric neural progenitor

ENS	Enteric nervous system
G	Glial (<i>in vitro</i> colonies)
GFAP	Glial fibrillary acidic protein
GI	Gastrointestinal
GMS	Gut muscle strip
IGF-1	Human insulin-like growth factor 1
HBSS	Hank's balanced salt solution
HSCR	Hirschsprung disease
JAX	The Jackson Laboratory
LD	Linkage disequilibrium
M	Myofibroblast (<i>in vitro</i> colonies)
N	Neuronal (<i>in vitro</i> colonies)
NBF	Neutral buffered formalin
NC	Neural crest
NCSC	Neural crest-derived stem cell
NDS	Normal donkey serum
OPA	Oligonucleotide pooled assay
P	Postnatal day (mouse age)
PBS	Phosphate buffered saline
PDL	Poly-D-lysine
PEG	Polyethylene glycol
PGP9.5	Protein gene product 9.5, now known as Uchl1
pH3	Phospho-Histone H3

PS	Penicillin-streptomycin
PSA	Penicillin-streptomycin-amphotericin
QTL	Quantitative trait locus
SAM	Sentrix Array Matrices
SDS	Sodium dodecyl sulfate
SMA	Smooth muscle actin
SNP	Single nucleotide polymorphism
SSC	Saline-sodium citrate
STR	Simple tandem repeat
TCA	Total colonic aganglionosis
TH	Tyrosine hydroxylase
UTR	Untranslated region
WS4	Waardenburg-Shah Syndrome, Type 4

LIST OF GENE ABBREVIATIONS

<i>Atp8a1</i>	ATPase, aminophospholipid transporter (APLT), class I, type 8A, member 1
<i>Edn3</i>	Endothelin 3
<i>EdnrB</i>	Endothelin receptor type B
<i>GDNF</i>	Glial cell line-derived neurotrophic factor
<i>GFAP</i>	Glial fibrillary acidic protein
<i>GFRα1</i>	Glial cell line-derived neurotrophic factor family receptor alpha 1
<i>HNK-1</i>	Also known as <i>B3gat1</i> , Beta-1,3-glucuronyltransferase 1 (glucuronosyltransferase P)
<i>HPRT</i>	Hypoxanthine guanine phosphoribosyl transferase
<i>Igta4</i>	Integrin alpha 4
<i>IKBKAP</i>	Inhibitor of kappa light polypeptide enhancer in B-cells, kinase complex-associated protein
<i>L1cam</i>	L1 cell adhesion molecule
<i>Mash1</i>	Mammalian achaete-scute complex homolog 1
<i>NRG1</i>	Neuregulin 1
<i>NTRK3</i>	Neurotrophic tyrosine kinase, receptor, type 3
<i>P75</i>	Also known as <i>NGFR</i> , Nerve growth factor receptor (TNFR superfamily, member 16)
<i>Phox2A</i>	Paired-like homeobox 2A

<i>Phox2B</i>	Paired-like homeobox 2B
<i>Slc30a9</i>	Solute carrier family 30 (zinc transporter), member 9
<i>SMA</i>	Smooth muscle actin
<i>Sox8</i>	SRY-box containing gene 8
<i>Sox10</i>	SRY-box containing gene 10
<i>Sox10m3</i>	Modifier interval on chr.5 (Owens et al. 2005)
<i>SVEP1</i>	Sushi, von Willebrand factor type A, EGF and pentraxin domain containing 1
<i>Tmem33</i>	Transmembrane protein 33
<i>Uchl1</i>	Ubiquitin carboxy-terminal hydrolase L1
<i>Uchl3</i>	Ubiquitin carboxyl-terminal esterase L3 (ubiquitin thiolesterase)
<i>Wnt1</i>	Wingless-related MMTV integration site 1
<i>Zfhx1B</i>	Also known as <i>Zeb2</i> , Zinc finger E-box binding homeobox 2

LIST OF MOUSE ALLELES

<i>Tg</i> ^{<i>Phox2B</i>-H2BCFP}	H2BCerulean reporter under control of <i>Phox2B</i> promoter (Corpening et al. 2008)
<i>Edn3</i> ^{<i>ls</i>}	Lethal spotting (spontaneous)
<i>EdnrB</i> ^{<i>S</i>}	Piebald (spontaneous)
<i>EdnrB</i> ^{<i>S-l</i>}	Piebald lethal (spontaneous)
<i>Phox2B</i> ^{<i>LacZ</i>}	Targeted knock-in of <i>LacZ</i> cassette (Pattyn et al. 1999)
<i>Rosa</i> ^{<i>26R</i>}	Gene-trap allele that expresses LacZ wherever Cre is expressed, also known as Gt(ROSA)26Sor ^{tm1Sor} (Soriano et al. 1999)
<i>Rosa</i> ^{<i>YFP</i>}	Gene-trap allele that expresses YFP wherever Cre is expressed, also known as Gt(ROSA)26Sor ^{tm1(EYFP)Cos} (Srinivas et al. 2001)
<i>Sox8</i> ^{<i>LacZ</i>}	Targeted knock-in of <i>LacZ</i> cassette (Sock et al. 2001)
<i>Sox10</i> ^{<i>LacZ</i>}	Targeted knock-in of <i>LacZ</i> cassette (Britsch et al. 2001)
<i>Sox10</i> ^{<i>Dom</i>}	Dominant megacolon (spontaneous)
<i>Uchl1</i> ^{<i>gad</i>}	Gracile axonal dystrophy (spontaneous)
<i>Uchl1</i> ^{<i>tm1Dgen</i>}	Targeted knockout (Deltagen)
<i>Zfhx1B</i> ^{<i>Δex7</i>}	Targeted knockout (Higashi et al. 2002)

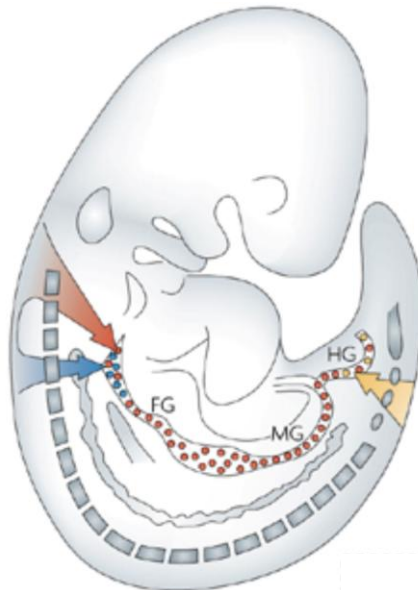
CHAPTER I

INTRODUCTION

Formation of the ENS

The ganglia of the enteric nervous system (ENS), composed of multiple neuronal subtypes and enteric glia, are formed by cells derived from the neural crest. In addition to the ENS, this small population of cells that migrates off the top of the neural tube also form craniofacial structures (including ganglia, cartilage, bone, and connective tissue), pigment cells, and other sensory ganglia (1). Normal ENS formation is a multi-step process that includes several migration phases, expansion of an initially small cell population, and creation of multiple cell lineages (2,3). Enteric neural progenitors (ENPs) originating from both the vagal and sacral levels of the neural tube contribute to the ENS [Figure 1.1; Figure 2A from Heanue & Pachnis 2007 (4)]. Vagal progenitors emigrate from the vagal neural tube at 9.5 days post-coitus (dpc) in the mouse and invade the proximal end of the developing gut. They then move caudally, colonizing the gut as it elongates and reaching the anus by 14.5dpc (5). Sacral ENPs enter the hindgut and migrate in a reverse direction to vagal ENPs up to the level of the post-umbilicus (6). During colonization, both vagal and sacral ENPs proliferate and differentiate into neurons and glia (2). The multi-step complex nature of ENS ontogeny makes it highly susceptible to alterations in gene function or expression.

Figure 1.1. Formation of the ENS by neural crest-derived progenitors.



Neural crest-derived progenitors enter the gut tube from the vagal region of the neural tube (red arrow; minor contributions from blue arrow) and migrate caudally as the gut tube elongates. A second population of progenitors enters from the sacral region (yellow arrow) and migrates rostrally to contribute to the hindgut. Figure 2A from Heanue & Pachnis 2007 (4).

Hirschsprung disease etiology

Hirschsprung disease (HSCR) is defined by a lack of enteric ganglia, aganglionosis, in a variable portion of the distal intestine (OMIM #142623) (7,8). Due to the lack of enteric ganglia in HSCR patients, stool cannot be passed through the colon, and a dilation of the bowel wall, or megacolon, results (9). Patients can be qualitatively classified as short-segment (when aganglionosis is present up to the recto-sigmoid junction, ~80% of cases) or long-segment (when aganglionosis extends proximally into the sigmoid colon ~20% of cases). A subclassification of long-segment HSCR is total colonic aganglionosis (TCA), in which aganglionosis is present up to the ileal-caecal junction (3-8% of cases) (9). In extremely rare cases, the small bowel is also affected (10). However, these

classifications are mainly used in clinical diagnosis. Studies in animal models do not support this rough dichotomization of the aganglionic phenotype. In particular, studies involving the *Sox10^{Dom}* mouse model of HSCR (11) have demonstrated that mutant animals on a mixed genetic background cover a wide spectrum of level of aganglionosis, similar to that seen in HSCR patients (12). Analysis of potential modifiers has shown that treating aganglionosis as a quantitative trait, rather than short vs. long segment, improves statistical power (12,13). Thus, a better understanding of variation in HSCR patients could be gained by analyzing aganglionosis quantitatively, instead of relying on clinical classifications.

Preliminary diagnosis of HSCR is predominantly made within the first week of life after failure to pass meconium (9). However, diagnosis can be delayed until later in infancy or even in adulthood (14). Definitive diagnosis is made by assaying suction biopsies of the colon for the presence of enteric ganglia (15). Treatment involves removal of the affected portion of the gut, pull-through of the unaffected portion, and reattachment to the anus (16,17).

This congenital disorder of the hindgut affects on average approximately 1/5000 live births, although significant differences exist in incidence between ethnic groups. HSCR is most common in Asian populations (1.4 cases per 5000 births) and least common in Hispanic populations (0.5 cases per 5000 births) (18). In addition, there is a strong sex bias; males are approximately four times as likely to develop short-segment HSCR as females. However, this sex bias is

not apparent in cases of long-segment HSCR (19). The reason for the preponderance of affected males is unknown.

Mutations in *RET* (20-22), *EDNRB* (23-25), *EDN3* (26,27), *GDNF* (28-30), and *SOX10* (31,32), genes that play important roles in the formation of the enteric nervous system (ENS), have been identified in HSCR patients. In addition, *EDNRB* and *SOX10* mutations are normally associated with Waardenburg-Shah Syndrome (Type 4) (WS4), which has additional neural crest (NC) defects beyond aganglionosis of the colon (32,33). Patients present with variable phenotypes depending in part on the primary gene defect. Patients with *RET* mutations typically exhibit greater extent of aganglionosis (24,34), while those with *EDNRB* mutations show lesser extent of aganglionosis (33).

Approximately 35% of cases have a mutation in one of the loci listed above. Another 15% of cases present with HSCR comorbid with another syndromic disorder; the most common of these is Down syndrome. The remaining 50% of cases have no identified mutation (9). However, even in familial cases that share an identical gene alteration between individual family members, a large degree of variation in penetrance (whether the phenotype is present) and severity (the extent of gut length affected) can occur (9). This variation among familial cases is thought to be the consequence of other regions of the genome, “modifiers,” that interact with the primary mutation to influence the final disease phenotype.

Modifiers of HSCR in humans

Disease modifiers of HSCR have been explored in human populations, with the focus being placed on modifiers of *RET*, as this gene is the most common location of HSCR mutations (9). Studies have highlighted chromosomal regions of interest, including chr.9q31 (35) and chr.3p21 (36), as well as genes known to be involved in the HSCR, including *GDNF* (30) and *EDN3* (37). Genes previously unassociated with HSCR have also been shown to modify *RET*; these include *NTRK3* (38) and *NRG1* (39). The chr.9q31 modifier has since been fine-mapped; association tests suggest that both *SVEP1* and *IKBKAP* may play a role in modifying HSCR (40). *RET* has been shown to act as a modifier itself in other syndromic diseases that display HSCR including congenital central hypoventilation syndrome (CCHS) (41), as well as Bardet-Biedl Syndrome and Down Syndrome (42). However, these studies have mainly focused on SNP-based or linkage screens, with little attention to biological processes. With the exception of *GDNF* and *EDN3*, the biological role of these modifier genes is not understood.

Mouse models of HSCR

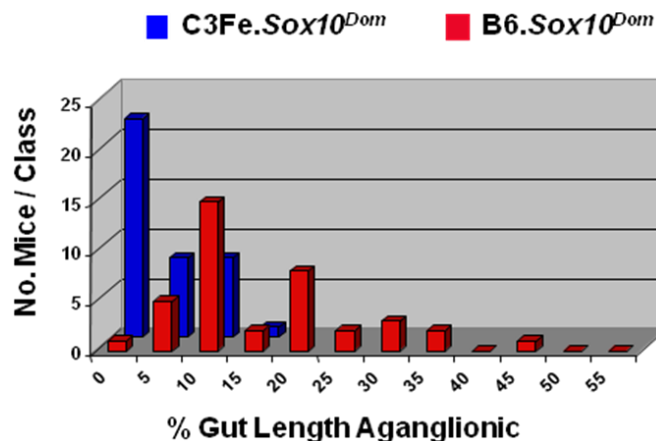
Studies in mouse models of HSCR have allowed greater mechanistic insight into the origins of aganglionosis. These models differ in the amount and location of aganglionosis within the gastrointestinal (GI) tract. Mice homozygous for knockouts of *Edn3* (43) or *EdnrB* (44) display aganglionosis in a variable portion of the distal colon, along with characteristic pigmentation defects. These

knockouts are engineered mutations of the lethal-spotting and piebald-lethal spontaneous mutations, respectively (45). Mice homozygous for knockouts of *Ret* (46), *GDNF* (47), or *GFR α 1* (48) display aganglionosis of the GI tract up to the esophageal sphincter in addition to severe defects in the renal system. In contrast, mice homozygous for a knockout of *Mash1* (49,50) only display aganglionosis of the esophagus; the remainder of the GI tract is populated. However, these mouse models are not perfect recapitulations of the human phenotype. First, homozygosity of the mutant allele is required for phenotypic presentation; in contrast, HSCR can be the result of heterozygous mutations. Second, aganglionosis is fully penetrant in each of these models; the incomplete penetrance of HSCR is one of its hallmark features. As a result, insights as to which developmental processes are affected by modifier interactions and the impact of these interactions on aganglionosis have been lacking.

The *Sox10*^{Dom/+} model is the only dominant HSCR mouse model that exhibits the variable penetrance and severity of aganglionosis seen between HSCR patients. *Sox10* encodes a transcription factor that is required to maintain the multipotency of ENPs and the differentiation of glial cells (51,52). The “*Dom*” mouse mutation arose spontaneously on a C57BL/6 (B6) haplotype in a B6xC3HeB/FeJLe-a/a intercross (53). The mutation is a single base-pair insertion that results in the retention of the DNA-binding domain but the loss of the transcriptional activation domain from the *Sox10* protein (11). The *Dom* protein has been shown to act in a dominant-negative fashion *in vitro* (54). Complete loss of *Sox10* leads to a total absence of enteric ganglia in

homozygotes (11). In addition to enteric deficits, *Sox10^{Dom/+}* mice also present pigmentation defects on the feet, ventrum, and head. The *Sox10^{Dom}* phenotype recapitulates features of WS4 in humans, which is characterized by intestinal aganglionosis and hypopigmentation as a consequence of mutations in the human *SOX10* gene (32). When bred on a mixed genetic background, *Sox10^{Dom/+}* mice exhibit variable aganglionosis. However, congenic lines of this allele maintained on B6 and C3Fe inbred genetic backgrounds differ significantly in phenotype [Figure 1.2; Figure 1D from Cantrell et al. 2004 (12)]. *Sox10^{Dom/+}* mice on the B6 background more frequently exhibit aganglionosis (greater penetrance) and a larger extent of the distal gut is affected by aganglionosis (greater severity) than when the mutation is bred onto the C3Fe background (12).

Figure 1.2. Variation in penetrance and severity of aganglionosis in congenic *Sox10^{Dom}* lines of mice.



B6.Sox10^{Dom} mice display high penetrance and severity of aganglionosis than *C3Fe.Sox10^{Dom}* mice. Figure 1D from Cantrell et al. 2004 (12).

A similar difference in severity of aganglionosis was documented by Kapur et al. in crosses between *Sox10^{Dom/+}* males of a mixed B6/C3Fe background and

inbred B6 or C3Fe females; the B6 cross always produced more severely affected progeny (55). However, the differences in phenotypic presentation were not explored in embryos, and the potential impact of strain background on the *Sox10^{Dom}* mutation was not discussed. While the studies by Cantrell et al. demonstrated the difference in aganglionic risk between the B6 and C3Fe inbred strains more clearly, analysis of *Sox10^{Dom}* animals on different strain backgrounds has only been performed postnatally (12). Previous studies have demonstrated that the *Sox10^{Dom}* mutation impacts the development of ENPs during ENS ontogeny; specifically, a decrease in extent of migration and density of enteric progenitors has been documented (11,55-57). However, the impact of strain background on the development of the ENS is not understood. As HSCR is a developmental disorder, a clearer picture of the role of genetic background, and the potential modifiers it contains, on the development of ENPs is vital.

Modulation of HSCR in mice

There have been two major types of studies concerning the modulation of the development and presentation of HSCR in mice. The first concerns gene interactions; these studies have sought to combine different mutant alleles of genes involved in NC biology to determine the overall effect on aganglionosis. The second concerns true modifiers; these studies attempt to show that “wild-type” alleles that differ in genetic background modulate the development of aganglionosis. The majority of studies have focused on interacting genes, as detailed below.

Some studies have sought to provide further evidence of potential HSCR modulation after finding association in humans, only to fail to produce evidence of an alteration of phenotype (41,58). Double heterozygote progeny from *Phox2B*^{+/-} X *Ret*^{+/-} crosses were not significantly different than wild-type littermates (41). Even though both of these genes play vital roles in NC biology, they may not interact in the development of HSCR. *TITF1* (also known as *NKX2-1*), a gene identified in HSCR association studies (58), was considered as a potential modifier, as homozygous knockout mice do not have any ENS defects (59-61). However, this gene is not expressed in mouse neurospheres or in embryonic gut, thereby excluding it as a modifier (58). Thus, genes identified by association screens in humans may not be recapitulated by studies in model organisms, either due to the design of the model studies or a spurious association in humans.

Nonetheless, several studies have conclusively demonstrated gene interactions that modulate the presentation of HSCR in mice. The interaction between *Ret* and *EdnrB* has been shown in multiple instances. Mice homozygous for a hypomorphic recessive *EdnrB* allele rarely present with aganglionosis; however, when combined with a heterozygous *Ret* mutation, a variable portion of the distal colon is aganglionic in all *Ret*^{+/-};*EdnrB*^{s/s} animals (62). These results were confirmed in a later study that also documented aganglionosis when *Ret* was heterozygous in the presence of a mixed *EdnrB*^{s/s-l} genotype (63). Interestingly, both of these studies found that the interaction between *Ret* and *EdnrB* produced a skewed sex ratio of affected status similar to

that seen in humans, with male animals presenting with higher levels of aganglionosis than females (62,63).

In addition, several genes that interact with *Sox10* to modulate aganglionosis have been identified. Heterozygosity at *Sox8* (64) or *Zfhx1B* (65) in conjunction with heterozygosity at *Sox10* significantly worsens the aganglionic phenotype. Both heterozygosity and homozygosity of mutant alleles of *Edn3* and *EdnrB* in conjunction with heterozygosity at *Sox10* increase aganglionosis (66). Loss of *L1cam*, an X-linked gene, also causes increased aganglionosis when paired with a heterozygous *Sox10* mutation (67).

While *EDN3* and *EDNRB* are known HSCR-related genes, the others have been associated with this disease only peripherally, if at all. *ZFHX1B* is the causative gene for Mowat-Wilson Syndrome, a dysmorphic disorder with mental retardation that is often comorbid with HSCR (68,69). *L1CAM* is mutated in a variety of X-linked mental retardation syndromes, collectively known as CRASH (70). It has been implicated in cases that present with both hydrocephalus and HSCR (71-73). In contrast, no disease has been associated with *SOX8*, and homozygous knockouts have no abnormal phenotype (64). The disparity of connection with HSCR in these genes underscores the need for further research into genes that interact and/or modify this disease.

Modifiers of Sox10^{Dom} aganglionosis

The variation in phenotype based on genetic background in *Sox10^{Dom/+}* mice made this model an ideal system for exploring the possibility of HSCR

modifiers in mice. A large C57BL/6JXC3HeB/FeJ.*Sox10^{Dom}* F₂ population was used for a genome-wide linkage scan for modifiers of aganglionosis (13). Five chromosomes had significant linkage results: mouse chr.3, 5, 8, 11, and 14. In the cases of the modifier intervals on chr.5, 8, 11, and 14, the B6 allele was associated with increased severity and penetrance of aganglionosis. For the chr.3 interval, the C3Fe background provided the risk allele (13). The chr.14 modifier interval was confirmed to be *EdnrB* in a separate study (12). *Sox10^{Dom/+};EdnrB^{S-/S-}* mice presented with significantly greater amounts of aganglionosis than *Sox10^{Dom/+};EdnrB^{+/+}*, *Sox10^{+/+};EdnrB^{S-/S-}*, or *Sox10^{Dom/+};EdnrB^{S-/+}* mice, which confirms an interaction between these two genes (12). In addition, the B6 allele of *EdnrB* was found to be associated with greater penetrance and severity of aganglionosis in a B6XC3Fe.*Sox10^{Dom}* F₂ population, which confirms that *EdnrB* is a modifier of *Sox10^{Dom}* aganglionosis (12). The modifier intervals on chr.3, 8, and 11 do not contain any genes previously associated with HSCR; these intervals will need to be studied further to determine the genes underlying their linkage with *Sox10^{Dom}* aganglionosis.

To be defined as a modifier, a gene should display several of the following characteristics: a biological function in line with the trait being studied; polymorphisms in coding or regulatory regions; an effect, either *in vitro* or *in vivo*, on the trait being studied when different alleles are compared; and a human homolog that has been associated with the trait of interest (74). These qualifications were used to determine which genes within the modifier intervals were the most promising candidates. The modifier interval on chr.5 was

narrowed with additional genotyping to an 8cM region; bioinformatic analysis identified 10 prospective candidate genes that displayed expression in the embryonic gut. Three candidates, *Uchl1*, *Atp8a1*, and *Phox2B*, were selected as the most likely genes to underlie this interval due to expression in enteric progenitors (13).

Atp8a1 has been characterized as the enzyme needed to shuttle phosphatidylserine and phosphatidylethanolamine between the inner and outer membrane leaflets of red blood cells (75). This gene is expressed in erythrocyte precursors (76) and may simply be a hallmark of precursor populations. In addition, mice homozygous for a targeted *LacZ* knock-in (Deltagen) have no morphological deficiencies. The lack of ENS phenotype in mutants removed this candidate from the list. *Uchl1*, also known as PGP9.5, is a commonly used marker of neural crest-derived precursors in the gut (77,78). It was determined to be the causative gene in *gracile axonal dystrophy (gad)* mice (79), a spontaneous mutant with progressive neuronal degeneration first described by Yamazaki et al. (80). Studies in the mouse brain have determined that *Uchl1* is expressed in neural progenitor cells and regulates progenitor cell morphology (81). The only known connection between this gene and the enteric nervous system is a report of dysphagia in *Uchl1;Uchl3* double mutant homozygotes (82). However, this phenotype is most likely due to central nervous system defects, rather than ENS deficits. In addition, test crosses using the *Uchl1^{tm1Dgen}* targeted knockout and the B6.*Sox10^{Dom}* line have shown no modifying effect of this locus

on aganglionosis (Southard-Smith EM, unpublished data). Thus, *Uchl1* is most likely not the modifying gene in the chr.5 interval.

Phox2B as a modifier of Sox10^{Dom} aganglionosis

The remaining candidate that is expressed in enteric progenitors, a vital requirement for modification of enteric aganglionosis, is *Phox2B*. This homeodomain transcription factor was first described by Pattyn et al. 1997 (83), with expression in the embryonic brain and autonomic nervous system. It is a reliable marker for ENPs throughout embryonic development (84-87). *Phox2B* is required for neural progenitors to exit the cell cycle and begin differentiation (88). In addition, it simultaneously promotes expression of proneural genes and inhibits expression of neurogenesis inhibitors (89). A transgenic *LacZ* knock-in allele was developed by Pattyn et al. 1999 (90). Analysis of this mutant demonstrated that *Phox2B* is necessary for development of the autonomic nervous system. Heterozygous animals have no discernible morphological abnormalities (90). Homozygous mutant embryos display *LacZ*⁺ cells in the foregut at 10.5dpc, but these degenerate by apoptosis by 13.5dpc; thus, the gastrointestinal tract is completely devoid of enteric progenitors (90). In addition, homozygous mutants lacked expression both of *Ret* and *Mash1*, genes required for development of the ENS (90). *Phox2B* plays a clear role in ENS ontogeny.

Phox2B also plays an important role in other parts of the autonomic nervous system. CCHS, characterized by lack of respiratory control primarily during sleep, was determined to be due to mutations in *PHOX2B* (91-93). In

particular, expansion of a polyalanine tract in exon 3 was found in the majority of patients (91,94). A subset of CCHS patients also present with HSCR, a condition known as Haddad Syndrome (95). Interestingly, these patients are much more likely to have mutations elsewhere in *PHOX2B*, rather than a polyalanine expansion; in particular, frameshift mutations in exon 3 are the most common form of variance (93,96-98). It has been postulated that the mutated forms of *PHOX2B* act in a dominant-negative fashion, rather than simply causing a decrease in protein (99). This is supported by the lack of a CCHS phenotype in the *Phox2B^{LacZ}* line of mice described above (90). However, a decrease in *Phox2B* activity could increase the appearance of HSCR-like phenotypes in a sensitized background.

Evidence for the modifying action of *Phox2B* can be found in both human and animal studies. An A→G transition in intron 2 has been associated with HSCR in the Han Chinese in two separate studies (100,101). This SNP alone would likely not be sufficient to cause HSCR, so *PHOX2B* is most likely acting in concert with another HSCR-related gene. Preliminary work by the Southard-Smith lab has demonstrated an effect of hemizyosity at *Phox2B* on *Sox10^{Dom}* aganglionosis. In crosses between B6D2.*Phox2B^{LacZ}* mice and both the B6 and C3Fe *Sox10^{Dom}* congenic lines, the only functional copy of *Phox2B* in double mutants comes from the genetic background of the *Sox10^{Dom}* line. In B6.*Sox10^{Dom/+};Phox2B^{LacZ/+}* mice, the severity of aganglionosis was much higher than in B6.*Sox10^{Dom/+};Phox2B^{+/+}* mice. In contrast, C3Fe.*Sox10^{Dom/+};Phox2B^{LacZ/+}* and C3Fe.*Sox10^{Dom/+};Phox2B^{+/+}* mice were

comparable in their levels of aganglionosis (Southard-Smith EM, unpublished data). If mere haploinsufficiency at *Phox2B* were to blame, double mutants of both backgrounds would be equally affected. As B6 double mutants present with greater severity than C3Fe double mutants, the genetic background of *Phox2B* is crucial to determining its effect of *Sox10^{Dom}* aganglionosis.

Summary

Numerous lines of evidence support the hypothesis that *Phox2B* plays a role in modulating the severity of aganglionosis. However, the mechanism behind this modulation and the effect of *Phox2B* during development of *Sox10^{Dom}* embryos is unknown. This study aims to answer the following questions: How does genetic background impact ENP development during ENS ontogeny? Is differential expression of *Phox2B* occurring between the B6 and C3Fe inbred strain backgrounds? What is the nature of sequence variation at this locus between these two strains? How do different alleles of *Phox2B* impact ENPs during ENS development in the *Sox10^{Dom}* model of aganglionosis?

A thorough analysis of different aspects of ENP development in the B6 and C3Fe *Sox10^{Dom}* lines will demonstrate the far-reaching impact of genetic background on the formation of the ENS. By utilizing the congenic *Sox10^{Dom}* lines and a variety of molecular techniques, differential expression of portions of *Phox2B* and potential for alternative splicing will be suggested between the B6 and C3Fe inbred strains. A combination of bacterial artificial chromosome (BAC) sequencing and focused multiplex genotyping will demonstrate the vast amount

of genetic diversity at the *Phox2B* locus between inbred strains of mice. Association tests between haplotype at *Phox2B* and aganglionic severity will demonstrate that *Phox2B* is at least one of the genes underlying the *Sox10m3* modifier interval. Finally, analysis of *Sox10^{Dom/+};Phox2B^{LacZ/+}* double mutants will highlight the impact of strain background at *Phox2B* on the development of the ENS. In total, this thesis work will decisively establish the importance of *Phox2B* in modifying aganglionosis.

References

1. Knecht,A.K., Bronner-Fraser,M. (2002) Induction of the neural crest: a multigene process. *Nat. Rev. Genet.*, **3**, 453-461.
2. Newgreen,D., Young,H.M. (2002) Enteric nervous system: development and developmental disturbances--part 2. *Pediatr. Dev. Pathol.*, **5**, 329-349.
3. Young,H.M. (2008) Functional development of the enteric nervous system--from migration to motility. *Neurogastroenterol. Motil.*, **20 Suppl 1**, 20-31.
4. Heanue,T.A., Pachnis,V. (2007) Enteric nervous system development and Hirschsprung's disease: advances in genetic and stem cell studies. *Nat. Rev. Neurosci.*, **8**, 466-479.
5. Young,H.M., Hearn,C.J., Newgreen,D.F. (2000) Embryology and development of the enteric nervous system. *Gut*, **47 Suppl 4**, iv12-iv14.
6. Burns,A.J., Champeval,D., Le Douarin,N.M. (2000) Sacral neural crest cells colonise aganglionic hindgut in vivo but fail to compensate for lack of enteric ganglia. *Dev. Biol.*, **219**, 30-43.
7. Hirschsprung H (1888) Stuhltragheit neugeborener infolge von dilatation und hypertrophic des colons. *Jb Kinderheilk*, **21**, 1-7.
8. WHITEHOUSE,F.R., KERNOHAN,J.W. (1948) Myenteric plexus in congenital megacolon; study of 11 cases. *Arch. Intern. Med. (Chic.)*, **82**, 75-111.
9. Chakravarti A, Lyonnet S (2006) *The Online Metabolic and Molecular Bases of Inherited Disease*. pp. 6231-6255.
10. ZUELZER,W.W., WILSON,J.L. (1948) Functional intestinal obstruction on a congenital neurogenic basis in infancy. *Am. J. Dis. Child*, **75**, 40-64.
11. Southard-Smith,E.M., Kos,L., Pavan,W.J. (1998) Sox10 mutation disrupts neural crest development in Dom Hirschsprung mouse model. *Nat. Genet.*, **18**, 60-64.
12. Cantrell,V.A., Owens,S.E., Chandler,R.L., *et al.* (2004) Interactions between Sox10 and EdnrB modulate penetrance and severity of aganglionosis in the Sox10Dom mouse model of Hirschsprung disease. *Hum. Mol. Genet.*, **13**, 2289-2301.
13. Owens,S.E., Broman,K.W., Wiltshire,T., *et al.* (2005) Genome-wide linkage identifies novel modifier loci of aganglionosis in the Sox10Dom model of Hirschsprung disease. *Hum. Mol. Genet.*, **14**, 1549-1558.

14. Parc,R., Berrod,J.L., Tussiot,J., *et al.* (1984) [Megacolon in adults. Apropos of 76 cases]. *Ann. Gastroenterol. Hepatol. (Paris)*, **20**, 133-141.
15. Kurer,M.H., Lawson,J.O., Pambakian,H. (1986) Suction biopsy in Hirschsprung's disease. *Arch. Dis. Child*, **61**, 83-84.
16. Pellerin,D. (1992) [Hirschsprung disease]. *Ann. Gastroenterol. Hepatol. (Paris)*, **28**, 99-103.
17. Swenson,O. (1996) Early history of the therapy of Hirschsprung's disease: facts and personal observations over 50 years. *J. Pediatr. Surg.*, **31**, 1003-1008.
18. Torfs CP (1998) *The Third International Meeting: Hirschsprung Disease and Related Neurocristopathies*. Evian, France.
19. Badner,J.A., Sieber,W.K., Garver,K.L., *et al.* (1990) A genetic study of Hirschsprung disease. *Am. J. Hum. Genet.*, **46**, 568-580.
20. Angrist,M., Kauffman,E., Slaugenhaupt,S.A., *et al.* (1993) A gene for Hirschsprung disease (megacolon) in the pericentromeric region of human chromosome 10. *Nat. Genet.*, **4**, 351-356.
21. Luo,Y., Ceccherini,I., Pasini,B., *et al.* (1993) Close linkage with the RET protooncogene and boundaries of deletion mutations in autosomal dominant Hirschsprung disease. *Hum. Mol. Genet.*, **2**, 1803-1808.
22. Lyonnet,S., Bolino,A., Pelet,A., *et al.* (1993) A gene for Hirschsprung disease maps to the proximal long arm of chromosome 10. *Nat. Genet.*, **4**, 346-350.
23. Amiel,J., Attie,T., Jan,D., *et al.* (1996) Heterozygous endothelin receptor B (EDNRB) mutations in isolated Hirschsprung disease. *Hum. Mol. Genet.*, **5**, 355-357.
24. Attie,T., Till,M., Pelet,A., *et al.* (1995) Mutation of the endothelin-receptor B gene in Waardenburg-Hirschsprung disease. *Hum. Mol. Genet.*, **4**, 2407-2409.
25. Kusafuka,T., Wang,Y., Puri,P. (1996) Novel mutations of the endothelin-B receptor gene in isolated patients with Hirschsprung's disease. *Hum. Mol. Genet.*, **5**, 347-349.
26. Edery,P., Attie,T., Amiel,J., *et al.* (1996) Mutation of the endothelin-3 gene in the Waardenburg-Hirschsprung disease (Shah-Waardenburg syndrome). *Nat. Genet.*, **12**, 442-444.

27. Hofstra,R.M., Osinga,J., Tan-Sindhunata,G., *et al.* (1996) A homozygous mutation in the endothelin-3 gene associated with a combined Waardenburg type 2 and Hirschsprung phenotype (Shah-Waardenburg syndrome). *Nat. Genet.*, **12**, 445-447.
28. Angrist,M., Bolk,S., Halushka,M., *et al.* (1996) Germline mutations in glial cell line-derived neurotrophic factor (GDNF) and RET in a Hirschsprung disease patient. *Nat. Genet.*, **14**, 341-344.
29. Ivanchuk,S.M., Myers,S.M., Eng,C., *et al.* (1996) De novo mutation of GDNF, ligand for the RET/GDNFR-alpha receptor complex, in Hirschsprung disease. *Hum. Mol. Genet.*, **5**, 2023-2026.
30. Salomon,R., Attie,T., Pelet,A., *et al.* (1996) Germline mutations of the RET ligand GDNF are not sufficient to cause Hirschsprung disease. *Nat. Genet.*, **14**, 345-347.
31. Pingault,V., Bondurand,N., Kuhlbrodt,K., *et al.* (1998) SOX10 mutations in patients with Waardenburg-Hirschsprung disease. *Nat. Genet.*, **18**, 171-173.
32. Southard-Smith,E.M., Angrist,M., Ellison,J.S., *et al.* (1999) The Sox10(Dom) mouse: modeling the genetic variation of Waardenburg-Shah (WS4) syndrome. *Genome Res.*, **9**, 215-225.
33. Chakravarti,A. (1996) Endothelin receptor-mediated signaling in hirschsprung disease. *Hum. Mol. Genet.*, **5**, 303-307.
34. Angrist,M., Bolk,S., Thiel,B., *et al.* (1995) Mutation analysis of the RET receptor tyrosine kinase in Hirschsprung disease. *Hum. Mol. Genet.*, **4**, 821-830.
35. Bolk,S., Pelet,A., Hofstra,R.M., *et al.* (2000) A human model for multigenic inheritance: phenotypic expression in Hirschsprung disease requires both the RET gene and a new 9q31 locus. *Proc. Natl. Acad. Sci. U. S. A.*, **97**, 268-273.
36. Garcia-Barcelo,M.M., Fong,P.Y., Tang,C.S., *et al.* (2008) Mapping of a Hirschsprung's disease locus in 3p21. *Eur. J. Hum. Genet.*, **16**, 833-840.
37. Sanchez-Mejias,A., Fernandez,R.M., Lopez-Alonso,M., *et al.* (2009) Contribution of RET, NTRK3 and EDN3 to the expression of Hirschsprung disease in a multiplex family. *J. Med. Genet.*, **46**, 862-864.
38. Fernandez,R.M., Sanchez-Mejias,A., Mena,M.D., *et al.* (2009) A novel point variant in NTRK3, R645C, suggests a role of this gene in the pathogenesis of Hirschsprung disease. *Ann. Hum. Genet.*, **73**, 19-25.

39. Garcia-Barcelo, M.M., Tang, C.S., Ngan, E.S., *et al.* (2009) Genome-wide association study identifies NRG1 as a susceptibility locus for Hirschsprung's disease. *Proc. Natl. Acad. Sci. U. S. A.*, **106**, 2694-2699.
40. Tang, C.S., Sribudiani, Y., Miao, X.P., *et al.* (2010) Fine mapping of the 9q31 Hirschsprung's disease locus. *Hum. Genet.*, **127**, 675-683.
41. de Pontual L., Pelet, A., Trochet, D., *et al.* (2006) Mutations of the RET gene in isolated and syndromic Hirschsprung's disease in human disclose major and modifier alleles at a single locus. *J. Med. Genet.*, **43**, 419-423.
42. de, P.L., Pelet, A., Clement-Ziza, M., *et al.* (2007) Epistatic interactions with a common hypomorphic RET allele in syndromic Hirschsprung disease. *Hum. Mutat.*, **28**, 790-796.
43. Baynash, A.G., Hosoda, K., Giaid, A., *et al.* (1994) Interaction of endothelin-3 with endothelin-B receptor is essential for development of epidermal melanocytes and enteric neurons. *Cell*, **79**, 1277-1285.
44. Hosoda, K., Hammer, R.E., Richardson, J.A., *et al.* (1994) Targeted and natural (piebald-lethal) mutations of endothelin-B receptor gene produce megacolon associated with spotted coat color in mice. *Cell*, **79**, 1267-1276.
45. Lane, P.W. (1966) Association of megacolon with two recessive spotting genes in the mouse. *J. Hered.*, **57**, 29-31.
46. Schuchardt, A., D'Agati, V., Larsson-Blomberg, L., *et al.* (1994) Defects in the kidney and enteric nervous system of mice lacking the tyrosine kinase receptor Ret. *Nature*, **367**, 380-383.
47. Pichel, J.G., Shen, L., Sheng, H.Z., *et al.* (1996) Defects in enteric innervation and kidney development in mice lacking GDNF. *Nature*, **382**, 73-76.
48. Tomac, A.C., Grinberg, A., Huang, S.P., *et al.* (2000) Glial cell line-derived neurotrophic factor receptor alpha1 availability regulates glial cell line-derived neurotrophic factor signaling: evidence from mice carrying one or two mutated alleles. *Neuroscience*, **95**, 1011-1023.
49. Guillemot, F., Lo, L.C., Johnson, J.E., *et al.* (1993) Mammalian achaete-scute homolog 1 is required for the early development of olfactory and autonomic neurons. *Cell*, **75**, 463-476.
50. Blaugrund, E., Pham, T.D., Tennyson, V.M., *et al.* (1996) Distinct subpopulations of enteric neuronal progenitors defined by time of development, sympathoadrenal lineage markers and Mash-1-dependence. *Development*, **122**, 309-320.

51. Kim,J., Lo,L., Dormand,E., *et al.* (2003) SOX10 maintains multipotency and inhibits neuronal differentiation of neural crest stem cells. *Neuron*, **38**, 17-31.
52. Paratore,C., Goerich,D.E., Suter,U., *et al.* (2001) Survival and glial fate acquisition of neural crest cells are regulated by an interplay between the transcription factor Sox10 and extrinsic combinatorial signaling. *Development*, **128**, 3949-3961.
53. Lane,P.W., Liu,H.M. (1984) Association of megacolon with a new dominant spotting gene (Dom) in the mouse. *J. Hered.*, **75**, 435-439.
54. Inoue,K., Khajavi,M., Ohyama,T., *et al.* (2004) Molecular mechanism for distinct neurological phenotypes conveyed by allelic truncating mutations. *Nat. Genet.*, **36**, 361-369.
55. Kapur,R.P., Livingston,R., Doggett,B., *et al.* (1996) Abnormal microenvironmental signals underlie intestinal aganglionosis in Dominant megacolon mutant mice. *Dev. Biol.*, **174**, 360-369.
56. Puliti,A., Poirier,V., Goossens,M., *et al.* (1996) Neuronal defects in genotyped dominant megacolon (Dom) mouse embryos, a model for Hirschsprung disease. *Neuroreport*, **7**, 489-492.
57. Kapur,R.P. (1999) Early death of neural crest cells is responsible for total enteric aganglionosis in Sox10(Dom)/Sox10(Dom) mouse embryos. *Pediatr. Dev. Pathol.*, **2**, 559-569.
58. Garcia-Barcelo,M.M., Lau,D.K., Ngan,E.S., *et al.* (2007) Evaluation of the thyroid transcription factor-1 gene (TTF1) as a Hirschsprung's disease locus. *Ann. Hum. Genet.*, **71**, 746-754.
59. Kimura,S., Hara,Y., Pineau,T., *et al.* (1996) The T/ebp null mouse: thyroid-specific enhancer-binding protein is essential for the organogenesis of the thyroid, lung, ventral forebrain, and pituitary. *Genes Dev.*, **10**, 60-69.
60. DeFelice,M., Silberschmidt,D., DiLauro,R., *et al.* (2003) TTF-1 phosphorylation is required for peripheral lung morphogenesis, perinatal survival, and tissue-specific gene expression. *J. Biol. Chem.*, **278**, 35574-35583.
61. Parlato,R., Rosica,A., Rodriguez-Mallon,A., *et al.* (2004) An integrated regulatory network controlling survival and migration in thyroid organogenesis. *Dev. Biol.*, **276**, 464-475.
62. Carrasquillo,M.M., McCallion,A.S., Puffenberger,E.G., *et al.* (2002) Genome-wide association study and mouse model identify interaction

between RET and EDNRB pathways in Hirschsprung disease. *Nat. Genet.*, **32**, 237-244.

63. McCallion,A.S., Stames,E., Conlon,R.A., *et al.* (2003) Phenotype variation in two-locus mouse models of Hirschsprung disease: tissue-specific interaction between Ret and Ednrb. *Proc. Natl. Acad. Sci. U. S. A.*, **100**, 1826-1831.
64. Maka,M., Stolt,C.C., Wegner,M. (2005) Identification of Sox8 as a modifier gene in a mouse model of Hirschsprung disease reveals underlying molecular defect. *Dev. Biol.*, **277**, 155-169.
65. Stanchina,L., Van de Putte,T., Goossens,M., *et al.* (2010) Genetic interaction between Sox10 and Zfhx1b during enteric nervous system development. *Dev. Biol.*, **341**, 416-428.
66. Stanchina,L., Baral,V., Robert,F., *et al.* (2006) Interactions between Sox10, Edn3 and Ednrb during enteric nervous system and melanocyte development. *Dev. Biol.*, **295**, 232-249.
67. Wallace,A.S., Schmidt,C., Schachner,M., *et al.* (2010) L1cam acts as a modifier gene during enteric nervous system development. *Neurobiol. Dis.*.
68. Cacheux,V., Dastot-Le,M.F., Kaariainen,H., *et al.* (2001) Loss-of-function mutations in SIP1 Smad interacting protein 1 result in a syndromic Hirschsprung disease. *Hum. Mol. Genet.*, **10**, 1503-1510.
69. Wakamatsu,N., Yamada,Y., Yamada,K., *et al.* (2001) Mutations in SIP1, encoding Smad interacting protein-1, cause a form of Hirschsprung disease. *Nat. Genet.*, **27**, 369-370.
70. Fransen,E., Lemmon,V., Van,C.G., *et al.* (1995) CRASH syndrome: clinical spectrum of corpus callosum hypoplasia, retardation, adducted thumbs, spastic paraparesis and hydrocephalus due to mutations in one single gene, L1. *Eur. J. Hum. Genet.*, **3**, 273-284.
71. Okamoto,N., Wada,Y., Goto,M. (1997) Hydrocephalus and Hirschsprung's disease in a patient with a mutation of L1CAM. *J. Med. Genet.*, **34**, 670-671.
72. Okamoto,N., Del,M.R., Valero,R., *et al.* (2004) Hydrocephalus and Hirschsprung's disease with a mutation of L1CAM. *J. Hum. Genet.*, **49**, 334-337.
73. Jackson,S.R., Guner,Y.S., Woo,R., *et al.* (2009) L1CAM mutation in association with X-linked hydrocephalus and Hirschsprung's disease. *Pediatr. Surg. Int.*, **25**, 823-825.

74. Abiola,O., Angel,J.M., Avner,P., *et al.* (2003) The nature and identification of quantitative trait loci: a community's view. *Nat. Rev. Genet.*, **4**, 911-916.
75. Soupene,E., Kemaladewi,D.U., Kuypers,F.A. (2008) ATP8A1 activity and phosphatidylserine transbilayer movement. *J. Receptor Ligand. Channel. Res.*, **1**, 1-10.
76. Soupene,E., Kuypers,F.A. (2006) Identification of an erythroid ATP-dependent aminophospholipid transporter. *Br. J. Haematol.*, **133**, 436-438.
77. Sidebotham,E.L., Woodward,M.N., Kenny,S.E., *et al.* (2001) Assessment of protein gene product 9.5 as a marker of neural crest-derived precursor cells in the developing enteric nervous system. *Pediatr. Surg. Int.*, **17**, 304-307.
78. Young,H.M., Bergner,A.J., Muller,T. (2003) Acquisition of neuronal and glial markers by neural crest-derived cells in the mouse intestine. *J. Comp Neurol.*, **456**, 1-11.
79. Saigoh,K., Wang,Y.L., Suh,J.G., *et al.* (1999) Intragenic deletion in the gene encoding ubiquitin carboxy-terminal hydrolase in gad mice. *Nat. Genet.*, **23**, 47-51.
80. Yamazaki,K., Wakasugi,N., Tomita,T., *et al.* (1988) Gracile axonal dystrophy (GAD), a new neurological mutant in the mouse. *Proc. Soc. Exp. Biol. Med.*, **187**, 209-215.
81. Sakurai,M., Ayukawa,K., Setsuie,R., *et al.* (2006) Ubiquitin C-terminal hydrolase L1 regulates the morphology of neural progenitor cells and modulates their differentiation. *J. Cell Sci.*, **119**, 162-171.
82. Kurihara,L.J., Kikuchi,T., Wada,K., *et al.* (2001) Loss of Uch-L1 and Uch-L3 leads to neurodegeneration, posterior paralysis and dysphagia. *Hum. Mol. Genet.*, **10**, 1963-1970.
83. Pattyn,A., Morin,X., Cremer,H., *et al.* (1997) Expression and interactions of the two closely related homeobox genes Phox2a and Phox2b during neurogenesis. *Development*, **124**, 4065-4075.
84. Young,H.M., Hearn,C.J., Ciampoli,D., *et al.* (1998) A single rostrocaudal colonization of the rodent intestine by enteric neuron precursors is revealed by the expression of Phox2b, Ret, and p75 and by explants grown under the kidney capsule or in organ culture. *Dev. Biol.*, **202**, 67-84.
85. Young,H.M., Ciampoli,D., Hsuan,J., *et al.* (1999) Expression of Ret-, p75(NTR)-, Phox2a-, Phox2b-, and tyrosine hydroxylase-immunoreactivity by undifferentiated neural crest-derived cells and different classes of enteric neurons in the embryonic mouse gut. *Dev. Dyn.*, **216**, 137-152.

86. Young,H.M., Jones,B.R., McKeown,S.J. (2002) The projections of early enteric neurons are influenced by the direction of neural crest cell migration. *J. Neurosci.*, **22**, 6005-6018.
87. Anderson,R.B., Stewart,A.L., Young,H.M. (2006) Phenotypes of neural-crest-derived cells in vagal and sacral pathways. *Cell Tissue Res.*, **323**, 11-25.
88. Dubreuil,V., Hirsch,M.R., Pattyn,A., *et al.* (2000) The Phox2b transcription factor coordinately regulates neuronal cell cycle exit and identity. *Development*, **127**, 5191-5201.
89. Dubreuil,V., Hirsch,M.R., Jouve,C., *et al.* (2002) The role of Phox2b in synchronizing pan-neuronal and type-specific aspects of neurogenesis. *Development*, **129**, 5241-5253.
90. Pattyn,A., Morin,X., Cremer,H., *et al.* (1999) The homeobox gene Phox2b is essential for the development of autonomic neural crest derivatives. *Nature*, **399**, 366-370.
91. Amiel,J., Laudier,B., Attie-Bitach,T., *et al.* (2003) Polyalanine expansion and frameshift mutations of the paired-like homeobox gene PHOX2B in congenital central hypoventilation syndrome. *Nat. Genet.*, **33**, 459-461.
92. Trang,H., Dehan,M., Beaufile,F., *et al.* (2005) The French Congenital Central Hypoventilation Syndrome Registry: general data, phenotype, and genotype. *Chest*, **127**, 72-79.
93. Trochet,D., O'Brien,L.M., Gozal,D., *et al.* (2005) PHOX2B genotype allows for prediction of tumor risk in congenital central hypoventilation syndrome. *Am. J. Hum. Genet.*, **76**, 421-426.
94. Weese-Mayer,D.E., Berry-Kravis,E.M., Zhou,L., *et al.* (2003) Idiopathic congenital central hypoventilation syndrome: analysis of genes pertinent to early autonomic nervous system embryologic development and identification of mutations in PHOX2b. *Am. J. Med. Genet. A*, **123A**, 267-278.
95. Haddad,G.G., Mazza,N.M., Defendini,R., *et al.* (1978) Congenital failure of automatic control of ventilation, gastrointestinal motility and heart rate. *Medicine (Baltimore)*, **57**, 517-526.
96. Sasaki,A., Kanai,M., Kijima,K., *et al.* (2003) Molecular analysis of congenital central hypoventilation syndrome. *Hum. Genet.*, **114**, 22-26.
97. Matera,I., Bachetti,T., Puppo,F., *et al.* (2004) PHOX2B mutations and polyalanine expansions correlate with the severity of the respiratory

phenotype and associated symptoms in both congenital and late onset Central Hypoventilation syndrome. *J. Med. Genet.*, **41**, 373-380.

98. Berry-Kravis,E.M., Zhou,L., Rand,C.M., *et al.* (2006) Congenital central hypoventilation syndrome: PHOX2B mutations and phenotype. *Am. J. Respir. Crit Care Med.*, **174**, 1139-1144.
99. Weese-Mayer,D.E., Berry-Kravis,E.M., Marazita,M.L. (2005) In pursuit (and discovery) of a genetic basis for congenital central hypoventilation syndrome. *Respir. Physiol Neurobiol.*, **149**, 73-82.
100. Garcia-Barcelo,M., Sham,M.H., Lui,V.C., *et al.* (2003) Association study of PHOX2B as a candidate gene for Hirschsprung's disease. *Gut*, **52**, 563-567.
101. Liu,C.P., Li,X.G., Lou,J.T., *et al.* (2009) Association analysis of the PHOX2B gene with Hirschsprung disease in the Han Chinese population of Southeastern China. *J. Pediatr. Surg.*, **44**, 1805-1811.

CHAPTER II

EFFECT OF STRAIN BACKGROUND ON ENTERIC DEVELOPMENT IN THE *SOX10^{DOM}* MODEL OF HSCR

Introduction

The impact of genetic background on development of ENPs has not previously been examined. Relative to wild-type progenitors, ENPs in *Sox10^{Dom/+}* mice are delayed in their migration as they traverse the gut (1). Modifier genes in the genetic background that produce the distinct amounts of aganglionosis seen in the *Sox10^{Dom/+}* congenic lines may be altering migration, enhancing or suppressing proliferation, or modulating developmental potential of ENPs. Developmental potential has been defined functionally as the ability of progenitors to form various lineages in response to developmental cues that regulate both the timing of differentiation and the proportions of cell types that are produced *in vivo* (2,3). *Sox10* could impact any of these processes because the gene is expressed early during the initial migratory phases of NC and is maintained in ENPs and adult enteric glia (4).

The connection between deficits in development of enteric progenitors and postnatal aganglionosis is not understood. The majority of developmental studies are undertaken at 9-14dpc, while postnatal aganglionosis is normally observed at P7-10 or even later. Many biological processes could be impacted in the intervening time span. Nonetheless, the analysis of these early time-points

can illuminate the initial points of divergence along the developmental track between deficient and functional progenitors. Determining the effects of genetic background on ENS development is critical to understanding the processes that lead to aganglionosis and the variation between HSCR patients.

It has been established that interplay between genes involved in ENS development can significantly affect the presentation of aganglionosis (5-8). The large disparity in aganglionosis severity and penetrance between the two congenic *Sox10^{Dom}* strains must result from the effects of other genes in the distinct B6 and C3Fe genetic backgrounds that are modulating basic developmental processes in ENPs. The search for modifiers of aganglionosis between these two strains has identified multiple intervals in the mouse genome, but specific genes within these regions remain to be identified (9). Understanding the biological effect(s) of genetic background will aid in the identification of modifier genes. More importantly, these studies can illuminate previously unrecognized aspects that contribute to the complex etiology of aganglionosis.

To define the effect of genetic background on ENS development, I have undertaken the developmental study of ENPs in the B6.*Sox10^{Dom}* and C3Fe.*Sox10^{Dom}* congenic lines. I hypothesized that the differences in postnatal aganglionosis were the result of differences in ENS ontogeny during fetal development. ENPs were assayed for differences in migration, proliferation, and developmental potential. Consistent with prior reports, I found that deficiency of *Sox10* alters migration and frequency of ENPs. In addition, I observed that

developmental potential of ENPs in *Sox10^{Dom}* mutants is substantially shifted but no effect on ENP proliferation was seen. Most importantly, these studies demonstrate that genetic background substantially impacts both migration and developmental potential of ENPs. Developmental potential reflects the capacity of NC-derived progenitors to respond to environmental cues and generate distinct lineages *in vivo*. This analysis suggests that genetic background can influence not only the migration of ENPs but, as a consequence of the effect on developmental potential, may also alter the composition of enteric ganglia that are formed in more proximal gut regions, thus contributing to the variation in HSCR-associated symptoms between patients.

Results

Both the Sox10^{Dom} mutation and strain background in the context of the Sox10^{Dom} allele alter ENP migration.

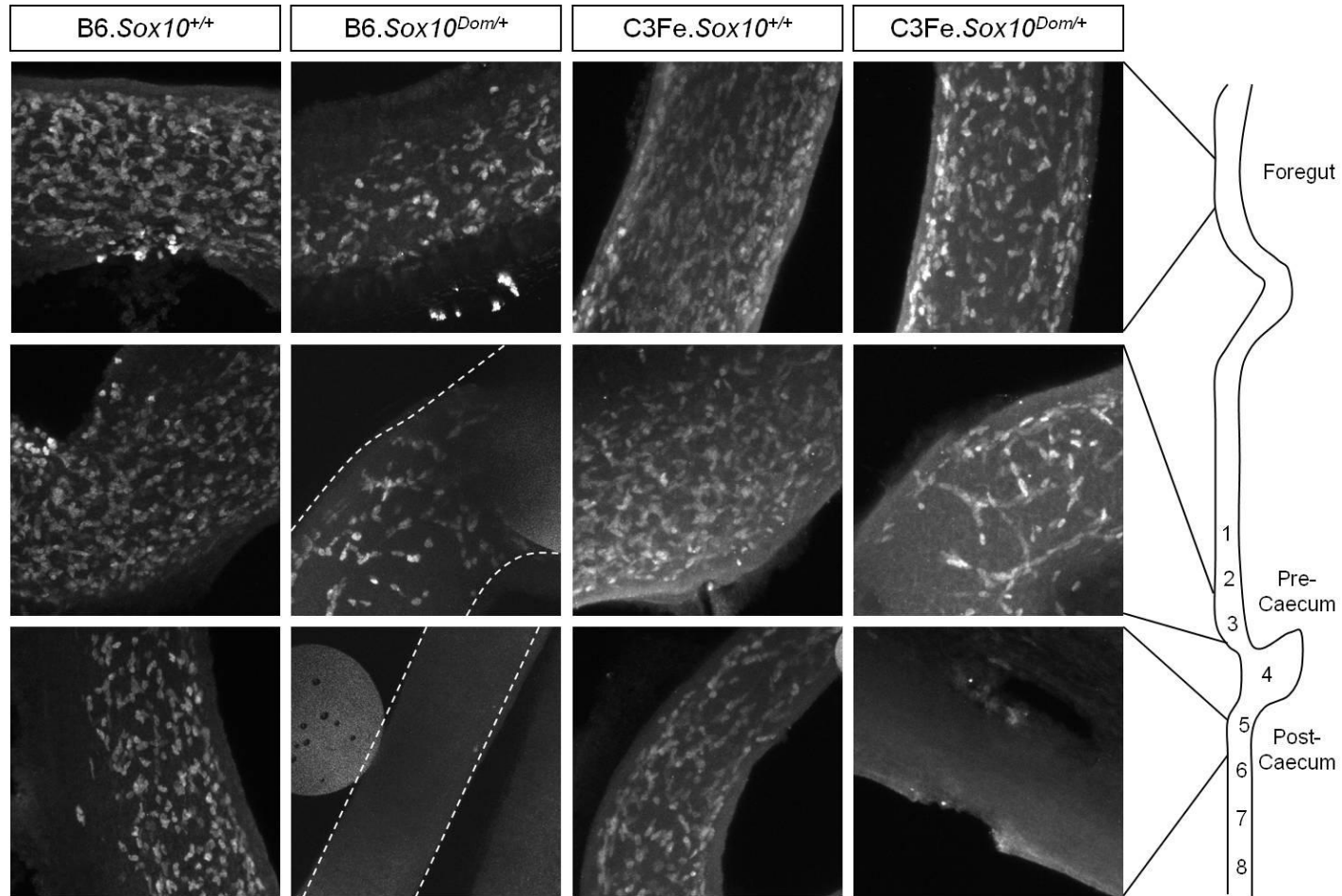
The initial migration of ENPs down the length of the fetal gut is an essential prerequisite for normal ENS development and function. Defective migration of ENPs has been documented in a variety of HSCR models, including *EdnrB^{sl/sl}* mice (10), *EdnrB^{sl/sl}* rats (11), and *Edn3^{sl/sl}* mice (12-14). In addition, several genes implicated in the development of HSCR have also been studied in regards to ENP migration, including *GDNF* (15,16) and cell adhesion molecule *L1* (17). It has been shown that mice with either the *Sox10^{Dom}* mutation or a targeted deletion of *Sox10* fail to completely colonize the distal bowel (1,18). Extent of aganglionosis in the *Sox10^{Dom}* model is influenced by genetic background, as evidenced by the difference in phenotype seen between the B6 and C3Fe strains (5). However, the impact of strain background on the migration process during development has yet to be investigated.

To examine the effect of the *Sox10^{Dom}* mutation and strain background on ENP migration, I used immunohistochemical detection of Phox2B, a known marker of all early ENPs (19), to quantify the extent of migration in whole-mount fetal gastrointestinal tracts from 12.5dpc *Sox10^{Dom/+}* and *Sox10^{+/+}* embryos on both B6 and C3Fe strain backgrounds. Each fetal gut sample was imaged in eight equal regions from mid-foregut to the anus, with the caecum being designated as region number four (Figure 2.1). Representative confocal images behind the migratory wave-front, immediately proximal to the caecum, and immediately distal to the caecum in individual gut samples were captured. The

density of Phox2B⁺ ENPs in each region was assigned on a four-point scale by an observer blinded to embryo genotype.

Wild-type (*Sox10*^{+/+}) embryos of either strain background displayed dense staining due to numerous Phox2B⁺ ENPs through the foregut and caecum. The density of Phox2B⁺ ENPs gradually declined in the hindgut where wave-front progenitors were populating the distal intestine (Table 2.1). In contrast, *Sox10*^{Dom/+} embryos of both strain backgrounds exhibited notably decreased Phox2B⁺ ENP staining with a marked reduction in extent of migration down the gut length and decreased density of Phox2B⁺ cells in the areas that were populated. This effect was most pronounced in *Sox10*^{Dom/+} embryos on the B6 background. Compared with littermate controls, ENPs in B6.*Sox10*^{Dom/+} embryos showed a two-thirds reduction both in cell density and the distance of migration. In contrast, ENPs in C3Fe.*Sox10*^{Dom/+} embryos were present at approximately half the density and had migrated one-third as far as ENPs in wild-type C3Fe embryos. The greater reduction of migration in B6.*Sox10*^{Dom/+} samples compared to C3Fe.*Sox10*^{Dom/+} samples indicates that genetic background exacerbates the effect of the *Sox10*^{Dom} mutation on ENP migration.

Figure 2.1. Effect of strain background and *Sox10^{Dom}* mutation on density and migration of ENPs.



Density and migration of ENPs in *Sox10^{Dom}* embryos and wild-type littermates can be seen in whole-mount 12.5dpc fetal guts by immunohistochemical staining for Phox2B. Confocal images (400X magnification) taken in the proximal foregut, before the caecum, and after the caecum are shown in relation to a schematic diagram of the developing gut. Image panels from representative single guts are shown for each genotypic class. Stippled lines outline the gut in the post-caecum image for *Sox10^{Dom}* embryos to emphasize the gut wall border.

Table 2.1. Effect of strain background and Sox10^{Dom} mutation on ENP migration.

Density of Phox2B⁺ cells was quantified on a four-point scale (1 = least dense, 4 = most dense) in eight equal-sized gut sections. Scores for individual guts and averages are shown (n≥6). The following coloring system was applied: 0.0-0.4 = white, 0.5-1.4 = light gray, 1.5-2.4 = medium gray, 2.5-3.4 = dark gray, and 3.5-4.0 = black.

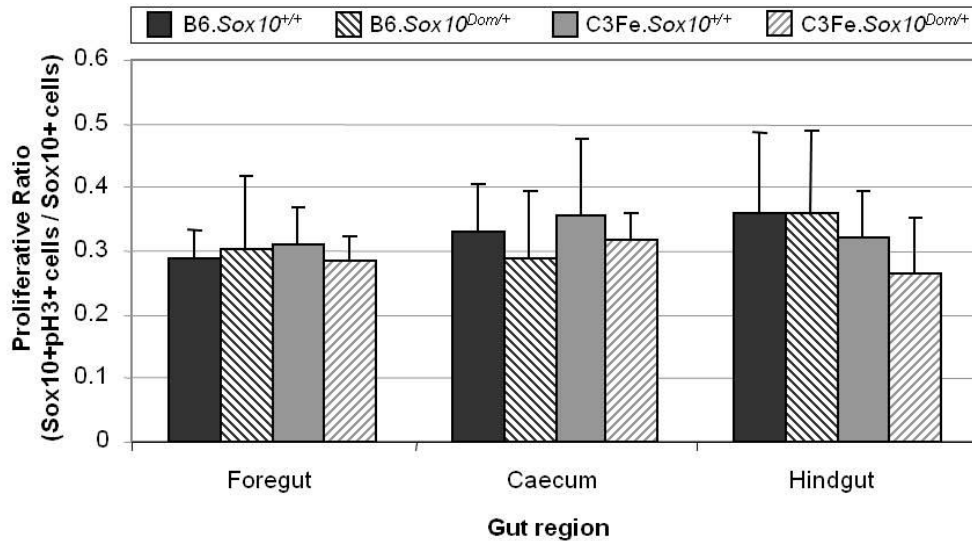
Genotypic Class	Density of Progenitor Cells along Gut							
	1	2	3	4	5	6	7	8
B6.Sox10 ^{+/+}								
Average	3.9	3.4	3.6	3.6	2.9	1.9	1.2	0.5
B6.Sox10 ^{Dom/+}								
Average	2.4	1.8	0.9	0.3	0.1	0.1	0	0
C3Fe.Sox10 ^{+/+}								
Average	4	4	4	4	3.2	1.7	0.9	0.2
C3Fe.Sox10 ^{Dom/+}								
Average	2.9	2.6	2.1	1.4	0.6	0.2	0	0

ENP proliferation is not affected by the Sox10^{Dom} mutation or by strain background.

ENPs are rapidly proliferating during colonization of the fetal intestine, and any loss of proliferative capacity could reduce the size of the progenitor pool needed to entirely populate the gut. Several NC genes are vital to the proliferation process, including *Edn3* (20) and *GDNF* (21-23). I investigated the possibility that the altered migration evident in Sox10^{Dom} mutants could be due to

a proliferative effect that is further influenced by genetic background. To identify proliferating ENPs, I implemented immunocytochemical detection of Sox10, which labels all ENPs, and phospho-Histone H3 (pH3), a known marker of proliferating cells, and specifically quantified the fraction undergoing mitosis. Cells were dissociated from three regions of sub-dissected fetal intestine (mid-small intestine, caecum, and hindgut) from 12.5dpc *Sox10^{Dom/+}* and wild-type littermate embryos. Cell suspensions were allowed to settle onto wells coated with poly-D-lysine and fibronectin, then fixed and stained for pH3 and Sox10 expression. Cells were classified into one of four categories: non-proliferating non-ENP cells (pH3⁻/Sox10⁻); proliferating non-ENP cells (pH3⁺/Sox10⁻); non-proliferating ENP cells (pH3⁻/Sox10⁺); and proliferating ENP cells (pH3⁺/Sox10⁺). The percentage of proliferative progenitors in each gut region was determined by calculating the number of proliferating ENPs (pH3⁺/Sox10⁺) divided by the total number of ENPs (all Sox10⁺ cells). Calculation of this percentage effectively normalized for any differences in total number of cells between wells so that the proliferative capacity of ENPs could be compared between genotype and strain classes for each gut region. This analysis found no significant differences in proliferation between wild-type and *Sox10^{Dom/+}* ENPs or between *Sox10^{Dom/+}* ENPs of either strain background (Figure 2.2).

Figure 2.2. Effect of strain background and Sox10^{Dom} mutation on proliferation of ENPs.



Proliferating enteric NC-derived cells from dissociated Sox10^{Dom} and wild-type littermate 12.5dpc fetal guts were visualized by immunohistochemical staining for Phospho-Histone H3 (pH3), Sox10, and DAPI. Proportion of proliferating ENPs (pH3⁺Sox10⁺ over all Sox10⁺) was determined in Sox10^{Dom} embryos and wild-type littermates. Values shown are average \pm S.D. (n \geq 6). Welch's t test was performed on B6 Sox10^{+/+} vs. C3Fe Sox10^{+/+}, B6 Sox10^{+/+} vs. B6 Sox10^{Dom/+}, C3Fe Sox10^{+/+} vs. C3Fe Sox10^{Dom/+}, and B6 Sox10^{Dom/+} vs. C3Fe Sox10^{Dom/+}.

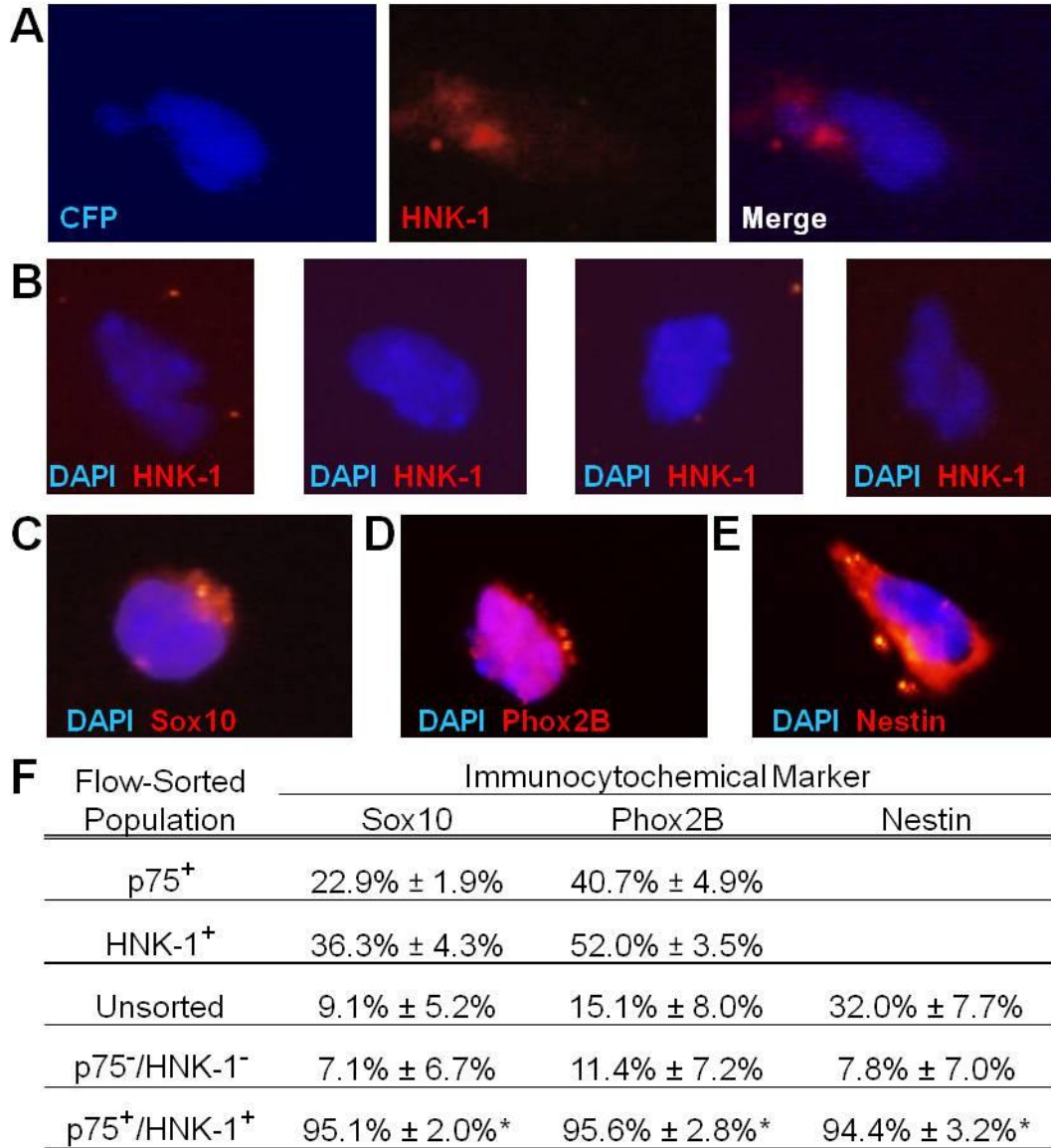
Isolation of ENPs by flow cytometry in the mouse.

Gut neural-crest-derived stem cells (NCSC) give rise to the ENS and comprise a few percent of fetal intestinal cells (2). NCSCs and progenitors can be identified *in situ* using probes for the transcription factors Sox10 or Phox2B. However, analysis of live cells requires use of cell surface markers. Surface antigens like p75, α 4-integrin, or HNK-1 (11,24) have been shown to reliably label ENPs in a variety of species, including quail, chick, and rat (25-32). Combinations of these surface antigens have been used extensively in the rat to purify NCSC populations from the peripheral nervous system, including the ENS (2,3,11,15,33,34). However, HNK-1 has not previously been utilized in mouse models, as prior efforts to localize this antigen by immunohistochemistry in fixed

cryo-sections were unsuccessful (30). The HNK-1 immunoreagent commonly used is an IgM monoclonal whose large size could sterically hinder its ability to cross-react with epitopes in fixed whole-mount tissues of other species (35). Moreover, loss of antigenicity with fixation can be a complicating factor in immunohistochemical detection. To investigate the presence of the HNK-1 epitope on live, unfixed suspensions of dissociated mouse ENPs, I utilized C3Fe-Tg^{Phox2B-H2BCFP} transgenic mice. This transgenic line expresses an H2BCerulean protein (CFP) under the control of the *Phox2B* promoter (36). As *Phox2B* is a widely recognized marker of ENPs, co-localization of HNK-1 with CFP⁺ fetal gut cells from these transgenic embryos would demonstrate that murine ENPs do express a cross-reactive HNK-1 epitope.

CFP⁺ cells were isolated from fetal guts of 14.5dpc C3Fe-Tg^{Phox2B-H2BCFP} embryos by flow cytometry. Cells were plated at a density of 150 cells per well and subjected to immunocytochemistry for p75 and HNK-1. Co-localization of the H2BCerulean marker and both p75 and HNK-1 cell surface markers was observed. In contrast, no HNK-1 immunoreactivity was noted in CFP⁻ cells isolated from the same guts (Figure 2.3A, B). Therefore, HNK-1 is expressed by ENPs in the developing murine gut.

Figure 2.3. Mouse fetal gut cells express HNK-1 on neural crest-derived enteric progenitors.



NC-derived fetal gut cells express HNK-1 and can be isolated based on p75/HNK-1 surface expression. (A) CFP⁺ cells from C3Fe-Tg^{Phox2B-CFP} fetal guts express HNK-1 (400X magnification). (B) CFP⁻ cells from C3Fe-Tg^{Phox2B-CFP} fetal guts were visualized by DAPI nuclear stain and lack HNK-1 expression (400X magnification). Flow-sorted p75⁺/HNK-1⁺ cells show co-expression of Sox10 (C), Phox2B (D), and Nestin (E) (400X magnification). p75⁺/HNK-1⁺ cells are significantly enriched for expression of these markers compared to p75⁻/HNK-1⁻ cells, unsorted cells, p75⁺ cells, and HNK-1⁺ cells from fetal gut. (F) Percentages of sorted cell populations that express NCSC markers. Averages ± S.D. are shown (n=8); *p<0.0001 p75⁺/HNK-1⁺ vs. all other sorted populations.

To evaluate the potential for use of HNK-1 labeling to isolate ENPs, I examined the frequency of Sox10 and Phox2B expression among cells purified by flow cytometry for HNK-1 surface expression. Single cell suspensions from dissociated fetal gut of 12.5dpc embryos were labeled for HNK-1 immunoreactivity. HNK-1⁺ cells were sorted into plates at a density of 150 cells per well and immediately subjected to immunocytochemistry for Sox10 and Phox2B, commonly used markers of ENPs (37). I observed that approximately half of enteric HNK-1⁺ cells are Phox2B⁺, while fewer than 40% are Sox10⁺ (Figure 2.3F). Thus, expression of HNK-1 alone is not sufficient to purify a population of ENPs, which are known to express both Sox10 and Phox2B.

As p75 surface expression has been used frequently to enrich for ENPs using a variety of methods (38-40), I examined the frequency of Sox10 and Phox2B expression in p75⁺ ENPs using flow cytometry to purify cells expressing this surface receptor. Interestingly, I found that less than half of total p75⁺ enteric cells express Phox2B and less than a quarter express Sox10 (Figure 2.3F). While these results could be due to the antibody source, purity, cross-reactivity, or the dilution of antibody applied, this analysis prompted an attempt of labeling with a combination of these two immunoreagents in an effort to obtain a population of ENPs that exhibited a high frequency of expression for Sox10 and Phox2B (36,37).

Double-labeling of dissociated fetal gut cell suspensions with both p75 and HNK-1 led to isolation of a population that is highly enriched for ENPs. When single cell suspensions from 14.5dpc fetal gut were exposed to both p75 and

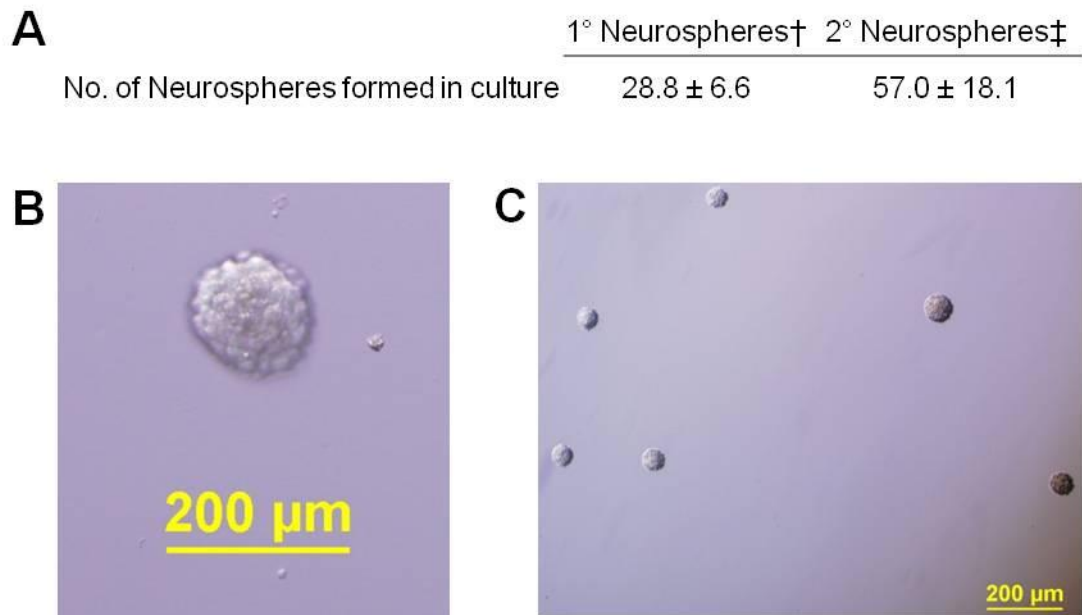
HNK-1 immunoreagents, plated, and immediately stained for Sox10 and Phox2B, I observed that ~95% of these cells express these known markers of enteric NC derivatives (Figure 2.3F). Moreover, p75⁺/HNK-1⁺ ENPs also express Nestin, a marker expressed in all stem cells (41). Thus, the use of both p75 and HNK-1 in combination for flow cytometry increases the purity of the isolated ENP population.

NCSC are also identified by their abilities to form neurospheres in non-adherent cultures and self-renew. To establish that p75⁺/HNK-1⁺ fetal gut cells isolated by flow cytometry possess these capabilities, I plated cells from wild-type 14.5dpc embryos at a density of 1000 cells per well in non-adherent plates. After seven days in culture, neurospheres were counted, dissociated, and replated at a density of 250 cells per well. The dissociated cells formed readily visible secondary neurospheres after seven days of culture (Figure 2.4). Thus, p75⁺/HNK-1⁺ cells in mouse fetal gut express markers of enteric NC-derived progenitors and exhibit both multipotency as well as self-renewal capacity.

Effect of the Sox10^{Dom} mutation and strain background on developmental potential of ENPs.

The ability to prospectively isolate ENPs provides the opportunity to assess the effect of genetic mutations and strain background on the multipotency, lineage potential, and growth factor responsiveness of a defined population (11,15,42,43). Developmental potential can be assessed *in vitro* by prospectively isolating distinct populations of NCSC and culturing these progenitors at low density (2,3,33).

Figure 2.4. Generation of neurospheres from p75⁺/HNK-1⁺ fetal gut cells.



Flow-sorted p75⁺/HNK-1⁺ cells form primary neurospheres in non-adherent culture. Primary neurospheres can be dissociated and replated to form secondary neurospheres after a population expansion. **(A)** Neurosphere counts after each growth period. †Plated at 1000 cells/well, n=9. ‡Plated at 250 cells/well, n=12. **(B)** Representative neurosphere from 1° culture (100X magnification). **(C)** Neurospheres from 2° culture (40X magnification).

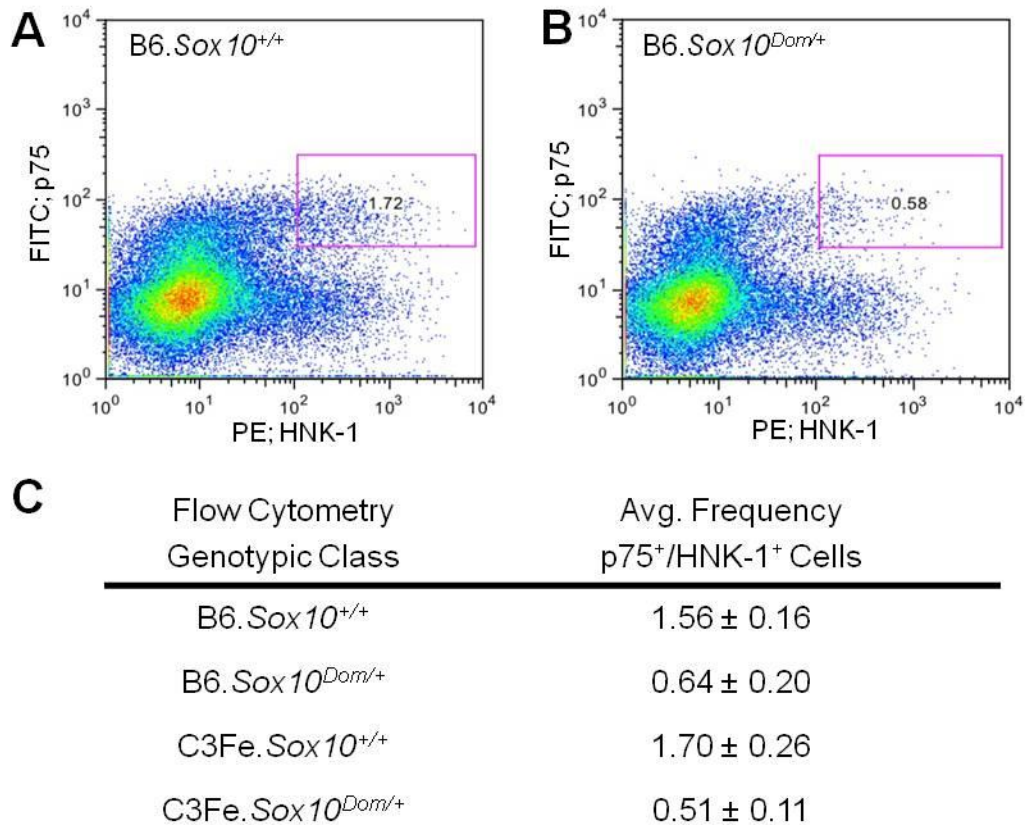
Under such conditions, individual cells form spatially distinct adherent colonies. The differentiation capacities of individual cells *in vivo* are reflected by the phenotypes of cells generated within each colony *in vitro* (2,3). The effect of genetic background on developmental potential of the progenitors that give rise to the ENS is unknown but is a crucial question as alterations in cell responsiveness and capacity to generate distinct lineages could alter the composition of enteric ganglia and potentially impact postnatal gastrointestinal function.

To investigate the effect of *Sox10*^{Dom/+} mutant genotype on ENPs in the B6 and C3Fe congenic lines, I isolated ENPs from fetal guts of 12.5dpc *Sox10*^{Dom/+} and *Sox10*^{+/+} embryos by flow cytometry. Representative flow

profiles of dissociated fetal gut populations stained for p75 and HNK-1 are shown in Figure 2.5. For *Sox10*^{+/+} guts, approximately 1.5-2% of total cells stained brightly for p75/HNK-1, consistent with percentages of NCSC reported by Bixby et al. 2002 (2). This fraction was collected for analysis of developmental potential *in vitro*. In contrast, *Sox10*^{Dom/+} littermate guts examined in parallel under identical gating conditions exhibited a consistent reduction in the percentage of ENPs present (0.4-0.8% of total cells), regardless of strain background. The fraction of fetal gut cells that are p75⁺/HNK-1⁺ differs significantly between wild-type and *Sox10*^{Dom} embryos (p<0.005). This observation is consistent with the reduced numbers of Phox2B⁺ cells observed in *Sox10*^{Dom} fetal guts by confocal microscopy.

To determine the effect of strain background and *Sox10* genotype on developmental potential of ENPs *in vitro*, I examined the phenotypes of colonies grown in adherent cultures at low density. I plated equal numbers of p75⁺/HNK-1⁺ progenitors for each genotype and strain background (500 cells per well, 52 cells/cm²). Colony phenotypes were examined by immunostaining for neuronal (peripherin), glial (GFAP), and myofibroblast (SMA) lineage markers. ENP-derived colonies were either multipotent (containing all three cell types within a single colony, Figure 2.6A, B) or restricted (containing only one or two cell types within a single colony; Figure 2.6C, D). Multiple colony types were produced from both *Sox10*^{Dom/+} and *Sox10*^{+/+} ENPs, regardless of strain background (Table 2.2).

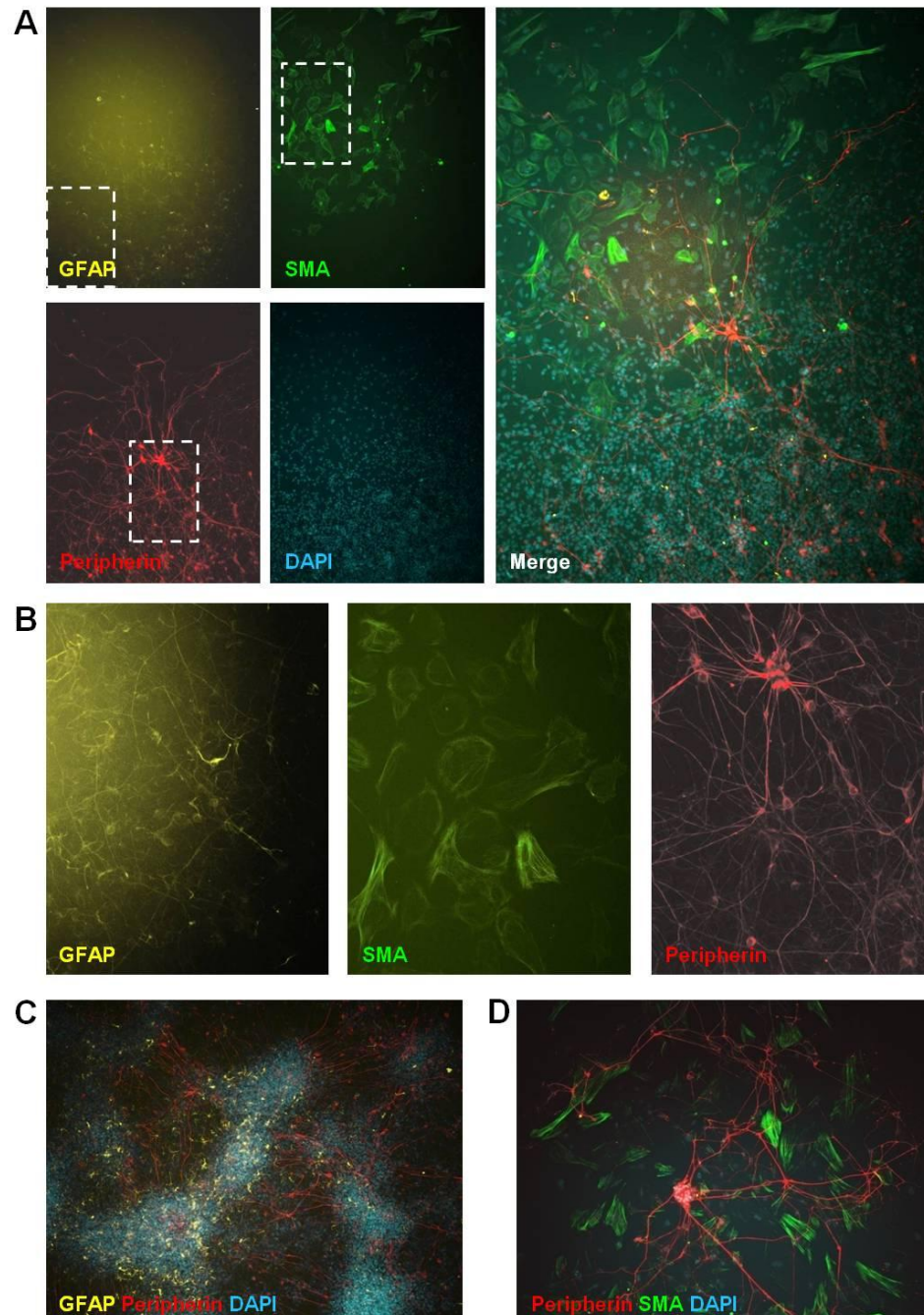
Figure 2.5. Effect of strain background and *Sox10^{Dom}* mutation on proportion of p75⁺/HNK-1⁺ ENPs in fetal gut.



ENPs are isolated by flow cytometry for p75⁺/HNK-1⁺ cells from dissociated 12.5dpc guts from *Sox10^{Dom}* embryos and wild-type littermates. A representative flow profile is shown for B6 *Sox10^{+/+}* (A) and B6 *Sox10^{Dom/+}* (B) fetal gut cell suspensions. Both flow profiles were generated using identical gate settings and are based on 5000 events. Average percentage of p75⁺/HNK-1⁺ cells from the total live population are shown for all four strain/genotype populations in (C) (n=4 independent sorts).

While all categories of ENPs were able to produce both restricted and multipotent colonies, we observed significant differences in the proportions of lineages produced by wild-type progenitors from the two strain backgrounds. B6.*Sox10^{+/+}* ENPs produced more glial derivatives, with 0.8% glial and 3.3% glial + myofibroblast colonies, when compared with C3Fe.*Sox10^{+/+}* ENPs, which produced no glial colonies and 0.7% glial + myofibroblast colonies. (Table 2.2)

Figure 2.6. Effect of strain background and *Sox10^{Dom}* mutation on developmental potential of *in vitro* cultures of flow-sorted ENPs.



Multiple colony types from cultured $p75^+$ /HNK-1⁺ ENPs from 12.5dpc guts from *Sox10^{Dom}* embryos and wild-type littermates are visualized by immunohistochemical staining for glial fibrillary acidic protein (GFAP, glia, yellow), smooth muscle actin (SMA, myofibroblasts, green), peripherin (neurons, red) and DAPI (blue). **(A)** A multipotent colony displays staining for all three cell lineage markers within a single colony (100X magnification). **(B)** Higher magnification (200X) images of cell types are shown from the regions indicated by the stipple boxes in **A**. **(C, D)** Restricted colonies display only a subset of cell-type markers within a single colony (neural/glial and neuronal/myofibroblast, respectively) (100X magnification).

Table 2.2. Effect of strain background and Sox10^{Dom} mutation on developmental potential.

Percentages of colony types (N = neuronal, G = glial, M = myofibroblasts) relative to total number of colonies per well. Values shown are average \pm S.D. (n \geq 10). B6.Sox10^{Dom/+} and C3Fe.Sox10^{+/+} were compared to B6.Sox10^{+/+} [\square Significant (p<0.05), \blacksquare Very Significant (p<0.01), *Highly Significant (p<0.001)]. C3Fe.Sox10^{Dom/+} was compared to C3Fe.Sox10^{+/+} [\bullet Very Significant (p<0.01), \dagger Highly Significant (p<0.001)].

Genotype	Total Colonies	Percentage of Cell Type						
		N	N+G	G	N+M	M	G+M	N+G+M
B6.Sox10 ^{+/+}	25.3 \pm 7.2	2.4 \pm 6.0	10.2 \pm 10.0	0.8 \pm 1.5	10.8 \pm 4.6	8.8 \pm 7.2	3.3 \pm 6.4	63.7 \pm 12.9
B6.Sox10 ^{Dom/+}	23.9 \pm 5.8*	5.3 \pm 5.4*	9.2 \pm 7.3	0.3 \pm 1.0*	18.3 \pm 12.4	8.1 \pm 5.7 \blacksquare	0.7 \pm 1.6*	58.2 \pm 14.2
C3Fe.Sox10 ^{+/+}	24.1 \pm 3.1 \square	10.5 \pm 7.3*	9.0 \pm 7.8	0.0 \pm 0.0*	24.8 \pm 10.7*	6.6 \pm 5.9 \blacksquare	0.7 \pm 1.7*	48.4 \pm 11.4 \square
C3Fe.Sox10 ^{Dom/+}	33.7 \pm 13.9	14.3 \pm 7.4	6.9 \pm 6.4 \bullet	0.0 \pm 0.0	25.2 \pm 11.9	6.4 \pm 5.1	1.1 \pm 1.8 \dagger	40.9 \pm 15.3

B6.*Sox10*^{+/+} ENPs produced significantly fewer neuronal derivatives, with 2.4% neuronal and 10.8% neuronal + myofibroblast colonies, compared with 10.5% neuronal and 24.8% neuronal + myofibroblast colonies from C3Fe.*Sox10*^{+/+} ENPs. The frequencies of multipotent colonies, which comprised the largest proportion of total colonies in all cases, were also significantly different. The highest percentage of multipotent (N+G+M) colonies was observed in B6.*Sox10*^{+/+} cultures (63.7%), compared with 48.4% in C3Fe.*Sox10*^{+/+} cultures. These results indicate that, even under “wild-type” conditions, genetic background can substantially shift the developmental potential of ENPs in wild-type embryos.

The presence of the *Sox10*^{Dom} mutation changed the developmental potential of ENPs and altered the ratios of colony types that were formed *in vitro*. This effect is more pronounced in progenitors isolated from B6.*Sox10*^{Dom/+} embryos. Four different categories of colony types were significantly shifted away from wild-type proportions in the B6 background: neuronal (5.3% Dom vs. 2.4% wild-type), glial (0.3% Dom vs. 0.8% wild-type), myofibroblast (8.1% Dom vs. 8.8% wild-type), and glial + myofibroblast (0.7% Dom vs. 3.3% wild-type). (Table 2.2) In contrast, only two classes of colonies from C3Fe.*Sox10*^{Dom/+} ENPs were significantly shifted away from proportions produced by wild-type embryos: neuronal + glial (6.9% Dom vs. 9% wild-type) and glial + myofibroblast (1.1% Dom vs. 0.7% wild-type). These results indicate that the *Sox10*^{Dom} allele alters developmental potential of ENPs at the time that these cells are migrating within

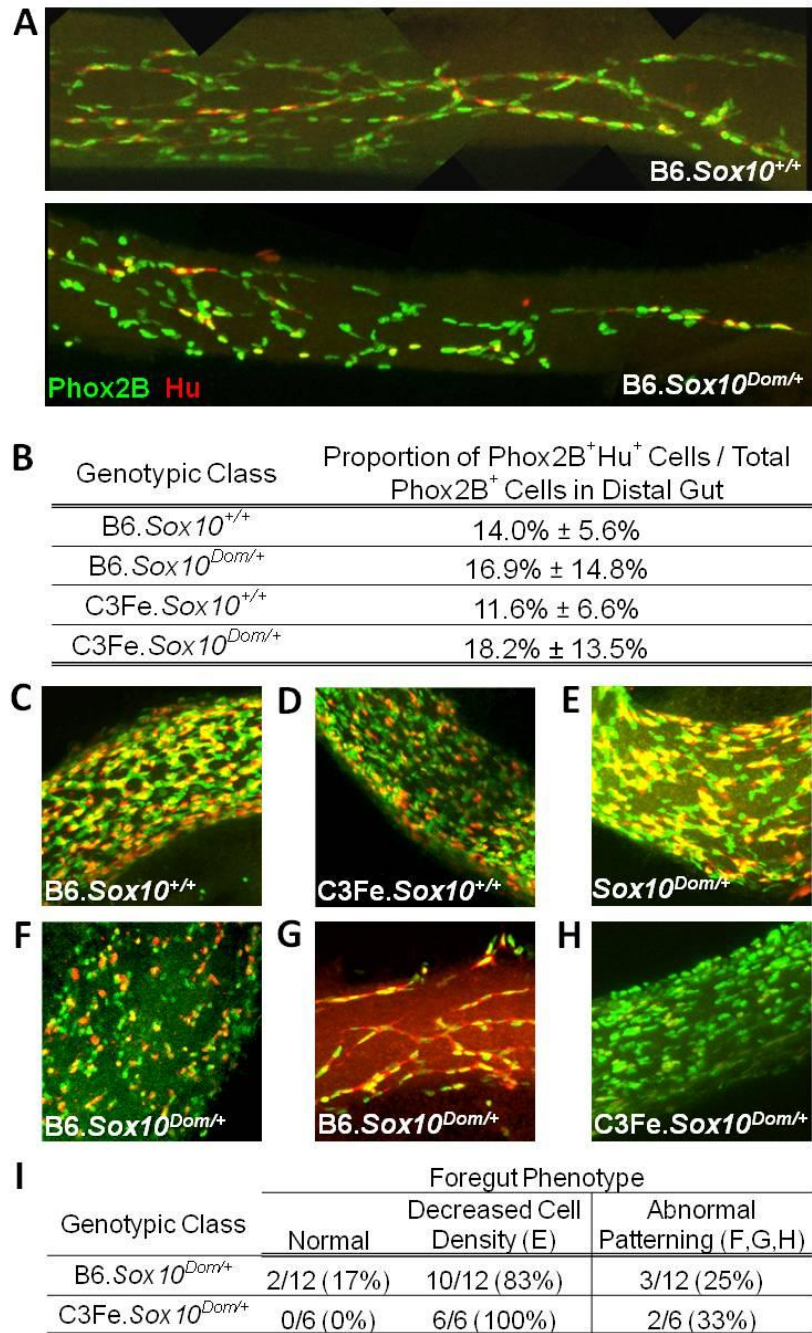
the gut. The greater number of colony classes shifted in the B6 strain reveals that developmental potential is a process impacted by genetic background.

Effect of the Sox10^{Dom} mutation and strain background on in vivo neurogenesis in the developing fetal gut.

The analysis of lineage potential *in vitro* demonstrated that the Sox10^{Dom} allele has a marked impact on the proportions of cell types that derive from ENPs. In particular, greater numbers of neuronal-restricted progenitors occur in Sox10^{Dom/+} mutants, particularly those on the B6 genetic background. Previous studies have shown that the presence of immature neurons is increased in Sox10^{LacZ/+} mutants at 15.5dpc, but this analysis did not take genetic background into account (18). An increase in neurons at this early developmental stage would have a patent affect on the functional ability of the fully-formed ENS.

To determine if the proportion of neurons in the developing fetal gut was altered in Sox10^{Dom/+} mutants *in vivo*, I used immunohistochemical detection of Phox2B, a known marker of all early ENPs (19), and Hu, an early marker of differentiating neurons (44) in fetal gastrointestinal tracts from 13.5dpc Sox10^{Dom/+} and Sox10^{+/+} embryos. The most distal 700um of the ENP-populated gut was identified, and the ratio of Phox2B⁺Hu⁺ cells to total Phox2B⁺ cells was calculated to determine the proportion of neurons in the developing fetal gut (Figure 2.7A).

Figure 2.7. *In vivo* neurogenesis in *Sox10^{Dom}* embryos.



(A) Gastrointestinal tracts from 13.5dpc *Sox10*^{+/+} and *Sox10*^{Dom/+} embryos were immunostained for Phox2B (green) and Hu (red) to visualize developing neurons at the distal wavefront of migration (400X magnification). (B) The proportion of double-positive (Phox2B⁺Hu⁺ / Phox2B⁺) cells was determined in the most distal 700um portion of the gut. The foregut region in these samples was also examined for cell staining and distribution (400X magnification). *Sox10*^{+/+} guts from the B6 (C) and C3Fe (D) backgrounds display normal dense population of the foregut. *Sox10*^{Dom/+} guts presented with decreased ENP density alone (E) or decreased density accompanied by abnormal patterning (F,G,H). (I) The phenotype of foregut ENP staining was characterized in *Sox10*^{Dom/+} guts.

Consistent with the *in vitro* analyses, the proportion of Phox2B⁺Hu⁺ neurons was highest in the C3Fe.Sox10^{Dom/+} fetal gut. This percentage was approximately 1.6-fold higher than that found in C3Fe.Sox10^{+/+} gastrointestinal tracts (18.2% vs. 11.6%), similar to the *in vitro* results (Figure 2.7B). Although the analyses of developmental potential were highly significant *in vitro* between wild-type and B6.Sox10^{Dom/+} mutants, the proportion of neurons was more similar between the B6.Sox10^{+/+} and B6.Sox10^{Dom/+} fetal gut samples *in vivo* at this stage of development (14.0% and 16.9%, respectively; approximately 1.2-fold difference). None of the ratios of Phox2B⁺Hu⁺/Phox2B⁺ cells, either between mutants and wild-type littermates or between strains, proved statistically significant. The lack of significant differences could be due to the highly variable nature of the ENP defects combined with the relatively small number of animals examined in this study (six to twelve in each class). Alternatively, significant differences may not have been seen due to the short time-frame between harvest of p75⁺/HNK-1⁺ ENPs at 12.5dpc for analysis of developmental potential and the double-label immunohistochemistry for Phox2B⁺/Hu⁺ ENPs at 13.5dpc. The 24-hour developmental window *in vivo* may not have been a sufficient time period for differentiation, whereas the *in vitro* cultures for analysis of lineage divergence are scored for cell types after two weeks. Interestingly, the variation was greater in the Sox10^{Dom/+} embryos, mirroring the wide spread of aganglionic severity seen in postnatal animals.

I postulated that the increase in neurons documented in B6.Sox10^{Dom/+} ENP colonies might be more visible in the foregut, which is completely populated

at 13.5dpc and further along in the differentiation process. In wild-type fetal gut from both the B6 and C3Fe strains, the density of cells in the proximal region was so great that quantification was not practical (Figure 2.7C, D). In contrast, the majority of gastrointestinal tracts from *Sox10^{Dom/+}* embryos from both strains had decreased numbers of progenitor cells in the foregut (Figure 2.7E, I). Moreover, a subset of B6.*Sox10^{Dom/+}* and C3Fe.*Sox10^{Dom/+}* gastrointestinal tracts also exhibited abnormal patterning of the ganglion network. (Figure 2.7F-I) The patterning defects in the proximal foregut were not correlated with an increase in the proportion of neurons found in the distal gut; samples that had the greatest proportions of Phox2B+Hu+ ENPs at the migratory wavefront did not exhibit more apparent abnormalities in the proximal fetal gut. No defects of patterning in the fetal foregut were detected in any of the wild-type samples of either strain.

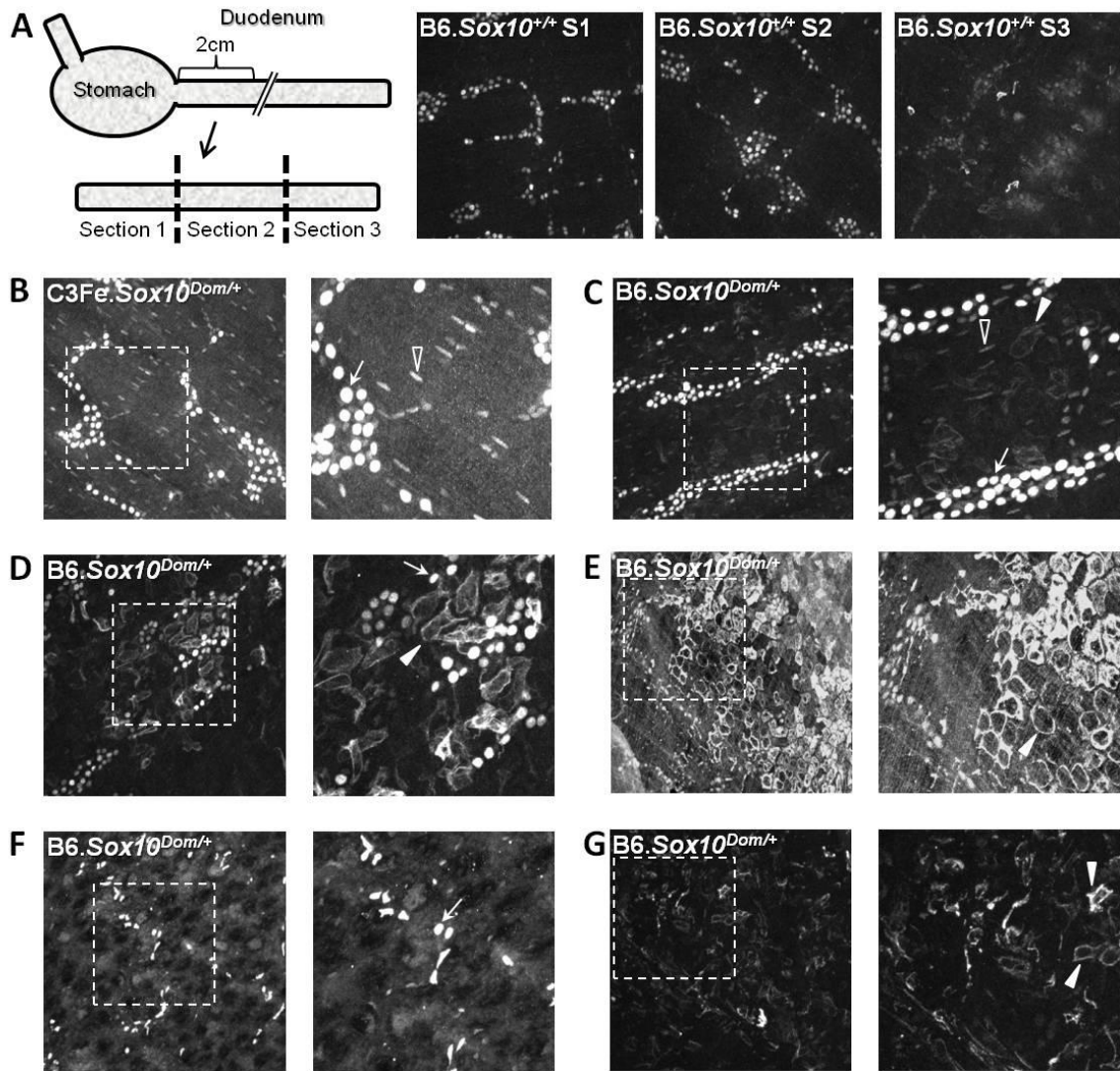
Effect of the Sox10^{Dom} mutation and strain background on postnatal ganglion patterning.

The abnormal cell density, distribution, and differentiation seen in 13.5dpc *Sox10^{Dom/+}* foreguts and the possibility that deficient migration in the hindgut might lead to an overabundance of ganglia in the foregut led me to investigate patterning of proximal foregut ganglion in postnatal *Sox10^{Dom/+}* mutants. Previous studies of the *Sox10^{Dom}* allele have utilized acetylcholinesterase staining to visualize the ganglion network (5). However, this method only labels cholinergic neurons and does not visualize all neurons or ancillary support cells. Examination of the enteric plexi separate from the gut mucosa as gut muscle strips (GMS) allows better visualization of the ganglion network of the small

intestine. Abnormal patterning of myenteric plexi in the proximal small intestine would be consistent with the concept that deficiencies in lineage divergence contribute to abnormalities of enteric ganglia development.

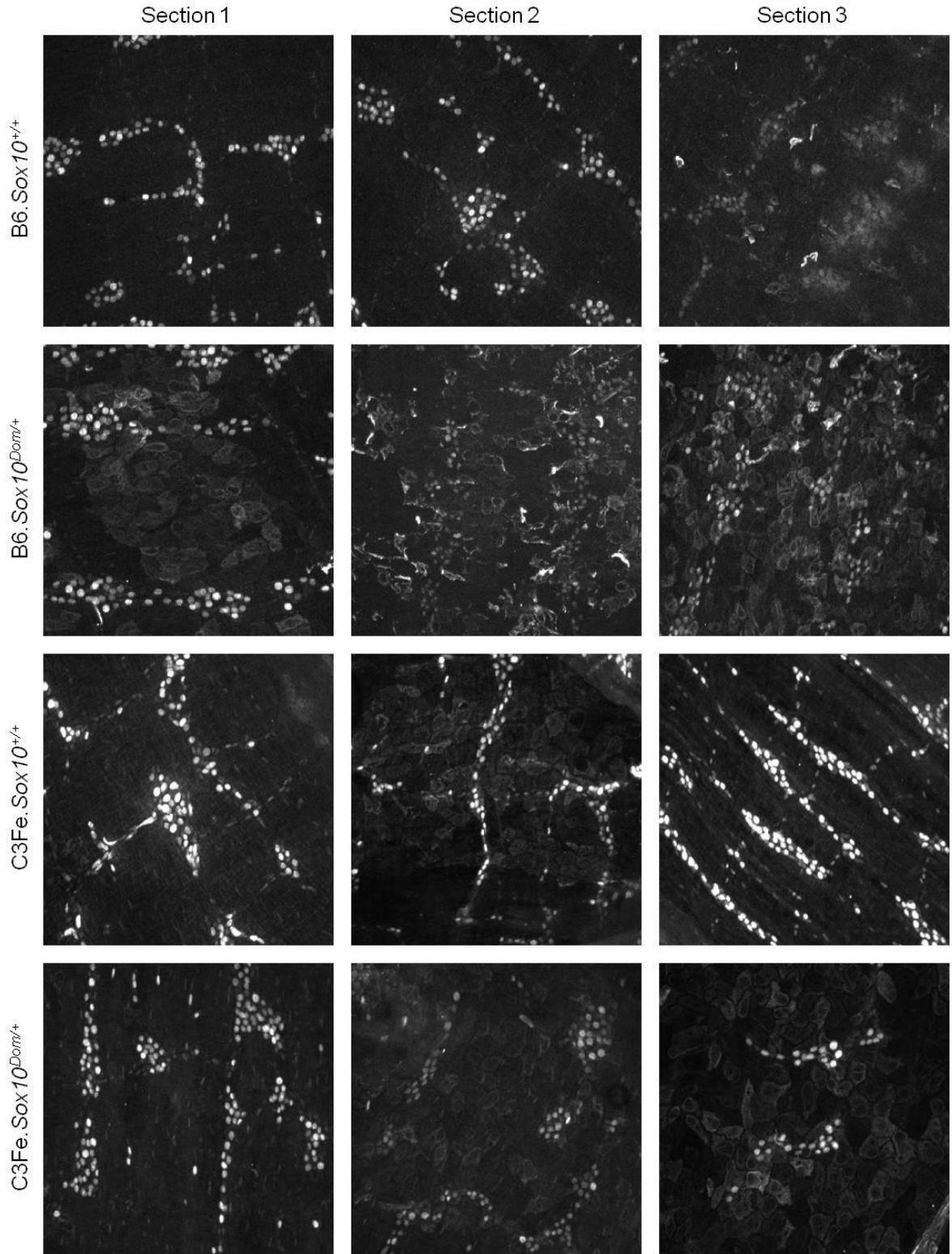
To examine the density and patterning of enteric ganglia in the proximal small intestine, GMS consisting of both the outer longitudinal and inner circular muscle layers were peeled away as an intact sheet from the proximal foregut of both postnatal (P15-P17) *Sox10^{Dom/+}* animals and wild-type littermates immediately below the gastric sphincter. These strips were divided into three sections to facilitate immunostaining with Phox2B antibody and imaged to view enteric ganglia (Figure 2.8A). GMS from wild-type, *Sox10^{+/+}*, animals exhibited large, round, brightly-Phox2B⁺ nuclei of neuronal cells forming chain-like networks interspersed with smaller, spindle-shaped, faintly-Phox2B⁺ enteric glia (Figure 2.8A). Images from adjoining sections of representative animals from each strain and genotype class are provided in Figure 2.9. Regions exhibiting normal latticework ganglion patterns were also present in *Sox10^{Dom/+}* animals, and I did not identify any areas with increased density of enteric ganglia in the mutants (Figure 2.8A-C). However, I did observe *decreased* density of enteric ganglia in the *Sox10^{Dom/+}* mutants. In addition, Phox2B-staining identified large cells exhibiting cytoplasmic Phox2B immunoreactivity and myofibroblast-like morphology within and around the enteric ganglia. These myofibroblast-like cells were present in all GMS of all genotypes, even the wild-types (Figure 2.9).

Figure 2.8. Ganglion patterning in *Sox10^{Dom}* mutants.



(A) Gut muscle layers were stripped intact from proximal foreguts, divided into three sections, and immunostained for Phox2B. *Sox10^{+/+}* ganglia present as chain-like arrangements of neurons with interspersed glia in all sections (200X magnification). (B) Similar ganglia can be found in *Sox10^{Dom/+}* gut muscle strips (200X magnification, 400X magnification designated by stippled outline; neurons identified by arrow, glia identified by open arrowhead). Myofibroblast-like cells (identified by closed arrowhead) labeled by Phox2B cytoplasmic staining were also visible in both wild-type and mutant GMS (C). The presence of myofibroblast-like cells is increased in *B6.Sox10^{Dom/+}* animals, normally in conjunction with neurons at the expense of glia (D, E). Severely affected *B6.Sox10^{Dom/+}* animals have additional patterning defects including abnormal morphology of neurons (F) and the presence of only myofibroblast-like cells (G).

Figure 2.9. Gut muscle strip sections.



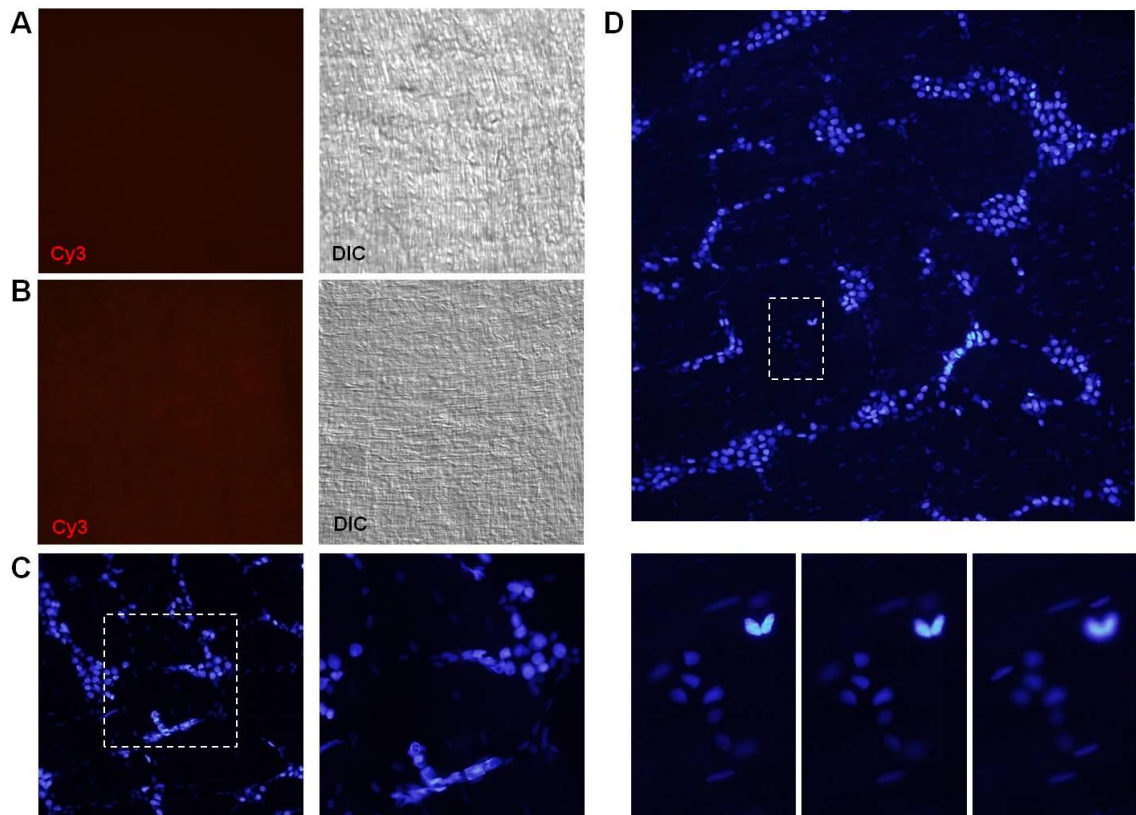
Consecutive gut muscle strip sections from individual animals immunostained for Phox2B are shown at 200X magnification. Phox2B⁺ myofibroblast-like cells can be seen in all strain and genotype classes.

These cells were present in larger areas of the GMS in *Sox10^{Dom/+}* mutants and at a higher frequency within those areas. These cytoplasmic Phox2B bright cells were seen in every genotype, although there was some variability in the intensity of Phox2B staining even when nearby neurons exhibited bright Phox2B nuclear stain. These cells were more prevalent in the distal-most region examined (Section 3, Figure 2.8 and Figure 2.9).

Abnormalities of ganglia composition were most evident in the B6.*Sox10^{Dom/+}* mutants where neurons were sparser with increased numbers of the myofibroblast-like cells as compared to C3Fe.*Sox10^{Dom/+}* mutants. While a greater proportion of the GMS area appeared normal in C3Fe.*Sox10^{Dom/+}* mutants (Figure 2.8B and data not shown), I did observe the myofibroblast-like cells in GMS of C3Fe.*Sox10^{Dom/+}* animals, but these were fewer in number and closer to the ganglia. In contrast, several types of deviant patterning were seen in B6.*Sox10^{Dom/+}* GMS. In B6.*Sox10^{Dom/+}* samples, large areas of the GMS lacked normal enteric ganglia and instead contained large numbers of cytoplasmic-Phox2B⁺ myofibroblast-like cells (Figure 2.8D). GMS from B6.*Sox10^{Dom/+}* animals with severe megacolon also displayed regional increases in myofibroblast-like cells at the expense of glia (Figure 2.8D, E), abnormal neuronal morphology (Figure 2.8F), and the presence of only myofibroblast-like cells (Figure 2.8G). These *in vivo* findings support and extend the *in vitro* analyses of developmental potential that showed that both the *Sox10^{Dom/+}* mutation and strain background impact lineage divergence.

The presence of myofibroblast-like cells in proximity to enteric ganglia that were immunoreactive for cytoplasmic Phox2B was unexpected. The Phox2B immunoreagent has been used extensively for studies of fetal ENP migration (19,45-47), and our group has previously described Phox2B expression in the distal foregut of adult wild-type mice (36). However, I reconfirmed the specificity of the antibody in control sections with no primary antibody and no secondary antibody (Figure 2.10). I only observed these myofibroblast-like cells in the Cy3 channel when both Phox2B primary antibody and donkey anti-rabbit Cy3 secondary antibody were applied to GMS. Thus, I have excluded the possibility that these myofibroblast-like cells are an unusual auto-fluorescent population. In addition, I examined GMS from the identical region of the foregut in P15 B6C3F1.Tg^{Phox2B-H2BCFP} animals that we have previously shown to recapitulate Phox2B expression (36). Analysis of Tg^{Phox2B-H2BCFP} GMS identified cells with large faintly H2B-CFP⁺ nuclei at a distance from normal ganglia in multiple areas of GMS (Figure 2.10). These results indicate that a previously unrecognized Phox2B⁺ cell type of unusual morphology is present in close proximity to postnatal enteric ganglia in the proximal foregut.

Figure 2.10. Controls for postnatal gut muscle strip analysis.



P16 C3Fe.*Sox10*^{+/+} gut muscles strips were used for immunohistochemistry controls: **(A)** Rabbit anti-Phox2B primary antibody only (200X magnification) and **(B)** Donkey anti-Rabbit Cy3 secondary antibody only (200X magnification). **(C)** Gut muscle strips from P15 C3Fe-Tg^{Phox2B-H2BCFP} mice (200X magnification, 400X magnification region designated by stippled outline). **(D)** Different focal places highlight variant cell morphology (200X magnification, 400X magnification designated by stippled outline).

Discussion

The mechanisms responsible for variation of aganglionosis between HSCR patients are unknown. The Southard-Smith lab has previously reported that genetic background contributes to differences in postnatal aganglionosis (5). To identify developmental processes that underlie aganglionosis differences between inbred strains, I utilized two congenic lines of *Sox10^{Dom}* mice that model multiple aspects of HSCR. The effects of the *Sox10^{Dom}* mutation and genetic background on migration, proliferation, and developmental potential were investigated. I found that genetic background had an effect on ENP migration in the presence of the *Sox10^{Dom}* mutation. The *Sox10^{Dom}* mutation also caused a decrease in the frequency of ENPs, regardless of strain background. This analysis further identified a previously unrecognized effect of the *Sox10^{Dom}* mutation on developmental potential, the balance of lineages normally generated by ENPs. Genetic background exacerbated the shift in developmental potential produced by the *Sox10^{Dom}* mutation. Moreover, I found that genetic background alone alters the proportions of cell types that derive from ENPs in wild-type animals, independent of *Sox10^{Dom}* genotype. *In vivo* analysis of enteric neural patterning in fetal and postnatal proximal intestine revealed that deficiency of Sox10 disrupts ENPs and enteric ganglia, respectively. Thus, this analysis has identified a novel pathological mechanism that likely contributes to abnormalities of enteric ganglia and may explain some of the variation in aganglionosis and post-surgical outcomes between HSCR patients.

Delayed migration of ENPs down the intestine is a consistent feature present in multiple HSCR mouse models, including *Sox10^{Dom}* (1,48), *EdnrB^{sl}* (10), and *Edn3^{sl}* (12,14). Kapur et al. 1996 (1) detailed the lack of complete bowel colonization in *Sox10^{Dom/+}* mutants utilizing the DBH-LacZ transgenic allele, assaying both fetal and postnatal time-points. However, this study used mice on a mixed B6-C3Fe background and was not able to assess the impact of genetic background on migration (1). I observed a marked difference in numbers and extent of migration of ENPs in *Sox10^{Dom/+}* embryos on two different strain backgrounds. B6.*Sox10^{Dom/+}* embryos had a more pronounced deficit than those on the C3Fe background. Thus, fetal ENP migration correlates closely with the significant differences in aganglionosis seen postnatally in these two congenic strains. Wild-type embryos were comparable between the two strains; therefore, strain background alone had no effect on ENP migration. It is only in the presence of the *Sox10^{Dom}* mutation that genetic modifiers in the B6 genetic background exert an effect on ENP migration; these are likely one or more of the *Sox10^{Dom}* modifier loci that have previously been mapped between these strains (9).

Multiple theories could be posited for the defect in migration seen in *Sox10^{Dom/+}* guts. The lack of complete population could be attributed to cell death in the progenitor population. While apoptosis has been demonstrated in early migrating NC derivatives just outside the neural tube in *Sox10^{Dom}* mutants (49), efforts investigating cell death within the intestinal wall of *Sox10^{Dom/+}* mutants have definitively shown no increase in apoptosis as compared to wild-

type littermates (18). Another possibility is a “blockade” against migration that holds progenitors in the foregut and prevents further progression down the developing gut. However, I did not observe increased density of progenitors in the foregut of *Sox10^{Dom/+}* mutants, regardless of age (12.5dpc, Figure 2.1; 13.5dpc, Figure 2.7E-H; P15-17, Figure 2.8B-G).

Current models of ENS development posit that ENPs at the migratory wave-front possess an increased capacity for proliferation and drive the extension of the cell population down the gut (50). However, these results show equal rates of proliferation across different regions of the gut. Previous work by Okamura and Saga (51) suggested that wild-type ENPs in the stomach and intestine had equal proliferative capacity. Young et al. (52) assayed proliferation in BALB/c embryonic guts and also detected no regional differences in proliferation in a wild-type situation. These studies examined multiple regions throughout the fetal intestine including the foregut and found no regional or strain-specific difference in ENP proliferation in wild-type animals, nor did they detect any significant differences in ENP proliferative capacity between *Sox10^{+/+}* and *Sox10^{Dom/+}* embryos at 12.5dpc. Other HSCR mouse models have similarly documented a defect in migration without any deficits in proliferation of ENPs (53). Even when I specifically assayed proliferation of wave-front ENPs in the distal hindgut, no effect of the *Sox10^{Dom}* allele on proliferation was detected. While proliferation is obviously essential to ENS ontogeny and may contribute to HSCR pathophysiology in some cases (21,51,54), it did not differ between

Sox10^{Dom} mutant and wild-type embryos and thus does not contribute to the etiology of aganglionosis in this particular HSCR model.

The ability to isolate viable ENPs for further study is vital to truly understanding the processes involved in ENS ontogeny. Surface p75 expression has been used routinely for enrichment of ENPs in mouse and rat (38-40). HNK-1, a marker of migrating NC, has also been used to this end in chick and rat (55-59). Isolation of pure enteric NCSC in the rat has been achieved by dual-labeling of p75 with other markers including P0 and α 4-integrin (2,3,11,33,34). This process has been hindered in the mouse due to a perceived lack of cell surface markers that could be utilized for flow cytometry. Use of HNK-1 immunoreactivity to capture mouse enteric NCSC has not been attempted because sectional analysis on fixed tissue was not successful (25). To eliminate any complications due to fixation or the physical size of the HNK-1 IgM monoclonal, I sought to immunostain freshly dissociated cells, thus circumventing problems of permeability. Using this methodology, I demonstrated that murine ENPs do in fact express HNK-1, thus allowing isolation by flow cytometric methods used in other species. Moreover, I demonstrated that double-labeling of mouse ENPs with p75 and HNK-1 identifies a population of highly enriched enteric stem cells. To conclusively demonstrate the progenitor characteristics of p75⁺/HNK-1⁺ enteric cells, I confirmed that these cells could form neurospheres, were able to self-renew, and expressed NC markers. Ready growth of primary and secondary neurospheres from cells isolated by p75/HNK-1 staining confirms that this cell population is made up of progenitors. Moreover, the significant enrichment of

cells expressing NC markers isolated by flow cytometry for p75/HNK-1 staining, especially compared to populations isolated using a single marker, indicates that this cell population contains specifically NC-derived progenitors. These qualities demonstrate the purity and utility of the p75⁺/HNK-1⁺ population for subsequent studies of enteric development.

Several studies have examined the frequency of enteric NC-derived progenitors in murine HSCR models. Decreased numbers of ENPs, ranging up to 60% of the total progenitor population, have been described in NC mutants (11,18,51). Our flow cytometric studies similarly identified a 65% reduction, on average, in numbers of p75⁺/HNK-1⁺ cells in *Sox10^{Dom/+}* fetal gut. This decrease in progenitors was not influenced by genetic background as the reduction in ENPs did not differ between B6 and C3Fe strains. Despite the reduction in frequency of p75⁺/HNK-1⁺ cells in *Sox10^{Dom/+}* mutants, I did not see any difference in the proportion of multipotent colonies between *Sox10^{Dom/+}* and *Sox10^{+/+}* ENPs. The proportions of multipotent colonies were also maintained in *EdnrB^{Sl}* mutant progenitors (11). Thus, while there is a substantial reduction in the number of p75⁺/HNK-1⁺ cells in *Sox10^{Dom/+}* mutant guts, the proportion of total progenitors that are multipotent remains the same. This raises an interesting question: what happens to the rest of the progenitor population *in vivo*? An obvious explanation for the decrease in p75⁺/HNK-1⁺ progenitors and the final fates of the missing progenitors in *Sox10^{Dom}* mutants is not apparent. Future studies using Cre-driven lineage tracing methods are needed to determine the fate of these cells in the gut.

Lineage divergence as a pathological mechanism has not been previously investigated in HSCR models. The majority of studies investigating ENS defects have focused strictly on hindgut aganglionosis and evaluated cell survival (60,61), or migration and proliferation, as detailed above. Those that have looked at lineage segregation have focused on strictly neuronal cell fates (51,62). The concurrent study of multiple lineages provides a complete picture of the cell fate capacity exhibited by ENPs. These *in vitro* studies of developmental potential demonstrate that the responsiveness of the p75⁺/HNK-1⁺ populations differs between strains and genotypes and, as a result, their ability to give rise to various lineages within the culture environment must also differ. Moreover, my *in vivo* analysis of enteric neurogenesis and postnatal ganglia are consistent with my *in vitro* developmental potential studies.

The analysis of early phases of lineage segregation revealed marked differences in developmental potential, the proportions of differentiated lineages that arose in culture, between wild-type and *Sox10*^{Dom/+} ENPs. Specifically, B6.*Sox10*^{Dom/+} ENPs increase the proportion of N-only colonies at the expense of other cell types. Paratore et al. 2001 (63) observed an analogous increase in neuronal derivatives within dorsal root ganglia cultures from *Sox10*^{LacZ/+} mutants and noted an increase in neuronal precursors in midgut sections from *Sox10*^{LacZ/+} embryos (18). My *in vivo* analysis of neurogenesis, performed earlier in development, identifies the onset of differential neuronal development between wild-type and *Sox10*^{Dom/+} ENPs. The consistency between these findings and

Paratore et al. (18,63) strengthen the concept that differences in lineage potential detected *in vitro* reflect differences of lineage segregation *in vivo*.

An increase in neurons *in vivo* could account for the decrease in cell density and migration seen in *Sox10^{Dom}* embryos by whole-mount. Premature differentiation of neurons could contribute to a decrease in migration (64,65). Studies by Hao et al. (64) demonstrated that immature TH⁺ neurons migrate at approximately 30-40% of the speed at which ENPs migrate. Wu et al. (65) also concluded that differentiating neurons have impaired migration in their studies of the effect of endothelin 3 on ENPs. The absence of proliferation among differentiated neurons (66) further limits the ability of ENPs to completely populate the intestine because a minimum density of enteric cells is required to provide the necessary cues for chain-based migration (50,67,68). Thus, the decreased rate of migration and lack of proliferation in committed neuroblasts may both contribute to aganglionosis. It is possible that the *Sox10^{Dom}* allele has a distinct effect on migration alone, separate from the migration defect caused by the primary effect on lineage divergence. However, it is not possible to uncouple these effects at this time. A recently reported conditional allele of *Sox10* will likely facilitate such studies in the future (69).

Most notably, these studies demonstrate a distinct and novel effect of genetic background on developmental potential independent of any mutation. I observed highly significant differences in enteric lineages produced by wild-type ENPs of the B6 and C3Fe strains, specifically an increase in neuronal lineages in the C3Fe strain. Because wild-type B6 and C3Fe mice have functional enteric

nervous systems, the differences in developmental capacity and responsiveness between these two strains were unexpected. These studies suggest that the ENS, similar to other biological systems, has a certain degree of plasticity in its composition. While neurons and glia must be present in the ganglia that comprise the ENS, the relative proportions of the two cell types appear to be flexible, at least at this developmental stage. It is only in the presence of a disease-causing mutation, like the *Sox10^{Dom}* allele, that these inherent differences modulate the threshold at which disease pathogenesis occurs. The fact that fewer lineage shifts occur in C3Fe.*Sox10^{Dom}* ENPs demonstrates that this genetic background provides a greater buffer to absorb disruptions in lineage divergence caused by mutations. This effect is consistent with the protective effect of the C3Fe genetic background (5). The molecular mechanisms behind this substantial difference in lineage segregation have not yet been identified. This overall effect of genetic background is most likely the cumulative result of multiple genes that participate in enteric NC development, as suggested by the identification of multiple aganglionosis modifiers between the B6 and C3Fe inbred strains (9).

In vivo imaging of neurogenesis based on detection of Phox2B⁺/Hu⁺ ENPs identified abnormal patterning in the proximal foregut of *Sox10^{Dom/+}* fetal intestine. This atypical patterning ranged from depletion of neuroblasts, seen in C3Fe.*Sox10^{Dom/+}* samples, to reduced ENP numbers and aberrant distributions in the gut wall including both punctate, disconnected cell bodies to sparse, chain-like ganglion arrangements in B6.*Sox10^{Dom/+}* mutants. The reduction of

progenitor cells in the proximal fetal gut of both strains demonstrates that the *Sox10^{Dom}* allele does not simply delay migration in a manner that causes accumulation of ENPs in the small intestine. Rather, these findings implicate the process of lineage divergence, both at the wavefront of migration and in patterning the distribution of ENPs in the proximal foregut.

I extended my *in vivo* analysis to examine the distribution of enteric ganglia in the proximal small intestine of postnatal *Sox10^{Dom/+}* mutants. I did not observe any increase in density of enteric ganglia in the mutants as compared to wild-type littermates. However, I did observe *decreased* density of enteric ganglia, as well as aberrant ganglia composition in the *Sox10^{Dom/+}* heterozygotes. The Southard-Smith lab has previously reported reduced density and altered patterning of enteric ganglia in the proximal foregut of *EdnrB* mutants based on acetylcholinesterase staining (5). My identification of altered patterning in proximal gut regions of *Sox10^{Dom/+}* mutants suggests that deficiencies of enteric ganglia in regions other than the distal aganglionic segment may be more prevalent than has previously been recognized.

The identification of large cells exhibiting myofibroblast-like morphology and weak cytoplasmic Phox2B immunoreactivity in the vicinity of postnatal enteric ganglia at low frequency in wild-type mice and higher frequencies in *Sox10^{Dom/+}* mutants prompted us to review the literature searching for any prior evidence of additional NC-derived cell types in the gut wall. Early work in fate-mapping contributions of different NC axial levels to the gut (70) only examined embryonic stages, used species-specific marking to track quail cells (Felgen

staining) and monitored only neural lineages based on the presence of ganglion cells (silver staining). Later studies that did incorporate immunohistochemical markers for analysis of lineage focused on neuronal (ANNA-1, now known as Hu) and glial (GFAP) cell types and examined the distribution of quail NC at embryonic stages to track migration pathways (71,72). Many subsequent studies in the analysis of enteric NC derivatives have simply not included additional lineage markers that might have been used to identify other cell types in or around the enteric ganglia. My results identify the presence of a previously unrecognized cell type near enteric ganglia that expresses cytoplasmic Phox2B and exhibits distinct myofibroblast-like morphology. Work investigating the timing of neuron birth dates in the ENS has shown that some NC-derived neurons in the gut withdraw from the cell-cycle in early postnatal development (P3-P14) (73); lineage diversification in the ENS is clearly ongoing even during postnatal development. Surprisingly, comprehensive lineage-mapping studies examining postnatal enteric NC-derived cell types with modern molecular tools like Wnt1-Cre have not yet been performed in the mouse. Thus, given that the vast majority of enteric neural development has focused on neural lineages, few if any markers of other lineages, including myofibroblast cell types, have been examined. In addition, fate-mapping studies in the postnatal mouse gut remain to be performed; thus, it is possible that additional NC-derived cell types reside within or near enteric ganglia in the intestine. An example of the recent discovery of previously unrecognized NC-derived cell types includes endoneurial fibroblasts that were identified as a novel NC derivative in peripheral nerve fibers (74).

Similar studies using Cre-mediated fate-mapping and multiple lineage markers are needed in the postnatal murine intestine.

My findings provide novel insight into the pathophysiology of aganglionosis in a mouse model that is likely relevant to enteric deficits in HSCR patients. I hypothesize that mutations which cause absence of enteric ganglia in the hindgut concurrently generate mispatterned and thus potentially dysfunctional enteric ganglia throughout the gastrointestinal tract. While the majority of patients have successful removal of the aganglionic region by rectal pull-through, 30-40% of patients post-resection continue to experience a spectrum of GI disturbances, including chronic constipation, enterocolitis, and dysmotility (75,76). These complications suggest abnormalities that impact initial development of ENPs may also affect function of enteric ganglia that are formed in more proximal gut regions. My studies in congenic mouse strains reveal that a large amount of natural variation exists in the population of ENPs that will eventually form the ganglia of the ENS. I hypothesize that these different progenitors may be able to give rise to functional ganglia in stress-free environment, but the addition of a disease-causing mutation renders them less able to generate a normal repertoire. The level at which they are still able to function obviously covers a wide spectrum, hence the variation in post-operative outcomes. These findings suggest that new methods to examine the functionality of residual proximal enteric ganglia are needed to improve patient outcomes after surgery.

In conclusion, I have shown that genetic background plays a key role in determining the final impact of disease-causing mutations, such as *Sox10^{Dom}*. The *Sox10^{Dom}* allele itself impacts migration, frequency, and developmental potential of the ENPs that go on to form the ENS. However, only migration and developmental potential are substantially modulated by genetic background. I also documented significant natural variation in developmental potential between “wild-type” strains of mice that appears to account for differences in penetrance and severity of aganglionosis when disease-causing mutations are introduced. The disruption of lineage divergence is a novel pathogenic mechanism for the development of aganglionosis and may explain the differential outcomes of HSCR patients post-resection. Studies such as these that explore both disease-causing mutations and the contribution of genetic background are vital to understanding complex diseases such as HSCR.

Materials and Methods

Animals. All animal protocols were approved by the Institutional Animal Care and Use Committee at Vanderbilt University. B6.*Sox10^{Dom}* and C3Fe.*Sox10^{Dom}* congenic lines were established and maintained by backcrosses to C57BL/6J and C3HeB/FeJ stocks, respectively. Both strains have been bred onto their respective inbred strains for >40 generations.

Fetal mouse dissections. Timed matings of congenic *Sox10^{Dom}* males and wild-type females were set up to obtain staged mouse fetuses, designating the morning of plug formation as 0.5 days post coitus (dpc). Fetal gastrointestinal tracts (stomach to anus) were sub-dissected for analysis.

Genotyping. Genomic DNA was isolated from limb buds by incubation in tail digest buffer (10mM Tris pH8.0, 100mM NaCl, 10mM EDTA, 0.5% SDS) with proteinase K at 55°C overnight, followed by phenol-chloroform extraction, ethanol precipitation, and resuspension in TE pH7.5. Genotype at the *Sox10* locus was determined using PCR-based methodology with the following primers: dcgs10 Bh2MidFa, CGGATGCAGCACAAAAAGGACC; and dcgs10 Bh2MidRB, GGCCAGGTGGGCACTCTTGTA (49). PCR products were run on a non-denaturing polyacrylamide gel.

For rapid genotyping, limb buds were digested in Fast Lysis Buffer (0.45% Tween, 2.5mM MgCl₂, 0.1M KCl, 10mM Tris pH8.3) with proteinase K at 90°C for

12 minutes. Genotype at the *Sox10* locus was determined using Real-Time Quantitative PCR (ABI). In brief, each reaction composed of 1X TaqMan Fast Universal PCR Master Mix-No AmpErase UNG (ABI, 4352042), 1X TaqMan *Sox10*Del SNP Genotyping Assay Mix (ABI, Custom Assay), 10% 1M Betaine, and 20% fast-prepped DNA was run in triplicate on the Fast Amplification Protocol (95°C for 20 seconds; 95°C for 1 second then 60°C for 20 seconds, 40 cycles) on a 7900HT Fast Real-Time PCR System (ABI). The *Sox10*Del SNP Genotyping assay was designed with the following specifications: *Sox10*Del F Primer, TCGGCGGCGGAAGAAC; *Sox10*Del R Primer, GCAGCAGCCCCTCCTT; *Sox10*Del VIC (*Sox10*^{+/+}) Probe, TCGGCTTCCCCCGCC; and *Sox10*Del FAM (*Sox10*^{Dom/+}) Probe, CTCGGCTTCCCCCGCC.

Analysis of migration. 12.5dpc fetal guts were dissected, and guts were fixed for 1-2 hours in ice-cold Neutral Buffered Formalin (NBF; Sigma, HT501128) with 0.5% Triton X-100. After fixation, guts were washed twice for a minimum of 10 minutes per wash in ice-cold PBS with 0.1% Triton X-100. Guts were then placed in blocking solution composed of PBS with 0.1% Triton X-100, 1% Bovine Serum Albumin-Fraction V (BSA; Sigma, A-4503), and 5% Normal Donkey Serum (NDS; Jackson ImmunoResearch, 017-000-121) for one hour at room temperature.

All antibodies were diluted in blocking solution. Guts were incubated in polyclonal rabbit anti-mouse Phox2B antibody (77) (1:750) overnight at 4°C, then

washed three times for a minimum of five minutes per wash in PBS with 0.1% Triton X-100. Guts were incubated in donkey anti-rabbit Cy3-conjugated secondary antibody (Jackson ImmunoResearch, 711-165-152, 1:1000) for 1 hour at room temperature. Guts were washed for a minimum of ten minutes in PBS with Triton X-100, then washed twice for a minimum of ten minutes in PBS. Guts were transferred to fresh PBS and allowed to sit at 4°C overnight to fully wash out secondary antibody. Stained guts were flat-mounted in Aqua Poly/Mount (PolySciences, Inc, 18606) on glass slides and cover-slipped for imaging. Clear nail polish was used to seal the edges of the coverslip to prevent mounting media from drying out.

Confocal microscopy was performed on a Zeiss Scanning Microscope LSM510 with a rhodamine (Cy3, Texas Red) band-pass filter at 200X and 400X magnifications to visualize ENPs expressing endogenous Phox2B in fetal guts. The HeNe1 laser, at a wavelength of 543nm, was set to 40% power. The pinhole was set to 79, with an optical slice less than 2.4µm. For z-stacks, the optimal interval of 6.43µm was used. Tiled confocal images of whole-mount fetal guts were divided into eight equal sections encompassing the mid-small intestine, caecum, and hindgut, with the caecum designated as section four. The density of Phox2B⁺ cells was qualitatively scored on a whole-number four-point scale, with zero being a lack of Phox2B⁺ cells and four being numerous Phox2B⁺ cells, for each individual section. Scoring was completed in a strain- and genotype-blinded fashion (78). Scores for each individual section of the gut were averaged

across strain- and genotype-matched embryos, with seven to nine embryos from two separate litters per genotypic class.

Analysis of proliferation. Fibronectin (1mg vial, Biomedical Technologies, BT-225) was reconstituted the night before analysis using the following protocol: addition of 0.5mL Biowhittaker water (Fisher Scientific, BW17-742Q), incubation at 37°C, 5% CO₂ for 1 hour, addition of 5.5mL Dulbecco's Phosphate Buffered Saline (DPBS; Gibco, 14040-182), and incubation at 37°C, 5% CO₂ overnight. 24-well plastic tissue culture plates (Falcon, 353047) were prepared using the following protocol: coating with Poly-D-Lysine (PDL, 150ug/mL; Biomedical Technologies, BT-227), removal of PDL, drying of wells by air in the tissue culture hood, rinsing with Biowhittaker water, removal of Biowhittaker water, and drying of wells by air in the tissue culture hood. Opti-MEM medium (Gibco, 31985070) was added to the wells, and the plates were incubated at 37°C, 5% CO₂ to allow the medium to equilibrate. In addition, L15 solution was prepared by combining Leibovitz's L-15 medium with 1mg/mL BSA (Sigma, A-3912), 10mM HEPES pH7.4 (Fisher Scientific, BW17-737E), 1% penicillin/streptomycin (PS; Gibco, 15140-122), and 10% Biowhittaker water.

12.5dpc fetal guts were dissected and then partitioned into segments comprised of the foregut (mid-small intestine, approximately equal in size to caecal), caecal, and hindgut (entire) regions. Individual gut segments were transferred to polypropylene tubes (Falcon, 353063) containing 3mL of Hanks' Balanced Salt Solution without calcium or magnesium (HBSS; Gibco, 14185-

052). Tubes were spun softly (1100rpm for five minutes at 4°C) in a pre-chilled swinging-bucket rotor (Sorvall RTH-750) to pellet the gut sections. While tubes were spinning, dissociation solution comprised of 0.5mg/mL Dispase (Gibco, 17105-041) in HBSS was made. The supernatant was aspirated off of the pelleted gut sections until approximately 100uL remained. 0.5mL of dissociation solution was added to each gut section. Tubes were incubated in a 37°C water bath for 10 minutes, and tubes were banged against the side of the water bath during the last two minutes of incubation.

Tubes were immediately transferred to ice, and 1mL of quench solution (L15 solution with 37.5ug/mL DnaseI [Sigma, D-4527]) was added. The solution was triturated six times and passed through a 45 micron nylon mesh membrane (Sefar America, 3-38/22) into a clean polypropylene tube. The old tube was washed with 1mL of dilute quench solution (L15 solution with 7.5ug/mL DnaseI), which was also filtered into the new tube. Cells were pelleted as before. The supernatant was aspirated off until approximately 100uL remained. The cell pellet was resuspended in 1mL dilute quench solution by triturating five times. The cell solution was passed through a membrane as above into a clean polypropylene tube. The old tube was washed with 1mL dilute quench solution, which was also filtered into the new tube. The top was topped off with dilute quench solution, and cells were pelleted as before. The supernatant was aspirated off until approximately 200uL remained. The solution was triturated ten times, and 50uL of dissociated cells were plated (approximately ~1/4 gut segment) per well in the 24-well plates.

Plates were incubated at 37°C, 5% CO₂ for 1 hour to allow cells to adhere to the plate surface and then fixed on ice in NBF with 0.5% Triton X-100. Cells were washed twice in wash buffer (PBS with 0.1% Triton X-100 and 0.5% BSA). Blocking solution was added, and cells were incubated at room temperature for 25 minutes. All antibodies were diluted in blocking solution. Cells were incubated in polyclonal rabbit anti-mouse Sox10 (79) (1:100) at room temperature for two hours, then washed twice in wash buffer. Cells were incubated in monoclonal mouse anti-mouse Phospho-Histone H3 (pH3, Abcam, ab14955, 1:2000) at 4°C overnight, then washed three times in wash buffer. Cells were incubated in donkey anti-rabbit Cy3-conjugated secondary antibody (1:500) at room temperature for 30 minutes, then washed twice in wash buffer. Cells were incubated in donkey anti-mouse Cy2-conjugated secondary antibody (Jackson ImmunoResearch, 715-225-150, 1:500) at room temperature for 30 minutes, then washed in wash buffer. Cells were washed in DAPI solution (Invitrogen, D1306, 1:50,000) and washed in wash buffer. The wash buffer was replaced, and the plates were stored at 4°C overnight before imaging.

Cells were imaged and counted using a DMI6000B microscope (Leica). A total count of Sox10⁺ and Sox10⁺/pH3⁺ cell numbers in each well was determined for each gut region. The ratio of double-positive (Sox10⁺/pH3⁺) cells relative to the total of all Sox10⁺ cells was calculated to determine the proliferative frequency of ENPs in each gut region. Ratios were averaged across strain- and genotype-matched embryos, with six to ten embryos per class. Averages and standard deviations were compared by Welch's t test and are shown in Figure

2.2. Statistics were performed using the GraphPad QuickCalcs web interface (<http://www.graphpad.com/quickcalcs/index.cfm>).

Identification of HNK-1 immunoreactivity on mouse ENPs. Fibronectin was prepared the night before analysis as above. 24-well tissue culture plates were prepared as above. Self-renewal medium was made to the following specifications: 50% Dulbecco's Modified Eagle's Medium with low glucose (DMEM-low; Gibco, 11885-084), 30% Neurobasal (Gibco 12348-017), 50uM 2-mercaptoethanol, 117nM retinoic acid, 15% chick embryo extract [CEE; prepared as described by (80)], 10ug/mL normocin (Amaxa, VZA-1001), 1% penicillin/streptomycin/amphotericin (PSA; Gibco, 15240-062), 1% N2 additive (Gibco, 17502-048), 2.5% B27 additive (Gibco, 17504-04), 20ng/mL human basic fibroblast growth factor (bFGF; R&D Systems, 233-FB-025), 20ng/mL human insulin-like growth factor 1 (IGF-1; R&D Systems, 291-G1-050), and 0.83ug/mL fibronectin (2). Medium was filtered using a 0.22um PES filter once assembled. The wells of the 24-well plates were washed with fibronectin (0.167mg/mL), which was then removed. Before the fibronectin solution dried, 0.4mL of self-renewal medium was added to each well. Plates were incubated at 37°C, 5% CO₂ to allow the medium to equilibrate. L15 solution was prepared as above.

Fetal guts from 14.5dpc C3Fe-Tg^{Phox2B-H2BCFP} mice (36) were dissected, and transgenic embryos were identified by CFP fluorescence. Transgenic (CFP⁺) and non-transgenic (CFP⁻) fetal guts were dissected and pooled into conical tubes with 15mL HBSS. Tubes were spun softly to pellet the guts. Guts

were dissociated as above to generate single cell suspensions, with the exception of the dissociation procedure. Guts were dissociated with 1mL Accumax (Sigma, A7089) at 37°C for 15 minutes, with trituration at the ten minute mark. Portions of the cell suspension were transferred to a fresh tube prior to the final spin to serve as compensation controls. A portion of the CFP⁻ cell suspension was used for a viability dye-only compensation control. A portion of the CFP⁺ cell suspension was used for a CFP only control.

The viability dye 7-Amino-Actinomycin (7-AAD, Molecular Probes, A-1310, 1:1,000 in L15 solution) was added to cell suspensions prior to FACS isolation to exclude dead cells. Cell sorts and analyses were performed on a BD FACSAria flow cytometer using a 100 micron nozzle. CFP⁻ and CFP⁺ cells were directly sorted the 24-well tissue culture plates at a density of 150 cells per well. Plates were spun softly to collect cells at the base of the wells.

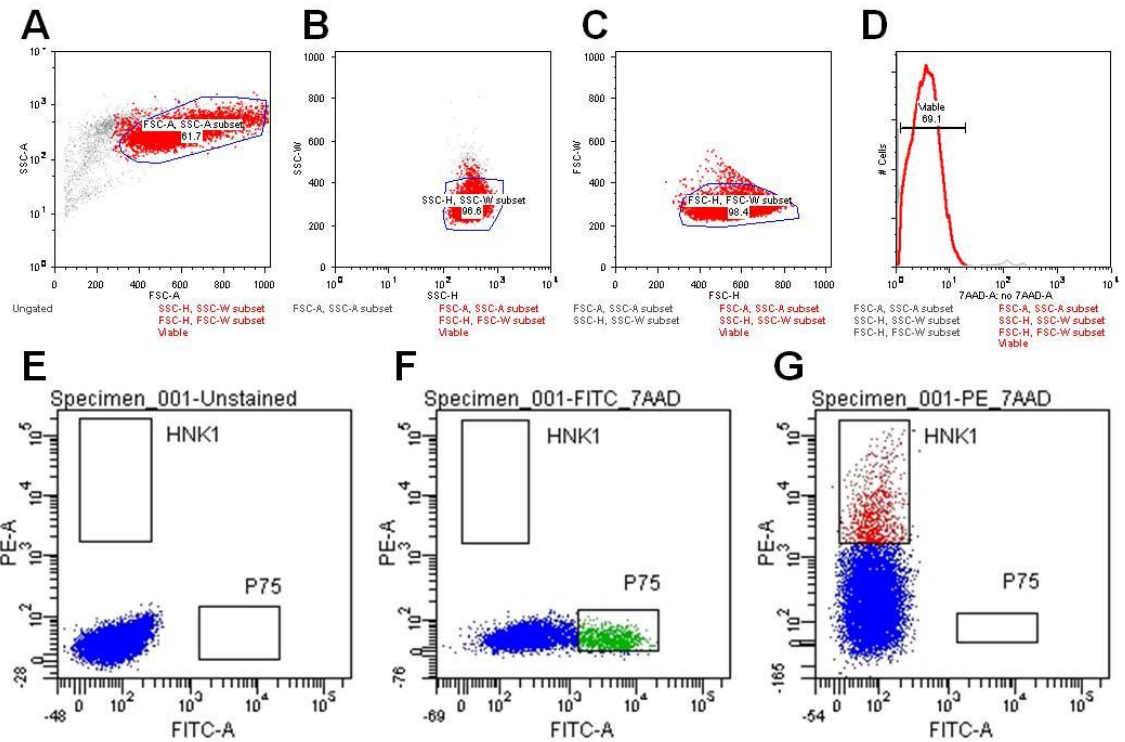
After incubating for two hours at 37°C, 5% CO₂ to allow cells to adhere to plate well surfaces, cells were fixed on ice in NBF with 0.5% Triton X-100. Immunocytochemistry was performed as in the analysis of proliferation section. Cells were immunostained with antibodies to polyclonal rabbit anti-mouse p75 (Chemicon, AB1554, 1:1000) or monoclonal mouse anti-human HNK-1 (BD Pharmingen, 559048, 1:400; cross-reactive with murine protein). Primary immunoreagents were detected with donkey anti-rabbit Cy3- and donkey anti-mouse Cy3-conjugated secondary antibodies (Jackson ImmunoResearch, 711-165-152 and 711-165-150, 1:1000) and DAPI. Cells were imaged using an Olympus IX71 inverted microscope.

Flow-cytometric isolation of p75⁺/HNK-1⁺ ENPs. 12.5dpc and 14.5dpc fetal guts were dissected and dissociated as above with the exception of the dissociation protocol. Guts were dissociated in HBSS with 0.0005% Trypsin-0.002% EDTA (Gibco, 25300-54) and 0.25mg/mL Collagenase Type IV (Worthington, CLS-4). Small portions of the cell suspension were transferred to fresh tubes prior to the final spin to serve as compensation controls.

Cells were immunostained with polyclonal rabbit anti-mouse p75 and/or monoclonal mouse anti-human HNK-1 primary antibodies on ice for 20 minutes. All antibody dilutions were made using dilute quench solution. Tubes were topped off with dilute quench solution and spun softly. The supernatant was aspirated off until approximately 200uL remained. Secondary fluorescent antibodies (goat anti-rabbit FITC, 111-096-144, Jackson ImmunoResearch, 1:400; goat anti-mouse PE, Jackson ImmunoResearch, 115-116-075, 1:400) were used to detect primary immunoreagents. Cells were incubated in secondary antibody on ice for 10 minutes. Tubes were topped off with dilute quench solution and spun softly. The supernatant was aspirated off until approximately 200uL remained.

7-AAD was added to cell suspensions prior to FACS isolation to exclude dead cells. Compensation controls included 7-AAD only, PE only, and FITC only. Cell sorts and analyses were performed on a BD FACSAria flow cytometer using a 100 micron nozzle. p75⁺/HNK-1⁺ cell measurements were determined by employing a series of gates to ensure this population only included single viable cells with high levels of marker staining (Figure 2.11).

Figure 2.11. Gating parameters used in flow cytometric isolation of eNCSC.



Panels from left to right above reflect (A) ungated population, (B) gated to exclude cell debris and multiplets based forward (FSC) and side (SSC) scatter area, (C) gated to further exclude doublet events by geometry gating for width and height measurement of FSC and SSC, and (D) gating to exclude non-viable cells 7AAD+ so that the 7AAD- population is retained before proceeding to selection of surface marker-positive population. Flow plots from the isolation of single-marker-positive cells are shown for unstained cells (E), p75⁺ cells (F), and HNK-1⁺ cells (G).

Immunocytochemical labeling of p75⁺/HNK-1⁺ progenitors.

p75⁺/HNK-1⁺ cells were directly flow-sorted into self-renewal medium within 24-well tissue culture plates coated with PDL and fibronectin at a density of 150 cells per well as described above. Equivalent numbers of unsorted, p75⁺, HNK-1⁺, and p75⁻/HNK-1⁻ cells were distributed into similar plates to serve as controls.

After incubating for two hours at 37°C, 5% CO₂ to allow cells to adhere to the plate well surface, cells were fixed on ice in NBF with 0.5% Triton X-100. Immunocytochemistry was performed as described in the analysis of proliferation section using antibodies for progenitor markers including polyclonal rabbit anti-

mouse Sox10 (79), polyclonal rabbit anti-mouse Phox2B (77), and monoclonal mouse anti-mouse Nestin (Chemicon, MAB353, 1:200) was performed. Primary immunoreagents were detected with donkey anti-rabbit Cy3- and donkey anti-mouse Cy3-conjugated secondary antibodies and DAPI.

Cells were visualized and counted using a DMI6000B microscope (Leica). The total number of DAPI⁺ cells and the number of DAPI⁺ cells positive for the individual progenitor marker being examined were determined for each individual well. The ratio of double-positive (DAPI⁺, Progenitor Marker⁺) relative to the total count of DAPI⁺ cells was calculated to determine the percentage of cells positive for each marker. Percentages were averaged across wells for each antibody, with eight replicates performed for each antibody in all three cell populations. Averages and standard deviations were compared between unsorted and p75⁻/HNK-1⁻ cells, unsorted and p75⁺/HNK-1⁺ cells, p75⁻/HNK-1⁻ and p75⁺/HNK-1⁺ cells, p75⁺ and p75⁺/HNK-1⁺ cells, and HNK-1⁺ and p75⁺/HNK-1⁺ cells using Welch's t test and are listed in Figure 2.3. Statistics were performed using the GraphPad QuickCalcs web interface (<http://www.graphpad.com/quickcalcs/index.cfm>).

Neurosphere culture of p75⁺/HNK-1⁺ progenitors. p75⁺/HNK-1⁺ cells were directly flow-sorted into self-renewal medium within 6-well non-adherent tissue culture plates (Costar, 3471) at a density of 1000 cells per well. Cultures were incubated in gas-tight modular incubator chambers (Billups-Rothenberg, MIC-101) that were flushed with 1% O₂/6% CO₂/balance N₂ to reach a final

concentration of 3-6% oxygen (34). After seven days of incubation at 37°C, neurospheres were counted using an Olympus IX71 inverted microscope. Neurospheres were pooled into a 15mL conical tube.

Neurospheres were pelleted by spinning softly as above for dissociation. The supernatant was aspirated off until approximately 200uL remained. The neurosphere pellet was washed with 5mL DMEM with low glucose and spun softly again. The supernatant was aspirated off until approximately 200uL remained. 0.5mL Accumax was added, and the neurosphere pellet was triturated five times. The neurosphere solution was incubated in a 37°C water bath for 30-45 minutes, with trituration every 10 minutes. The neurosphere solution was placed on ice, and 1mL quench solution (self-renewal medium with 37.5ug/mL DnaseI) was added. The solution was triturated ten times. The solution was spun softly, and the supernatant was aspirated off until approximately 200uL remained. The cell pellet was resuspended in 5mL dilute quench solution (self-renewal medium with 7.5ug/mL DnaseI). The solution was spun softly, and the supernatant was aspirated off until approximately 100uL remained. 900uL of self-renewal medium was added to bring the volume to 1mL. The solution was vortexed to resuspend the cell pellet.

The concentration of cells (cells/mL) was determined using a hemacytometer, and dissociated cells were replated into self-renewal medium in 6-well non-adherent tissue culture plates at a density of 250 cells per well. After seven days of incubation at 37°C, 3-6% oxygen, neurospheres were again

counted. This analysis was performed on two biological replicates. The number of isolated neurospheres can be found in Figure 2.4.

Analysis of developmental potential. 12.5dpc fetal guts were dissected, pooled according to strain and *Sox10* genotype, dissociated, and isolated by flow cytometry as described in the flow-cytometric isolation of p75⁺/HNK-1⁺ ENPs section. p75⁺/HNK-1⁺ cells were directly sorted at low density (500 cells per well, 52 cells/cm²) into self-renewal medium within 6-well tissue culture plates coated with PDL and fibronectin as described above. Identical gating conditions were used for *Sox10*^{+/+} and *Sox10*^{Dom/+} cells.

After seven days in culture, the medium was changed to promote cellular differentiation of the p75⁺/HNK-1⁺ colonies. All incubations took place in tissue culture incubators at 37°C, 5% CO₂, as opposed to gas-tight chambers as in Bixby et al. (2). Differentiation medium was made to the following specifications: 59.3% DMEM-low, 35.6% Neurobasal, 50uM 2-mercaptoethanol, 117nM retinoic acid, 1% CEE, 10ug/mL normocin, 1% PSA, 1% N2 additive, 2% B27 additive, 10ng/mL bFGF, and 20ng/mL IGF-1 (2). Differentiation medium was filtered through a 0.22um PES filter and allowed to equilibrate at 37°C, 5% CO₂ for 30 minutes before the cell culture medium was switched.

Following seven days at 37°C, 5% CO₂ in differentiation medium, immunohistochemistry was performed to determine the composition of resulting colonies. Cultures were washed in Dulbecco's Phosphate Buffered Saline (DPBS; Gibco, 14040-182) and then fixed on ice in NBF with 0.1% Triton X-100

for 15 minutes. After fixation, cultures were washed twice with wash buffer (PBS with 0.1% Triton X-100 and 0.5% BSA) and incubated in blocking solution (PBS with 1% BSA and 5% NDS) for 30 minutes at 37°C, 5% CO₂.

All antibody dilutions were made in blocking solution. Cultures were incubated in polyclonal rabbit anti-peripherin primary antibody (Chemicon, AB1530, 1:1000) for 30 minutes. Cultures were washed twice with wash buffer and then incubated in donkey anti-rabbit Cy5-conjugated secondary antibody (Jackson Immuno Research, 711-175-152, 1:1000) for 30 minutes. Cultures were washed twice in wash buffer and then incubated in blocking solution again for 15 minutes at 37°C, 5% CO₂. Cultures were incubated in a mixture of monoclonal mouse anti-human GFAP-Cy3 (Sigma, C9205, 1:800) and monoclonal mouse anti-human α SMA-FITC (Sigma, F3777, 1:800) for 30 minutes. Cultures were washed three times in wash buffer and then fixed in NBF with 0.1% Triton X-100 again for 15 minutes on ice. Cultures were washed in wash buffer, washed in DAPI, and washed in wash buffer. The wash buffer was replaced, and cultures were stored overnight at 4°C to allow antibodies to wash out.

The number of total colonies per well were counted. Colonies were classified based on detection of distinct lineage IHC markers within individual colonies. Peripherin detected neurons, glial fibrillary acidic protein (GFAP) detected glia, and smooth muscle actin (SMA) detected myofibroblasts. Colonies were categorized as either multipotent (neuronal + glial + myofibroblast, N+G+M) or uni- or bi-potent based on the observation of IHC staining within the colony:

neuronal only (N), glial only (G), myofibroblast only (M), neuronal + glial (N+G), neuronal + myofibroblast (N+M), or glial + myofibroblast (G+M). Each well comprised one replicate. Colony-type percentages were determined by dividing the number of colonies displaying a particular phenotype by the total number of colonies in a single well. Percentages were averaged across replicates. Non-parametric statistical analyses were applied because standard deviations were not equivalent. Average percentages were compared by the Wilcoxon Rank Sum Test. Statistics were performed by hand using the critical ranges listed in Essential Medical Statistics (81).

Analysis of *in vivo* neurogenesis. 13.5dpc embryonic guts were dissected and fixed on ice for one hour in NBF with 0.5% Triton X-100. Guts were washed twice for a minimum of ten minutes on ice in PBS with 0.1% Triton X-100. All washes were done in PBS with 0.1% Triton X-100 unless otherwise stated. Guts were incubated in blocking solution (as described in the analysis of migration section) for one hour.

All antibody dilutions were made with blocking solution. Guts were incubated in polyclonal rabbit anti-mouse Phox2B antibody (77) for three hours and then washed four times for a minimum of 15 minutes. Guts were incubated in polyclonal human anti-human Hu antibody (44) (1:800; cross-reactive with murine protein) at 4°C overnight. Guts were washed four times for a minimum of five minutes. Guts were incubated in donkey anti-rabbit Cy2-conjugated secondary antibody (Jackson ImmunoResearch, 715-225-152, 1:500) for 1 hour

and then washed three times for a minimum of five minutes. Guts were incubated in donkey anti-human Texas Red-conjugated secondary antibody (Jackson Immuno Research, 709-075-149, 1:100) and then washed for a minimum of ten minutes. Guts were washed twice in PBS for a minimum of ten minutes and then placed in fresh PBS at 4°C overnight to allow antibodies to completely wash out.

Embryonic guts were mounted for imaging as described in the analysis of migration section. Confocal microscopy was performed on a Zeiss Scanning Microscope LSM510 using rhodamine (Cy3, Texas Red) and FITC (GFP, Cy2, Alexa 488) band-pass filters. The HeNe1 laser, at a wavelength of 543nm, was set to 15% power. The Argon/2 laser, as a wavelength of 488nm, was set to 3% power. The pinhole was set to 440, with an optical slice less than 5.5um. For z-stacks, the optimal interval of 2.72um was used.

The most distal 700um of populated gut was identified in tiled confocal images. Numbers of Phox2B⁺ cells and Phox2B⁺/Hu⁺ cells were determined in this portion of the gut, with the ratio of double-positive to all Phox2B⁺ cells providing the neuronal percentage of the recently populated gut. Neuronal percentages were averaged across strain- and genotype-matched embryos, with six to twelve embryos from four to five separate litters per class. Non-parametric statistical analyses were applied because standard deviations were not equivalent. Average percentages were compared by the Wilcoxon Rank Sum Test. Statistics were performed by hand using the critical ranges listed in

Essential Medical Statistics (81). The foregut was also imaged with confocal microscopy using identical settings and parameters as above.

Analysis of postnatal ganglion patterning. The foregut region including the gastric sphincter and 2cm of proximal small intestine from P15-P17 *Sox10^{Dom/+}* pups and wild-type littermates was removed and flushed with PBS. It was dropped into ice-cold NBF with 0.5% TX-100 and fixed on ice for 20 minutes. After fixation, the tissue was divided into three sections, taking care to retain their biological linearity. The inner and outer enteric muscle layers, together with the myenteric plexus, were stripped off as an intact sheet. Gut muscle strips (GMS) were washed twice for a minimum of ten minutes in ice-cold PBS with 0.1% Triton X-100. Immunohistochemistry was performed as described in the analysis of migration section using polyclonal rabbit anti-mouse Phox2B antibody (77) and donkey anti-rabbit Cy3-conjugated secondary antibody.

GMS were mounted for imaging as described in the analysis of migration section. Confocal microscopy at 200X and 400X magnifications was performed on a Zeiss Scanning Microscope LSM510 using a rhodamine (Cy3, Texas Red) band-pass filter to visualize the ganglion network in postnatal guts. The HeNe1 laser, at a wavelength of 543nm, was set to 12% power. The pinhole was set to 440, with an optical slice less than 5.5um. For z-stacks, the interval was set to 1um. Gut muscle strips from P15 C3Fe-Tg^{Phox2B-H2BCFP} mice (36) were dissected, and fixed and washed as above before mounting. These samples were imaged on a BX41 Fluorescent Microscope (Olympus) at 200X and 400X magnifications.

References

1. Kapur,R.P., Livingston,R., Doggett,B., *et al.* (1996) Abnormal microenvironmental signals underlie intestinal aganglionosis in Dominant megacolon mutant mice. *Dev. Biol.*, **174**, 360-369.
2. Bixby,S., Kruger,G.M., Mosher,J.T., *et al.* (2002) Cell-intrinsic differences between stem cells from different regions of the peripheral nervous system regulate the generation of neural diversity. *Neuron*, **35**, 643-656.
3. Kruger,G.M., Mosher,J.T., Bixby,S., *et al.* (2002) Neural crest stem cells persist in the adult gut but undergo changes in self-renewal, neuronal subtype potential, and factor responsiveness. *Neuron*, **35**, 657-669.
4. Kuhlbrodt,K., Herbarth,B., Sock,E., *et al.* (1998) Sox10, a novel transcriptional modulator in glial cells. *J. Neurosci.*, **18**, 237-250.
5. Cantrell,V.A., Owens,S.E., Chandler,R.L., *et al.* (2004) Interactions between Sox10 and EdnrB modulate penetrance and severity of aganglionosis in the Sox10Dom mouse model of Hirschsprung disease. *Hum. Mol. Genet.*, **13**, 2289-2301.
6. Stanchina,L., Baral,V., Robert,F., *et al.* (2006) Interactions between Sox10, Edn3 and Ednrb during enteric nervous system and melanocyte development. *Dev. Biol.*, **295**, 232-249.
7. Carrasquillo,M.M., McCallion,A.S., Puffenberger,E.G., *et al.* (2002) Genome-wide association study and mouse model identify interaction between RET and EDNRB pathways in Hirschsprung disease. *Nat. Genet.*, **32**, 237-244.
8. McCallion,A.S., Stames,E., Conlon,R.A., *et al.* (2003) Phenotype variation in two-locus mouse models of Hirschsprung disease: tissue-specific interaction between Ret and Ednrb. *Proc. Natl. Acad. Sci. U. S. A*, **100**, 1826-1831.
9. Owens,S.E., Broman,K.W., Wiltshire,T., *et al.* (2005) Genome-wide linkage identifies novel modifier loci of aganglionosis in the Sox10Dom model of Hirschsprung disease. *Hum. Mol. Genet.*, **14**, 1549-1558.
10. Kapur,R.P., Sweetser,D.A., Doggett,B., *et al.* (1995) Intercellular signals downstream of endothelin receptor-B mediate colonization of the large intestine by enteric neuroblasts. *Development*, **121**, 3787-3795.
11. Kruger,G.M., Mosher,J.T., Tsai,Y.H., *et al.* (2003) Temporally distinct requirements for endothelin receptor B in the generation and migration of gut neural crest stem cells. *Neuron*, **40**, 917-929.

12. Rothman,T.P., Goldowitz,D., Gershon,M.D. (1993) Inhibition of migration of neural crest-derived cells by the abnormal mesenchyme of the presumptive aganglionic bowel of Is/Is mice: analysis with aggregation and interspecies chimeras. *Dev. Biol.*, **159**, 559-573.
13. Woodward,M.N., Sidebotham,E.L., Connell,M.G., *et al.* (2003) Analysis of the effects of endothelin-3 on the development of neural crest cells in the embryonic mouse gut. *J. Pediatr. Surg.*, **38**, 1322-1328.
14. Coventry,S., Yost,C., Palmiter,R.D., *et al.* (1994) Migration of ganglion cell precursors in the ileoceca of normal and lethal spotted embryos, a murine model for Hirschsprung disease. *Lab Invest*, **71**, 82-93.
15. Iwashita,T., Kruger,G.M., Pardal,R., *et al.* (2003) Hirschsprung disease is linked to defects in neural crest stem cell function. *Science*, **301**, 972-976.
16. Fu,M., Sato,Y., Lyons-Warren,A., *et al.* (2010) Vitamin A facilitates enteric nervous system precursor migration by reducing Pten accumulation. *Development*, **137**, 631-640.
17. Anderson,R.B., Turner,K.N., Nikonenko,A.G., *et al.* (2006) The cell adhesion molecule I1 is required for chain migration of neural crest cells in the developing mouse gut. *Gastroenterology*, **130**, 1221-1232.
18. Paratore,C., Eichenberger,C., Suter,U., *et al.* (2002) Sox10 haploinsufficiency affects maintenance of progenitor cells in a mouse model of Hirschsprung disease. *Hum. Mol. Genet.*, **11**, 3075-3085.
19. Young,H.M., Hearn,C.J., Ciampoli,D., *et al.* (1998) A single rostrocaudal colonization of the rodent intestine by enteric neuron precursors is revealed by the expression of Phox2b, Ret, and p75 and by explants grown under the kidney capsule or in organ culture. *Dev. Biol.*, **202**, 67-84.
20. Nagy,N., Goldstein,A.M. (2006) Endothelin-3 regulates neural crest cell proliferation and differentiation in the hindgut enteric nervous system. *Dev. Biol.*, **293**, 203-217.
21. Gianino,S., Grider,J.R., Cresswell,J., *et al.* (2003) GDNF availability determines enteric neuron number by controlling precursor proliferation. *Development*, **130**, 2187-2198.
22. Heuckeroth,R.O., Lampe,P.A., Johnson,E.M., *et al.* (1998) Neurturin and GDNF promote proliferation and survival of enteric neuron and glial progenitors in vitro. *Dev. Biol.*, **200**, 116-129.
23. Focke,P.J., Swetlik,A.R., Schilz,J.L., *et al.* (2003) GDNF and insulin cooperate to enhance the proliferation and differentiation of enteric crest-derived cells. *J. Neurobiol.*, **55**, 151-164.

24. Pisano, J.M., Colon-Hastings, F., Birren, S.J. (2000) Postmigratory enteric and sympathetic neural precursors share common, developmentally regulated, responses to BMP2. *Dev. Biol.*, **227**, 1-11.
25. Tucker, G.C., Aoyama, H., Lipinski, M., *et al.* (1984) Identical reactivity of monoclonal antibodies HNK-1 and NC-1: conservation in vertebrates on cells derived from the neural primordium and on some leukocytes. *Cell Differ.*, **14**, 223-230.
26. Tucker, G.C., Ciment, G., Thiery, J.P. (1986) Pathways of avian neural crest cell migration in the developing gut. *Dev. Biol.*, **116**, 439-450.
27. Pomeranz, H.D., Gershon, M.D. (1990) Colonization of the avian hindgut by cells derived from the sacral neural crest. *Dev. Biol.*, **137**, 378-394.
28. Epstein, M.L., Poulsen, K.T., Thiboldeaux, R. (1991) Formation of ganglia in the gut of the chick embryo. *J. Comp Neurol.*, **307**, 189-199.
29. Newgreen, D.F., Southwell, B., Hartley, L., *et al.* (1996) Migration of enteric neural crest cells in relation to growth of the gut in avian embryos. *Acta Anat. (Basel)*, **157**, 105-115.
30. Tucker, G.C., Delarue, M., Zada, S., *et al.* (1988) Expression of the HNK-1/NC-1 epitope in early vertebrate neurogenesis. *Cell Tissue Res.*, **251**, 457-465.
31. Erickson, C.A., Loring, J.F., Lester, S.M. (1989) Migratory pathways of HNK-1-immunoreactive neural crest cells in the rat embryo. *Dev. Biol.*, **134**, 112-118.
32. Newgreen, D.F., Hartley, L. (1995) Extracellular matrix and adhesive molecules in the early development of the gut and its innervation in normal and spotting lethal rat embryos. *Acta Anat. (Basel)*, **154**, 243-260.
33. Morrison, S.J., White, P.M., Zock, C., *et al.* (1999) Prospective identification, isolation by flow cytometry, and in vivo self-renewal of multipotent mammalian neural crest stem cells. *Cell*, **96**, 737-749.
34. Morrison, S.J., Csete, M., Groves, A.K., *et al.* (2000) Culture in reduced levels of oxygen promotes clonogenic sympathoadrenal differentiation by isolated neural crest stem cells. *J. Neurosci.*, **20**, 7370-7376.
35. Abo, T., Balch, C.M. (1981) A differentiation antigen of human NK and K cells identified by a monoclonal antibody (HNK-1). *J. Immunol.*, **127**, 1024-1029.
36. Corpening, J.C., Cantrell, V.A., Deal, K.K., *et al.* (2008) A Histone2BCerulean BAC transgene identifies differential expression of

- Phox2b in migrating enteric neural crest derivatives and enteric glia. *Dev. Dyn.*, **237**, 1119-1132.
37. Young,H.M., Newgreen,D. (2001) Enteric neural crest-derived cells: origin, identification, migration, and differentiation. *Anat. Rec.*, **262**, 1-15.
 38. Chalazonitis,A., Rothman,T.P., Chen,J., *et al.* (1998) Age-dependent differences in the effects of GDNF and NT-3 on the development of neurons and glia from neural crest-derived precursors immunoselected from the fetal rat gut: expression of GFRalpha-1 in vitro and in vivo. *Dev. Biol.*, **204**, 385-406.
 39. Chalazonitis,A., Pham,T.D., Li,Z., *et al.* (2008) Bone morphogenetic protein regulation of enteric neuronal phenotypic diversity: relationship to timing of cell cycle exit. *J. Comp Neurol.*, **509**, 474-492.
 40. Chalazonitis,A., D'Autreaux,F., Guha,U., *et al.* (2004) Bone morphogenetic protein-2 and -4 limit the number of enteric neurons but promote development of a TrkC-expressing neurotrophin-3-dependent subset. *J. Neurosci.*, **24**, 4266-4282.
 41. Wiese,C., Rolletschek,A., Kania,G., *et al.* (2004) Nestin expression--a property of multi-lineage progenitor cells? *Cell Mol. Life Sci.*, **61**, 2510-2522.
 42. Kotani,M., Osanai,T., Tajima,Y., *et al.* (2002) Identification of neuronal cell lineage-specific molecules in the neuronal differentiation of P19 EC cells and mouse central nervous system. *J. Neurosci. Res.*, **67**, 595-606.
 43. White,P.M., Morrison,S.J., Orimoto,K., *et al.* (2001) Neural crest stem cells undergo cell-intrinsic developmental changes in sensitivity to instructive differentiation signals. *Neuron*, **29**, 57-71.
 44. Fairman,C.L., Clagett-Dame,M., Lennon,V.A., *et al.* (1995) Appearance of neurons in the developing chick gut. *Dev. Dyn.*, **204**, 192-201.
 45. Young,H.M., Ciampoli,D., Hsuan,J., *et al.* (1999) Expression of Ret-, p75(NTR)-, Phox2a-, Phox2b-, and tyrosine hydroxylase-immunoreactivity by undifferentiated neural crest-derived cells and different classes of enteric neurons in the embryonic mouse gut. *Dev. Dyn.*, **216**, 137-152.
 46. Young,H.M., Jones,B.R., McKeown,S.J. (2002) The projections of early enteric neurons are influenced by the direction of neural crest cell migration. *J. Neurosci.*, **22**, 6005-6018.
 47. Anderson,R.B., Stewart,A.L., Young,H.M. (2006) Phenotypes of neural-crest-derived cells in vagal and sacral pathways. *Cell Tissue Res.*, **323**, 11-25.

48. Southard-Smith,E.M., Angrist,M., Ellison,J.S., *et al.* (1999) The Sox10(Dom) mouse: modeling the genetic variation of Waardenburg-Shah (WS4) syndrome. *Genome Res.*, **9**, 215-225.
49. Southard-Smith,E.M., Kos,L., Pavan,W.J. (1998) Sox10 mutation disrupts neural crest development in Dom Hirschsprung mouse model. *Nat. Genet.*, **18**, 60-64.
50. Simpson,M.J., Landman,K.A., Hughes,B.D., *et al.* (2006) Looking inside an invasion wave of cells using continuum models: proliferation is the key. *J. Theor. Biol.*, **243**, 343-360.
51. Okamura,Y., Saga,Y. (2008) Notch signaling is required for the maintenance of enteric neural crest progenitors. *Development*, **135**, 3555-3565.
52. Young,H.M., Turner,K.N., Bergner,A.J. (2005) The location and phenotype of proliferating neural-crest-derived cells in the developing mouse gut. *Cell Tissue Res.*, **320**, 1-9.
53. Breau,M.A., Pietri,T., Eder,O., *et al.* (2006) Lack of beta1 integrins in enteric neural crest cells leads to a Hirschsprung-like phenotype. *Development*, **133**, 1725-1734.
54. Barlow,A., de,G.E., Pachnis,V. (2003) Enteric nervous system progenitors are coordinately controlled by the G protein-coupled receptor EDNRB and the receptor tyrosine kinase RET. *Neuron*, **40**, 905-916.
55. Pisano,J.M., Colon-Hastings,F., Birren,S.J. (2000) Postmigratory enteric and sympathetic neural precursors share common, developmentally regulated, responses to BMP2. *Dev. Biol.*, **227**, 1-11.
56. Pisano,J.M., Birren,S.J. (1999) Restriction of developmental potential during divergence of the enteric and sympathetic neuronal lineages. *Development*, **126**, 2855-2868.
57. Chalazonitis,A., Rothman,T.P., Chen,J., *et al.* (1994) Neurotrophin-3 induces neural crest-derived cells from fetal rat gut to develop in vitro as neurons or glia. *J. Neurosci.*, **14**, 6571-6584.
58. Hearn,C.J., Murphy,M., Newgreen,D. (1998) GDNF and ET-3 differentially modulate the numbers of avian enteric neural crest cells and enteric neurons in vitro. *Dev. Biol.*, **197**, 93-105.
59. Hendershot,T.J., Liu,H., Sarkar,A.A., *et al.* (2007) Expression of Hand2 is sufficient for neurogenesis and cell type-specific gene expression in the enteric nervous system. *Dev. Dyn.*, **236**, 93-105.

60. Bordeaux,M.C., Forcet,C., Granger,L., *et al.* (2000) The RET proto-oncogene induces apoptosis: a novel mechanism for Hirschsprung disease. *EMBO J.*, **19**, 4056-4063.
61. Uesaka,T., Enomoto,H. (2010) Neural precursor death is central to the pathogenesis of intestinal aganglionosis in ret hypomorphic mice. *J. Neurosci.*, **30**, 5211-5218.
62. Paratore,C., Hagedorn,L., Floris,J., *et al.* (2002) Cell-intrinsic and cell-extrinsic cues regulating lineage decisions in multipotent neural crest-derived progenitor cells. *Int. J. Dev. Biol.*, **46**, 193-200.
63. Paratore,C., Goerich,D.E., Suter,U., *et al.* (2001) Survival and glial fate acquisition of neural crest cells are regulated by an interplay between the transcription factor Sox10 and extrinsic combinatorial signaling. *Development*, **128**, 3949-3961.
64. Hao,M.M., Anderson,R.B., Kobayashi,K., *et al.* (2009) The migratory behavior of immature enteric neurons. *Dev. Neurobiol.*, **69**, 22-35.
65. Wu,J.J., Chen,J.X., Rothman,T.P., *et al.* (1999) Inhibition of in vitro enteric neuronal development by endothelin-3: mediation by endothelin B receptors. *Development*, **126**, 1161-1173.
66. Gershon,M.D. (1999) Endothelin and the development of the enteric nervous system. *Clin. Exp. Pharmacol. Physiol*, **26**, 985-988.
67. Barlow,A.J., Wallace,A.S., Thapar,N., *et al.* (2008) Critical numbers of neural crest cells are required in the pathways from the neural tube to the foregut to ensure complete enteric nervous system formation. *Development*, **135**, 1681-1691.
68. Simpson,M.J., Zhang,D.C., Mariani,M., *et al.* (2007) Cell proliferation drives neural crest cell invasion of the intestine. *Dev. Biol.*, **302**, 553-568.
69. Finsch,M., Schreiner,S., Kichko,T., *et al.* (2010) Sox10 is required for Schwann cell identity and progression beyond the immature Schwann cell stage. *J. Cell Biol.*, **189**, 701-712.
70. Le Douarin,N.M., Teillet,M.A. (1973) The migration of neural crest cells to the wall of the digestive tract in avian embryo. *J. Embryol. Exp. Morphol.*, **30**, 31-48.
71. Burns,A.J., Champeval,D., Le Douarin,N.M. (2000) Sacral neural crest cells colonise aganglionic hindgut in vivo but fail to compensate for lack of enteric ganglia. *Dev. Biol.*, **219**, 30-43.

72. Burns,A.J., Le Douarin,N.M. (2001) Enteric nervous system development: analysis of the selective developmental potentialities of vagal and sacral neural crest cells using quail-chick chimeras. *Anat. Rec.*, **262**, 16-28.
73. Pham,T.D., Gershon,M.D., Rothman,T.P. (1991) Time of origin of neurons in the murine enteric nervous system: sequence in relation to phenotype. *J. Comp Neurol.*, **314**, 789-798.
74. Joseph,N.M., Mukouyama,Y.S., Mosher,J.T., *et al.* (2004) Neural crest stem cells undergo multilineage differentiation in developing peripheral nerves to generate endoneurial fibroblasts in addition to Schwann cells. *Development*, **131**, 5599-5612.
75. Miele,E., Tozzi,A., Staiano,A., *et al.* (2000) Persistence of abnormal gastrointestinal motility after operation for Hirschsprung's disease. *Am. J. Gastroenterol.*, **95**, 1226-1230.
76. Faure,C., Ategbo,S., Ferreira,G.C., *et al.* (1994) Duodenal and esophageal manometry in total colonic aganglionosis. *J. Pediatr. Gastroenterol. Nutr.*, **18**, 193-199.
77. Pattyn,A., Morin,X., Cremer,H., *et al.* (1999) The homeobox gene Phox2b is essential for the development of autonomic neural crest derivatives. *Nature*, **399**, 366-370.
78. Tsai,Y.H., Garipey,C.E. (2005) Dynamic changes in the proximal gut neural crest stem cell population are associated with successful development of the distal enteric nervous system in rats. *Pediatr. Res.*, **58**, 636-643.
79. Mollaaghababa,R., Pavan,W.J. (2003) The importance of having your SOX on: role of SOX10 in the development of neural crest-derived melanocytes and glia. *Oncogene*, **22**, 3024-3034.
80. Stemple,D.L., Anderson,D.J. (1992) Isolation of a stem cell for neurons and glia from the mammalian neural crest. *Cell*, **71**, 973-985.
81. Kirkwood,B.R., Sterne,J.A.C. (2003) *Essential Medical Statistics*. Blackwell Science, Malden, MA.

CHAPTER III

DIFFERENTIAL EXPRESSION OF *PHOX2B* BETWEEN INBRED STRAINS OF MICE

Introduction

The substantial differences in both postnatal and embryonic phenotypes between the B6 and C3Fe *Sox10^{Dom}* strains have an underlying basis in the genetic backgrounds of these two inbred strains. The most promising candidate for explaining some of these differences is *Phox2B*, the gene postulated to be the *Sox10m3* modifier. *Phox2B* is an essential neural crest transcription factor involved in autonomic neurogenesis (1). Differential expression of this gene could cause the differences in development of ENPs described in Chapter II.

Normal *Phox2B* expression patterns in the developing ENS have been well studied (2,3). *Phox2B*⁺ cells are apparent in the mesenchyme adjacent to the foregut at 9.5dpc. They then invade the foregut and migrate down the developing gut tube, reaching the anus by 14.5dpc (2,3). *Phox2B* expression is maintained in adult neurons (2) and, at lower levels, in enteric glia (4). In addition, this disparate expression can be seen in developing ENPs, which display both bright and dim levels of CFP under the control of a *Phox2B* promoter (4). Thus, the expression of *Phox2B* is dynamic and required through both the development and maintenance of the ENS.

Homozygous knockout mutants of *Phox2B* are embryonic lethal, but heterozygous knockouts have no morphological abnormalities (1). Thus, 50% of “normal” expression levels are sufficient for proper development. *Sox10* is required for initial expression of *Phox2B* in the developing gastrointestinal tract; loss of functional Sox10 protein results in a failure to induce *Phox2B* expression (5,6). As the *Dom* mutation decreases the amount of available functional Sox10 protein, the sensitized environment found in mutants may cause a drop in *Phox2B* expression below the acceptable threshold for normal ENS ontogeny.

Relative expression levels of *Phox2B* have not been explored in different mouse strains. In order to determine if strain background affected *Phox2B* expression, I compared wild-type and *Sox10^{Dom/+}* mRNA from both the B6 and C3Fe strains through a variety of methods. The results of allele-specific expression analysis suggest that *Phox2B* is differentially expressed between the B6 and C3Fe strains in terms of mRNA architecture. Differences in overall expression of *Phox2B*, as assayed by real-time PCR and Northern blots, are not conclusively demonstrated. These studies suggest that strain-specific regulation of *Phox2B* expression may contribute to the differences in *Sox10^{Dom}* aganglionosis between the B6 and C3Fe strains due to *Sox10m3*.

Results

Quantitative Real-Time PCR highlights variation of Phox2B expression between pooled RNA samples.

Quantitative real-time PCR is a molecular tool that enables the user to quantify very small amounts of input RNA due to the exponential amplification of the initial cDNA sample produced by reverse transcription. The expression level of the gene in question can be reliably quantified when compared to a standard curve of input amounts. In addition, this technique can be used to compare relative expression levels between experimental conditions when the expression of a housekeeping gene, which should be equal between samples, is also assayed. The expression of the housekeeping gene, which should be comparable between samples, can then be used to account for minor discrepancies in input amounts of cDNA due to unequal reverse transcription efficiencies or loading errors.

In order to compare the expression levels of *Phox2B* between the B6.*Sox10^{Dom}* and C3Fe.*Sox10^{Dom}* lines, quantitative real-time PCR was performed using Taqman Gene Expression Assays (ABI). Two assays for *Phox2B*, one that spanned exons one and two (Phox2Bex1-2) and a second in exon three (Phox2Bex3), were custom-designed. Guts from 12.5dpc *Sox10^{Dom/+}* embryos and wild-type littermates were pooled by strain and genotype. RNA was isolated from these gut pools and then reverse-transcribed into cDNA. cDNA samples were used as template in triplicate real-time PCR reactions using the Phox2Bex1-2 and Phox2Bex3 assays, in addition to an 18S ribosomal

subunit control assay. Data analysis consisted of averaging Ct values for each triplicate set, normalizing the Phox2B Ct values to the 18S Ct values (ΔCt), and comparing the normalized values for each genotype against B6.*Sox10*^{+/+} ($\Delta\Delta\text{Ct}$) to determine the fold-difference ($2^{-\Delta\Delta\text{Ct}}$) (7).

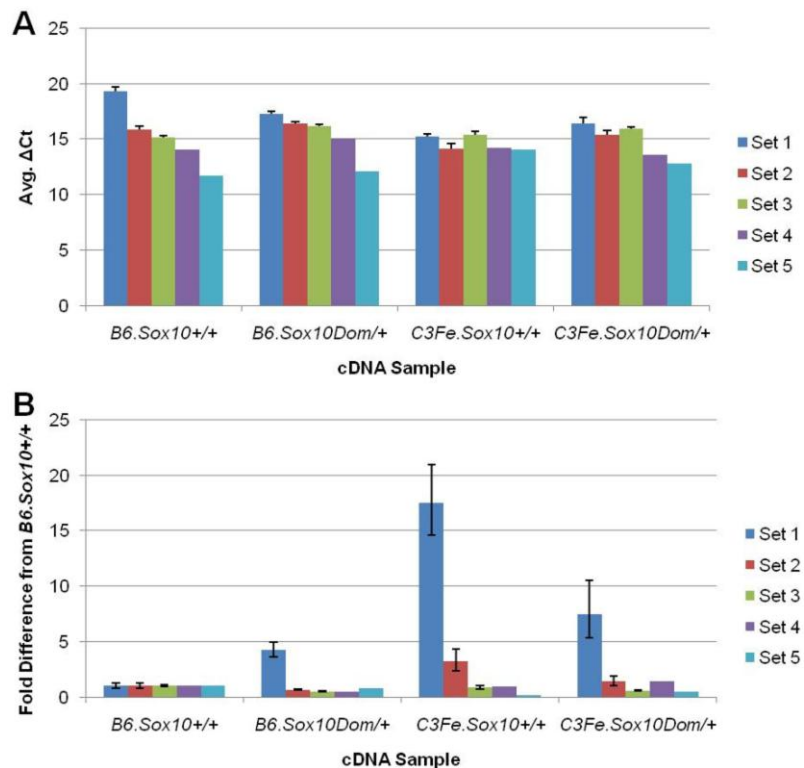
The results of these experiments when comparing fold differences relative to B6.*Sox10*^{+/+} were inconclusive due to the large amount of variation between biological replicates. Five separate pool sets (each containing pooled gut RNA from B6.*Sox10*^{+/+}, B6.*Sox10*^{Dom/+}, C3Fe.*Sox10*^{+/+}, and C3Fe.*Sox10*^{Dom/+} embryos) were tested by this methodology (Table 3.1). Three of the pool sets had multiple technical replicates; real-time PCR reactions were performed (in triplicate with both control and experimental assays) eleven, six, and four times for Sets 1, 2, and 3, respectively. Sets 4 and 5 did not have technical replicates; only a single real-time PCR run was performed. Both the Phox2Bex1-2 and Phox2Bex3 assays produced similar results (data not shown). Individual pools were consistent from run to run (technical replicates) in terms of average ΔCt (Figure 3.1A), but extremely disparate results in differences of expression levels between strain and genotype classes were obtained between individual pools (biological replicates) (Figure 3.1B).

Table 3.1. Composition of RNA sets used in expression analyses.

The numbers of individual guts from each strain/genotype class that were pooled for RNA isolation, as well as the developmental stage of the embryos and isolation details, are listed below. RNA Integrity Number (RIN) is a measure of RNA quality on a 0-10 scale determined by the amount of sample degradation; only samples with RINs higher than 7.0 were used for analysis.

RNA Set	Isolator	RINs	Number of 12.5dpc embryonic guts			
			B6. <i>Sox10</i> ^{+/+}	B6. <i>Sox10</i> ^{Dom/+}	C3Fe. <i>Sox10</i> ^{+/+}	C3Fe. <i>Sox10</i> ^{Dom/+}
1	MSS	9.5,10,10,9.1	11	9	6	9
2	LCW	9.8,10,10,10	9	8	10	9
3	LCW	10,10,10,10	19	21	14	12
4	LCW	10,10,10,10	18	7	18	33
5	MSS	10,10,10,10	21	32	23	19

Figure 3.1. Variation of *Phox2B* expression levels with real-time PCR using the *Phox2B*ex1-2 assay.



Real-time PCR was used to assay expression of *Phox2B* using a probe that spanned the junction between exons one and two in five distinct sets of pooled gut RNA from 12.5dpc B6.*Sox10*^{+/+}, B6.*Sox10*^{Dom/+}, C3Fe.*Sox10*^{+/+}, and C3Fe.*Sox10*^{Dom/+} embryos. (A) Expression levels (shown as average ΔCt) are very consistent for individual RNA pools. (B) Comparative expression levels (shown as average fold difference from B6.*Sox10*^{+/+}, $2^{-\Delta\Delta\text{Ct}}$) are highly variable between biological replicates.

When individual sets are analyzed, significant differences in expression between strain and genotype classes are seen. For Set 1, the C3Fe background produces a significantly higher level of *Phox2B* expression in wild-type embryos (fold difference of 17.5, $p < 0.0001$). However, the *Sox10^{Dom}* mutation has disparate effects between the strain backgrounds; it causes an increase in expression in the B6 strain (fold difference of 4.2, $p < 0.0001$) but causes a decrease in expression in the C3Fe strain (fold difference of 0.4, $p < 0.0001$). Regardless, C3Fe.*Sox10^{Dom/+}* embryos have a significantly higher expression level than B6.*Sox10^{Dom/+}* embryos (fold difference of 1.8, $p = 0.0002$).

For Set 2, the C3Fe background again produces a higher level of *Phox2B* expression in wild-type embryos, albeit a lower relative increase (fold difference of 3.2, $p = 0.0002$). However, in this set, the *Sox10^{Dom}* mutation causes a decrease in expression in both the B6 and C3Fe strain backgrounds (fold difference of 0.7, $p = 0.0145$; and fold difference of 0.4, $p = 0.0006$, respectively). C3Fe.*Sox10^{Dom/+}* embryos have a significantly higher expression level than B6.*Sox10^{Dom/+}* embryos (fold difference of 2.1, $p = 0.0014$).

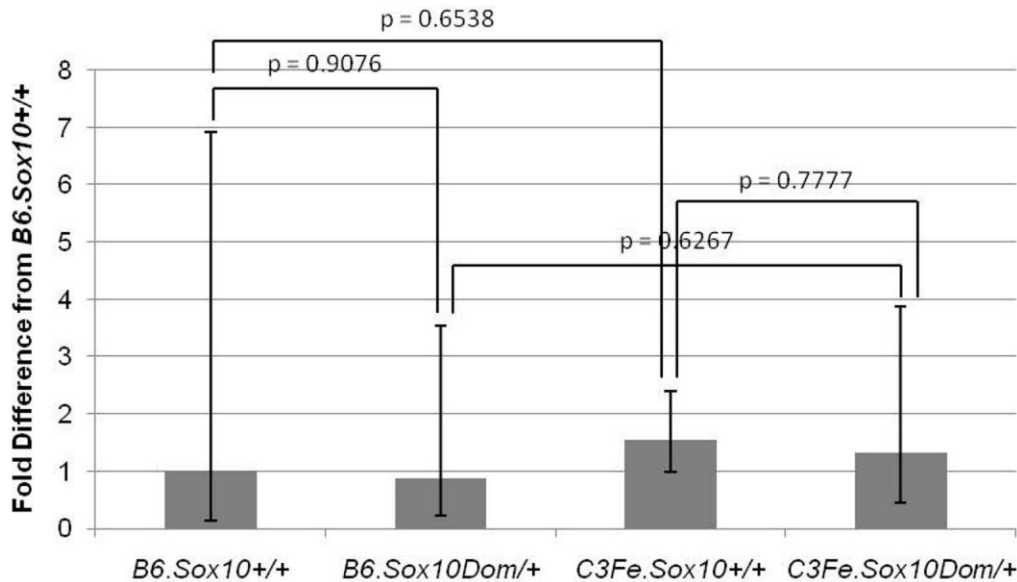
Finally, for Set 3, strain background has no effect on *Phox2B* expression in wild-type embryos ($p = 0.2052$). As in Set 2, the *Sox10^{Dom}* causes a decrease in expression in both the B6 and C3Fe strain backgrounds (fold difference of 0.5, $p < 0.0001$; and fold difference of 0.7, $p = 0.0132$, respectively). In this case, the difference in expression between C3Fe.*Sox10^{Dom/+}* embryos and B6.*Sox10^{Dom/+}* embryos is not statistically significant but follows the same trend (fold difference

of 1.2, $p = 0.0807$). Sets 4 and 5 were not analyzed for statistical significance due to the lack of technical replicates.

To compensate for variation between the biological replicates found in each RNA set, statistical analyses were performed on the combined data. However, when all five sets are averaged as biological replicates, the differences in expression between strain and genotype classes are no longer significant (Figure 3.2). For this analysis, average ΔCt values for each RNA set were averaged across all five sets; average values were used to prevent bias toward sets with more technical replicates. Averaged ΔCt values were then compared to B6.*Sox10*^{+/+} and used to determine fold differences in expression ($2^{-\Delta\Delta\text{Ct}}$). No pairwise comparisons were significant. This lack of significance persisted after removal of Set 1, the most obvious outlier. Similar results were obtained upon removal of Set 5, another potential outlier, and upon removal of both Sets 1 and 5, given the possibility that variation existed between RNA isolators.

However, the trend that C3Fe background imparts a higher level of *Phox2B* expression than the B6 background, regardless of *Sox10* genotype, remains. While certainly not conclusive, this analysis suggests that both the *Sox10*^{Dom} mutation and genetic background are important determinants of expression of the *Phox2B* locus.

Figure 3.2. Relative quantification of *Phox2B* expression levels by real-time PCR using the Phox2Bex1-2 assay.



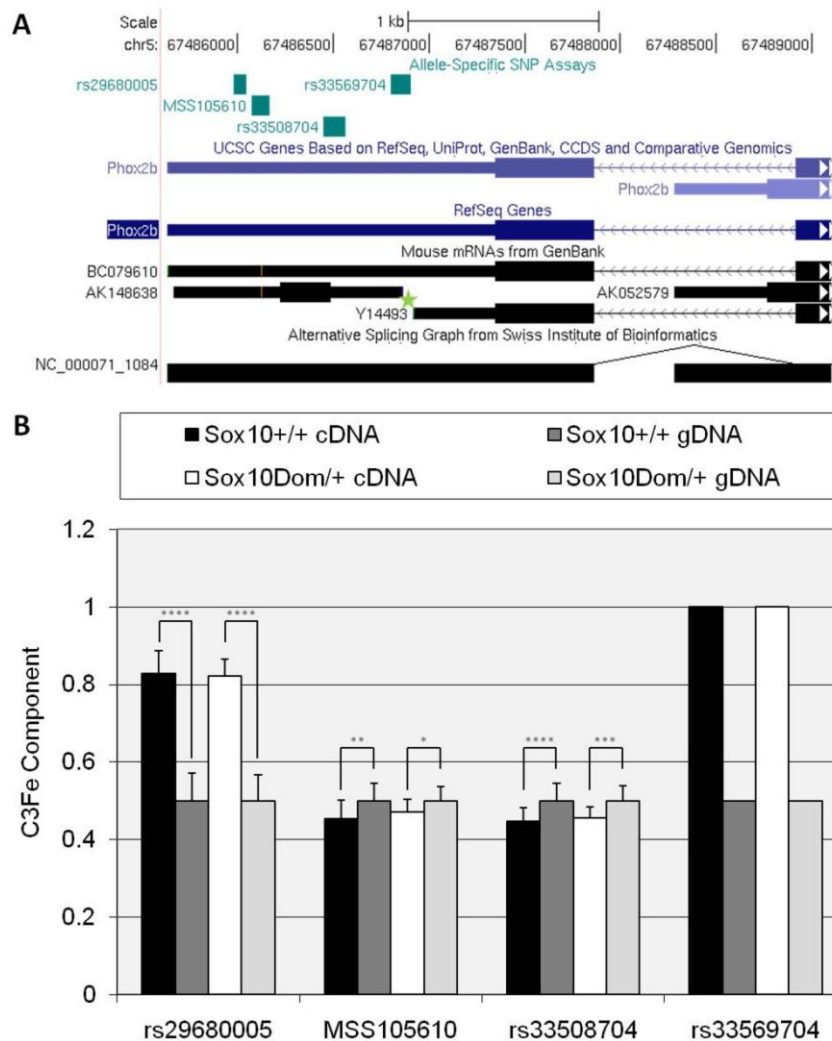
Comparison of expression levels between strain and genotype classes using five biological replicates of RNA pools from 12.5dpc B6.Sox10^{+/+}, B6.Sox10^{Dom/+}, C3Fe.Sox10^{+/+}, and C3Fe.Sox10^{Dom/+} embryos fails to demonstrate differential expression of *Phox2B*. Average ΔCt values for each biological replicate were averaged. These averaged values were compared to B6.Sox10^{+/+} to generate a fold difference ($2^{-\Delta\Delta\text{Ct}}$). Strain and genotype class ΔCt values were compared using Welch's t test.

B6 and C3Fe alleles of Phox2B are differentially expressed across the 3' UTR.

To avoid the confounding issue of biological variation, I sought to assay the expression of the B6 and C3Fe alleles of *Phox2B* within a single animal. Taqman SNP Genotyping Assays (ABI) can be used to determine the expression level of each allele when the output data is analyzed quantitatively (8). Four assays were custom-designed in the 3' UTR of *Phox2B*, as no SNPs are present within the coding regions (Figure 3.3A). Individual guts from 12.5dpc C3Fe.Sox10^{+/+} X B6.Sox10^{Dom/+} embryos were processed for RNA isolation.

Thirteen *Sox10*^{+/+} samples and nine *Sox10*^{Dom/+} samples with confirmed genotypes and RINs of 9.6-10 were used for analysis.

Figure 3.3. Allele-specific expression of *Phox2B* across the 3' UTR.



Taqman SNP Genotyping assays were designed for four SNPs in the 3' UTR of *Phox2B*. cDNA generated from gut RNA from individual 12.5dpc C3Fe. *Sox10*^{+/+} X B6. *Sox10*^{Dom/+} F₁ embryos was used as the assay input. **(A)** Schematic representation of *Phox2B* transcript, alternate splice forms, and placement of SNP assays. The gap between splice forms AK148638 and Y14493 is designated by a star. **(B)** Expression at each of the SNPs was variable between the B6 and C3Fe alleles, but this variation was not consistent across the 3' UTR. cDNA allele-specific expression levels were normalized against genomic DNA expression levels, where 50% of the expression should derive from each allele. The proportion of expression originating from the C3Fe allele is shown. Averages \pm SD are shown; **p*<0.05, ***p*<0.01, ****p*<0.001, *****p*<0.0001 by Student's t test.

cDNA from these individual guts, as well as genomic DNAs from the same embryos, were run in triplicate with each of the SNP Genotyping assays. A standard curve was produced by mixing B6 and C3Fe genomic DNA in 10% increments. The Ct values were averaged across triplicates, and a ratio of the B6 allele Ct over the C3Fe allele Ct was determined. The experimental sample Ct ratios were compared to those on the standard curve to derive the proportion of the expression that was produced by a given allele (B6 or C3Fe). The genomic DNA ratios were normalized to one to represent 50% expression from each allele. The normalization factor was then applied to the cDNA ratios. Each assay was run a total of three times; the two runs for each individual assay with the genomic DNA expression ratios closest to 50% were used for analysis.

Phox2B expression based on strain-specific allele varies across the 3' UTR (Figure 3.3B). At the most proximal SNP to exon three, rs33569704, the B6 allele was never detected in cDNA samples, even though it was readily amplified from F₁ genomic DNA. Thus, 100% of the expression of this SNP is due to the C3Fe allele; statistical analysis on this SNP was not performed due to lack of variance. The expression profile of this SNP could be due to the placement of one of the assay primers in between alternative transcripts identified in public databases. The forward primer for the rs33569704 assay (Figure 3.3A, right side of box in assay track) falls between the splice forms AK148638 and Y14493 (Figure 3.3A, green star).

Both the B6 and C3Fe alleles were detected for the remaining SNPs. The two SNPs in the middle of the 3' UTR, rs33508704 and MSS105610, derived

approximately 45% of their expression from the C3Fe allele. The most distal SNP, rs29680005, derived approximately 80% of its expression from the C3Fe allele. The *Sox10^{Dom}* allele had no impact on the expression of any of the SNPs; there were no statistical differences between wild-type and mutant F₁ samples. Therefore, expression of *Phox2B* varies between the B6 and C3Fe strains in specific regions of the 3' UTR.

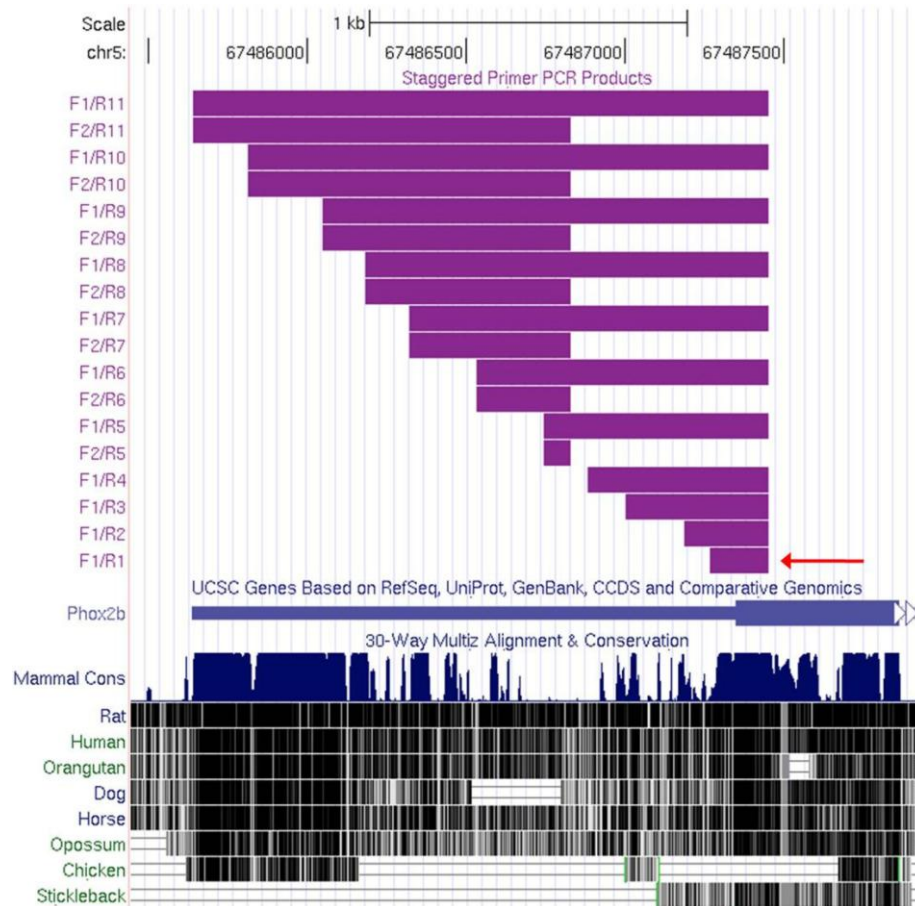
Reverse-transcriptase PCR reveals unanticipated architecture of the Phox2B 3' UTR.

To determine if alternative splicing was the underlying cause of the variable expression of the 3' UTR SNPs, the analysis of the 3' UTR was expanded to look at larger regions at a time. Staggered primers across the 3' UTR would produce differently-sized amplification products if alternative splicing was occurring in this region. Several alternatively-spliced transcripts have been identified; these include truncations of the 3' UTR, exclusion of exon 3, and a transcript that only contains the 3' UTR (Figure 3.3A).

Eleven reverse primers that spanned the 3' UTR and two forward primers, one at the distal end of exon 3 and one between reverse primers four and five, were designed to be complementary to cDNA (Figure 3.4). RNA from the pooled gut sets was reverse-transcribed and used as template in PCR amplification with each of the primer sets (18 in total). cDNA was also amplified with primers for *HPRT* as a positive reverse transcription control. Regardless of the RNA pool set used for template, the only amplification product in *Phox2B* was the 185bp

fragment between the forward primer in exon three and the most proximal reverse primer (Figure 3.4). Even though the remainder of the 3' UTR is present, as it can be amplified from cDNA in the allele-specific expression assays, it is not amenable to amplification of large contiguous segments needed for production of RT-PCR products for this assay.

Figure 3.4. Staggered primer PCR fails to detect majority of 3' UTR.



Two forward primers and eleven reverse primers were used in reverse-transcription PCR to assess the amplification of 18 total fragments of the *Phox2B* 3' UTR. cDNA generated from pooled gut RNA from 12.5dpc B6.*Sox10*^{+/+}, B6.*Sox10*^{Dom/+}, C3Fe.*Sox10*^{+/+}, and C3Fe.*Sox10*^{Dom/+} embryos was used as the PCR template. Regardless of strain or genotype, the only detectable PCR fragment was F1/R1, designated by the arrow.

Analysis of Phox2B expression by Northern blot suggests differential expression between strain backgrounds.

Examination of expression levels by Northern methodology is the gold-standard for demonstrating disparate expression. This method has the advantage of being able to detect multiple RNA species, if present, with a single probe. However, it requires a significantly larger amount of input RNA than the other methods employed previously.

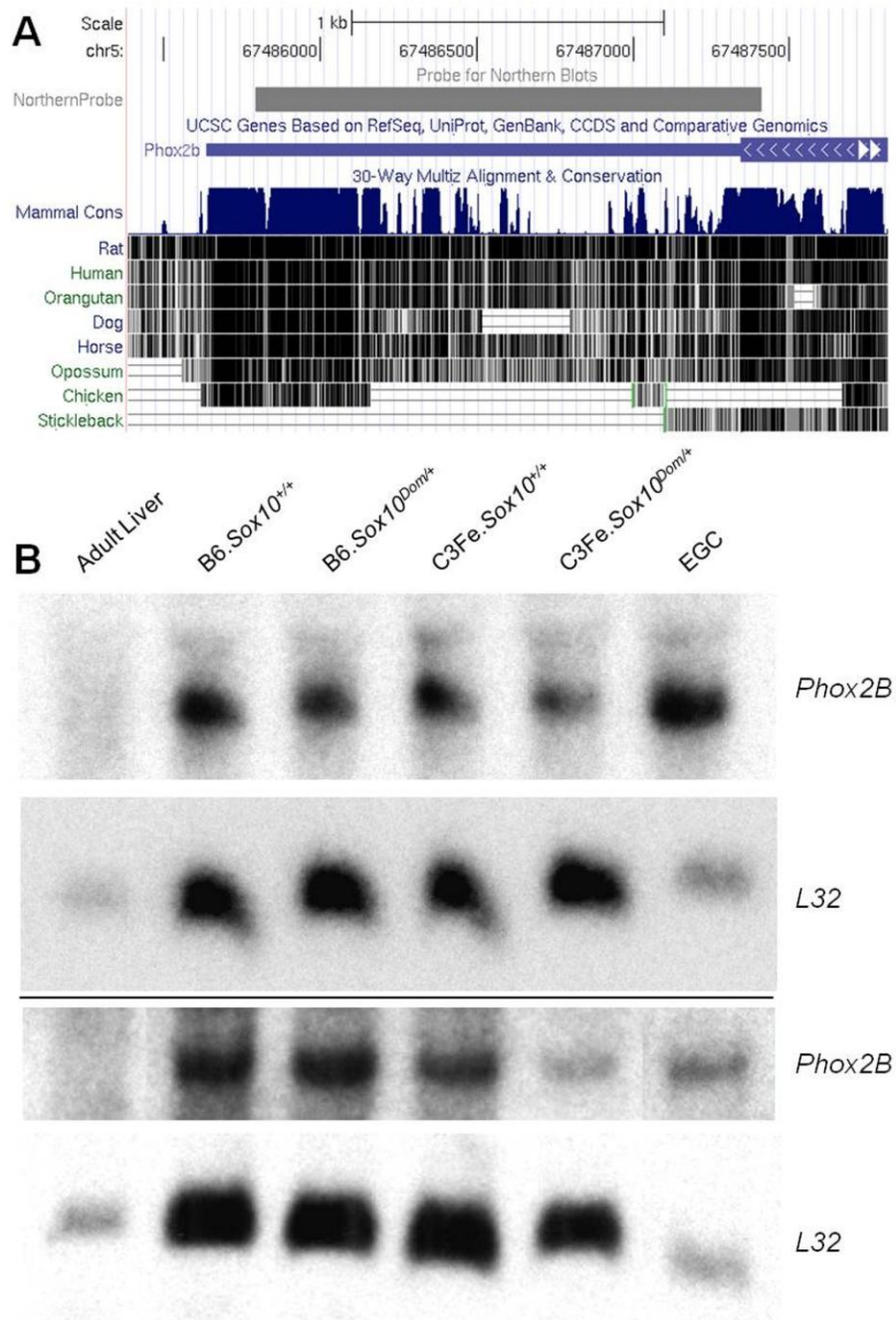
Previous experiments involving Northern blots had used a small (300bp) probe that spanned exons one and two. However, these analyses failed to produce a readable signal. For this round of experiments, a large probe (1.6kb) that covered the majority of the 3' UTR was designed (Figure 3.5A). This probe would include more radioactive nucleotides and thus produce a more intense signal band when exposed to autoradiography film. In addition, this probe would allow us to determine if large deletions or insertions were occurring in the 3' UTR of *Phox2B*, as the size of the band on the film would shift if this were the case.

To minimize the effect of biological sampling, the gut pool set with the largest number of guts within each pooled sample was chosen for analysis (Set 5; see Table 3.1). Positive and negative control tissues were also included; liver RNA should have no *Phox2B* expression, while primary rat enteroglial cells (EGCs) should have high levels of *Phox2B* expression (9). 10ug of each RNA sample (total RNA) was run on a methylmercury gel, transferred to a nitrocellulose membrane, and UV cross-linked to secure RNA to the membrane.

The RNA was hybridized separately to the 1.6kb *Phox2B* 3' UTR probe and a 300bp probe to the *L32* ribosomal subunit (used for a loading control) (Figure 3.5B). Hybridized membranes were exposed to autoradiography film for three days before development. The *Phox2B* probe produced several bands. The strongest band was present at approximately 2.8kb, the expected size of the annotated transcript. Other bands were seen at approximately 3.7kb and 1.6kb; however, these bands were most likely due to repetitive regions, as they could be eliminated by genomic DNA-blocking the probe before hybridization. A single band at approximately 1kb was seen for the *L32* probe. Bands were quantified, and the *L32* band probe intensities were used to normalize those for *Phox2B* (2.8kb band).

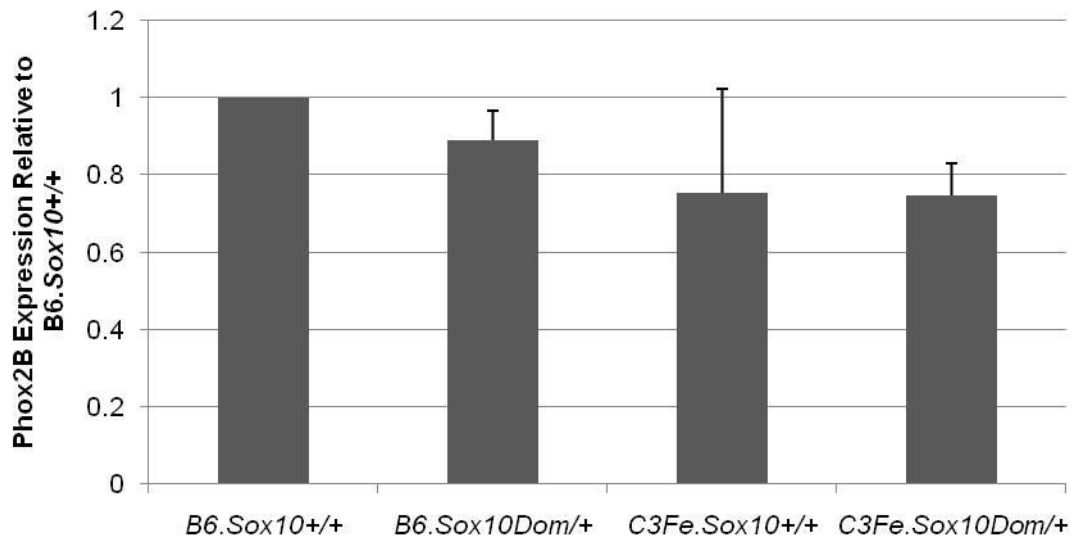
The relative levels of *Phox2B* expression across the congenic *Sox10^{Dom}* samples ran contrary to the real-time PCR analysis (Figure 3.6). Expression of *Phox2B* was highest in B6.*Sox10^{+/+}* samples, followed closely by B6.*Sox10^{Dom/+}* samples. Expression in C3Fe.*Sox10^{+/+}* samples was decreased compared to B6.*Sox10^{+/+}*. However, the presence of the *Sox10^{Dom}* allele on this background did not affect the expression of *Phox2B*. Although not statistically significant, these results suggest that differential expression of this locus is a possibility.

Figure 3.5. *Phox2B* expression across congenic *Sox10^{Dom}* lines by Northern blot analysis.



(A) A 1.6kb probe was designed to cover the majority of the 3' UTR of *Phox2B*. **(B)** Purified RNA samples from rat enteroglial cells (EGCs), adult murine liver, and pooled 12.5dpc guts from the *Sox10^{Dom}* congenic strains (Set 5) were used for Northern analysis and probed for *Phox2B* (2.8kb expected band) and the *L32* ribosomal subunit (1kb expected band). Two separate blots are shown (separated by line).

Figure 3.6. Relative quantification of *Phox2B* expression levels by Northern blot analysis.



L32 expression levels were used to normalize input RNA amount across the congenic strain samples. Normalized *Phox2B* expression levels were compared to B6.Sox10^{+/+}. See Methods for a complete description of analysis. Averages ± S.D. (n=2) are shown. Samples were compared by Welch's t test.

In summary, the methods utilized to discern the expression levels of *Phox2B* across different strain backgrounds in the Sox10^{Dom} congenic lines provide disparate results. The results from real-time PCR and Northern analyses were not statistically significant. However, allele-specific expression studies indicated that strain background is vital when assaying expression of certain portions of the *Phox2B* 3' UTR. When combined with the intriguing results of the staggered primer PCR analyses, it is clear that strain background may play a key role in determining the transcript architecture of *Phox2B*.

Discussion

While the spatiotemporal pattern of *Phox2B* expression in enteric progenitors has been well-documented (2,3), little is known about the differences in expression of this gene between different inbred strains of mice, whether in a normal or mutant state. To determine if *Phox2B* expression was affected by genetic background and/or the presence of the *Sox10^{Dom}* mutation, wild-type and *Sox10^{Dom/+}* RNA from both the B6 and C3Fe strains were compared using real-time PCR, allele-specific expression assays, staggered primer reverse-transcriptase PCR, and Northern blot analysis. While both real-time PCR and Northern blot analysis were not statistically significant, both methods suggested differential expression of *Phox2B* between strain and genotype classes. Allele-specific expression studies demonstrated strain bias in expression of certain portions of the 3' UTR, and staggered primer reverse-transcriptase PCR suggested that secondary structure might be affecting *Phox2B* transcripts. These results indicate that strain background possibly plays a role in determining both the amount and the composition of *Phox2B* RNA. These suggested differences in expression could account for the effect of this locus on *Sox10^{Dom}* aganglionosis.

Real-time PCR has the ability to detect very low levels of mRNA in a small amount of sample with a high throughput capability [see Guilietti et al. (10) for a review on its use in murine immunology]. As the population of cells that express *Phox2B* at 12.5dpc is relatively low (8-10%; Southard-Smith EM, unpublished data), a large amount of embryonic gut tissue is required to isolate an amount of

RNA substantial enough to detect this transcript by traditional means. Thus, the ability to use an input of 25ng into a reverse-transcription reaction is much preferable to an input of 10ug onto a methylmercury gel to generate a Northern blot. However, the small amount of input could be partially to blame for the wide variability in *Phox2B* levels seen by real-time PCR. As with any solution, non-homogenous composition could lead to irreproducible results. Nonetheless, individual samples themselves produced very consistent expression level readings.

The more likely explanation for the variation in expression level is biological sampling. As seen in Cantrell et al. (11), there exists a wide spectrum of severity of aganglionosis even among animals on the same inbred background with the same causative mutation. If we assume that animals with low levels of aganglionosis have different expression levels of *Phox2B* than those with high levels of aganglionosis, the issue of population sampling becomes apparent. A random selection of 10-20 animals would not fully represent the overall population. If one pool oversampled from the low aganglionosis group and another oversampled from the high aganglionosis group, those two groups would have vastly different *Phox2B* expression levels. The same concept holds true for wild-type animals, as seen by the variation in *in vitro* developmental potential (see Chapter II, Table 2.2). Clearly, the *Sox10^{Dom}* mutation is not the only component varying the amount of *Phox2B* expression. Thus, the real-time PCR results may be skewed based on the inability to experimentally replicate the distribution of *Phox2B* expression levels within a given genotype and strain class.

Comparison of biological replicates failed to reach statistically significant results, but analysis of individual RNA pools suggests that *Phox2B* is differentially expressed between the B6 and C3Fe strains. Indeed, the most likely factor contributing to the lack of significant difference between wild-type B6 and C3Fe samples is the large standard deviation for expression level in B6 wild-type RNA, which in turn is probably due to biological sampling. The magnitude of decrease in expression between B6.*Sox10*^{Dom/+} and B6.*Sox10*^{+/+} is most likely a false assessment, as the *Dom* samples have much lower numbers of enteric progenitors than their wild-type counterparts (see Chapter II, Figures 2.1 and 2.5 and Table 2.1). The same could be said for C3Fe.*Sox10*^{+/+} and C3Fe.*Sox10*^{Dom/+} samples, although this effect would not be as large.

One could postulate that the *Dom* samples actually have an *increased* level of *Phox2B* expression compared to wild-type samples when cell number is taken into account, with the B6.*Sox10*^{Dom/+} samples having a higher level of expression than C3Fe.*Sox10*^{Dom/+} samples. While there is a substantial decrease in the number of neural crest-derived stem cells in *Sox10*^{Dom/+} guts in both strains (see Chapter II, Figure 2.5), the number of *Phox2B*⁺ cells seen by immunohistochemistry is much higher in C3Fe. *Sox10*^{Dom/+} embryos than in B6.*Sox10*^{Dom/+} embryos (see Chapter II, Figure 2.1 and Table 2.1). Both of these cell populations express *Phox2B*. In the analysis of all biological replicates, C3Fe.*Sox10*^{Dom/+} samples had an approximately 1.5-fold increase in expression over B6.*Sox10*^{Dom/+} samples. However, when the number of cells that express *Phox2B* is considered, this difference is erased. The migration analyses detailed

in Chapter II demonstrate that C3Fe.*Sox10*^{Dom/+} samples have almost twice as many *Phox2B*+ cells as their B6 counterparts. Thus, the difference in expression seen by real-time PCR is likely due to cell number, not an actual difference in amount of transcript produced.

This confounding issue of cell number could be eliminated by performing real-time PCR on flow-isolated cell populations. The number of cells used to generate an RNA sample could be controlled, thereby allowing a direct comparison of cellular *Phox2B* expression. By utilizing the flow cytometry methods described in Chapter II, enteric NCSC could be isolated from each of the four strain and genotype classes. While this analysis would not eliminate the problem of biological sampling, as only so many embryos can be harvested on a single day, it would generate a clearer picture of the expression profile of *Phox2B* between genetic backgrounds.

An increase in *Phox2B* expression in C3Fe wild-type RNA compared to B6 wild-type RNA in two out of three pools supports the *in vitro* developmental potential data discussed in Chapter II that demonstrated that neurons are more prevalent in the C3Fe strain background (see Chapter II, Table 2.2). A higher level of *Phox2B* expression in *Dom* embryos relative to wild-type in the B6 strain would also confirm the *in vitro* developmental potential data in Chapter II (see Chapter II, Table 2.2). B6.*Sox10*^{Dom/+} ENPs produced significantly higher numbers of neuronal derivatives than their wild-type counterparts, while C3Fe *Sox10*^{+/+} and *Sox10*^{Dom/+} progenitors did not differ in that category. Therefore, it remains possible that *Phox2B* is differentially expressed between the B6 and

C3Fe inbred strains, and this difference in expression partially explains the difference in behavior of ENPs. Further analysis with additional biological replicates is necessary to overcome the hurdle of population sampling.

Analysis of both strain alleles within a single animal avoids the issue of biological sampling. Thus, allele-specific expression analysis in C3Fe X B6.*Sox10^{Dom}* embryos was undertaken using Taqman SNP Genotyping assays (ABI). This method has been used previously on human samples (8,12,13), along with the SNaPshot assay system (ABI), which employs a similar method of determining allelic ratios by comparing relative amounts of different fluorophores (14-20). However, no studies have explored variable expression of strain alleles in mice.

The results of the allelic expression studies in the 3' UTR of *Phox2B* were striking. Four SNPs were assayed across the 1.7kb 3' UTR. The two SNPs in the middle of the 3' UTR, rs33508704 and MSS105610, owed approximately 45% of their expression levels to the C3Fe allele. In contrast, the most distal SNP, rs29680005, had approximately 80% of its expression derived from the C3Fe allele. Most shockingly, the SNP most proximal to exon 3, rs33569704, displayed monoallelic expression in cDNA templates. The B6 allele was never detected in this template during assay optimization, which utilized combinations of B6 and C3Fe strain cDNA in known quantities. None of these results were affected by the presence of the *Sox10^{Dom}* mutation. Therefore, not only does strain background possibly play a role in determining the level of *Phox2B* expression, my data suggests it also determines the architecture of the transcript.

The composition of the 3' UTR was also the focus of study in staggered primer reverse-transcriptase PCR in RNA isolates from the congenic *Sox10^{Dom}* strains. The results of the allele-specific expression analysis demonstrated that strain-specific allele expression in F₁ samples was markedly skewed from the expected 50:50 ratio. It was postulated that alternative splicing was occurring in a strain-specific fashion. To determine if this was the case, 18 primer pairs were designed to assay the *Phox2B* 3' UTR for strain-specific differences in amplicon length. This approach would pinpoint the exact location of alternative splicing.

However, only one amplicon was produced, regardless of strain and *Sox10* genotype. The smallest and most proximal amplicon, which covered the distal end of exon 3 and the first 80bp of the 3' UTR, was readily produced, but no other regions could be amplified from cDNA. It is clear that the remainder of the 3' UTR is present from other experiments. It is possible that the base composition of the 3' UTR (51.9% GC) prevented robust PCR amplification. However, amplicons were readily produced when primers were optimized on genomic DNA, so this explanation is not likely. It is also possible that the RNA became degraded during storage, and full-length cDNA was not produced during reverse transcription, which utilized by oligo (dT) and random nonamer primers. However, this is also not likely, as the same RNA samples were used in Northern blots that detected the full-length 3' UTR.

The disparity in the detection of longer transcripts is likely due to a combination of secondary structure and GC-content. The reverse transcriptase reaction was performed at room temperature (~22°C) according to

manufacturer's specifications. However, the presence of secondary structure and high GC-content can produce the need to perform the reaction at higher temperatures to produce larger amplicons (42-55°C). As experiments with real-time PCR and SNP genotyping assays did not require this deviation from protocol, it was not used for staggered primer PCR. A final explanation is that secondary structure is forming during the annealing stage of PCR and preventing amplification. Unfortunately, this prevents analysis of alternative splicing through this methodology. Future studies using different approaches will be needed to determine the composition of the 3' UTR of *Phox2B* in the B6 and C3Fe strains.

As the results of real-time PCR analyses were inconclusive, a different methodology was employed to confirm differential expression of *Phox2B* between the B6 and C3Fe strains. Northern blot analysis was first developed in 1977 as a method of analyzing RNA expression (21). It has the advantage of being highly specific; in addition, RNA molecules of different sizes can be visualized using the same probe. Finally, it allows for the analysis of both a target gene and a control gene on a single membrane. Thus, this analysis would generate data both on relative amounts of *Phox2B* RNA in B6 and C3Fe *Sox10^{Dom}* samples and their relative sizes.

In order to ensure that all splice forms would be ascertained, a probe was designed to cover the majority of the 3' UTR, as well as the distal end of exon 3. A control probe for the *L32* ribosomal subunit was also used as a loading control. This analysis, while not statistically significant, suggested that the B6 background had higher levels of *Phox2B* expression than the C3Fe background. In addition,

it was suggested that the *Sox10^{Dom}* mutation caused a decrease in expression in samples with a B6 background but had no effect in the C3Fe background. Additional bands (1.6kb and 3.7kb) were seen when the probe for *Phox2B* was hybridized to the membrane; however, these bands were not seen when the probe was genomic DNA-blocked, indicating that they are artifacts of repetitive regions. However, the possibility that transcripts of alternate size exist cannot be discredited by this analysis. The resolution on the Northern blot in the area of interest, as determined by comparison to the size standard run on the gel, is approximately 100bp per 1mm. The *Phox2B* band itself is 2mm; thus, this band could encompass transcripts of a small range of sizes. In addition, if alternatively spliced transcripts are in the minority, it is possible that the resulting faint bands were not detected, as the level of background within the experimental RNA lanes was high.

These results are contradictory to those from the real-time PCR analysis. The first possibility is centered on probe design. The real-time PCR probes were positioned within the coding region; one covered the exon 1-exon 2 junction, and the other was located in exon 3. In contrast, the Northern probe is in the 3' UTR. The advantage of the *Phox2B*ex1-2 probe is that it skips an intron, thereby eliminating the appearance of signal from contaminating DNA. It is possible that DNA contamination occurred in the Northern analyses, which would alter the amount of signal produced based on the amount of contamination. However, this is highly unlikely, as genomic DNA would produce a high molecular weight smear on a Northern blot, which was not noted on any of the membranes. In addition,

no genomic DNA contamination was seen in PCR reactions using No-RT control samples from the same RNA pools.

Secondly, these probes assay for very different regions. If alternative splicing is occurring, it could disrupt the congruity between these analysis methods. In particular, the real-time PCR probe target (Phox2Bex1-2) is found in the majority of sequenced mRNAs and spliced ESTs seen in public databases. In contrast, there is disparity among these sequenced products in the presence and length of the 3' UTR, which was used in Northern hybridization (see Figure 3.5). One transcript, AK052579, does not contain the 3' UTR and thus would not be visualized using this probe. The alternative transcripts are shorter in total length and contain a smaller portion of the 3' UTR; therefore, they would not incorporate as much radioactivity. It is possible that the films were not exposed long enough to detect fainter bands corresponding to these other transcripts. The films used in this analysis were exposed at -80°C for three days in an intensifying cassette; longer exposures were not used due to the high levels of background hybridization.

However, once again, the conflicting results may be due to biological sampling. Only one set of RNA was used for Northern blot analysis; it was chosen because it had the greatest number of individuals in the pools (19-32 embryos per strain and genotype class). Encouragingly, the results from Northern analysis are similar to those obtained by real-time PCR for this particular RNA set (Figure 3.1A, Set 5) in that the B6 samples have higher levels of expression than the C3Fe samples. Therefore, if all RNA sets had been

analyzed using this methodology and compared, it is most likely that similar results to the real-time PCR analysis would be obtained. However, this is not a viable experimental plan, as many of these RNA sets have been depleted by other analyses. Future experiments that utilize both methods in tandem on multiple RNA sets are necessary to confirm this hypothesis.

Finally, it is possible that no differences in expression exist between the B6 and C3Fe strains. The methods employed in this body of work have failed to produce statistically significant results. This may be due to experimental issues with biological sampling or unequal cell number, as discussed above. However, the possibility that the strain backgrounds have equal levels of *Phox2B* mRNA expression cannot be excluded. Further analysis using cell-number-equalized samples will provide a more definitive answer to the question of expression levels.

If expression at the mRNA level does not differ between the B6 and C3Fe strains, it is possible that expression at the protein level does. The presence of SNPs in the 3' UTR could indicate a strain-specific effect on mRNA stability and/or translation. Either of these could affect the overall amount of Phox2B protein, which would then have downstream effects on the transcriptional activation of Phox2B targets. Future studies on mRNA stability and protein levels will provide insight into this aspect of *Phox2B* regulation.

While association studies seeking to link *Phox2B* and HSCR have been performed (22,23), no association has previously been made between *Phox2B* and *Sox10* in humans. In addition, no studies concerning *Phox2B* expression

levels have been done in HSCR patients. However, *in vitro* studies of *Phox2B* mutations found in CCHS patients indicate that mutations in this gene lead to a decrease in transcriptional activation of targets (24). In addition, these *in vitro* studies documented a strict correlation between length of a polyalanine repeat and decreased ability to activate transcription of target genes (24). The work by de Pontual et al. (22) observed a preponderance of longer repeat lengths in CCHS patients that also presented with HSCR (22). Interestingly, previous work in the Southard-Smith lab identified differences in length of repeat tracts between the B6 and C3Fe strains in intron 2; the B6 sequence contained more repeats in both locations. While not polyalanine tracts in the final transcript, the expansion of repeat regions may play a role in determining final *Phox2B* function in the mouse. As numerous *Phox2B* transcripts are present in public databases, these repeat expansions may have an impact on alternative splicing, which could disrupt the activity of the *Phox2B* protein. Therefore, the biological consequences of different alleles of *Phox2B* may not be due simply to differences in expression but also in the ability of this transcription factor to perform its tasks. Future studies testing the *in vitro* transcriptional activation abilities of the B6 and C3Fe alleles of *Phox2B* will shed light on this possible pathological mechanism.

In conclusion, a variety of methods suggest that strain background is important in determining the amount and composition of *Phox2B* transcript, in terms of possible alternative splicing, that is produced. Allele-specific expression analyses demonstrated evidence of strain-specific 3' UTR composition; however,

there was no evidence that the *Sox10^{Dom}* mutation impacted the potential for alternative splicing of the resulting transcript. The suggested differences in expression and composition most likely explain some of the variation in aganglionosis seen between the B6 and C3Fe *Sox10^{Dom}* congenic strains.

Materials and Methods

Animals. All animal protocols were approved by the Institutional Animal Care and Use Committee at Vanderbilt University. B6.*Sox10^{Dom}* and C3Fe.*Sox10^{Dom}* congenic lines were established and maintained by backcrosses to C57BL/6J and C3HeB/FeJ stocks, respectively. Both strains have been bred onto their respective inbred strains for >40 generations.

Fetal mouse dissections. Timed matings of congenic *Sox10^{Dom}* males and wild-type females were set up to obtain staged mouse fetuses, designating the morning of plug formation as 0.5 days post coitus (dpc). Fetal gastrointestinal tracts (stomach to anus) were sub-dissected for analysis. Guts were stored in RNA*later* Solution (Ambion, AM7020) at -20°C until RNA isolation.

Genotyping. Genomic DNA was isolated from limb buds by incubation in tail digest buffer (10mM Tris pH8.0, 100mM NaCl, 10mM EDTA, 0.5% SDS) with proteinase K at 55°C overnight, followed by phenol-chloroform extraction, ethanol precipitation, and resuspension in TE pH7.5. Genotype at the *Sox10* locus was determined using PCR-based methodology with the following primers: dcgs10 Bh2MidFa, CGGATGCAGCACAAAAGGACC; and dcgs10 Bh2MidRB, GGCCAGGTGGGCACTCTTGTA (25). PCR products were run on a non-denaturing polyacrylamide gel.

RNA isolation. Tissue was transferred from RNA*later* to the side of polypropylene tubes (Falcon, 352063) containing 500uL TRIzol (Invitrogen, 15596-026). Guts were pushed into the TRIzol and immediately homogenized using a Tissuemizer (Tekmar) for 45 seconds. Homogenized solutions were transferred to 1.5mL tubes. 125ug glycogen (Ambion, AM9510) and 100uL Chloroform were added, and solutions were vigorously vortexed for 15 seconds. Solutions were incubated on ice for 15 minutes and then centrifuged at 10,000RCF for 15 minutes at 4°C. The aqueous layer was transferred to a new 1.5mL tube and 500uL isopropanol was added. The solution was mixed by inversion, and RNA was precipitated by incubation at -20°C for 1-4 hours.

RNA was pelleted by centrifugation at 12,000RCF for 15 minutes at 4°C. The supernatant was removed by pipetting, and 1mL ice-cold 80% ethanol was added to wash the pellet. The RNA was pelleted by centrifugation at 7,500RCF for 15 minutes at 4°C. The supernatant was removed, and the pellet was air-dried for 2-3 minutes. The pellet was resuspended in 30uL nuclease-free water and incubated at room temperature for five minutes. The RNA was combined with 3.5uL DNase I 10X Buffer (Ambion, AM8170G), 2uL DNase I (Ambion, AM2222), and 2uL RNasin (Promega, N251A). The solution was incubated at 37°C for 20 minutes.

The RNA was then purified using a Qiagen RNeasy Kit (Qiagen, 74104) and eluted in 60uL nuclease-free water. An aliquot was removed for quality analysis; the remainder of RNA was stored at -80°C until further use. RNA quality analysis was performed by the Vanderbilt Microarray Shared Resource

(VMSR). An aliquot of 2uL of RNA (non-diluted) at concentrations ranging from 400-2200ng/uL for gut pools and 10-250ng/uL for single guts was given to the VMSR. RNA was run on a NanoDrop for concentration and on a Bioanalyzer for integrity. The details for the different RNA sets are in Table 3.1.

Reverse transcription. cDNA was generated from RNA using the High Capacity cDNA Reverse Transcription Kit (ABI, 4368813). RNA stocks were diluted to a concentration of 25ng/uL in nuclease-free (DEPC-treated) water. A 25uL reverse transcription reaction was used with an input of 25-150ng RNA. The reaction was composed of the following: 1uL 10mM dNTPS (Invitrogen, 18427-013); 2.5uL 15uM Oligo d(T)₂₃ VN (NEB, S1327S); 2.5uL 15uM Random Primer 9 (NEB, S1254S); 2.5uL 10X Kit Buffer; 1uL RNasin (Promega, N2111); 1uL diluted RNA; 1uL Multiscribe reverse transcriptase (kit); and 13.5uL nuclease-free water. The reaction was incubated at room temperature for 10 minutes and then at 37°C for two hours. The cDNA was immediately used in further applications.

Real-Time PCR. For analysis of expression of *Phox2B*, RNA from pools of 12.5dpc guts from *Sox10^{Dom/+}* and *Sox10^{+/+}* embryos from both congenic lines was used. Guts were pooled by strain, genotype at *Sox10*, and age before isolation of RNA as described above. The cDNA generated by reverse transcription was diluted by adding two volumes of nuclease-free water. 3uL of diluted cDNA was then added to the wells of an optically-clear 384-well plate

(ABI, 4309849). Each sample was run in triplicate. cDNA was dried into the wells by placing the plates on 37°C hot blocks for 2 hours.

Real-time PCR was performed with pre-designed and custom-designed assays from ABI. A Taqman MGB probe for the junction between exons one and two (Phox2Bex1-2) was generated with the sequence 6FAMCCGCAGTTCCATACAAMGBNFQ. Primers were designed separately and generated by Invitrogen with the following sequences: Phox2BMGBF, AGTATAACCCGATAAGGACCACTTTTG; Phox2BMGBR, GCCGTGGTCGGTGAAGAGT. A Taqman assay was generated for a region in exon 3 (Phox2Bex3) with the following specifications: Forward Primer, GCCTTAGTGAAGAGCAGTATGTTCT; Reverse Primer, AACTAGCCTTGGGTCTACCC; Probe, FAMCCCACTCGCCAGCCCGNFQ. A pre-designed Taqman assay for the 18S ribosomal subunit (ABI, 4333760F) was used as a control.

For the Phox2Bex1-2 assay, each reaction consisted of the following: 0.74uL 6.6uM Phox2BMGBF Primer, 0.74uL 6.6uM Phox2BMGBR Primer, 0.01 Phox2Bex1-2 MGB Probe, 5.66uL Taqman 2X Universal PCR Master Mix, No AmpErase UNG (ABI, 4324018), and 2.85uL water. For the Phox2Bex3 and 18S assays, each reaction consisted of the following: 0.25uL 40X assay mix, 5uL Taqman 2X Universal PCR Master Mix, and 3.75uL water. Plates were covered with optically clear adhesive covers (ABI, 4311971) and centrifuged to draw all liquid to the bottom of the well. Plates were run on a 7900HT Fast Real-Time PCR System (ABI, 4329002) operated by the Vanderbilt DNA Resources Core.

Data was analyzed using the SDS software package (ABI, version 2.3). Outlier Ct values within each sample triplicate were discarded, and Ct values were averaged. Experimental gene (Phox2B) Ct values were normalized by subtracting the control gene (18S) Ct values (ΔCt). Normalized Ct values were then compared to those in the B6 WT sample ($\Delta\Delta\text{Ct}$) to determine a fold-difference in level of expression ($2^{-\Delta\Delta\text{Ct}}$) (7). For statistical analyses, ΔCt values were compared between strain and genotype classes using Welch's t test. Statistics were performed using the GraphPad QuickCalcs web interface (<http://www.graphpad.com/quickcalcs/index.cfm>).

One real-time PCR run is comprised of one reverse-transcription reaction for each of the four samples within an RNA set followed by triplicate real-time PCR reactions for both the Phox2B assay and the 18S control assay for all four samples. Each real-time PCR run is equal to one technical replicate for a given RNA set. The separate RNA sets correspond to biological replicates.

Staggered primer PCR. For analysis of amplicon length in the 3' UTR of *Phox2B*, pooled gut cDNA from the congenic *Sox10^{Dom}* lines was used, as described in the real-time PCR section. PCR primers were designed to span the entire 3' UTR of *Phox2B*. A forward primer at the distal end of exon three and eleven reverse primers across the 3' UTR were produced. The range of size of amplicons was 185bp to 1810bp. In addition, a second forward primer between the fourth and fifth reverse primers was designed. The primer sequences are listed in Table 3.2.

Each PCR reaction consisted of the following: 2uL 10X PCR Buffer, 0.75uL 6.6uM Forward Primer, 0.75uL 6.6uM Reverse Primer, 0.4uL 10mM dNTPs, 0.1uL Taq Polymerase, 30ng cDNA, and water to final volume of 20uL. Some reactions generated cleaner products with the addition of Dimethyl Sulfoxide (DMSO). For these reactions (1071F/R4, 1071F/R6, and 1071F/R9), 1uL of DMSO was added to a 20uL PCR reaction. Some reactions generated cleaner products with the addition of Betaine. For these reactions (1071F/R1, 1071F/R3, 1071F/R8, 1071F/R10, and 1071F/R11), 4uL of 5M Betaine was added to a 20uL PCR reaction. PCR conditions were optimized using B6 and C3Fe genomic DNA.

Table 3.2. Primers used for staggered primer PCR.

The following primers were used in standard PCR reactions with cDNA templates to assay the composition of the *Phox2B* 3'UTR.

Primer Name	Sequence
Phx2b_mRNA_1071F	ACCTCCATCCCAGATTC
Phx2b_Ribo3F	ATTTGAAAATACAAAGGAGACG
Phx2b_3UTR_R1	GACACTAGCCTTGGGTCTAC
Phx2b_3UTR_R2	ACGTCATTTTCTCGTTGTTT
Phx2b_3UTR_R3	GACATACACCCGTCCTCA
Phx2b_3UTR_R4	CCTTTTGTATCTTTGCTGCT
Phx2b_3UTR_R5	GTCGTGAGCGAGAGAATTTA
Phx2b_3UTR_R6	AGAGTGTGGGAAATCAGTTG
Phx2b_3UTR_R7	TACAACACTGACTCCAATGCAA
Phx2b_3UTR_R8	ACAGTCTGTCCACCCTACAG
Phx2b_3UTR_R9	GCTGTAGAAAGACACCGAAA
Phx2b_3UTR_R10	TAGTCCCAACGAGAAGAAAA
Phx2b_3UTR_R11	TGCTTAGACTTGCTTTTTTCTT

Reactions were run in a thermocycler using the following program: 94°C, 5 minutes; 94°C, 30 seconds; 55°C, 30 seconds, 72°C, *n* seconds; repeat steps 2-4 34 times; 72°C, 10 minutes; 4°C, hold. For 1071F/R1-3 and Ribo3F/R5-7, *n* equals 30 seconds. For 1071F/R4-6 and Ribo3F/R8-10, *n* equals 60 seconds. For 1071F/R7-9 and Ribo3F/R11, *n* equals 90 seconds. For 1071F/R10-11, *n* equals 120 seconds.

In addition, amplification of the *HPRT* gene was used as a control for reverse transcription success. These primers were HPRT9F, TGAGATTGTATCTGTAAGAAGGA, and HPRT9R, GGGAAAATACAGCCAACACTG. PCR products were run on a non-denaturing polyacrylamide gel.

Allele-specific expression. For analysis of allele-specific expression of *Phox2B*, guts from individual B6.*Sox10*^{Dom/+} X C3Fe.*Sox10*^{+/+} F₁ embryos were used. RNA was isolated from single guts as described above, and cDNA was generated as described above. Taqman SNP Genotyping Assays (ABI) were custom-designed for four SNPs in the 3' UTR of *Phox2B*. The specifications for each assay are listed in Table 3.3.

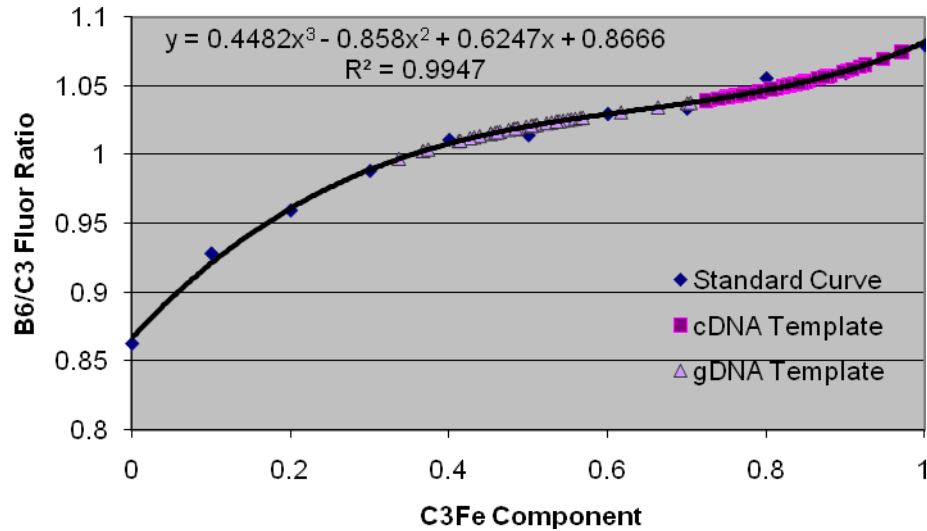
In addition, a standard curve of 10% incremental mixtures of B6 and C3Fe genomic DNA were used as templates. Samples of genomic DNA from both strains, at known concentrations, were mixed to a final concentration of 10ng/uL. This standard curve was used as PCR template with each technical replicate.

Finally, genomic DNA samples for each of the F₁ embryonic samples at 10ng/uL were also used as PCR template.

For all assays, the reaction mix contained 10ng cDNA diluted in water to a total volume of 9.5uL, 10 uL Taqman Universal PCR Master Mix, and 0.5uL Taqman assay. Plates were covered with optically clear adhesive covers and centrifuged to draw all liquid to the bottom of the well. Plates were run on a 7900HT Fast Real-Time PCR System operated by the Vanderbilt DNA Resources Core.

Data was analyzed using the SDS software package. Outlier Ct values within each sample triplicate were discarded, and Ct values were averaged. Ct values for the B6 allele (FAM) were divided by the Ct values for the C3Fe allele (VIC) to determine the B6/C3Fe expression ratio. The ratios of allele fluorophores were plotted for the standard curve and used to generate a trinomial (rs29580005) or linear (rs33508704, MSS105610) line equation (best fit model, $R^2 > 0.97$, Windows Excel). This equation, where x equals the proportion of the expression due to the C3Fe allele in the input cDNA and y equals the B6/C3Fe fluorophore Ct ratio, was used to back-calculate the amount of C3Fe allelic expression in experimental samples (value of x determined using Maxima software). This equation was used for each of the F₁ samples, both cDNA and genomic DNA, for which the fluorophore ratio was known (Figure 3.6). A separate standard curve, and thus a separate equation, was generated for each individual run of the set of F₁ samples.

Figure 3.7. Allele-specific expression analysis.



The standard curve equation for rs29680005 is shown along with plotted values for cDNA and genomic DNA (gDNA) templates. The equation, derived from the standard curve of known C3Fe components, is used to determine the C3Fe components of the F₁ samples.

The average C3Fe allele expression for the genomic DNA samples was normalized to 50%, representing equal expression of alleles. A separate normalization factor was determined for wild-type and *Sox10^{Dom/+}* samples. The proper normalization factor was applied to the average C3Fe allele expression of the cDNA samples to generate the final percentage of *Phox2B* expression due to the C3Fe allele. Averages and standard deviations were compared between wild-type cDNA and genomic DNA samples and between *Sox10^{Dom/+}* cDNA and genomic DNA samples using Welch's t test. Statistics were performed using the GraphPad QuickCalcs web interface (<http://www.graphpad.com/quickcalcs/index.cfm>).

Table 3.3. Specifications for Taqman SNP Genotyping Assays.

The following primers and probes were used in Taqman SNP Genotyping assays to study allele-specific expression in C3Fe X B6.*Sox10^{Dom}* F₁ embryos.

SNP	Forward Primer	Reverse Primer	VIC Probe	FAM Probe
rs33569704	TCCCTCGTCTCCTTTGTATTT TCAAATTA	GGAAAGCAGCAAAGATA CAAAGGA	AAATAAATTACAAAAG TTTTTTTAA	AAATTACAAAAGTGT TTTTAA
rs33508704	CTGGAGGGTGAGAAGGGAT CT	CGCCATTAGCGCAACTG ATTT	CCTGAGAGATGATGCC CTGTACA	CCTGAGAGATGATGC CCTATACA
MSS105610	GCCTCAACATTCAACTAATA TCTATAGTTTTGTG	CCTTCTATGCGCAGTTTA GACATCT	TGGGCTTTTTTTTTAAAT TT	TTGGGCTTTTTTTTTAT ATTT
rs29680005	CGGTCACGTAGAGGAGACG	AGCTGTGTTCTGTGACT CAATTGTA	TCTGTAAGAGAGTAAC AC	TCTGTAAGATAGTAA CAC

Northern blot generation. For analysis of *Phox2B* expression by Northern blots, RNA from pools of 12.5dpc guts from *Sox10^{Dom/+}* and *Sox10^{+/+}* embryos from both congenic lines was used. Control RNAs from adult murine liver and rat enterogial cells [ATCC, CRL-2690; (9)] were also loaded in parallel on the same gel. Guts were pooled by strain, genotype at *Sox10*, and age before isolation of RNA as described above. 10ug of RNA was ethanol-precipitated at -20°C overnight. Glass plates with 0.5mm spacers secured by binder clamps were warmed in a 60°C oven for 5 minutes. The corners of the plates were sealed with molten 1% agarose.

The plate setup was returned to the 60°C oven for 20 minutes. 900mL of 1X Gel Buffer was made by diluting 90mL 10X Gel Buffer (0.5M Boric Acid, 0.05M Sodium Borate-septahydrate, 0.1M Sodium Sulfate, and 0.01M Tetrasodium salt EDTA) in 810mL water. 0.6g Pulsed Field Certified Agarose (Bio-Rad, 162-0137) was dissolved in 50mL 1X Gel Buffer and incubated in a 55°C water bath for 10 minutes. The plate setup was removed from the oven, and 0.25mL of 1M Methyl Mercury Hydroxide was added to the agarose solution. The solution was swirled to mix and immediately poured into the pre-warmed plate setup. A 15-well comb was inserted and clamped into place. The gel was allowed to solidify for 30 minutes.

RNA was pelleted by centrifugation at 13,200rpm at 4°C for 10 minutes. The supernatant was removed, and the pellet was air-dried for 2-3 minutes. The pellet was resuspended in 6uL of 2X Sample Buffer (20mM Methyl Mercury

Hydroxide, 5% Ficoll, and 0.1% bromophenol blue in 1X Gel Buffer) and stored on ice until loading.

The gel was placed in a vertical electrophoresis rig, which included a pump for recirculating the 1X Gel Buffer. Samples were loaded along with molecular weight markers (1kb DNA Ladder, Invitrogen, 15615-016; RNA Ladder, Promega, G3191). The gel was run at 10mA for 45 minutes and then at 45mA for two hours. The gel was stained with 1ug/mL ethidium bromide in 0.5M Ammonium Acetate for 30 minutes and destained in water for 30 minutes. The gel was then photographed on a UV light box at multiple exposures for later comparisons.

The gel was then washed in water five times for a minimum of ten minutes. The gel was nicked in 10mM sodium hydroxide for 15 minutes, then rinsed in water and held in 10X SSC before transfer. A capillary transfer setup utilizing the Whatman Schleicher & Schuell Turboblotter was used. The setup was as follows (bottom to top): 20 sheets dry thick blotting paper (Whatman, GB004); 4 sheets dry thin blotting paper (Whatman, 3030-347); 1 sheet thin blotting paper prewet in 10X SSC; Zetaprobe membrane (Bio-Rad, 162-0155) prewet in 10X SSC; Gel; Strips of Parafilm on edges of gel; 3 sheets thin blotting paper prewet in 10X SSC; 2 wicks of thin blotting paper prewet in 10X SSC with ends immersed in buffer tray filled with 10X SSC.

The transfer was run for five hours. The transfer stack was disassembled, and the gel was stained in 1ug/mL ethidium bromide for 10 minutes. The gel was destained in water for 10 minutes and photographed on a UV light box at multiple

exposures. The membrane was UV cross-linked, rinsed in 2X SSC, and stained with Methylene Blue for 2 minutes. The membrane was destained in several rinses of water and left to air-dry.

Northern probe generation. To generate a probe for *Phox2B*, a 1.6kb portion of the 3' UTR was amplified by PCR from B6 genomic DNA using the Phox2b_mRNA_ex3_F, TATGACGCTCATGTTACAAA, and Phox2b_mRNA_3UTR_R, CTTATCTTCGCTCCAAAGACC, primers. Twelve PCR reactions were pooled and ethanol-precipitated overnight at -20°C. DNA was pelleted by centrifugation at 10,000rpm at 4°C for ten minutes. The supernatant was removed, and the pellet was air-dried for 2-3 minutes. The pellet was resuspended in 15uL TE and run on a 1% agarose gel. The 1.6kb band was purified by running the band into PEG, followed by phenol-chloroform extraction.

This purified product was cloned using the TOPO TA cloning kit (pCR2.1-TOPO vector, Invitrogen, K2040-01). Several clones were grown up in liquid culture and minipreped using the Wizard Plus Miniprep Kit (Promega, A7100). DNA was sequenced by the Vanderbilt Sequencing Core. Three clones (5, 11, and 17) had three base changes from the reference *Phox2B* sequence over the 1.6kb sequence; the high percentage of matching sequence was sufficient for hybridization. Clone 5 was selected for maxiprep using the Wizard Plus Maxiprep Kit (Promega, A7270). 10ug of maxipreped DNA was subjected to a restriction enzyme digest using *EcoRI* at 37°C overnight. The 1.6kb band was

purified by PEG/phenol-chloroform as described above. The probe concentration was quantified by running 1uL of probe with λ *HindIII* standards on an agarose minigel.

The same procedure was followed for an *L32* ribosomal subunit control probe (generated using primers L32F, CAGCTGTGCTGCTCTTTCTAC, and L32R, TAGTGGATCCTGATGCCCAAC).

Northern probe labeling. To generate a labeled probe for Northern hybridization, 200-300ng of probe was combined with water to a final volume of 34uL. This solution was boiled for 5 minutes, then combined with 10uL Oligo Labeling Buffer (1M HEPES, 0.24M Tris-HCl pH 8.0, 24mM MgCl₂, 0.35% β -mercaptoethanol, 97uM dATP, 97uM dGTP, 97uM dTTP, and 27 unit/mL hexadeoxynucleotides in TE pH 8.0). The solution was cooled at room temperature for 1-2 minutes. 2uL 10mg/mL BSA, 2uL Klenow polymerase (NEB, M0210S), and 3uL P³²γdCTP (10uCi/uL, Perkin Elmer, BLU013H250UC) were added. The solution was incubated in a 37°C heat block with water in the well overnight.

To determine the percent incorporation of the radiolabel, 1uL of probe solution was spotted on a DE81 filter (Whatman, 3658324). The filter was transferred to a 1.5mL tube and analyzed in a scintillation counter for cpm ("Before"). The filter was washed four times in 0.4M Sodium Phosphate (dibasic), followed by washes in water and 95% ethanol. The filter was air-dried for ten minutes and transferred to a fresh 1.5mL tube. The washed filter was

analyzed in a scintillation counter for cpm (“After”). The “After” cpm count was divided by the “Before” cpm count to determine the percent incorporation of the radiolabel. Only probes with >60% incorporation were used.

The northern blot membrane was rinsed in 2X SSC and transferred to a hybridization bag (Kapak Corporation, 405). 25mL of Church Hybridization Buffer (0.5M Dibasic Sodium Phosphate, 1mM EDTA, 1% BSA, 7% SDS) was filtered using a 0.8um filter and added to the hybridization bag. The bag was heat-sealed and incubated in a 60°C shaking water bath for 3-4 hours.

The labeled probe was combined with 100uL water, 20uL TE pH 6.0, 1uL 10mg/mL salmon sperm DNA, and 20uL 1% CPB. The solution was frozen on dry ice until solid and then thawed in a 37°C heat block with water in the well. The probe was pelleted by centrifugation at 13,200rpm for two minutes. The supernatant was removed, and the pellet was washed with water. The probe was pelleted again. The supernatant was removed, and the pellet was washed with water. The probe was pelleted again. The supernatant was removed, and the pellet was washed with 80% ethanol in 0.1M Sodium Acetate pH 4.5. The supernatant was removed, and the pellet was air-dried for 2-3 minutes.

The pre-hybridization solution was poured off of the membrane into a 50mL conical tube. 500uL was used to resuspend the probe pellet, which was transferred to a new 50mL conical tube. The probe tube was washed at least three times with pre-hybridization solution to ensure complete transfer of probe. Pre-hybridization solution was added to the new 50mL conical tube to bring the volume of probe solution to 15mL. The probe solution was filtered using a 0.8um

filter and transferred to the hybridization bag. Bubbles were removed, and the hybridization bag was heat-sealed. The bag was placed inside a lidded bin with water, and the bin was incubated in the 60°C shaking water bath overnight.

Wash Buffers 1 (2X SSC, 1% SDS, 0.1% Sodium Pyrophosphate) and 2 (0.2X SSC, 0.5% SDS, 0.1% Sodium Pyrophosphate) were preheated to 55°C. The probe solution was poured off of the membrane into a 50mL conical tube and discarded. The membrane was transferred to a lidded bin and washed with Wash Buffer 1 at room temperature and Wash Buffer 2 at 60°C. The exact number and length of washes was dependent on the adherence of the probe to the membrane.

The washed membrane was wrapped in Saran Wrap and placed in a Kodak BioMax Autoradiography Cassette (Fisher Scientific, 05-728-14) with Kodak BioMax MR Film (Fisher Scientific, 8701302). The cassette was incubated at -80°C for three days before the film was developed.

Northern blot labeling analysis. Films were scanned at a resolution of 1200dpi. The images were imported using QuantityOne software (Bio-Rad). Using the Band Outline tool, an equal-sized box was placed around each individual band. An identical box was placed in an area of the lane that did not contain a band; this box identified the individual backgrounds. The Volume Analysis tool was used to determine the intensity of each boxed region, both band and background. The background intensity was subtracted from the band intensity for each

individual sample to generate a corrected intensity value. This process was performed on both the *L32* and *Phox2B* bands.

The *L32* corrected intensities were used to normalize for loading amount. Normalized *Phox2B* intensity values were determined by dividing the corrected *Phox2B* intensity values by the corrected *L32* corrected intensity values. B6.*Sox10*^{+/+} was set as the biological baseline, similar to real-time PCR analysis. To determine the fold-change from B6.*Sox10*^{+/+}, each normalized *Phox2B* intensity was divided by the B6.*Sox10*^{+/+} normalized intensity. Fold-changes were averaged and compared using Welch's t test. Statistics were performed using the GraphPad QuickCalcs web interface (<http://www.graphpad.com/quickcalcs/index.cfm>).

References

1. Pattyn,A., Morin,X., Cremer,H., *et al.* (1999) The homeobox gene Phox2b is essential for the development of autonomic neural crest derivatives. *Nature*, **399**, 366-370.
2. Young,H.M., Hearn,C.J., Ciampoli,D., *et al.* (1998) A single rostrocaudal colonization of the rodent intestine by enteric neuron precursors is revealed by the expression of Phox2b, Ret, and p75 and by explants grown under the kidney capsule or in organ culture. *Dev. Biol.*, **202**, 67-84.
3. Young,H.M., Ciampoli,D., Hsuan,J., *et al.* (1999) Expression of Ret-, p75(NTR)-, Phox2a-, Phox2b-, and tyrosine hydroxylase-immunoreactivity by undifferentiated neural crest-derived cells and different classes of enteric neurons in the embryonic mouse gut. *Dev. Dyn.*, **216**, 137-152.
4. Corpening,J.C., Cantrell,V.A., Deal,K.K., *et al.* (2008) A Histone2BCerulean BAC transgene identifies differential expression of Phox2b in migrating enteric neural crest derivatives and enteric glia. *Dev. Dyn.*, **237**, 1119-1132.
5. Kim,J., Lo,L., Dormand,E., *et al.* (2003) SOX10 maintains multipotency and inhibits neuronal differentiation of neural crest stem cells. *Neuron*, **38**, 17-31.
6. Elworthy,S., Pinto,J.P., Pettifer,A., *et al.* (2005) Phox2b function in the enteric nervous system is conserved in zebrafish and is sox10-dependent. *Mech. Dev.*, **122**, 659-669.
7. Livak,K.J., Schmittgen,T.D. (2001) Analysis of relative gene expression data using real-time quantitative PCR and the 2(-Delta Delta C(T)) Method. *Methods*, **25**, 402-408.
8. Riancho,J.A., Valero,C., Naranjo,A., *et al.* (2007) Identification of an aromatase haplotype that is associated with gene expression and postmenopausal osteoporosis. *J. Clin. Endocrinol. Metab*, **92**, 660-665.
9. Ruhl,A., Trotter,J., Stremmel,W. (2001) Isolation of enteric glia and establishment of transformed enteroglial cell lines from the myenteric plexus of adult rat. *Neurogastroenterol. Motil.*, **13**, 95-106.
10. Giulietti,A., Overbergh,L., Valckx,D., *et al.* (2001) An overview of real-time quantitative PCR: applications to quantify cytokine gene expression. *Methods*, **25**, 386-401.
11. Cantrell,V.A., Owens,S.E., Chandler,R.L., *et al.* (2004) Interactions between Sox10 and EdnrB modulate penetrance and severity of

- aganglionosis in the Sox10Dom mouse model of Hirschsprung disease. *Hum. Mol. Genet.*, **13**, 2289-2301.
12. Suda,T., Kato,M., Hiratsuka,M., *et al.* (2003) Use of real-time RT-PCR for the detection of allelic expression of an imprinted gene. *Int. J. Mol. Med.*, **12**, 243-246.
 13. Zhu,G., Lipsky,R.H., Xu,K., *et al.* (2004) Differential expression of human COMT alleles in brain and lymphoblasts detected by RT-coupled 5' nuclease assay. *Psychopharmacology (Berl)*, **177**, 178-184.
 14. Zhang,Y., Wang,D., Johnson,A.D., *et al.* (2005) Allelic expression imbalance of human mu opioid receptor (OPRM1) caused by variant A118G. *J. Biol. Chem.*, **280**, 32618-32624.
 15. Zhang,Y., Bertolino,A., Fazio,L., *et al.* (2007) Polymorphisms in human dopamine D2 receptor gene affect gene expression, splicing, and neuronal activity during working memory. *Proc. Natl. Acad. Sci. U. S. A*, **104**, 20552-20557.
 16. Wang,D., Papp,A.C., Binkley,P.F., *et al.* (2006) Highly variable mRNA expression and splicing of L-type voltage-dependent calcium channel alpha subunit 1C in human heart tissues. *Pharmacogenet. Genomics*, **16**, 735-745.
 17. Johnson,A.D., Zhang,Y., Papp,A.C., *et al.* (2008) Polymorphisms affecting gene transcription and mRNA processing in pharmacogenetic candidate genes: detection through allelic expression imbalance in human target tissues. *Pharmacogenet. Genomics*, **18**, 781-791.
 18. Johnson,A.D., Gong,Y., Wang,D., *et al.* (2009) Promoter polymorphisms in ACE (angiotensin I-converting enzyme) associated with clinical outcomes in hypertension. *Clin. Pharmacol. Ther.*, **85**, 36-44.
 19. Alachkar,H., Kataki,M., Scharre,D.W., *et al.* (2008) Allelic mRNA expression of sortilin-1 (SORL1) mRNA in Alzheimer's autopsy brain tissues. *Neurosci. Lett.*, **448**, 120-124.
 20. Yuferov,V., Ji,F., Nielsen,D.A., *et al.* (2009) A functional haplotype implicated in vulnerability to develop cocaine dependence is associated with reduced PDYN expression in human brain. *Neuropsychopharmacology*, **34**, 1185-1197.
 21. Alwine,J.C., Kemp,D.J., Stark,G.R. (1977) Method for detection of specific RNAs in agarose gels by transfer to diazobenzyloxymethyl-paper and hybridization with DNA probes. *Proc. Natl. Acad. Sci. U. S. A*, **74**, 5350-5354.

22. de Pontual L., Pelet,A., Trochet,D., *et al.* (2006) Mutations of the RET gene in isolated and syndromic Hirschsprung's disease in human disclose major and modifier alleles at a single locus. *J. Med. Genet.*, **43**, 419-423.
23. Liu,C.P., Li,X.G., Lou,J.T., *et al.* (2009) Association analysis of the PHOX2B gene with Hirschsprung disease in the Han Chinese population of Southeastern China. *J. Pediatr. Surg.*, **44**, 1805-1811.
24. Bachetti,T., Matera,I., Borghini,S., *et al.* (2005) Distinct pathogenetic mechanisms for PHOX2B associated polyalanine expansions and frameshift mutations in congenital central hypoventilation syndrome. *Hum. Mol. Genet.*, **14**, 1815-1824.
25. Southard-Smith,E.M., Kos,L., Pavan,W.J. (1998) Sox10 mutation disrupts neural crest development in Dom Hirschsprung mouse model. *Nat. Genet.*, **18**, 60-64.

CHAPTER IV

SEQUENCE VARIATION IN THE SOX10M3 INTERVAL

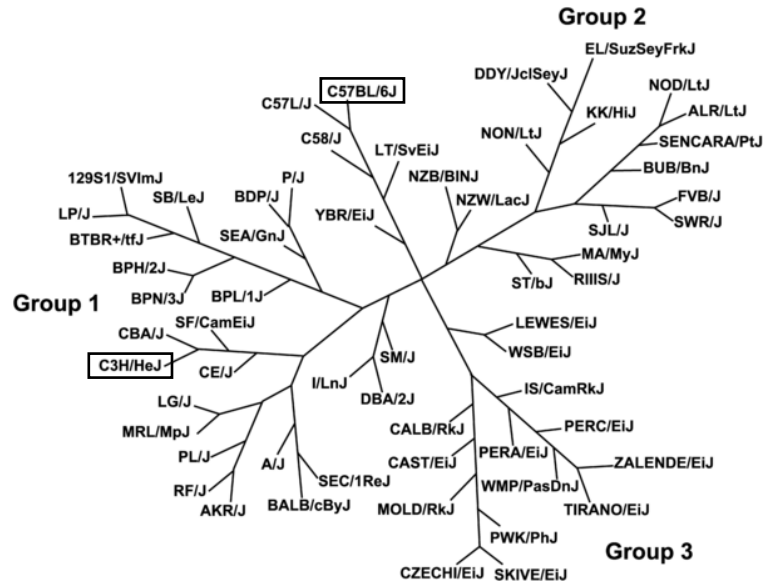
Introduction

The differences in ENP development, postnatal *Sox10*^{Dom} aganglionosis and/or *Phox2B* expression between the B6 and C3Fe strains are most likely due to variation in the genetic sequence in the region surrounding this locus. However, the amount of sequence information in this region is severely lacking, both for C3Fe and other commonly used inbred strains. The B6 strain was sequenced as the mouse reference genome (1), but sequence information for other strains relies on the action of individual researchers or contracted companies with the ability to perform high-throughput sequencing.

There are currently nine publicly available SNPs in the transcript region of *Phox2B*; one in the 5' UTR, three in introns, and five in the 3' UTR. The C3H/HeJ (C3H, a strain closely related to C3Fe) allele is known for only three of these SNPs. If the field of view is extended to 1Mb on either side of the *Phox2B* locus, 9074 publicly available SNPs are found; the C3H allele is known for 6787 of these. More importantly, both the B6 and C3H alleles are known for only 516 SNPs in a region larger than 2Mb. Of those, only 337 (~65%) are polymorphic between these two strains, and only one, rs29776386, is found within the transcript region. As these two strains represent highly divergent branches on

the laboratory mouse phylogenetic tree [Figure 4.1; Figure 1 from Petkov et al. 2005 (2)], a much larger number of SNPs would be expected.

Figure 4.1. Phylogenetic tree of the laboratory mouse.



B6 and C3H are members of disparate branches of the phylogenetic tree and therefore should differ by a large number of genetic variants. Figure 1 from Petkov et al. 2005 (2).

In order to determine the effect of the different genetic backgrounds at *Phox2B*, it was necessary to generate a complete picture of the genetic variation at this locus, both in the transcript proper and the surrounding genomic region. Therefore, a need was present for more sequence information at the *Phox2B* locus. Previous work by the Southard-Smith lab identified six sequence variants in the transcript region between B6 and C3Fe. Two SNPs were identified, one in the 5' UTR and one in intron 2; the 5' UTR SNP has since been disproved. Two insertions were identified in intron 2, each a single base in the C3Fe strain. Finally, two repeat polymorphisms were identified in intron 2, both with four extra

repeats in the B6 strain. However, due to experimental constraints, this analysis could not be extended to surrounding regions. The likelihood of a variant in the transcript region being causative for the action of a modifier is not 100%; variants in modifier genes have been found in both the transcript (3) and in regulatory regions (4). Therefore, additional sequencing in potential regulatory regions was necessary.

Secondarily, additional evidence to identify *Phox2B* as the causative gene in the *Sox10m3* modifier interval was needed. An association with aganglionic severity would provide more weight to the linkage peak identified in the original modifier screen (5). Additional crosses between the B6.*Sox10^{Dom}* strain and multiple inbred strains performed by other members of the Southard-Smith lab have produced a body of information concerning the relative susceptibility of different strain backgrounds to aganglionosis. The association of *Phox2B* with aganglionic severity in strains other than B6 and C3Fe would further support the notion that this gene is the *Sox10m3* modifier.

In order to increase the knowledge base of sequence information in the *Phox2B* region, C3H BAC sequencing was undertaken. A large number of novel and newly informative SNPs between B6 and C3H were discovered. In addition, high-throughput, multiplex sequencing was performed in the *Sox10m3* modifier interval to identify haplotypes that associated with aganglionic severity in B6.*Sox10^{Dom}* F₁ progeny. A 10-SNP haplotype 3' of *Phox2B* was significantly associated and most likely points to a key regulatory region of this gene. These

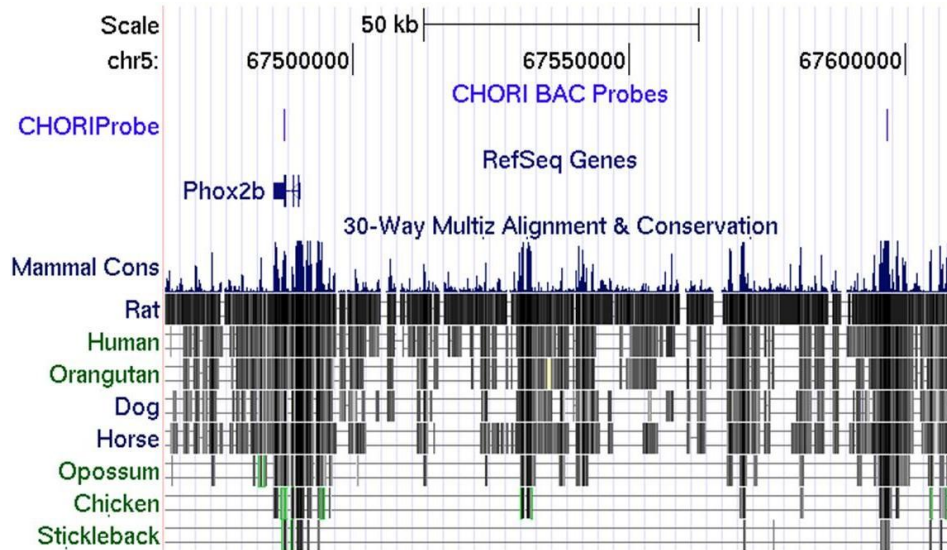
studies confirm that *Phox2B* is a modifier underlying the *Sox10m3* interval and demonstrate its modifying properties in additional strains.

Results

B6 and C3Fe genetic backgrounds are highly divergent around Phox2B

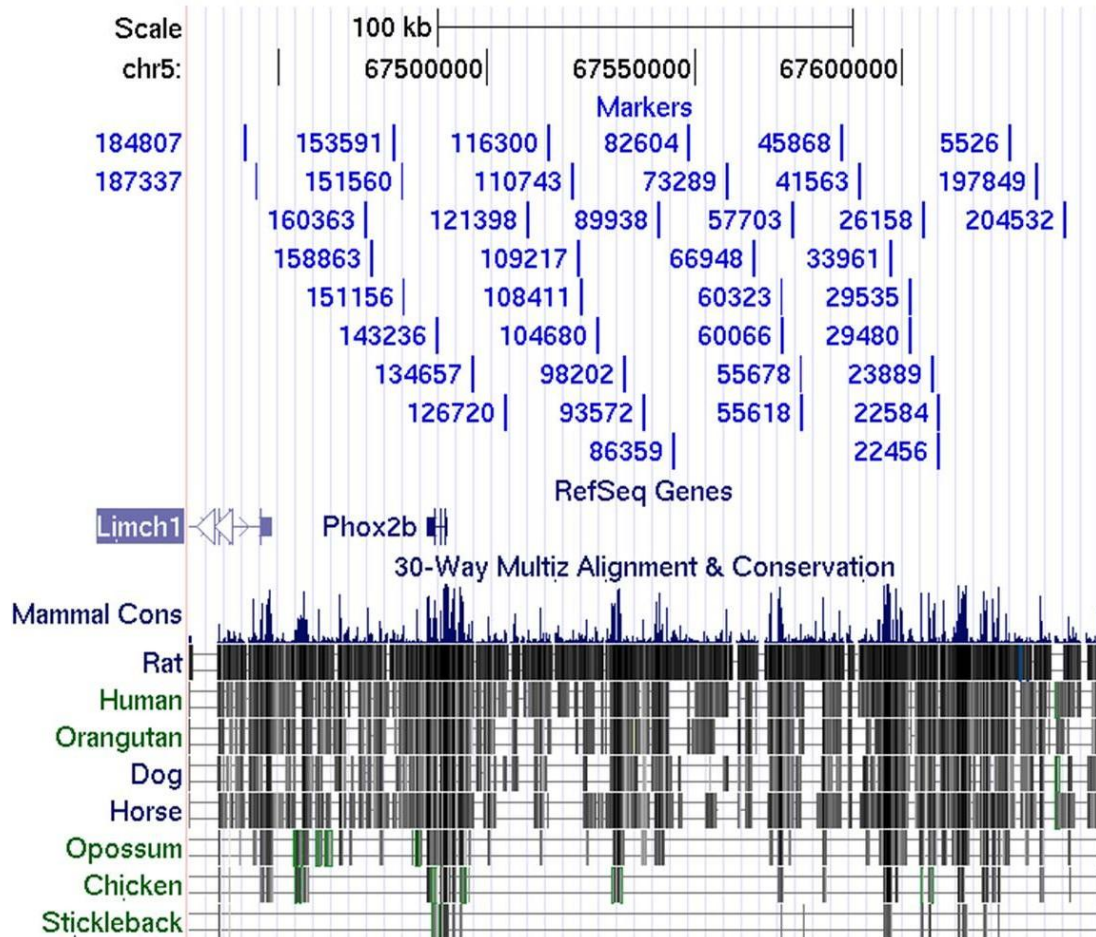
In order to discover the underlying cause of the differential expression of *Phox2B*, I sought to explore genetic variation between the B6 and C3Fe genetic backgrounds. However, sequence information for strains other than B6, the reference genome for mouse, is very scarce in this region. I obtained bacterial artificial chromosomes (BACs) from the CHORI-34 C3H/HeJ BAC library that were probed for the presence of two separate regions in the vicinity of *Phox2B* (Figure 4.2). The first probe was in exon three of *Phox2B*, and the second probe was 5' of the gene locus. Eleven BAC clones were positive for at least one of these probes.

Figure 4.2. Probes used to select CHORI BACs.



Two probes, one in exon three of *Phox2B* and one 5' of the gene locus, were used to select C3H CHORI BACs that contained at least a portion of the desired genomic region for future analysis.

Figure 4.3. STR markers used for BAC quality analysis.

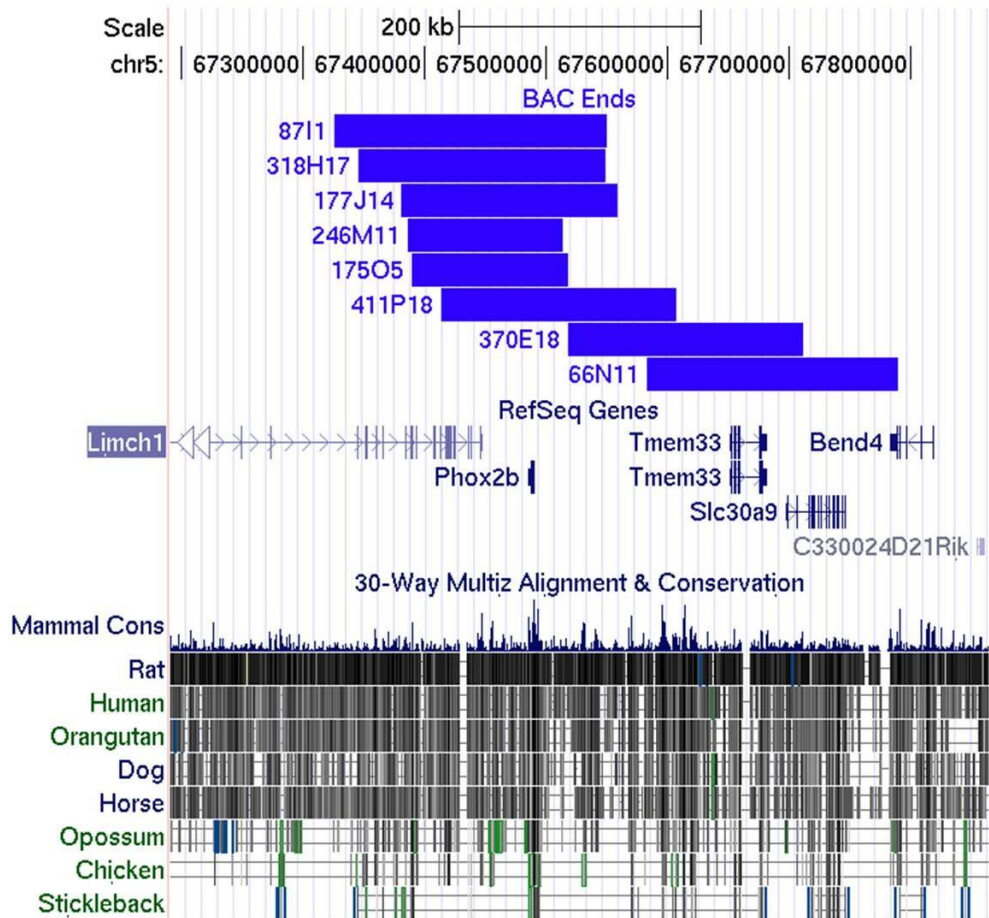


40 STR markers across the *Phox2B* locus and surrounding regions were used to test the CHORI BACs for deletions and assay relative position.

The exact genomic position of the BAC inserts was determined by Simple Tandem Repeat (STR) genotyping and end sequencing. For STR genotyping, a panel of STR markers across the *Phox2B* region known to be required for proper expression of the gene (Figure 4.3) was typed in each of the BAC clones using mini-prepped DNA. This analysis allowed me to determine if deletions were present within the inserts and give a rough estimate of the proportion of the region of interest that each BAC insert covered. Clone 126G was discarded at

this step due to the small number of present STRs. For end sequencing, maxi-prepped DNA was used as template for sequencing with T7 and Sp6 primers to specifically map the ends of the BAC insert. Clones 49H9 and 260E2 were discarded at this step due to aberrant end sequences; these clones mapped to genomic regions other than chromosome 5. Thus, eight clones passed quality analysis (correct end sequence placement and lack of deleted STRs) (Figure 4.4).

Figure 4.4. Genomic positions of CHORI BACs.

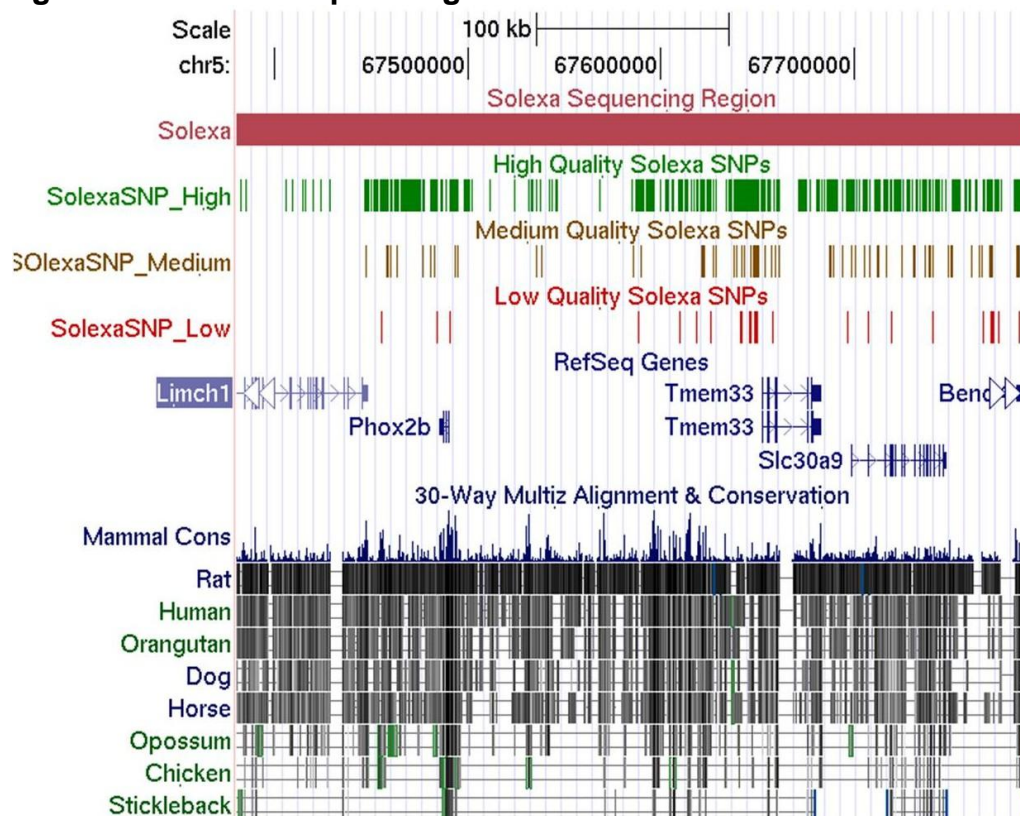


Genomic positions of CHORI BACs that passed quality analysis as determined by Sp6 and T7 end sequencing.

Four clones that covered a large portion of the total genomic span of the BAC panel were selected for sequencing on the Solexa Gene Analyzer. To generate high-quality DNA for sequencing, DNA from BAC clones 66N11, 177J14, 370E18, and 411P18 was isolated by cesium chloride (CsCl) extraction. However, after analysis of restriction digests on a CHEF gel, the DNA isolations from clones 177J14 and 411P18 were exchanged for DNA isolated using a maxiprep kit due to smearing of genomic DNA. This indicated that the DNA had been sheared during the isolation process, and thus the integrity was compromised. DNA isolations were combined from pairs of BACs to decrease the number of samples to be sequenced. 177J14 was paired with 370E18, and 411P18 was paired with 66N11. DNA was processed by the Vanderbilt Microarray Shared Resource for analysis on the Solexa Gene Analyzer. The genomic region covered by all four BACs totaled approximately 409kb, which amounted to approximately 900X coverage based on the number of sequence reads.

Sequence reads of 35bp were aligned to the reference genome. In total, 909 SNPs between B6 and C3H were identified. These SNPs were ranked for quality using an algorithm developed by Kevin Bradley in the laboratory of Dr. Jeffrey Smith based on frequency of variant and reference allele calls. After quality analysis, 678 SNPs were designated as high quality, 82 SNPs were designated as medium quality, 36 SNPs were designated as low quality, and 113 SNPs did not pass quality assessment and were discarded (Figure 4.5).

Figure 4.5. Solexa sequencing identified SNPs between B6 and C3H.



SNPs between B6 and C3H were identified in the genomic region sequenced using Solexa technology (burgundy). Based on a quality-assigning algorithm, SNPs were either of high quality (green), medium quality (brown), low quality (red), or junk (discarded, not shown).

Of the high quality SNPs, 235 were not present in public databases and thus represented newly discovered SNPs. Of those that were publicly known, 310 (~70%) were newly informative for C3H and thus C3Fe, given the highly related nature of these strains. The SNPs appeared to cluster into two blocks; one block was located 5' of *Phox2B* and contained the genes *Tmem33* and *Slc30a9*, while the other was located 3' of *Phox2B*. The large amount of variation in the 3' block led us to hypothesize that genetic differences in regulatory regions of *Phox2B* could explain the differential expression seen for this gene between the B6 and C3Fe strains.

Focused genotyping reveals mouse strain phylogeny at sub-chromosomal level

The amount of variation surrounding *Phox2B* and the discovery of a large number of new SNPs uncovered the need for additional genotype information. The number of inbred strains available for research numbers in the hundreds, and sequence information for the vast majority of these strains is decidedly lacking. In order to amass genetic information in the most efficient fashion, a large-scale focused genotyping approach was taken.

An Illumina GoldenGate genotyping panel was designed to genotype 1536 SNPs in 96 strains of mice. The SNP selection process involved combining SNPs from the Solexa screen with SNPs from dbSNP for the Solexa region as well as the other potential candidate genes for *Sox10m3*, *Uchl1* and *Atp8a1*. When performing original SNP screening for assay design, it was apparent that the close proximity (<60bp apart) of the Solexa SNPs would preclude the use of all of them in the final Illumina panel. Thus, only 386 SNPs from the original Solexa screen were chosen. These SNPs were supplemented by an additional 703 SNPs from dbSNP within the genomic region covered by the Solexa screen, for a total of 1089 SNPs. Of these 703 SNPs from dbSNP, 619 were non-polymorphic between B6 and C3H, 71 were missing allelic information for C3H, and 13 were missing allelic information for both B6 and C3H. All known SNPs (34) in *Uchl1* were included in the panel. 413 SNPs within *Atp8a1* were selected; this set was weighted toward SNPs with B6/C3H variance and equal spread

throughout the gene. The SNP panel was designed by Kevin Bradley in the laboratory of Dr. Jeffrey Smith.

Two panels of mouse strains were assembled for genotyping. The first panel was selected based on prior use in the laboratory and availability of live mice for use in future studies. The original strains used in the Solexa screen, B6 and C3H, were included as controls. 28 strains had been used in F₁ crosses with the B6.*Sox10*^{Dom} line and thus were included. Four recombinant inbred lines were included due to putative haplotype breaks within the region of interest. Two individuals from C3Fe-Tg^{*Phox2B*-H2BCFP} Line C (6) were included to further define the deletion 3' of *Phox2B* originally detected through STR mapping of founder mice. The remaining 60 strains were available from the Jackson Laboratory (JAX) either from active breeding stocks (15 strains), a live repository (26 strains), or a cryogenic repository of frozen embryos or sperm (19 strains). The second panel was selected to maximize the presence of rare alleles. 21 wild-derived strains were included, four of which had been used in F₁ crosses. 51 additional inbred strains were included, one of which had been used in F₁ crosses. 18 individuals from various generations of C3Fe-Tg^{*Phox2B*-H2BCFP} Line C were included to confirm the SNP deletion region identified in Panel I. Six control samples (two each from B6, C3Fe, and C3HeB/FeJ-Lea/a) were included for quality control. A complete list of strains used in both Illumina panels can be found in the Materials and Methods section.

DNA samples from each of the chosen strains were tested for quality and concentration before genotyping. The vast majority of the DNA samples were

obtained from JAX as highly concentrated liver DNA isolations (87/96 for Panel I, 71/96 for Panel II). The remaining DNA samples were either isolated by the laboratory (8/96 for Panel I, 25/96 for Panel II) or from the laboratory of Dr. Robert Williams (1/96 for Panel I). Samples were tested for amplification ability by PCR with control primers; all samples passed. Samples were tested for concentration by Joan Breyer in the laboratory of Dr. Jeffrey Smith using PicoGreen analysis before final dilution for genotyping.

SNP quality control removed 54 SNPs that had a call rate of <82% in Panel I. 48 SNPs were removed in Panel II. This amounted to a SNP dropout rate of 3-4%. Greater than 97% of SNPs that passed quality control produced usable allele calls for all strains. One strain in Panel I, BXD78, was removed due to an overwhelmingly high proportion of heterozygous allele calls, most likely due to contamination of the sample. All other heterozygous allele calls were excluded from analysis.

Genotype calls were sorted by genomic position. The recombinant inbred strains did not have recombination breakpoints in the region of interest and thus were not analyzed further. The C3Fe-Tg^{Phox2B-H2BCFP} Line C samples were used in a separate analysis. The remaining inbred strains were sorted into haplotype groups using polymorphic SNPs. In Panel I, only 726 SNPs were polymorphic. In Panel II, 1439 SNPs were polymorphic. Among the Panel I strains, 24 haplotype groups were identified in 90 strains. Among the Panel II strains, 29 haplotype groups were identified in 70 strains. When the panels were combined,

41 haplotype groups were identified in 158 strains; 26 of the haplotype groups were comprised of a single strain (Table 4.1).

Table 4.1. Haplotype groups identified by Illumina genotyping.

Haplotype groups were assigned by visual inspection of SNP genotype data. Bold face indicates wild-derived strains. Italics indicate strains used in association tests.

Haplotype Group Number	Number of strains within group	Strain names
1	26	<i>C57BL/6J</i> , <i>C57BL/10J</i> , <i>C57BL/10ScN</i> , <i>C57BL/10ScSn</i> , <i>C57BL/10SnJ</i> , <i>C57BL/6By</i> , <i>C57BL/6ByJ</i> , <i>C57BL/6JEiJ</i> , <i>C57BL/6NJ</i> , <i>C57BLKS/J</i> , <i>C57BR/cdJ</i> , <i>C57L/J</i> , <i>C58/J</i> , <i>BPN/3J</i> , CALB/Rk , <i>CHMU/LeJ</i> , <i>CIN/Ls</i> , <i>HP/EiT_y</i> , <i>IDH2/Ei</i> , <i>LDH2/Ei</i> , <i>PN/nBSwUmabJ</i> , <i>PRO/Re</i> , <i>PRO/Re-Pro-1a</i> , RBA/DnJ , <i>SESV/Ei</i> , <i>ZRDCTRax+/ChUmdJ</i>
2	1	WB/Re
3	7	<i>BDP/J</i> , <i>BPH/2J</i> , <i>BUB/BnJ</i> , <i>CE/J</i> , <i>FVB/NJ</i> , <i>P/J</i> , <i>RIII/ImrNhs/J</i>
4	2	<i>NZL/LtJ</i> , <i>NZO/HILtJ</i>
5	1	<i>NZO/H1Lt</i>
6	1	LEWES/Ei
7	2	TIRANO/EiJ , ZALENDE/EiJ
8	1	IS/CamEi
9	1	<i>SOD/Ei</i>
10	1	WMP/Pas
11	1	CAST/EiJ
12	1	CZECHI/EiJ
13	1	CZECHII/EiJ
14	1	JF1/Ms
15	1	MSM/Ms
16	1	MOLG/DnJ
17	2	PWD/PhJ , PWK/PhJ
18	1	SKIVE/EiJ
19	1	WSB/EiJ
20	1	PERA/EiJ
21	1	PERC/EiJ
22	8	<i>129/SvJ</i> , <i>129P1/ReJ</i> , <i>129P3/J</i> , <i>129S1/SvImJ</i> , <i>129SvEvTac</i> , <i>129T2/SvEmsJ</i> , <i>LP/J</i> , <i>SB/LeJ</i>
23	1	<i>DDY/Jc1DidSeyFrkJ</i>
24	1	IS/CamRk
25	1	RIIS/J

Table 4.1, Cont'd.

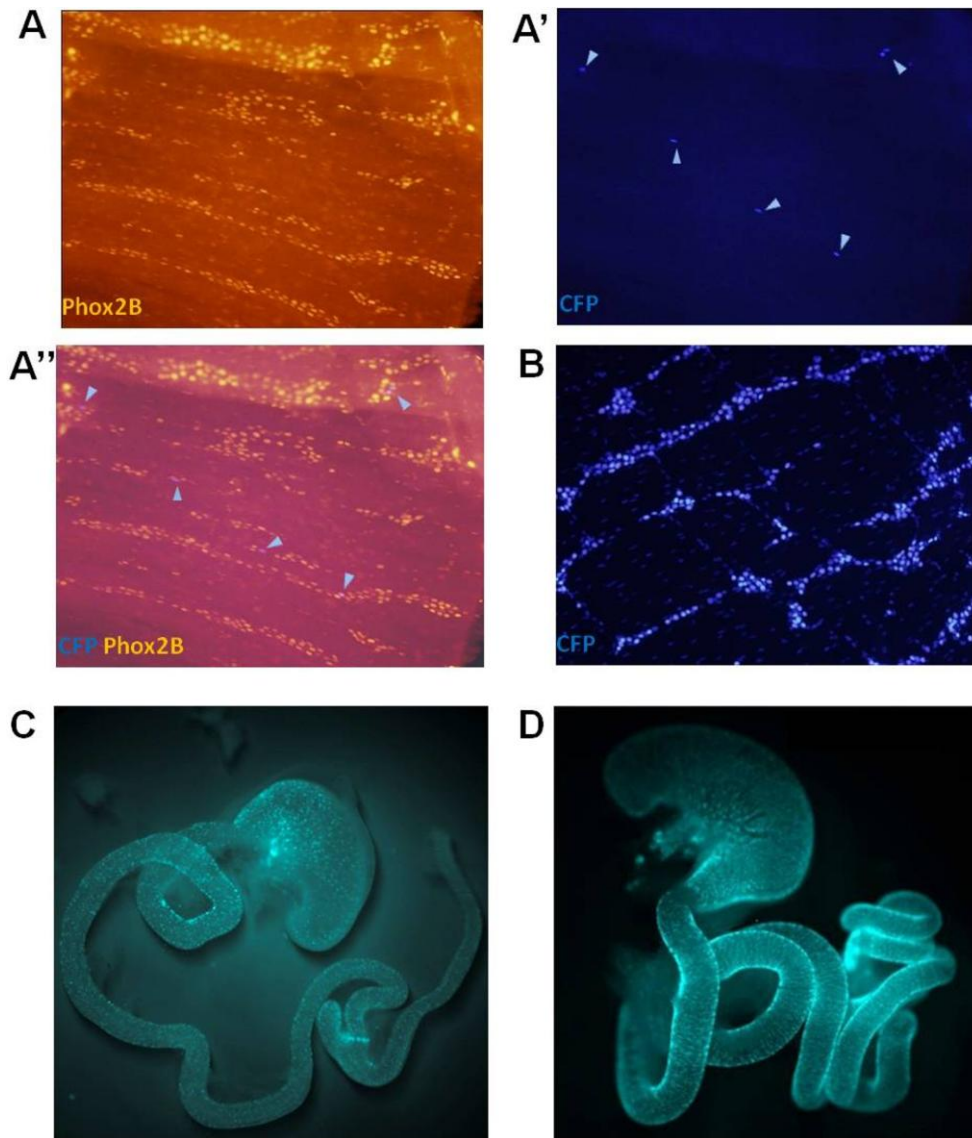
26	1	<i>SM/J</i>
27	1	RIII/DmMob
28	2	NON, <i>NON/ShiLtJ</i>
29	1	TALLYHO/JngJ
30	12	BALB/cBiDsm MMTV-, BALB/cBy, BALB/cGa, BALB/cGrLs, BALB/cGrRk, BALB/cWt, DBA/HaSmn, LT/ChRe, LT/ChReSv, LT/SvEi, LT/SvEiJ, SEC/1ReJ
31	5	<i>BALB/cByJ</i> , BALB/cJ, BALB/cWtWi, HTG/GoSfSn, <i>SEA/GnJ</i>
32	4	ALR/Lt, ALS/Lt, RBF/Dn, RBF/DnJ
33	1	<i>NOD/ShiLtJ</i>
34	1	<i>NZW/LacJ</i>
35	4	<i>AKR/J</i> , <i>LG/J</i> , <i>MRL/MpJ</i> , RF/J
36	26	A/HeJ, A/J, A/WySnJ, BPL/1J, <i>BTBR T+ tf/J</i> , DA/HuSn, EL/SuzSeyFrkJ, GR/J, <i>MA/MyJ</i> , MOLF/EiJ , NOD/Lt, NOR/Lt, NOR/LtJ, <i>NZB/B1NJ</i> , NZM2328/J, NZM2410/J, NZM391/J, NZM64/J, NZM88/J, <i>PL/J</i> , SJL/Bm, <i>SJL/J</i> , SJL/Wt, ST/bJ, SWR/Bm, <i>SWR/J</i>
37	1	RBB/Dn
38	2	<i>DBA/2J</i> , <i>DBA/2J-GpnmB+/SjJ</i>
39	1	YBR/Ei
40	20	AuSsJ, CBA/CaGnLe, CBA/CaJ, <i>CBA/J</i> , CBA/JLs, CD10/J1sJ, CD3/J1sJ, CD7/J1sJ, CD9/J1sJ, <i>DBA/1J</i> , <i>DBA/1LacJ</i> , <i>DBA/2DeJ</i> , <i>DBA/8BiDsm</i> , I/LnJ, <i>KK/HIJ</i> , NH/KiPt, SENCARA/PtJ, SENCARB/PtJ, SENCARC/PtJ, VM/Dk
41	10	FL/1Re, FL/4ReJ, LPT/LeJ, SF/CamEi, SI/Col Tyrp1Dnahc11/J, <i>C3H/HeJ</i> , C3H/HeJBirLtJ, CeH/HeOuJ, C3HeB/FeJ-Lea/a, <i>C3HeB/FeJ</i>

Reporter expression in C3Fe-Tg^{Phox2B-H2BCFP} Line C points to a regulatory region 3' of Phox2B

C3Fe-Tg^{Phox2B-H2BCFP} Line A has been shown to express the CFP reporter in an appropriate temporal and spatial pattern (6) (Figure 4.6B). However, analysis of Line C has shown that this transgenic line is lacking a significant amount of reporter expression in the adult (Figure 4.6A-A"). In particular, expression is confined to small number of neurons, whereas CFP expression can be seen in both neurons and glia in Line A samples. Additional studies have

demonstrated that CFP expression is present at 10.5dpc but starts to diminish after 14.5dpc (Figure 4.6C,D).

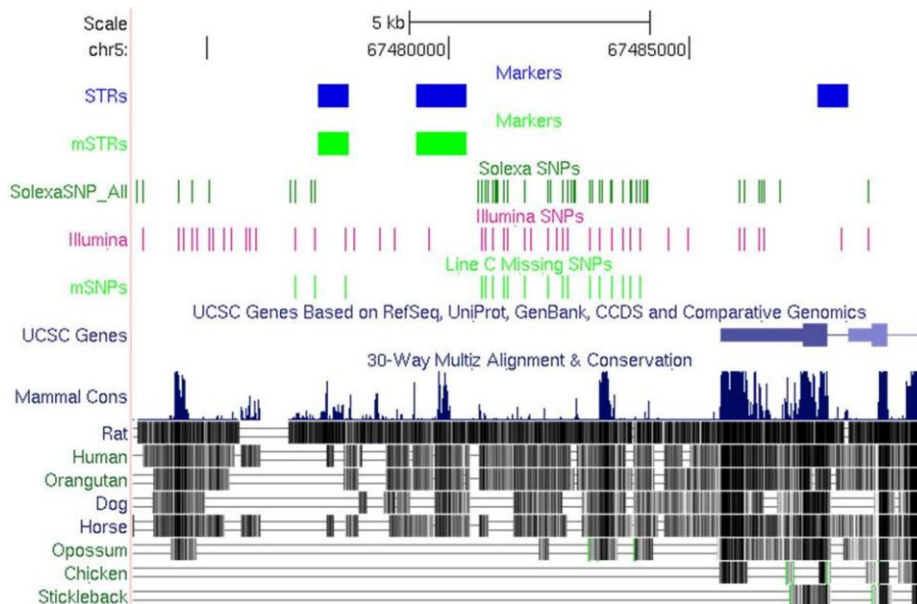
Figure 4.6. Inappropriate reporter expression in C3Fe-Tg^{Phox2B-H2BCFP} Line C.



Gut muscle strips immunostained for Phox2B (Cy3) (**A**) from an adult C3Fe-Tg^{Phox2B-H2BCFP} Line C animal show restricted CFP expression (**A'**) in only a fraction of the neurons in the enteric ganglia, highlighted by arrowheads (**A''**, Merge of **A** and **A'**). (**B**) Gut muscle strips from an adult C3Fe-Tg^{Phox2B-H2BCFP} Line A animal show CFP expression through the enteric ganglia. Differences in CFP expression can also be seen in whole-mount images of 14.5dpc fetal guts from Line C (**C**) and Line A (**D**) embryos (300X magnification). Panel D adapted from Figure 1D, Corpening et al. 2008 (6).

Initial STR mapping of the transgenic founders by previous members of the lab identified a deletion 3' of *Phox2B* (Figure 4.7). Due to the wide spacing of STR markers, the deletion region could only be narrowed to an interval of approximately 15kb. By utilizing the Illumina panel, I could narrow this region further through identification of homozygous C3Fe SNPs within the C3Fe-Tg^{*Phox2B*-H2BCFP} Line C samples. 18 SNPs produced homozygous allele calls and thus were deleted in Line C (Figure 4.7). The nearest flanking polymorphic SNPs that were heterozygous in Line C samples were rs29579671 (Build 37 position chr5: 67475023) and rs51589489 (Build 37 position chr5: 67484533). The tighter spacing of the Illumina SNPs narrowed the deletion region to an interval of approximately 9.5kb.

Figure 4.7. A deleted regulatory region in C3Fe-Tg^{*Phox2B*-H2BCFP} Line C.



Initial STR mapping identified three missing STRs in Line C (all STRs in blue, missing STRs in light green). SNP genotyping identified fifteen missing SNPs in the same region (Solexa SNPs in dark green,, Illumina SNPs in pink, missing SNPs in light green).

Haplotype at *Phox2B* is significantly associated with severity of aganglionosis

Previous studies involving F₁ crosses between a variety of inbred strains and the B6.*Sox10^{Dom}* congenic line have demonstrated that there is a large amount of variation in severity of aganglionosis dependent on genetic background. When F₁ *Sox10^{Dom/+}* pups are analyzed for the presence of enteric ganglia at P7-P10, the average percent of the gut presenting with aganglionosis ranges from 0.12% to 23.32%. These strains can be dichotomized into mild (<10% aganglionosis) and severe (>10% aganglionosis) groups (Table 4.2; unpublished data, Southard-Smith EM). As the disease-causing mutation remains the same, modifiers elsewhere in the genome are clearly impacting disease presentation.























Table 4.2. Severity of aganglionic phenotype across F₁ crosses with the B6.*Sox10^{Dom}* congenic strain.

Gastrointestinal tracts from postnatal animals (P7-P10) from crosses between various inbred strains and the B6.*Sox10^{Dom}* strain were stained for acetylcholinesterase activity. The percentage of the gut lacking ganglia was determined by comparing the size of the unstained region to the total gut length. Percentages were averaged across 21-67 individuals per cross. Strains were classified as either mild (<10% aganglionosis) or severe (>10% aganglionosis).

Phenotypic Classification	Inbred Strains
Mild	AKR/J, BALB/cByJ, BTBR T+ tf/J, BUB/BnJ, C3H/HeJ, C3HeB/FeJ, C57BR/cdJ, CBA/J, DBA/1J, DBA/2J, KK/HIJ, MA/MyJ, NON/ShiLtJ, NZB/B1NJ, NZO/HILtJ, NZW/LacJ, PL/J, PWD/PhJ, SJL/J, SM/J, SWR/J, WSB/EiJ, ZALENDE/EiJ
Severe	129/SvJ, 129S1/SvImJ, A/J, CAST/EiJ, C57BL/6J, FVB/NJ, LG/J, LP/J, MRL/MpJ, NOD/ShiLtJ, P/J, SEA/GnJ

In order to determine if haplotype within the *Sox10m3* interval was associated with aganglionic severity in strains other than B6 and C3Fe, haplotype within the candidate genes was first analyzed (Figure 4.8). For this analysis, only haplotype at SNPs within the transcript region was considered. The average % aganglionosis for the 35 strains used in the F₁ crosses was the phenotype being tested, with severe strains representing the cases and mild strains representing the controls. Fisher's Exact Test was used to compare each haplotype group against the others for association with phenotypic severity.

Figure 4.8. Association of candidate gene haplotypes with aganglionic severity.

Haplotypes		# of Strains Mildly Affected	# of Strains Severely Affected	p Value
<i>Uchl1</i> (23 SNPs)	 S	4	3	129 = 0.0336
	 S	1	0	
	 S	0	1	
	 S	0	3	
	 ★	1	0	
	 S	17	5	
<i>Phox2B</i> (5 SNPs)	 ★	3	6	B6 = 0.0378
	 S	0	1	
	 S	1	0	C3 = 0.0223
	 ★	19	5	
<i>Atp8a1</i> (166 SNPs)		2	1	None Significant
	 S	1	0	
	 S	0	1	
	 S	1	0	
		1	1	
		1	2	
	 S	1	0	
	 S	1	0	
		8	5	
		1	2	
	 S	1	0	
		5	0	

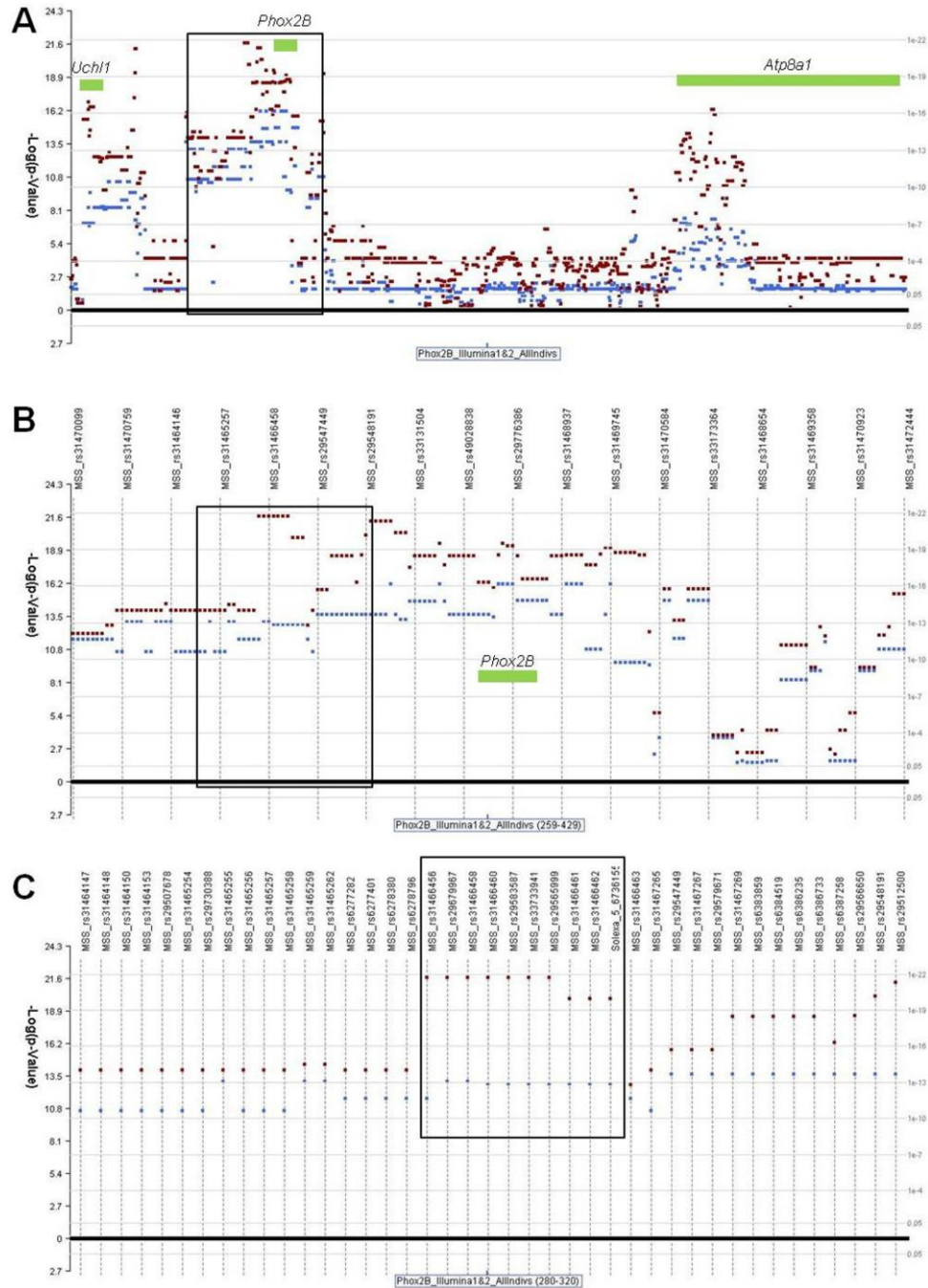
Haplotype at each of the candidate genes within the *Sox10m3* interval was tested for association with aganglionic severity in the F₁ progeny of 35 inbred strains crossed to the B6.*Sox10^{Dom}* line. Haplotypes are represented schematically for the different alleles: B6 (red), C3H (blue), common allele (yellow), and variant allele (orange). Single-strain haplotypes are designated by an "s". Strains were dichotomized into mildly affected (<10% aganglionosis) and severely affected (>10% aganglionosis) groups. Association was tested using Fisher's Exact test; significant haplotypes designated by stars.

At *Uchl1*, six haplotype groups were present in the 35 strains. Fisher's Exact analysis showed that one haplotype at this gene was significantly associated with phenotypic severity (129/SvJ, 129/SvImJ, LP/J; uncorrected $p = 0.0336$). At *Atp8a1*, 12 haplotype groups were present in the 35 strains. Fisher's Exact analysis showed that no haplotypes at this gene were significantly associated with phenotypic severity (lowest uncorrected $p = 0.1412$). At *Phox2B*, four haplotype groups were present in the 35 strains. Fisher's Exact analysis showed that two haplotypes at this gene were significantly associated with phenotypic severity. The B6 haplotype (C57/BL/6J, C57BR/cdJ, BUB/BnJ, FVB/NJ, P/J, 129/SvJ, 129S1/SvImJ, LP/J, SM/J) was associated with phenotypic severity with an uncorrected p value of 0.0378. The C3 haplotype (C3HeB/FeJ, C3H/HeJ, ZALENDE/EiJ, NZO/HILtJ, WSB/EiJ, NZW/LacJ, NOD/ShiLtJ, A/J, AKR/J, BALB/cByJ, BTBR T+ tf/J, LG/J, NON/ShiLtJ, CBA/J, DBA/1J, KK/HIJ, DBA/2J, MA/MyJ, MRL/MpJ, SEA/GnJ, NZB/B1NJ, PL/J, SJL/J, SWR/J) was associated with phenotypic severity with an uncorrected p value of 0.0223. Upon stringent correction for multiple testing (Bonferroni correction, $\alpha = 0.05/\text{number of tests}$; $\alpha=0.008$ for *Uchl1*, 0.013 for *Phox2B*), none of the significant haplotypes retained their statistical significance. However, the *Phox2B* haplotypes displayed the strongest trend toward significance. As the modifier intervals were originally identified in a B6 X C3Fe intercross population, haplotype analysis within the *Sox10m3* interval identifies *Phox2B* as a gene underlying this modifier region.

To further refine the region of *Phox2B* that was the cause of the association, sliding window haplotype analysis was used. 21 individual animals were selected from each of the 35 strains, with the exception of 18 animals for CAST/EiJ, for a total of 732 animals. The individuals were sorted by % aganglionosis, and the extremes of the phenotype distribution were used to increase power to detect an association. 171 animals were identified as controls, with 0% aganglionosis. 105 animals were identified as cases, with $\geq 15\%$ aganglionosis. The algorithm used for this analysis was developed by Kevin Bradley in the laboratory of Dr. Jeffrey Smith.

Sliding window haplotype analysis identified a ten SNP haplotype 3' of *Phox2B* that was highly significantly associated with aganglionic severity ($p = 1.58 \times 10^{-22}$ by χ^2) (Figure 4.9A-C). One haplotype, ATGCCTCGCC, was present in 39 cases and 2 controls, for a p value of 1.53×10^{-21} for risk. Another haplotype, CCGATGTGCC, was present in 34 cases and 156 controls, for a p value of 7.31×10^{-11} for protection. This analysis demonstrates that this region is clearly associated with *Sox10^{Dom}* aganglionosis and may play a role in the regulation of *Phox2B*.

Figure 4.9. Sliding window haplotype analysis in the *Phox2B* genomic region.



(A) Haplotypes across all polymorphic SNPs in the Illumina panel were subjected to sliding window haplotype analysis using both X^2 (red) and logistic regression (blue) analyses. Gene locations are designated by green boxes. **(B)** A closer view of the most significant region designated by the box in **(A)**. **(C)** A single SNP-level view of the most significant region designated by the box in **(B)**. The most significant haplotype, a ten SNP block, is designated by a box.

Discussion

Sequence information at the *Phox2B* locus in strains other than B6, the reference genome for the mouse, is decidedly lacking. As sequence variants between B6 and C3Fe are the most likely cause for the differential expression of *Phox2B* between these two strains, I sought to discover new genetic variation, both within the *Phox2B* locus and the surrounding genomic region. To accomplish this end, C3H BAC clones were sequenced using the Solexa Gene Analyzer. In addition, a large number of other inbred mouse strains were used for high density genotyping in the *Sox10m3* modifier interval to determine if *Phox2B* was associated with aganglionic severity in strains other than B6 and C3Fe. A highly significant haplotype in a region 3' of *Phox2B* was associated with phenotypic severity in a panel of 35 inbred strains. This analysis is consistent with *Phox2B* being a gene within the *Sox10m3* modifier interval and highlights a potential regulatory region that controls expression for further study.

Government-contracted high-throughput sequencing projects have been the main source of information on genetic variation in the mouse. The first major project was completed by Perlegen Life Sciences; 15 inbred mouse strains were sequenced to identify 8.27 million SNPs (7). The strains that were sequenced were: 129S1/SvImJ, A/J, AKR/J, BALB/cByJ, BTBR T+ tf/J, C3H/HeJ, CAST/EiJ, DBA/2J, FVB/NJ, KK/HIJ, MOLF/EiJ, NOD/LtJ, NZW/LacJ, PWD/PhJ, and WSB/EiJ. 4,484 SNPs were typed in our area of interest, encompassing the genomic region from *Uchl1* to *Atp8a1*. However, 491 of them did not produce genotype data for C3H; 49 of these are found within the *Phox2B* BAC region

known to contain necessary regulatory regions (7). However, the Perlegen algorithm was designed to minimize false-positives, thereby maximizing false-negatives; the actual number of SNPs present between these strains is estimated to be 45 million (8). Thus, even though the Perlegen data is impressive, it is still missing the vast majority of SNPs present in mouse genomes.

In parallel, smaller-scale sequencing projects were performed. The Broad Institute genotyped 138,000 SNPs in 49 inbred strains, including C3H (9). In our region of interest, only 13 SNPs were typed, one of which had no allele information for C3H (9). The Wellcome Trust genotyped a very low density panel (13,370 SNPs) in 499 strains that mainly focused on recombinant inbred panels and heterogeneous stock outbred lines (10). The purpose of this study was to create a high-density genetic map.

From the combination of all of these genotyping studies, additional groups imputed the genotypes from the high density panel for the strains genotyped in the low density studies. The genotypes at approximately 7.9 million SNPs in 49 strains were imputed using a Hidden Markov Model (11). However, in the C3H/HeJ strain, of the 941,292 SNPs whose genotype was imputed, only 1,337 of these could be validated. From that validation set, the error rate was approximately 15%; this value varied widely among the inbred strains (11)). Another imputation study also used a Hidden Markov Model to expand the SNP genotype base to 94 strains to create a mouse HapMap (12). In contrast, the error rate in imputation for the C3Fe strain in this study was only 0.065%. This

study generated a map of approximately 6.57 million SNPs (12). While these imputation studies vastly increased the knowledge base of SNP information, they still lack the majority of postulated SNPs in the mouse genome.

By sequencing complete BACs and comparing them to the reference B6 genome, the problem of SNP selection for genotyping was avoided. The majority of variation could be detected; unfortunately, the short length of sequence reads produced by the Solexa Gene Analyzer made it difficult to correctly identify repeat expansions and deletions. Even with these limitations, 35% of the high-quality SNPs identified between B6 and C3H were novel, and 70% of the publicly available SNPs were newly informative for C3H. Therefore, this analysis greatly increased the knowledge base of variation between B6 and C3H in our region of interest.

Nonetheless, the sequence information for other inbred strains in this region was still not dense enough to facilitate association studies. The need to look for association outside of the *Phox2B* locus proper was evident, as more subtle variation in regulatory regions rather than coding changes was likely the cause of the original linkage. The most commonly sequenced inbred strains obviously did not have allele information for the novel SNPs. Even among the publicly available SNPs, the majority of the strains were missing significant numbers of allele calls. Thus, focused genotyping using the Illumina GoldenGate system was chosen to fill in the gaps.

The Illumina panel was designed to cover the top candidates in the *Sox10m3* modifier region. The focus was clearly on *Phox2B* and its surrounding

regions, but SNPs were included for *Uchl1* and *Atp8a1* to provide further evidence that they were *not* the modifier genes. Nonvariant SNPs between B6 and C3H were included to ensure that haplotype formation was not biased by exclusion of rare SNP alleles. Strains were selected based on previous use in the Southard-Smith lab, as well as public availability (and therefore use by other investigators). In addition, a number of wild-derived strains were included to assay the total amount of variation in this region.

A side benefit of designing the Illumina panel was the ability to fine-map the deletion in C3Fe-Tg^{*Phox2B*-H2BCFP} Line C. This subline, nicknamed “Starry Sky,” loses expression of the transgenic reporter after 14.5dpc in the majority of Phox2B⁺ cells. During initial mapping, a deletion was identified 3’ of the transgene. However, due to the wide spacing of the STR markers used for mapping, the size of the deletion was unknown and could range up to 15kb. The close spacing of the SNPs genotyped in the Illumina panel decreased the size of the putative deleted region to 9.5kb. As the complete transgene [Line A, described in Corpening et al. (6)] imparts correct expression, this deleted region must be the cause of the loss of transgene expression and therefore contains a key regulatory element. Analysis of regulatory regions of *Phox2B* has been performed in zebrafish, with a predominant focus on the genomic region 5’ of the gene (13,14). Several smaller deletions (3-4kb) were noted in Line C in the distant 5’ region (45-55kb from the transcript); however, studies in zebrafish have not explored this region. Interestingly, it is possible that the deleted region in Line C corresponds to the +6.7 amplicon shown to promote *Phox2B* expression

by McGaughey et al. (13). Future studies to define the exact boundaries of this deleted region and to test its regulatory functions are necessary.

The process of haplotype grouping in the inbred strains provided interesting results. In particular, the differences from the traditional laboratory mouse phylogenetic tree at the sub-chromosomal level became quite apparent. Some branches held their shape; in particular, AKR/J, LG/J, MRL/MpJ, and RF/J are closely related on the traditional tree, and they maintain this relationship throughout the *Sox10m3* interval. In contrast, 129S1/SvImJ and BTBR T+ tf/J are closely related on the traditional tree but present with vastly different haplotypes throughout the *Sox10m3* interval; the same is true for B6 and YBR/Ei. This analysis demonstrates the importance of focused sequencing in determining the most appropriate group of strains for one's particular region of interest when pursuing phenotypic associations.

In addition, the sheer amount of diversity in the *Sox10m3* interval was astounding. Even when limited to 1536 SNPs over 1.17Mb, 41 haplotype groups were identified in 158 strains. More importantly, 25 of those groups remain when wild-derived strains are removed from the analysis. Combined with the fact that over half of the SNPs identified in the Solexa screen were not used, this region is clearly one of high variation. This variation was maintained in the 35 strains used for haplotype association tests; 18 haplotype groups across the entire interval were present. This region is clearly part of the one-third of the mouse genome that contains 95% of the variation (15); as our parental strains (B6 and C3Fe) are very different, the power to detect an association should be high.

Test of haplotype association with phenotype have been in use in the mouse for over a decade. However, the techniques have significantly improved over the years. The first association test was performed in 2001 by Grupe et al. (16). They tested approximately 3400 SNPs in 15 inbred strains for association with a variety of phenotypes that had previously published QTLs. In all cases, *in silico* mapping confirmed the published QTLs while excluding a vast majority of the mouse genome (16). This type of analysis was refined by Pletcher et al. in 2004, which tested approximately 11,000 SNPs in 48 inbred strains for association with HDL and gallstone phenotypes (17). Haplotype association mapping has since been used to validate and narrow the intervals of known QTLs, as well as identify novel ones (18-21). Combining the results between mouse haplotype association mapping and human genome-wide association studies can provide powerful evidence for the involvement of a locus with a phenotype (22,23). Nonetheless, there is the risk of false positives by using a strict *in silico* approach (24). Thus, the best approach is to combine haplotype association mapping with experimental crosses, as this study has done.

For preliminary analysis, a simple association between candidate gene haplotype and aganglionic severity was tested. As opposed to the large number of haplotype groups in our strain set across the entire interval, the number of groups markedly decreased when haplotype groups were formed in only the transcript regions of our candidate genes. For *Atp8a1*, the candidate gene with the largest number of SNPs, the group number fell to twelve. For *Uchl1*, the next largest SNP number, only six haplotype groups were present. Finally, for

Phox2B, only four haplotype groups could be formed, two of which were composed of single, wild-derived strains. Even with this small number of haplotype groups, preliminary association tests found significant associations between aganglionic severity and both the B6 and C3Fe haplotypes at *Phox2B*.

The strain group used for association analysis was designed for maximum power. Strains were selected to cover the wide breadth of phylogeny within the laboratory mouse field. Indeed, of the 43 priority strains used in Svenson et al. 2007, a gold standard study for QTL analysis, our strain group included 27 (PWK/PhJ is closely related to PWD/PhJ) (25). According to power calculations done by Kirby et al. (12), the use of our strain group imparts approximately 80% power to detect a component that accounts for 5% of the trait variance when the background genetic effect (a measure of the strain relatedness) is 25% across a 10Mb region (12). The power decreases with rising background genetic effect (the strains are more related) and increases with rising trait variance impact (12). However, as our genotyped region is only 1.17Mb, the actual power is likely higher. In addition, the use of only the extremes of the phenotypic distribution also increased the power to detect a statistical association by clearing out the biological “noise” from the middle of the distribution. Thus, this study was primed to find an association if one existed.

Once it was determined that an association could be detected in this strain population, the entire interval was subjected to sliding window haplotype analysis. This algorithm, developed by Kevin Bradley in the laboratory of Dr. Jeffrey Smith, has been used previously in cancer association studies in humans

(26-28). A similar statistical method has also been utilized by other groups (29,30). The benefit of sliding window haplotype analysis, as opposed to single SNP association tests, is that it allows for combinatorial effects.

Sliding windows of 1-10 SNP haplotypes were tested for association with aganglionic severity using both X^2 and unconditional logistic regression tests. The study population was comprised of cases with $\geq 15\%$ aganglionosis and controls with 0% aganglionosis. A 10-SNP haplotype 3' of *Phox2B* proved to be highly significant ($p = 1.58 \times 10^{-22}$ by X^2). Both a risk-conferring haplotype ($p = 1.53 \times 10^{-21}$) and a protection-conferring haplotype ($p = 7.31 \times 10^{-11}$) were found. Simulations by Kirby et al. (12) set the $\alpha = 0.05$ significance level for a 10Mb region at $p = 2 \times 10^{-4}$. Thus, these results retain their significance even after correction.

However, there is a major caveat to this analysis. While model organisms, particularly mice, are powerful tools to explore genetic effects, the inbred nature of the populations can lead to false positive genetic associations due to population structure. This analysis has not been corrected for strain relatedness. There are several methods that can be used to overcome this issue. Efficient mixed-model association (EMMA) is an extension of traditional linear mixed model statistical tests that increases efficiency by removing redundant computations; it has been applied to several organisms, including mouse (31). Another option is permutation testing, which randomly reorganizes the input data to generate a background threshold above which true positives should be readily visible. This approach has been successfully used in the study of mouse

quantitative traits (32). The haplotype association data will need to be corrected for strain relatedness before the veracity of the association can be ascertained.

The region covered by the significant haplotype block contains several peaks of conservation. However, recent studies in zebrafish have shown that conservation is not an infallible indicator of regulatory activity (13,14). Future studies are needed to determine if this region is in fact the cause of the association or if it is simply in LD with the true causative factor. In addition, if this region is indeed associated, studies on its regulatory activity are needed to determine the effect of different haplotypes on *Phox2B* expression.

The importance of this study is wide-reaching. Previous attempts to associate *Phox2B* with HSCR have focused completely on the coding regions of this gene (33,34). It is clear that regulatory regions outside of the locus proper can have significant effects on phenotypic severity. However, current genome-wide association studies utilize SNP chips that predominantly concentrate on coding region variation. If regulatory elements are included, it is almost always confined to the proximal promoter. It is true that variation in these regions is often connected to large disturbances in gene function, thereby allowing an obvious correlation between sequence and phenotype. However, *Phox2B* functions as a modifier; its effects on phenotype are only seen in a sensitized environment. Until studies in humans expand their reach to distant regulatory elements, the effects of modifiers like *Phox2B* in human disease will remain unknown.

In conclusion, sequencing the *Phox2B* genomic region demonstrated that a large amount of variation exists at this locus between B6 and C3H. Newly discovered SNPs were included on a genotyping panel that showcased the genetic diversity among inbred mouse strains. Haplotype association studies in 35 inbred strains demonstrated a significant association between a region 3' of *Phox2B* and aganglionic severity. This region is most likely a regulatory element that controls *Phox2B* expression and solidifies the placement of *Phox2B* as a *Sox10m3* modifier gene.

Materials and Methods

BAC selection. Bacterial artificial chromosomes (BACs) were obtained from Children's Hospital Oakland Research Institute (CHORI). The CHORI-34 Mouse C3H BAC library, generated from the kidney cells of a male C3H mouse, was screened for a sequence in exon three of *Phox2B* (CGCTCCAAAGACCCAACGGTGCCAAAGCCGCCTTAGTGAAGAG). Seven clones were obtained as LB agar stab cultures: 12G6, 87I1, 175O5, 177J14, 246M11, 318H17, and 411P18. The same library was also screened for a sequence in an evolutionarily-conserved region 5' of *Phox2B* (GAAATTTGGCCCGCTTGTGGTGTAAATTCCTCGGAGACGA). Five clones were obtained as LB agar stab cultures: 49H9, 66N11, 260E2, 370E18, and 411P18 (same as previous screening).

BAC purification for STR analysis. Clones were streaked onto LB/chloramphenicol (CAM) plates and incubated overnight at 37°C. Four individual colonies were picked into liquid LB/CAM cultures and incubated overnight at 37°C. BAC DNA was isolated using the Wade-Martins BAC plasmid miniprep protocol. In short, 1.4mL of overnight culture was transferred to a 1.5mL tube, and cells were pelleted by centrifugation at 5,000rpm for ten minutes. The supernatant was removed, and the cell pellet was resuspended in 70uL STET buffer (8% sucrose, 5% Triton X-100, 50mM EDTA, 50mM Tris-HCl). The cells were lysed with 200uL Lysis buffer (1% SDS, 0.2M sodium hydroxide),

and the lysate was neutralized with 150uL 7.5M ammonium acetate. The lysate was incubated on ice for five minutes and then centrifuged at 13,000rpm for 20 minutes at 4°C. The supernatant was transferred to a fresh 1.5mL tube, and 250uL isopropanol was added. The DNA was pelleted by centrifugation at 10,000rpm for eight minutes. The supernatant was removed, and the pellet was washed with 200uL 70% ethanol. The DNA was pelleted by centrifugation again. The supernatant was removed, and the pellet was air-dried for 5-10 minutes. The DNA was resuspended in 50uL TE.

BAC STR analysis. The BAC miniprep DNA samples were diluted to 5ng/uL in water. The diluted BAC DNA was used as a template for PCR using a panel of Simple Tandem Repeat (STR) markers that spanned the genomic region contained by the 95M11 BAC used in the C3Fe-Tg^{Phox2B-H2BCFP} line (6). The primers used for these PCR reactions are listed in Table 4.3. All PCR reactions contained the following: 13uL water, 2uL PCR Buffer, 0.4uL 10mM dNTPs, 0.75uL 6.6uM Forward Primer, 0.75uL 6.6uM Reverse Primer, 0.1uL Taq Polymerase, and 3uL 5ng/uL BAC DNA. Reactions were run in a thermocycler using the following program: 94°C, 5 minutes; 94°C, 30 seconds; 55°C, 30 seconds, 72°C, 30 seconds; repeat steps 2-4 34 times; 72°C, 10 minutes; 4°C, hold. The PCR products were run on non-denaturing acrylamide gels.

Table 4.3. Primers used in BAC STR analysis.

Sequences of primer pairs used to amplify STRs in C3H BACs for quality analysis.

STR	Forward Primer Sequence	Reverse Primer Sequence
5526	CCCTTTGTAAACTGCAAG	CCAAACTCAGAATGCTAGG
12976	TGACCTCTGCTTGACTGAC	CCAAGTCAGTATGCTTGCC
22456	TTTGACTAGAAAGGGCCAG	GAGGAAGAGGGGAAGAAG
22584	CTTCCTCCTCCTCCTCATA	GTCTACAAAGTGAGTTCCAGG
23889	GTCAACAGTGCCTCCTTTA	CTCCTCGTATGGATCCAAG
26158	CTCGATGGTACCTGAATG	GAACATCCTGATGAACTG
26874	GTTACCTAATCAGGGCTGC	CTAAGGCTGATCTAGGCCTT
29480	CAGGCAGACTCTTGGTACTG	CTCAGCAGTAATTCGTTCC
29535	CAGGCAGACTCTTGGTACTG	CTCAGCAGTAATTCGTTCC
33961	GATGGTTTGAGGCAATCAG	CTTTCGGAACATACTGGGA
41563	GTTGCTAGCAGGATGAGC	GGATGTTTCCCTAATAGCAG
45868	GTGGACATCTGCCTACAAAG	CCATCAAGGAAGCTACTGG
55618	CTGGCTACAATCTGGAGAAC	CCTTGGGTACTGTACTGC
55678	CTGGCTACAATCTGGAGAAC	CCTTGGGTACTGTACTGC
57703	GCCCTGATCTATCTTTGTAAG	GTGCTTCACTACCGAAGATG
59157	GACCTTTGACTCAGGATAGC	CTTCCTCCTTCTTCCTCCT
60066	CCTCAGACCTGGAAATGTAT	CTGTATCCTAGCCAGGAAG
60323	CCTGGAAGTTAGAACAACAG	CAAGGTCTAAGCAGTTTGTG
73289	GAGAAGGAGAAGGAGAAGG	GTGTCATGCAAGGCTTC
82604	ACAGTCCTAACTGGCTTGG	GTTATCTGCATAAGACAGGG
86359	GAGCCATACAGGAGCCTT	CTCTGGTCAGGACTTTCTG
89938	CAGACTTCTCAGGGTTCAC	GTAGTTTCCCTGGTGGACA
93572	GAAGCTTACTCCGGGTAGT	CAGCAAGGTTTCTTGTAGA
98202	CAATGGAGTGTAGTTGTAGGG	GCATGAACTGGCTTTGAAC
104680	TATCCATGGAGCCATCAGTC	CACCAGATACTGTCTACTGGC
108411	GTA ACTCCAGCATTGCGAG	CTGAACTCGGGTCTTCTG
109217	GACCCTCAAGTTCTGAGTG	CACTGTCACATACTGTCTCAC
110743	TAAGCATTACAATGCCTCG	GCCCTTCATACATGTACAGC
114258	GCAAAAGTTAGCGCAATCTC	ATTCAGTGAGAGACCTTGTG
116300	ACCACCAGTTGACATCTTC	CTGACCTTAAAGCCGATTG
121398	GCAGCTTGTC AACCAGTTC	GTATGTGAGTGCATGGTGTA
126720	GTATGACCAGTCTAGCCAGC	CACAGATCTAGACATTTTGC
134657	CAATGTGCTTCACTTGAG	CCACCTTGTAAGACCTC
143236	GGTCCATTACATACAGCG	GCTTGCGAACTTAGCC
151156	TCACTCAAAGCTTAGCCTG	CTTTGACATGGACAGATAGC
151560	GACAAACCTGGTTTGCTTG	CTCAAGACAGTACGTGCAA

Table 4.3 Cont'd.

STR	Forward Primer Sequence	Reverse Primer Sequence
153591	ATGAGTTTGAGGTCAGCC	GACTTCAGTGGCAACACTTC
160363	GGTGGCTTACGACTTCAATC	CTGGCCTTGAACAACTCAG
184807	GCAGATGTCTTCCACAGTC	CTTGGTCCTGTAAAGGCTC
187337	AGTGGACTGTTTGAAACTCG	TAGGCTCAGTCAAACAGGC
197849	GTGGCTGCACTCATACATAC	ATGGAGCTACTGTCCCAG
204532	CAGTGAGCATTTCAGGATCA	GCATAGACAGGCAGATTTC

BAC purification for sequence analysis. To generate high-quality DNA, BAC clones were maxiprepmed using the Nucleobond AX500 Kit (now called the Nucleobond BAC 100 Kit; Clontech, 740579). BAC DNA was sequenced using T7 and Sp6 primers to determine the orientation of the insert by the Vanderbilt Sequencing Core.

Cesium chloride DNA extraction. Two 500mL cultures of BAC clones 66N11, 177J14, 370E18, and 411P18 were incubated at 32°C overnight. Cells were pelleted in centrifuge bottles by centrifugation at 6000rpm (all rotor speeds for Sorvall SLA-1500 rotor prior to -80°C incubation) for 10 minutes at 4°C. The pellets were resuspended in 40mL chilled 10mM EDTA pH 8.0 by pipetting. The cells were lysed by adding 40mL 0.2M Sodium Hydroxide/1% SDS, swirling to mix, and incubating at room temperature for five minutes. The lysis was neutralized by adding 40mL chilled 7.5M Potassium Acetate, swirling to mix, and incubating on ice for 30 minutes. The lysate was centrifuged at 10,000rpm at 4°C for 20 minutes. The supernatant was filtered through Whatman #1 circles

(Whatman, 1001125) into fresh centrifuge bottles. An equal volume of isopropanol was added, and the solutions were mixed by inversion.

The DNA was pelleted by centrifugation at 10,000rpm at 4°C for 20 minutes. The supernatant was removed, and the pellet was resuspended in 9mL 10mM Tris-HCl pH 8.0 / 50mM EDTA pH 8.0. The solution was transferred to an Oakridge tube and combined with 4.5mL 7.5M Potassium Acetate. The solution was incubated at -80°C overnight and thawed at room temperature. The solution was centrifuged at 4500rpm (all rotor speeds for Sorvall HB-6 rotor) at 4°C for ten minutes. The supernatant was transferred to a new Oakridge tube, combined with 2.5 volumes of 100% ethanol, and mixed by inversion. The DNA was pelleted by centrifugation at 4500rpm at 4°C for ten minutes. The supernatant was removed, and the pellet was resuspended in 1.3mL 50mM Tris-HCl pH 8.0 / 50mM EDTA pH 8.0.

The DNA solutions from identical clones were pooled into a 14mL tube (Falcon, 352059). 0.5 volumes of phenol were added, and the solution was rocked at room temperature for three minutes. An equal volume (compared to phenol) of chloroform was added, the solution was rocked briefly, and the phases were separated by centrifugation at 4500rpm at 4°C for ten minutes. The aqueous layer was transferred to a new 14mL tube. The DNA was ethanol-precipitated with 0.1 volumes of 3M Sodium Acetate pH 7.0 and 3 volumes of 100% ethanol at -20°C for two hours. The DNA was pelleted at 6000rpm at 4°C for 15 minutes.

The supernatant was removed, and the pellet was resuspended by swirling in 2mL 50mM Tris-HCl pH 8.0 / 25mM EDTA pH 8.0. 9.63g Cesium Chloride was dissolved in a 14mL tube in 6mL 50mM Tris-HCl pH 8.0 / 25mM EDTA pH 8.0 by rolling in hands. The DNA suspension was added and mixed by rolling in hands. 0.8mL 10mg/mL ethidium bromide was added, and the solution was protected from light hereafter. The solution was centrifuged at 3000rpm at 4°C for 10 minutes. The supernatant was transferred to an ultracentrifuge tube (Beckman, 362181) with a Pasteur pipet such that the tube was filled to just below the neck. The tubes were heat-sealed and covered with caps. The tubes were transferred to a Beckman Ti70.1 rotor and spun in an ultracentrifuge at 55,000rpm at 20°C for 16 hours.

The tubes were removed from the rotor and clamped onto a ring stand. The tubes were vented with a 27g needle. The tubes were illuminated with a UV lamp, and the lower (circularized) band was removed using an 18g needle on a 1mL syringe. The DNA solution was transferred to a 15mL conical tube. The ethidium bromide was extracted by adding an equal volume of TE/NaCl-saturated butanol (10mM Tris pH 7.5, 1mM EDTA, 100mM Sodium Chloride), inverting to mix, and discarding the upper layer. This process was repeated at least five times, or until the DNA solution was free of orange color. The DNA was dialyzed in three washes of at least four hours in dialysis buffer (10mM Tris pH 7.4, 1mM EDTA pH 8.0) at 4°C.

CHEF gel analysis. 2ug of AX500-maxiprepped DNA and CsCl-prepped DNA was digested with *NotI* at 37°C for four hours. Each reaction contained the following: 2uL NEBuffer 3, 2uL 10X BSA, 2uL *NotI*, 2ug DNA, and water to a final volume of 20uL. 3.5L of 0.5X TBE Buffer (45mM Tris, 45mM Borate, 1mM EDTA pH 8.3) was prechilled to 14°C in the gel rig. 150mL of 0.5X TBE Buffer was combined with 1.5g Pulsed Field Certified Agarose (Bio-Rad, 162-0137). The agarose was dissolved by boiling. Approximately 140mL of agarose solution was used to pour the gel, which was left at room temperature for 30 minutes to solidify. The remainder of the agarose solution was kept at 55°C. The gel was dry-loaded on the benchtop. The complete restriction digest was loaded into the wells, as well as 1kb DNA Ladder (Invitrogen, 15615-016), Low Range PFG Marker (NEB, N0350S), and MidRange I PFG Marker (NEB, N3551S). The wells were sealed with the conserved agarose solution. The gel was placed in the gel rig, and current was run in a contour-clamped homogenous electrical field for 17 hours at 14°C with circulating buffer. The gel was stained for 30 minutes with 1ug/mL ethidium bromide and destained for 30 minutes with water. The gel was photographed on a UV light box.

Solexa sequencing of BAC clones. BAC clones were combined into pairs for minimal overlap. 3ug of AX500-prepped DNA from BAC Clone 177J14 was combined with 3ug of CsCl-prepped DNA from BAC Clone 370E18. 3ug of AX500-prepped DNA from BAC Clone 411P18 was combined with 3ug of CsCl-prepped DNA from BAC Clone 66N11. The DNA was ethanol-precipitated at -

20°C overnight. The DNA was pelleted by centrifugation at 10,000rpm at 4°C for ten minutes. The supernatant was removed, and the pellet was air-dried for ten minutes. The pellet was resuspended in 5uL 10mM Tris pH 8.0. The DNA was prepared for sequencing by the Vanderbilt Microarray Shared Resource. In brief, the DNA was randomly fragmented and ligated to adapters. The DNA fragments were attached to the flow cell surface and amplified. The sequencing was performed on the Solexa Gene Analyzer by the Vanderbilt Microarray Shared Resource. In brief, a combination of fluorescent reversible terminating nucleotides, DNA polymerase, and primers was added to the flow cell, and the flow cell was scanned to determine the identity of the first base. The terminators were removed, and the process was repeated.

The coverage was ~900X with 35bp sequence reads. The sequence output was aligned to the B6 reference genome for SNP identification (Genome Technology Core), and SNP quality was classified by a ratio of SNP calls to reference calls (Kevin Bradley). The algorithm was designed as follows: $SNPScore1 = (\text{Sum of Most Frequent Alternate Allele Calls} + 1) / (\text{Sum of Reference Allele Calls} + 1)$; $SNPScore2 = SNPScore1 / (\text{Sum of } 2^{\text{nd}} \text{ Most Frequent Alternate Allele Calls} + 1)$; $SNPScoreFinal = SNPScore2 / [3(\text{Sum of Other Alternate Allele Calls} + 1)]$. $SNPScoreFinal$ was used to designate SNP quality: 0 to <5 = Junk, 5 to <20 = Low, 20 to <50 = Medium, and ≥ 50 = High.

Illumina panel design. A 1536-SNP GoldenGate Illumina panel (Illumina,GT-103-1213 and GT-95-205) was designed to genotype 96 inbred strains across

the *Phox2B* region, as well as at *Atp8a1* and *Uchl1*. All SNPs identified by Solexa sequencing, non-variant SNPs in the Solexa region identified by dbSNP, and SNPs within *Atp8a1* and *Uchl1* identified by dbSNP were submitted to Illumina for a ranking of ease of assay design. The most common error code was 340, which labeled adjacent SNPs that were less than 60bp apart. A panel of 1536 SNPs was designed to include 1089 SNPs from the Solexa region (both variant and non-variant), 34 SNPs from *Uchl1*, and 413 SNPs from *Atp8a1*. SNPs from the Solexa region included 386 variant SNPs, 619 non-variant SNPs, and 84 SNPs with missing genotype information for B6 and/or C3H. All SNPs within *Uchl1* were included. SNPs within *Atp8a1* were chosen with a preference for variance between B6 and C3H and equal coverage across the gene. The SNP panel was designed by Kevin Bradley in the laboratory of Dr. Jeffrey Smith.

Illumina DNA selection. 96 mouse strains were selected for genotype analysis on the Illumina panel. 90 inbred strains were chosen based on prior use in the laboratory for phenotype analysis in conjunction with the *Sox10*^{Dom} allele and availability of live mice from the Jackson Laboratory. Four recombinant-inbred strains were chosen based on putative recombination breakpoints within the region of interest. Two individuals from C3Fe-Tg^{Phox2B-H2BCFP} Line C (6) were chosen to further define the deletion 3' of *Phox2B*. A second set of 96 mouse strains was selected for genotype analysis on the second round with the Illumina panel. 72 inbred strains were chosen to maximize the presence of rare alleles within the panel. 18 individuals from different generations of C3Fe-Tg^{Phox2B-}

^{H2BCFP} Line C (6) were chosen to confirm the SNP deletion region identified in Illumina Panel I. Six controls (two samples each from B6, C3Fe, and C3HeB/FeJ-Lea/a) were chosen for quality control.

Illumina DNA quality analysis. DNA samples for the Illumina panel were obtained from liver DNA preparations made previously in the laboratory, the DNA Resource at the Jackson Laboratory (JAX), or the lab of Dr. Robert Williams at UNC-Chapel Hill. The strains used in the panel and the source of the DNA samples are listed in Tables 4.4 and 4.5 (for Illumina Panel I and II, respectively). All samples were diluted to ~10ng/uL and used as template in PCR. All PCR reactions contained the following: 13uL water, 2uL 10X PCR Buffer, 0.4uL 10mM dNTPs, 0.75uL 6.6uM RapSyn Sense Primer (AGGACTGGGTGGCTTCCAACCTCCAGACAC), 0.75uL 6.6uM RapSyn Antisense Primer (AGCTTCTCATTGGTGCGCGCCAGGTTTCAGG), 0.1uL Taq Polymerase, and 3uL 10ng/uL DNA. PCR products were run on non-denaturing acrylamide gels.

All samples were also diluted to ~250ng/uL for PicoGreen concentration analysis, which was performed by Joan Breyer in the laboratory of Jeff Smith. Serial dilutions in TE (10mM Tris, 1mM EDTA, pH 7.4; Accugene, 51235) at 1:55, 1:550, and 1:5500 were made of the 250ng/uL stock. 5uL of each dilution was transferred to a well in a 384-well black plate. 5uL Quant-iT PicoGreen (Invitrogen, P7589) DNA dye diluted 1:200 in TE was added to the solutions, and the plate was incubated in the dark for five minutes. The fluorescence intensity

was read on a LJL Analyst (Molecular Devices, 0200-6044). The concentrations of the experimental DNA samples were determined by comparison to a standard curve of λ DNA (8.70ng/mL, 15.23ng/mL, 26.66ng/mL, 81.63ng/mL, 142.86ng/mL, and 250ng/mL).

Table 4.4. Mouse strains used in Illumina Panel I.
Strain information and source for strains genotyped in Illumina Panel I.

Strain Name	JAX Stock #	Source
C3H/HeJ	000659	JAX Prep
C57BL/6J	000664	Lab Liver Prep
DBA/2J	000671	JAX Prep
A/J	000646	JAX Prep
AKR/J	000648	JAX Prep
C3HeB/FeJ	000658	Lab Liver Prep
SJL/J	000686	JAX Prep
MRL/MpJ	000486	JAX Prep
LP/J	000676	JAX Prep
PL/J	000680	JAX Prep
BTBR T+ tf/J	002282	JAX Prep
NZW/LacJ	001058	JAX Prep
SM/J	000687	JAX Prep
BUB/BnJ	000653	JAX Prep
LG/J	000675	JAX Prep
NOD/ShiLtJ	001976	JAX Prep
129S1/SvImJ	002448	JAX Prep
129/SvJ	000691	JAX Prep
NZO/HILtJ	002105	JAX Prep
129P3/J	000690	JAX Prep
A/HeJ	000645	JAX Prep
ALR/Lt	003070	JAX Prep
ALS/Lt	003072	JAX Prep
BALB/cByJ	001026	JAX Prep
BALB/cJ	000651	JAX Prep
C3H/HeOuj	000635	JAX Prep
C57BL/10J	000665	JAX Prep

Table 4.4 Cont'd.

Strain Name	JAX Stock #	Source
C57BL/10SnJ	000666	JAX Prep
C57BL/6NJ	005304	JAX Prep
C57BLKS/J	000662	JAX Prep
C57BR/cdJ	000667	JAX Prep
C57L/J	000668	JAX Prep
CBA/CaJ	000654	JAX Prep
CBA/J	000656	JAX Prep
CE/J	000657	JAX Prep
DBA/1J	000670	JAX Prep
DBA/1LacJ	001140	JAX Prep
FVB/NJ	001800	JAX Prep
KK/HIJ	002106	JAX Prep
MA/MyJ	000677	JAX Prep
NON/ShiLtJ	002423	JAX Prep
NOR/LtJ	002050	JAX Prep
SWR/J	000689	JAX Prep
TALLYHO/JngJ	005314	JAX Prep
WSB/EiJ	001145	JAX Prep
129P1/ReJ	001137	JAX Prep
129T2/SvEmsJ	002065	JAX Prep
A/WySnJ	000647	JAX Prep
Au/SsJ	000649	JAX Prep
BDP/J	000652	JAX Prep
BPH/2J	003005	JAX Prep
BPL/1J	003006	JAX Prep
BPN/3J	003004	JAX Prep
C57BL/10ScN	003752	JAX Prep
C57BL/10ScSn	000476	JAX Prep
C57BL/6JEiJ	000924	JAX Prep
C58/J	000669	JAX Prep
CBA/CaGnLe	001143	JAX Prep
CD3/J1sJ	006177	JAX Prep
CD7/J1sJ	006178	JAX Prep
CD9/J1sJ	006179	JAX Prep
DDY/Jc1DidSeyFrkJ	002243	JAX Prep
I/LnJ	000674	JAX Prep
NZL/LtJ	005067	JAX Prep
NZM2410/J	002676	JAX Prep

Table 4.4 Cont'd.

Strain Name	JAX Stock #	Source
RBF/Dn	000611	JAX Prep
RIII/ImrNhsJ	005221	JAX Prep
RIIS/J	000683	JAX Prep
SEA/GnJ	000644	JAX Prep
SOD1/Ei	001224	JAX Prep
BALB/cWtWi	001311	JAX Prep
BXA12/PgnJ	001700	JAX Prep
C3H/HeJBirLtJ	005972	JAX Prep
CHMU/LeJ	000293	JAX Prep
DA/HuSn	000660	JAX Prep
DBA/8BiDsm	002860	JAX Prep
EL/SuzSeyFrkJ	001956	JAX Prep
FL/1Re	000023	JAX Prep
HTG/GoSfSn	000556	JAX Prep
LPT/LeJ	000220	JAX Prep
NH/KiPt	003091	JAX Prep
PN/nBSwUmabJ	005052	JAX Prep
PRO/Re	000059	JAX Prep
RF/J	000682	JAX Prep
SB/LeJ	000269	JAX Prep
SENCARA/PtJ	002746	JAX Prep
SI/Col Tyrp1 Dnahc11<iv>/J	001045	JAX Prep
YBR/Ei	000933	JAX Prep
P/J	000679	Lab Liver Prep
Zalende/EiJ	001392	JAX Prep
Phox2B-CFP Line C #1 (11528)	---	Lab Liver Prep
Phox2B-CFP Line C #2 (12008)	---	Lab Tail Prep
129SvEvTac	---	Lab Tail Prep
BXD43 F	---	Lab Tail Prep
BXD100 F	---	Lab Tail Prep
BXD78 F	---	RW Prep

Table 4.5. Mouse strains used in Illumina Panel II.
Strain information and source for strains genotyped in Illumina Panel II.

Strain Name	JAX Stock #	Source
Phox2bLineC - N2, 7830	--	Lab Tail Prep
Phox2bLineC - N2, 7835	--	Lab Tail Prep
Phox2bLineC - N3, 8484	--	Lab Tail Prep
Phox2bLineC - N3, 1340 E5	--	Lab Tail Prep
Phox2bLineC - N4, 8645	--	Lab Tail Prep
Phox2bLineC - N4, 1387 A5	--	Lab Tail Prep
Phox2bLineC - N5, 8703	--	Lab Tail Prep
Phox2bLineC - N5, 8829	--	Lab Tail Prep
Phox2bLineC - N6, 9287	--	Lab Tail Prep
Phox2bLineC - N6, 1492 B1	--	Lab Tail Prep
Phox2bLineC - N7, 10197	--	Lab Tail Prep
Phox2bLineC - N7, 1644 C4	--	Lab Tail Prep
Phox2bLineC - N8, 11074	--	Lab Tail Prep
Phox2bLineC - N8, 11073	--	Lab Tail Prep
Phox2bLineC - N9, 1918 A2	--	Lab Tail Prep
Phox2bLineC - N9, 1918 A3	--	Lab Tail Prep
Phox2bLineC - N10, 12897	--	Lab Tail Prep
Phox2bLineC - N10, 2076 D2	--	Lab Tail Prep
BALB/cAnLil	002846	JAX
BALB/cBiDsm MMTV<->	002861	JAX
BALB/cBy	000650	JAX
BALB/cGa	001905	JAX
BALB/cGrLs	001751	JAX
BALB/cGrRk	000921	JAX
BALB/cWt	000922	JAX
C57BL/6By	000663	JAX
C57BL/6ByJ	001139	JAX
CBA/JLs	000705	JAX
CD10/J1sJ	006180	JAX
CIN/Ls	002179	JAX
DBA/2DeJ	000052	JAX
DBA/2J-Gpnmbs<+>/SjJ	007048	JAX
DBA/HaSmn	000973	JAX
FL/4ReJ	000025	JAX
GR/J	006131	JAX
HP/EiTy	000337	JAX

Table 4.5 Cont'd.

Strain Name	JAX Stock #	Source
IDH2/Ei	000633	JAX
IS/Cam Ei	000925	JAX
LDH2/Ei	001266	JAX
LT/ChRe	000111	JAX
LT/ChReSv	000398	JAX
LT/SvEi	003588	JAX
LT/SvEiJ	006252	JAX
NOD/Lt	001289	JAX
NON	001290	JAX
NOR/Lt	001761	JAX
NZB/B1NJ	000684	JAX
NZM2328/J	002706	JAX
NZM391/J	003108	JAX
NZM64/J	002673	JAX
NZM88/J	002808	JAX
NZO/H1Lt	002589	JAX
PRO/Re-Pro-1<a>	000173	JAX
RBF/DnJ	000726	JAX
RIII/DmMob	001088	JAX
SEC/1ReJ	000685	JAX
SENCARB/PtJ	002747	JAX
SENCARC/PtJ	002748	JAX
SESV/Ei	001204	JAX
SJL/Bm	001902	JAX
SJL/Wt	001097	JAX
ST/bJ	000688	JAX
SWR/Bm	001900	JAX
VM/Dk	001524	JAX
WB/Re	000175	JAX
ZRDCT Rax<+>/ChUmdJ	005005	JAX
CALB/Rk	001489	JAX
CAST/EiJ	000928	JAX
CZECHI/EiJ	002799	JAX
CZECHII/EiJ	001144	JAX
IS/CamRk	000573	JAX
JF1/Ms	003720	JAX
LEWES/Ei	002798	JAX

Table 4.5 Cont'd.

Strain Name	JAX Stock #	Source
MOLF/EiJ	000550	JAX
MOLG/DnJ	000555	JAX
MSM/Ms	003719	JAX
Mus caroli/EiJ	000926	JAX
Mus pahari/Ei	002655	JAX
PANCEVO/Ei	001384	JAX
PERA/EiJ	000930	JAX
PERC/EiJ	001307	JAX
PWK/PhJ	003715	JAX
RBA/DnJ	000874	JAX
RBB/Dn	000609	JAX
SF/CamEi	000280	JAX
SKIVE/EiJ	001393	JAX
SPRET/EiJ	001146	JAX
TIRANO/EiJ	000929	JAX
WMP/Pas	001746	JAX
PWD/PhJ	004660	Lab Liver Prep
C57BL/6J 4-5-00	--	Lab Liver Prep
C57BL/6J 10-16-07	--	Lab Liver Prep
C3HeB/FeJ 4-5-00	--	Lab Liver Prep
C3HeB/FeJ 4-17-08	--	Lab Liver Prep
C3HeB/FeJ-Lea/a 2-24-05	--	Lab Liver Prep
C3HeB/FeJ-Lea/a 6-7-01	--	Lab Liver Prep

Illumina panel genotyping. Experimental strain DNA samples were diluted to 50ng/uL using the PicoGreen-determined concentrations from the ~250ng/uL stocks. Illumina genotyping was performed by Joan Breyer in the laboratory of Dr. Jeffrey Smith. DNA was activated using the Illumina Single Use DNA Activation protocol (Illumina, GT-95-201). In short, biotin was incorporated into the DNA in a non-biased fashion, and unincorporated biotin was removed. Activated DNA was hybridized to the oligonucleotide pool assay (OPA) by

binding the biotinylated DNA to streptavidin beads and then binding the primers to the DNA. Mismatched primers were removed, and the allele-specific and locus-specific primers were extended and ligated together. The ligated oligos were amplified using PCR. The amplified DNA was hybridized to the array using the Sentrix Array Matrices (SAM) hybridization cartridge. The SAM was imaged using a BeadArray reader (Illumina). Genotypes were called by multiple viewers using Bead Reader software (Illumina). SNPs were discarded if the call rate was less than 82%. Heterozygous calls for all strains other than the Phox2B-CFP Line C samples were discarded.

Haplotype Generation. The genotype data for the 158 inbred strains was sorted by genomic position. All non-variant SNPs were removed from the dataset. SNP alleles were colored for greater ease of sorting (B6/C3H variant SNPs: red = B6 allele, blue = C3H allele; B6/C3H non-variant SNPs: yellow = B6/C3H shared allele, orange = rare variant allele). Haplotype groups were assigned by visual inspection of the dataset.

Haplotype Analysis. For simple association tests between phenotypic severity and haplotype at a candidate gene, 35 strains were dichotomized into mildly affected (<10% total aganglionosis) and severely affected (>10% total aganglionosis) based on strain mean values. Strain mean values were generated from dissections performed by Shelley Stein, Alex Nickle, Stacy Rogers, Jean-Marc DeKeyser; all data was collated by Jean-Marc DeKeyser in

the Southard-Smith Laboratory. Haplotype groups were assigned by visual inspection of SNPs within the gene transcript (*Uchl1*, 23 SNPs; *Phox2B*, 5 SNPs; *Atp8a1*, 166 SNPs). Fisher's exact tests were used to assess association. Statistics were performed using the GraphPad QuickCalcs web interface (<http://www.graphpad.com/quickcalcs/index.cfm>). For sliding window haplotype analysis, 732 individual animals, 21 per strain except for CAST/EiJ, were sorted by % aganglionosis. The extremes of the phenotypic spread were used to increase power to detect an association. Controls were classified as 0% aganglionosis; 171 animals were in this category. Cases were classified as $\geq 15\%$ aganglionosis; 105 animals were in this category. Genotypes at all SNPs in the Illumina panel that passed QC for both panels (1426 SNPs) were uploaded to the Association Test 2 algorithm developed by Kevin Bradley in the laboratory of Dr. Jeffrey Smith. Genotypes were classified as X/Y data, as all genotypes were homozygous. A sliding window of 1-10 SNP haplotypes was tested for association with aganglionosis using either X^2 or unconditional logistic regression statistics.

References

1. Waterston,R.H., Lindblad-Toh,K., Birney,E., *et al.* (2002) Initial sequencing and comparative analysis of the mouse genome. *Nature*, **420**, 520-562.
2. Petkov,P.M., Graber,J.H., Churchill,G.A., *et al.* (2005) Evidence of a large-scale functional organization of mammalian chromosomes. *PLoS. Genet.*, **1**, e33.
3. Park,Y.G., Zhao,X., Lesueur,F., *et al.* (2005) Sipa1 is a candidate for underlying the metastasis efficiency modifier locus Mtes1. *Nat. Genet.*, **37**, 1055-1062.
4. Wang,X., Ria,M., Kelmenson,P.M., *et al.* (2005) Positional identification of TNFSF4, encoding OX40 ligand, as a gene that influences atherosclerosis susceptibility. *Nat. Genet.*, **37**, 365-372.
5. Owens,S.E., Broman,K.W., Wiltshire,T., *et al.* (2005) Genome-wide linkage identifies novel modifier loci of aganglionosis in the Sox10Dom model of Hirschsprung disease. *Hum. Mol. Genet.*, **14**, 1549-1558.
6. Corpening,J.C., Cantrell,V.A., Deal,K.K., *et al.* (2008) A Histone2BCerulean BAC transgene identifies differential expression of Phox2b in migrating enteric neural crest derivatives and enteric glia. *Dev. Dyn.*, **237**, 1119-1132.
7. Frazer,K.A., Eskin,E., Kang,H.M., *et al.* (2007) A sequence-based variation map of 8.27 million SNPs in inbred mouse strains. *Nature*, **448**, 1050-1053.
8. Yang,H., Bell,T.A., Churchill,G.A., *et al.* (2007) On the subspecific origin of the laboratory mouse. *Nat. Genet.*, **39**, 1100-1107.
9. Wade,C.M., Daly,M.J. (2005) Genetic variation in laboratory mice. *Nat. Genet.*, **37**, 1175-1180.
10. Shifman,S., Bell,J.T., Copley,R.R., *et al.* (2006) A high-resolution single nucleotide polymorphism genetic map of the mouse genome. *PLoS. Biol.*, **4**, e395.
11. Szatkiewicz,J.P., Beane,G.L., Ding,Y., *et al.* (2008) An imputed genotype resource for the laboratory mouse. *Mamm. Genome*, **19**, 199-208.
12. Kirby,A., Kang,H.M., Wade,C.M., *et al.* (2010) Fine mapping in 94 inbred mouse strains using a high-density haplotype resource. *Genetics*, **185**, 1081-1095.

13. McGaughey,D.M., Vinton,R.M., Huynh,J., *et al.* (2008) Metrics of sequence constraint overlook regulatory sequences in an exhaustive analysis at phox2b. *Genome Res.*, **18**, 252-260.
14. McGaughey,D.M., Stine,Z.E., Huynh,J.L., *et al.* (2009) Asymmetrical distribution of non-conserved regulatory sequences at PHOX2B is reflected at the ENCODE loci and illuminates a possible genome-wide trend. *BMC. Genomics*, **10**, 8.
15. Wade,C.M., Kulbokas,E.J., III, Kirby,A.W., *et al.* (2002) The mosaic structure of variation in the laboratory mouse genome. *Nature*, **420**, 574-578.
16. Grupe,A., Germer,S., Usuka,J., *et al.* (2001) In silico mapping of complex disease-related traits in mice. *Science*, **292**, 1915-1918.
17. Pletcher,M.T., McClurg,P., Batalov,S., *et al.* (2004) Use of a dense single nucleotide polymorphism map for in silico mapping in the mouse. *PLoS. Biol.*, **2**, e393.
18. Liu,P., Vikis,H., Lu,Y., *et al.* (2007) Large-scale in silico mapping of complex quantitative traits in inbred mice. *PLoS. One.*, **2**, e651.
19. Leme,A.S., Berndt,A., Williams,L.K., *et al.* (2010) A survey of airway responsiveness in 36 inbred mouse strains facilitates gene mapping studies and identification of quantitative trait loci. *Mol. Genet. Genomics*, **283**, 317-326.
20. Lightfoot,J.T., Turner,M.J., Pomp,D., *et al.* (2008) Quantitative trait loci for physical activity traits in mice. *Physiol Genomics*, **32**, 401-408.
21. Lightfoot,J.T., Leamy,L., Pomp,D., *et al.* (2010) Strain screen and haplotype association mapping of wheel running in inbred mouse strains. *J. Appl. Physiol*, **109**, 623-634.
22. Tang,P.L., Cheung,C.L., Sham,P.C., *et al.* (2009) Genome-wide haplotype association mapping in mice identifies a genetic variant in CER1 associated with BMD and fracture in southern Chinese women. *J. Bone Miner. Res.*, **24**, 1013-1021.
23. Tsaih,S.W., Pezzolesi,M.G., Yuan,R., *et al.* (2010) Genetic analysis of albuminuria in aging mice and concordance with loci for human diabetic nephropathy found in a genome-wide association scan. *Kidney Int.*, **77**, 201-210.

24. Burgess-Herbert,S.L., Tsaih,S.W., Stylianou,I.M., *et al.* (2009) An experimental assessment of in silico haplotype association mapping in laboratory mice. *BMC. Genet.*, **10**, 81.
25. Svenson,K.L., Von,S.R., Magnani,P.A., *et al.* (2007) Multiple trait measurements in 43 inbred mouse strains capture the phenotypic diversity characteristic of human populations. *J. Appl. Physiol*, **102**, 2369-2378.
26. Yaspan,B.L., Breyer,J.P., Cai,Q., *et al.* (2007) Haplotype analysis of CYP11A1 identifies promoter variants associated with breast cancer risk. *Cancer Res.*, **67**, 5673-5682.
27. Yaspan,B.L., McReynolds,K.M., Elmore,J.B., *et al.* (2008) A haplotype at chromosome Xq27.2 confers susceptibility to prostate cancer. *Hum. Genet.*, **123**, 379-386.
28. Breyer,J.P., McReynolds,K.M., Yaspan,B.L., *et al.* (2009) Genetic variants and prostate cancer risk: candidate replication and exploration of viral restriction genes. *Cancer Epidemiol. Biomarkers Prev.*, **18**, 2137-2144.
29. Fallin,D., Cohen,A., Essioux,L., *et al.* (2001) Genetic analysis of case/control data using estimated haplotype frequencies: application to APOE locus variation and Alzheimer's disease. *Genome Res.*, **11**, 143-151.
30. Mathias,R.A., Gao,P., Goldstein,J.L., *et al.* (2006) A graphical assessment of p-values from sliding window haplotype tests of association to identify asthma susceptibility loci on chromosome 11q. *BMC. Genet.*, **7**, 38.
31. Kang,H.M., Zaitlen,N.A., Wade,C.M., *et al.* (2008) Efficient control of population structure in model organism association mapping. *Genetics*, **178**, 1709-1723.
32. Bell,T.A., Casa-Esperon,E., Doherty,H.E., *et al.* (2006) The paternal gene of the DDK syndrome maps to the Schlafen gene cluster on mouse chromosome 11. *Genetics*, **172**, 411-423.
33. Garcia-Barcelo,M., Sham,M.H., Lui,V.C., *et al.* (2003) Association study of PHOX2B as a candidate gene for Hirschsprung's disease. *Gut*, **52**, 563-567.
34. Liu,C.P., Li,X.G., Lou,J.T., *et al.* (2009) Association analysis of the PHOX2B gene with Hirschsprung disease in the Han Chinese population of Southeastern China. *J. Pediatr. Surg.*, **44**, 1805-1811.

CHAPTER V

EFFECT OF STRAIN-SPECIFIC ALLELES OF *PHOX2B* ON ENS DEVELOPMENT

Introduction

The final, and most biologically relevant, characteristic of modifier loci is their ability to modulate a phenotype in conjunction with a disease-causing mutation that significantly differs from the phenotype of either the initial mutation or the modifier alone (1). In some cases, the modifier allele itself has little to no phenotype. It is only in the presence of the predisposing allele that its effect is realized. The threshold for phenotypic presentation is lowered enough such that the effect of the modifier is visible.

Phenotypic alteration due to a modifier has previously been shown by combining the *EdnrB^{s-l}* allele with the *Sox10^{Dom}* allele (2). *EdnrB^{s-l/s-l}* mice present with aganglionosis in a short portion of the distal colon (3)). It was demonstrated that the B6 allele at *EdnrB* was associated with phenotypic severity in a large B6C3Fe pedigree. In addition, *EdnrB^{s-l/s-l};Sox10^{Dom/+}* mice were significantly more affected with aganglionosis than *EdnrB^{s-l/+};Sox10^{Dom/+}* or *EdnrB^{+/+};Sox10^{Dom/+}* mice (2). Thus, *EdnrB* is a modifier of *Sox10^{Dom}* aganglionosis and corresponds to the *Sox10m1* modifier region identified by Owens et al. (4).

In order to explore the effects of combining mutant alleles at *Phox2B* with the *Sox10^{Dom}* allele, we utilized the *Phox2B^{LacZ}* allele (5). Homozygotes lack components of the enteric nervous system past the stomach due to early apoptosis of neural crest-derived cells that arrive in the foregut. They also lack expression of key genes involved in formation of neural crest-derived structures, including *Ret*, *Mash1*, and *Sox10*. In contrast, heterozygotes display no morphological abnormalities and are born in Mendelian proportions (5).

Previous studies by the Southard-Smith laboratory have demonstrated that *Sox10^{Dom/+};Phox2B^{LacZ/+}* double mutants display strain-specific modification of aganglionosis compared to single mutants when analyzed postnatally (Southard-Smith EM, unpublished data) through the use of a quantitative complementation test-cross (6). Double mutants on the C3Fe background are very similar to *Sox10^{Dom/+};Phox2B^{+/+}* animals. Thus, hemizyosity at *Phox2B* when the C3Fe allele is present does not affect aganglionosis. In stark contrast, the addition of the *Phox2B^{LacZ}* allele on the B6 background is highly detrimental. Double mutants are significantly more affected than single mutants; therefore, hemizyosity of the B6 allele of *Phox2B* is the cause of the increased severity of aganglionosis. Thus, *Phox2B* displays a strain-specific modifying effect on the severity of *Sox10^{Dom}* aganglionosis.

However, the modifying action of *Phox2B* has not been studied in a developmental context. As postnatal aganglionosis originates during development, we sought to understand the role of *Phox2B* during the early stages of ENS ontogeny. The processes of ENP migration, proliferation, and

early patterning were assayed in the progeny of crosses between the congenic *Sox10^{Dom}* strains and *Phox2B^{LacZ}* mice. We determined that strain-specific alleles at *Phox2B* have a significant effect on ENP migration. Consistent with prior studies, *Phox2B* hemizyosity had no effect on ENP proliferation. Allele-specific effects of *Phox2B* were also seen in early foregut patterning. Our studies provide significant evidence that *Phox2B* is a modifier of *Sox10^{Dom}* aganglionosis and that strain-specific differences in this locus partially explain the differences in severity and penetrance seen in the B6 and C3Fe congenic *Sox10^{Dom}* lines.

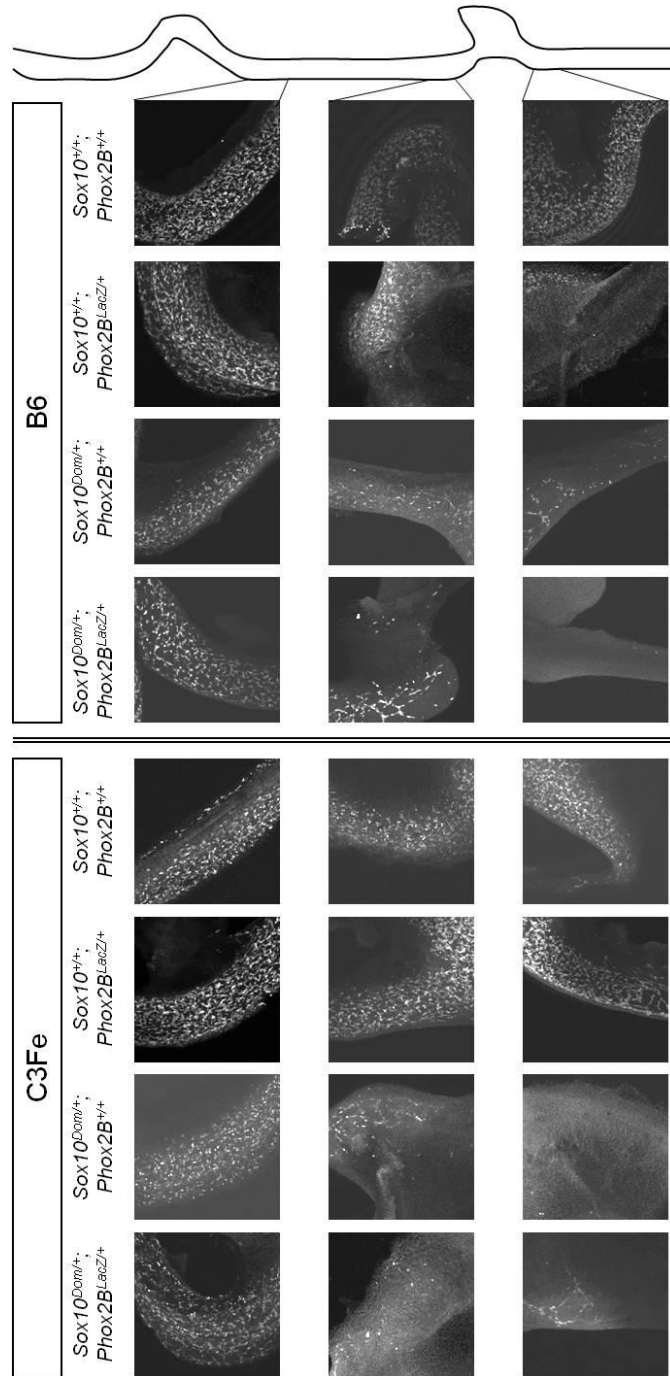
Results

Hemizyosity at *Phox2B* impacts the effects of the *Sox10^{Dom}* allele and strain background on ENP migration.

Previous studies have shown that the *Sox10^{Dom}* allele has a negative effect on the migration of ENPs down the developing gastrointestinal tract. In addition, this effect is modulated by strain background, with a more severe deficit in the B6 genetic background (7). Thus, genetic modifiers that differ between B6 and C3Fe play a role in ENP migration.

To determine if *Phox2B* impacted this developmental process, ENP migration was assayed in B6D2.*Phox2B^{LacZ/+}* X B6.*Sox10^{Dom/+}* and B6D2.*Phox2B^{LacZ/+}* X C3Fe.*Sox10^{Dom/+}* embryos. For brevity, strain background will be referred to as either B6 or C3Fe. 12.5dpc fetal gastrointestinal tracts were immunostained for *Phox2B*, a known marker of all early ENPs (8), to quantify the extent of migration. Representative confocal images behind the migratory wavefront, immediately proximal to the caecum, and immediately distal to the caecum in individual gut samples were captured (Figure 5.1). The density of *Phox2B⁺* ENPs in eight equally-sized regions was assigned on a four-point scale by an observer blinded to embryo genotype.

Figure 5.1. Effect of *Phox2B* hemizyosity in conjunction with the *Sox10^{Dom}* allele and strain background on ENP migration.



Density and migration of ENPs can be seen in whole-mount 12.5dpc fetal guts by immunohistochemical staining for Phox2B. Confocal images (200X magnification) taken in the proximal foregut, before the caecum, and after the caecum are shown in relation to a schematic diagram of the developing gut. Image panels from representative single guts are shown for each genotypic class.

Wild-type (*Sox10*^{+/+};*Phox2B*^{+/+}) embryos of either strain background displayed dense staining due to numerous *Phox2B*⁺ ENPs through the foregut and caecum. The density of *Phox2B*⁺ ENPs gradually declined in the hindgut where wave-front progenitors were populating the distal intestine (Table 5.1). This staining pattern was also seen in all *Sox10*^{+/+};*Phox2B*^{LacZ/+} embryos, confirming earlier reports that did not find gastrointestinal defects in heterozygotes (5) (Table 5.1). As previously detailed in congenic studies (7), *Sox10*^{Dom/+};*Phox2B*^{+/+} embryos of both strain backgrounds exhibited notably decreased *Phox2B*⁺ ENP staining with a marked reduction in extent of migration down the gut length and decreased density of *Phox2B*⁺ cells in the areas that were populated.

Contrary to prior studies, the extent of migration and density of ENPs in this genotypic class were similar between the B6 and C3Fe strains (Table 5.1). This is most likely to the “dilution” of the C3Fe background caused by the introduction of B6 genetic components. However, the disparate effects of genetic background were clearly visible in the *Sox10*^{Dom/+};*Phox2B*^{LacZ/+} embryos. Those on the B6 background were even more severely affected than the B6.*Sox10*^{Dom/+};*Phox2B*^{+/+} embryos. Double mutants had approximately half the extent of migration and one-third the cell density as the single mutants (Table 5.1). In contrast, the C3Fe.*Sox10*^{Dom/+};*Phox2B*^{LacZ/+} embryos were roughly comparable, both in extent of migration and cell density, to C3Fe.*Sox10*^{Dom/+};*Phox2B*^{+/+} embryos. Therefore, hemizyosity at *Phox2B*

negatively impacts ENP migration in a strain background-specific manner that is consistent with the effect of the *Sox10^{m3}* modifier.

Table 5.1. Effect of *Phox2B* hemizyosity in conjunction with the *Sox10^{Dom}* allele and strain background on ENP migration.

Density of *Phox2B*⁺ cells was quantified on a four-point scale (1 = least dense, 4 = most dense) in eight equal-sized gut sections. Scores for individual guts and averages are shown (n≥6). The following coloring system was applied: 0.0-0.4 = white, 0.5-1.4 = light gray, 1.5-2.4 = medium gray, 2.5-3.4 = dark gray, and 3.5-4.0 = black.

Genotypic Class	Density of Progenitor Cells along Gut							
	1	2	3	4	5	6	7	8
B6. <i>Sox10^{+/+}</i> ; <i>Phox2B^{+/+}</i>								
Average	4.0	4.0	3.9	3.3	2.7	2.0	1.0	0.5
C3Fe. <i>Sox10^{+/+}</i> ; <i>Phox2B^{+/+}</i>								
Average	4.0	4.0	4.0	3.9	2.9	2.2	1.0	0.0
B6. <i>Sox10^{+/+}</i> ; <i>Phox2B^{LacZ/+}</i>								
Average	4.0	4.0	4.0	3.4	2.3	1.9	1.0	0.2
C3Fe. <i>Sox10^{+/+}</i> ; <i>Phox2B^{LacZ/+}</i>								
Average	4.0	4.0	4.0	3.6	3.0	1.7	0.7	0.0
B6. <i>Sox10^{Dom/+}</i> ; <i>Phox2B^{+/+}</i>								
Average	3.4	2.8	1.7	0.7	0.2	0.2	0.1	0.0
C3Fe. <i>Sox10^{Dom/+}</i> ; <i>Phox2B^{+/+}</i>								
Average	3.1	2.3	1.4	0.3	0.1	0.1	0.0	0.0
B6. <i>Sox10^{Dom/+}</i> ; <i>Phox2B^{LacZ/+}</i>								
Average	1.9	1.2	0.3	0.0	0.0	0.0	0.0	0.0
C3Fe. <i>Sox10^{Dom/+}</i> ; <i>Phox2B^{LacZ/+}</i>								
Average	3.3	2.7	1.1	0.2	0.1	0.1	0.0	0.0

Hemizyosity at Phox2B has no impact on ENP proliferation.

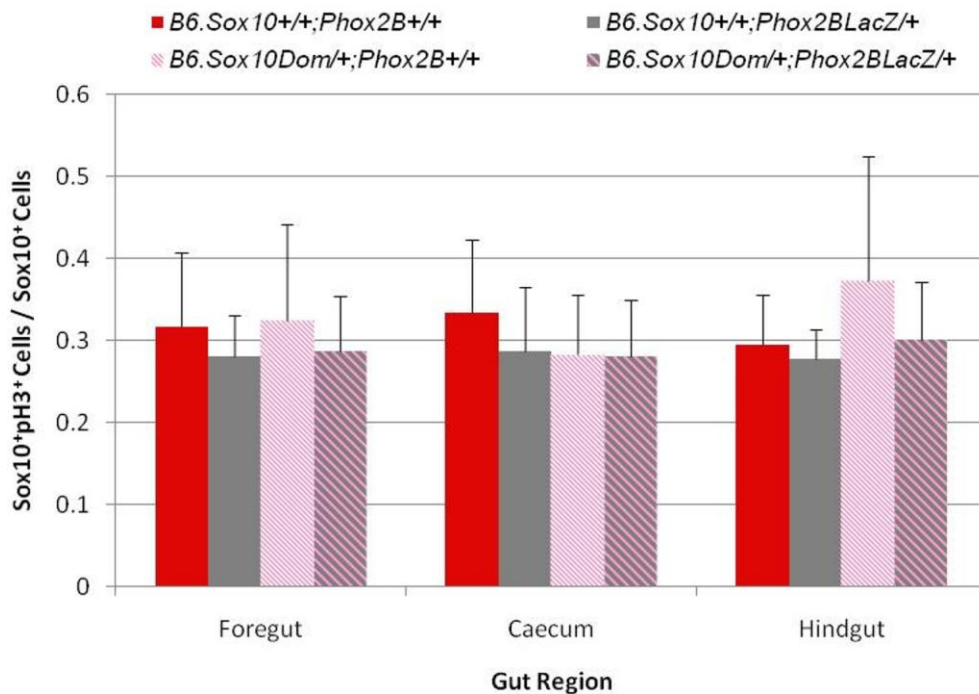
Previous studies have shown that neither the *Sox10^{Dom}* allele nor strain background affect ENP proliferation (7). However, it remains possible that loss of one allele of *Phox2B* could impact proliferation in the sensitized *Sox10^{Dom}* environment. As the B6 strain background is more severely affected, this analysis was undertaken in this strain only to increase the possibility of detecting an effect.

To determine if *Phox2B* affected ENP proliferation, this developmental process was assayed in B6D2.*Phox2B^{LacZ/+}* X B6.*Sox10^{Dom/+}* embryos. To identify proliferating ENPs, I implemented immunocytochemical detection of Sox10, which labels all ENPs, and phospho-Histone H3 (pH3), a known marker of proliferating cells, and specifically quantified the fraction undergoing mitosis. Cells were dissociated from three regions of sub-dissected fetal intestine (mid-small intestine, caecum, and hindgut) from 12.5dpc embryos. Cell suspensions were allowed to settle onto wells coated with poly-D-lysine and fibronectin, then fixed and stained for pH3 and Sox10 expression.

Cells were classified into one of four categories: non-proliferating non-ENP cells (pH3⁻/Sox10⁻); proliferating non-ENP cells (pH3⁺/Sox10⁻); non-proliferating ENP cells (pH3⁻/Sox10⁺); and proliferating ENP cells (pH3⁺/Sox10⁺). The percentage of proliferative progenitors in each gut region was determined by calculating the number of proliferating ENPs (pH3⁺/Sox10⁺) divided by the total number of ENPs (all Sox10⁺ cells). Calculation of this percentage effectively normalized for any differences in total number of cells between wells so that the

proliferative capacity of ENPs could be compared between genotype and strain classes for each gut region. Proliferative percentages were compared between $Sox10^{+/+};Phox2B^{+/+}$ ENPs, $Sox10^{+/+};Phox2B^{LacZ/+}$ ENPs, $Sox10^{Dom/+};Phox2B^{+/+}$ ENPs, and $Sox10^{Dom/+};Phox2B^{LacZ/+}$ ENPs for all three gut regions. This analysis found no significant differences in proliferation between any classes of ENPs (Figure 5.2). Thus, ENP proliferation is not impacted by hemizyosity at *Phox2B*, indicating that this developmental process is not affected by *Sox10m3*.

Figure 5.2. Effect of *Phox2B* hemizyosity in conjunction with the *Sox10^{Dom}* allele and strain background on ENP proliferation.



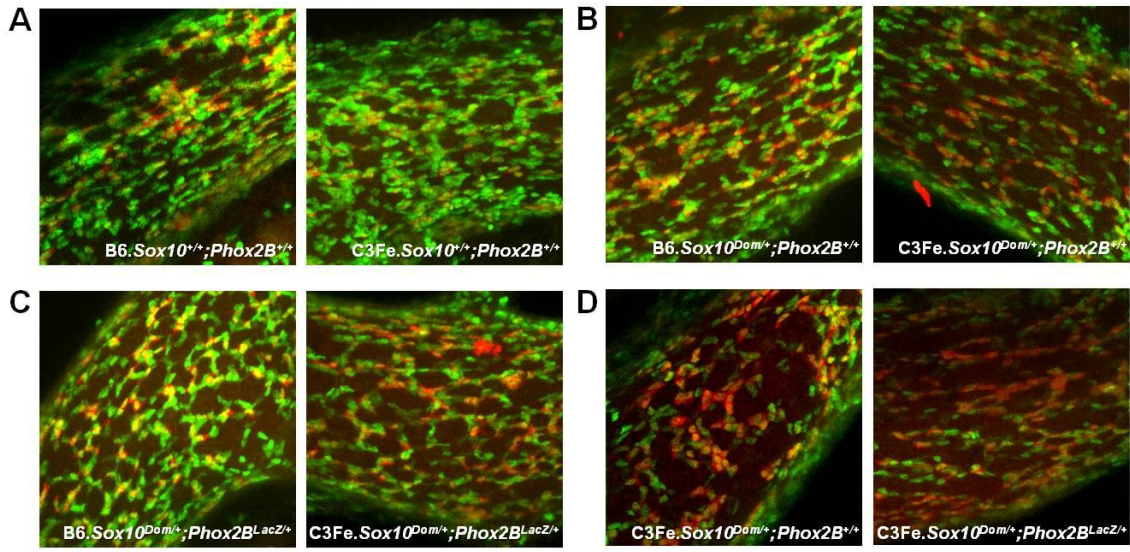
Proliferating enteric NC-derived cells from dissociated B6.Sox10^{Dom/+} X B6D2.Phox2B^{LacZ/+} 12.5dpc fetal guts were visualized by immunohistochemical staining for Phospho-Histone H3 (pH3), Sox10, and DAPI. Proportion of proliferating ENPs (pH3⁺Sox10⁺ over all Sox10⁺) was determined in all embryos. Values shown are average ± S.D. (n≥6). Welch's t test was performed on B6 Sox10^{+/+};Phox2B^{+/+} vs. B6 Sox10^{+/+};Phox2B^{LacZ/+}, B6 Sox10^{+/+};Phox2B^{+/+} vs. B6 Sox10^{Dom/+};Phox2B^{+/+}, B6 Sox10^{+/+};Phox2B^{+/+} vs. B6 Sox10^{Dom/+};Phox2B^{LacZ/+}, B6 Sox10^{+/+};Phox2B^{LacZ/+} vs. B6 Sox10^{Dom/+};Phox2B^{+/+}, B6 Sox10^{+/+};Phox2B^{LacZ/+} vs. B6 Sox10^{Dom/+};Phox2B^{LacZ/+}, and B6 Sox10^{Dom/+};Phox2B^{+/+} vs. B6 Sox10^{Dom/+};Phox2B^{LacZ/+} for all gut regions.

Hemizyosity at *Phox2B* differentially affects foregut ENP patterning.

Previous studies have shown that the *Sox10^{Dom}* allele causes a decrease in the number of ENPs present in the foregut of 13.5dpc embryos (7). In addition, abnormal patterning of the developing ENS was seen in several *Sox10^{Dom}* embryos, both on the B6 and C3Fe strain backgrounds (7). As *Phox2B* clearly played a role in the migration of ENPs, the analysis of foregut patterning was repeated in double mutants to determine if this gene also impacted the spatial distribution of ENPS in the developing ENS.

To determine if the patterning of the developing ENS was disturbed in the proximal foregut of double mutants, I used immunohistochemical detection of *Phox2B*, a known marker of all early ENPs (8), and Hu, an early marker of differentiating neurons (9) in fetal gastrointestinal tracts from 13.5dpc *Sox10^{+/+};Phox2B^{LacZ/+}* X *Sox10^{Dom/+};Phox2B^{+/+}* embryos. In wild-type fetal gut from both the B6 and C3Fe strains, the density of cells in the proximal region was high enough to cover the majority of the gut tube (Figure 5.3A). However, there appeared to be a trend towards higher density in the wild-type C3Fe embryos. As compared to wild-type B6 gastrointestinal tracts, those from B6.*Sox10^{Dom/+};Phox2B^{+/+}* embryos did not differ in the majority of cases (Figure 5.3B, Table 5.2). In contrast, all of the gastrointestinal tracts from C3Fe.*Sox10^{Dom/+};Phox2B^{+/+}* embryos had decreased numbers of progenitor cells in the foregut (Figure 5.3B, Table 5.2). As mentioned previously, the greater severity of phenotype in the “protective” strain background is most likely due to the “dilution” of this effect by introduction of the B6 genetic material.

Figure 5.3. Foregut patterning in $Sox10^{Dom/+};Phox2B^{LacZ/+}$ embryos.



Gastrointestinal tracts from 13.5dpc $Sox10^{+/+};Phox2B^{LacZ/+}$ X $Sox10^{Dom/+};Phox2B^{+/+}$ embryos were immunostained for Phox2B (green) and Hu (red) to visualize developing neurons in the proximal foregut (400X magnification). (A) $Sox10^{+/+};Phox2B^{+/+}$ guts from the B6 and C3Fe backgrounds display normal dense population of the foregut. (B) B6. $Sox10^{Dom/+};Phox2B^{+/+}$ guts presented with normal density. C3Fe. $Sox10^{Dom/+};Phox2B^{+/+}$ guts presented with decreased ENP density alone (B) or decreased density accompanied by abnormal patterning (D). (C) $Sox10^{Dom/+};Phox2B^{LacZ/+}$ guts from both strain backgrounds presented with decreased ENP density. Those from the C3Fe background also demonstrated abnormal patterning (D).

Table 5.2. Foregut patterning in $Sox10^{Dom/+};Phox2B^{LacZ/+}$ embryos.

Gastrointestinal tracts from 13.5dpc $Sox10^{+/+};Phox2B^{LacZ/+}$ X $Sox10^{Dom/+};Phox2B^{+/+}$ embryos were immunostained for Phox2B and Hu to visualize developing neurons in the proximal foregut. The staining pattern for mutants ($Sox10^{Dom/+};Phox2B^{+/+}$ and $Sox10^{Dom/+};Phox2B^{LacZ/+}$) was compared to wild-type embryos of the same strain.

Genotypic Class	Foregut Phenotype		
	Normal (Figure 5.3A)	Decreased Density (Figure 5.3B,C)	Abnormal Patterning (Figure 5.3D)
B6. $Sox10^{Dom/+};Phox2B^{+/+}$	4/5 (80%)	1/5 (20%)	0/5 (0%)
C3Fe. $Sox10^{Dom/+};Phox2B^{+/+}$	0/4 (0%)	4/4 (100%)	2/4 (50%)
B6. $Sox10^{Dom/+};Phox2B^{LacZ/+}$	0/4 (0%)	4/4 (100%)	0/4 (0%)
C3Fe. $Sox10^{Dom/+};Phox2B^{LacZ/+}$	1/7 (14%)	6/7 (86%)	2/7 (29%)

Decreased progenitor density was seen in all guts from B6.*Sox10^{Dom/+};Phox2B^{LacZ/+}* embryos and a majority of guts from C3Fe.*Sox10^{Dom/+};Phox2B^{LacZ/+}* embryos (Figure 5.3C, Table 5.2). In addition, a subset of C3Fe.*Sox10^{Dom/+};Phox2B^{+/+}* and C3Fe.*Sox10^{Dom/+};Phox2B^{LacZ/+}* gastrointestinal tracts also exhibited abnormal patterning of the ganglion network, presenting with increased Hu staining (Figure 5.3D, Table 5.2). However, as this phenotype was present in both *Phox2B^{+/+}* and *Phox2B^{LacZ/+}* embryos, it is not due to the action of the *Sox10m3* locus. In contrast, the phenotype of B6.*Sox10^{Dom/+}* embryos markedly deteriorated with the loss of one allele of *Phox2B*. Thus, hemizyosity at *Phox2B* worsens the effect of the *Sox10^{Dom}* allele on foregut patterning in a strain-specific fashion.

Discussion

While several lines of evidence supported the identification of *Phox2B* as the gene underlying the *Sox10^{m3}* modifier interval on chromosome 5, the most significant would be phenotypic alteration by different alleles of this gene. Preliminary studies performed postnatally were promising, but a demonstration of an impact during development would be more informative. To accomplish this end, progeny of crosses between the *Sox10^{Dom}* congenic strains and *Phox2B^{LacZ}* mice were assayed for differences in ENP migration, proliferation, and early ENS patterning. I discovered that strain-specific alleles at *Phox2B* differentially affected ENP migration. In addition, early ENS patterning was altered in a strain-specific fashion when embryos were hemizygous at *Phox2B*. Thus, haplotype at *Phox2B* differentially modifies ENP development and eventually *Sox10^{Dom}* aganglionosis. These studies highlight the role of modifying genes in the phenotypic presentation of complex diseases such as HSCR.

Previous work on the role of modifying genes in HSCR-related phenotypes has focused both on postnatal analyses (2,10) and embryonic analyses (11-13). However, the role of genetic background at a modifying locus has not been previously examined. By utilizing a knock-in *LacZ* allele (5), I was able to assay the effects of both decreased *Phox2B* expression and the strain-specific haplotype at this locus.

Numerous studies have detailed the delayed migration of ENPs down the developing gut tube in the *Sox10^{Dom}* mouse model of HSCR (7,14,15). In addition, studies of modifiers of *Sox10* have noted delayed migration in crosses

with *Edn3* mutants (11), *EdnrB* mutants (11), *Sox8* mutants (12), and *Zfhx1B* mutants (13). However, strain background was not taken into consideration in any of these studies. The *Sox10^{Dom}* animals used by Stanchina et al. 2006 were maintained on a mixed B6 X C3H/HeOJ genetic background, while the *Edn3^{ls}* and *EdnrB^s* mutants were maintained on LS/LeJ and SSL/LeJ backgrounds, respectively (11). The *Sox10^{LacZ}* and *Sox8^{LacZ}* mice used by Maka et al. were both maintained on a mixed B6 X C3Fe genetic background (12). The *Sox10^{LacZ}* and *Zfhx1B^{Δex7}* mice used by Stanchina et al. 2010 were both maintained on a C3Fe genetic background (13). As demonstrated by Walters et al., strain background modulated the severity of the *Sox10^{Dom}* phenotype; the B6 background caused decreases in both ENP density and extent of migration (7). Thus, genetic background is a key factor to consider when studying the effects of potential modifiers.

In order to determine if haplotype at *Phox2B* was at least partially behind this phenomenon, ENP migration was assayed in 12.5dpc *Sox10^{+/+};Phox2B^{LacZ/+}* X *Sox10^{Dom/+};Phox2B^{+/+}* embryos. As seen previously, the presence of the *Sox10^{Dom}* allele caused a decrease in cell density and extent of migration, regardless of strain background. In addition, the combined genotype of *Sox10^{Dom/+};Phox2B^{LacZ/+}* led to an even larger deficit, specifically in the B6 strain. These embryos displayed approximately one-third of the cell density and half of the extent of migration as their *Sox10^{Dom/+};Phox2B^{+/+}* littermates. No such difference was seen in the C3Fe strain; single mutants and double mutants had roughly identical cell density and extent of migration. Thus, the presence of the

B6 haplotype at the only functional allele of *Phox2B* markedly increased the severity of the phenotype.

ENP proliferation is a necessary process for ENS ontogeny, as an initially small population of cells must undergo a massive expansion to fully populate the gut (16). However, previous work with the *Sox10^{Dom}* congenic strains demonstrated that this process was not impacted by the *Sox10^{Dom}* mutation (7). This was also the case in crosses between *Sox10^{Dom}* and *EdnrB^S* mutants (11) and between *Sox10^{LacZ}* and *Sox8^{LacZ}* mutants (12). In contrast, proliferation has played a role in phenotypic presentation in other studies of modifiers of *Sox10*, specifically crosses between *Sox10^{LacZ}* and *Zfhx1B^{Δex7}* mutants; in this case, double mutants had a significant decrease in ENP proliferation that could account for the decreased extent of migration (13). Nonetheless, as stated previously, strain background was not taken into account in these studies. In particular, no study specifically looked at the B6 strain, which is more severely affected. The mixed genetic background in the Stanchina et al. 2006 (11) and Maka et al. (12) studies could mask an effect on proliferation that may be more apparent on a pure background.

In order to confirm that ENP proliferation was not affected by modifying action, this process was assayed in 12.5dpc B6D2.*Phox2B^{LacZ/+}* X B6.*Sox10^{Dom/+}* embryos. Only the B6 strain was used as this background is predisposing to a more severe phenotype. If any effect was to be visible, it would be seen in the “risk” strain. However, in accordance with previous studies (7), ENP proliferation was not affected by genotype at *Sox10* or *Phox2B*. Regardless of the gut region,

approximately 30% of ENPs were proliferative in all genotypes. Thus, ENP proliferation is not affected by the modifying action of *Phox2B* in conjunction with the *Sox10^{Dom}* allele.

ENPs differentiate into multiple cell types that form the ENS (16). The relative proportions of these cell types, as well as the timing of their differentiation, can have a significant impact on ENS ontogeny. Inappropriate cell differentiation during development can manifest postnatally as abnormal patterning (2). As shown by Walters et al. (7), the *Sox10^{Dom}* mutation has a significant effect on the *in vitro* fate of enteric NCSC. This was reflected *in vivo* by the appearance of abnormal foregut patterning in 13.5dpc *Sox10^{Dom/+}* embryos (7). The fate of ENPs has also been of interest in studies of *Sox10* modifiers. The combination of mutant alleles of *Sox10* and *Sox8* caused a decrease in gliogenesis (12). In contrast, an increase in neurogenesis was seen when a mutant allele of *Sox10* was combined with *EdnrB* or *Zfhx1B* mutant alleles (11,13). As stated previously, strain background was not examined in these studies. Walters et al. demonstrated that genetic background alone can have a substantial impact on *in vitro* differentiation (7). Thus, the effects on differentiation postulated to be due to the modifier in question might actually be caused by genetic background.

In order to determine if strain-specific alleles of *Phox2B* modulated neuronal differentiation, guts from 13.5dpc *Phox2B^{LacZ}* X *Sox10^{Dom}* embryos were immunostained for Hu and *Phox2B*, and the foreguts were analyzed for differences in patterning. In *Sox10^{Dom/+};**Phox2B^{+/+}* embryos, a decrease in cell

density was noted for both strains. However, the prevalence of this deficiency was not equal; while all C3Fe single mutants displayed this phenotype, less than a quarter of B6 single mutants were affected. This is in stark contrast to previous studies (7). However, this could be attributed to the mixed B6 X DBA/2J background of the *Phox2B^{LacZ}* mice. DBA/2J is a highly protective strain background in terms of *Sox10^{Dom}* aganglionosis. It is possible that the introduction of DBA/2J genetic material into the B6 background ameliorated some of the phenotypic severity, while the introduction of B6 genetic material into the C3Fe background increased the propensity for phenotypic consequences.

In *Sox10^{Dom/+};Phox2B^{Phox2B/+}* embryos, a decrease in cell density was again seen. In this case, the majority of embryos from both strains displayed this phenotype. Interestingly, a small minority (less than 15%) of double mutants on the C3Fe background presented with a normal phenotype, thus providing another piece of evidence that hemizyosity at *Phox2B* is actually protective in this strain background. The shift from a normal phenotype in the single mutants to a deficit of ENPs in the double mutants specifically in the B6 strain signifies that *Phox2B* is acting as a modifier of this consequence of the *Sox10^{Dom}* mutation.

A separate phenomenon was noted in both single and double mutants on the C3Fe genetic background. In both genotypic classes, a minority of embryos displayed abnormal patterning, specifically an increase in the amount of Hu staining corresponding to developing neurons. This is in stark contrast to the lack of neuroblasts seen in a minority of C3Fe.*Sox10^{Dom/+}* foreguts in previous studies (7). As this occurred both in the presence and absence of the

Phox2B^{LacZ} allele, it is not due to the modifying action of the locus. Nonetheless, it raises interesting questions concerning the exact nature of the regulation of ENP development in the *Sox10*^{Dom} congenic strains. While the embryos used in the double mutant analyses are labeled B6 or C3Fe for brevity, they are in fact a combination of several strain backgrounds. In particular, the C3Fe embryos also contain genetic material from the B6 and DBA/2J inbred strains. The *in vitro* developmental potential studies detailed in Chapter II demonstrated an increase in neurons in B6.*Sox10*^{Dom/+} samples. It is possible that the increase in neuronal staining in the “C3Fe”.*Sox10*^{Dom/+};*Phox2B*^{X/+} embryos is due to the addition of B6 genetic material. It is also possible that the DBA/2J genetic material is promoting neurogenesis in this mixed background. This would be unexpected, as the DBA/2J inbred strain background is highly protective against *Sox10*^{Dom} aganglionosis (Southard-Smith EM, unpublished data). While the final biological endpoint (a functional ENS) may be the same, the mechanisms that control ENP development could differ between strains.

From the evidence presented above, it is clear that *Phox2B* modifies *Sox10*^{Dom} aganglionosis in a strain-specific fashion. However, the molecular mechanisms underlying this modification remain unclear. We have shown that ENP proliferation is not affected. However, a decrease in ENP density and extent of migration, on top of that normally observed in B6.*Sox10*^{Dom/+} embryos, is apparent through multiple analyses. It did not appear that neurogenesis was increased *in vivo*, which could account for both deficits (as detailed in Chapter II). Nonetheless, we only analyzed a single time-point; a time course of studies may

be necessary to fully rule out increased neuronal differentiation as a causative mechanism. However, as detailed in Chapter II, the distribution of multiple cell types was different between the B6 and C3Fe strains, even under “wild-type” conditions. It is possible that the overall proportions of the cell types that comprise the ENS are altered by strain-specific alleles of *Phox2B*. Further studies of *in vitro* developmental potential utilizing these double mutants will shed light onto the exact nature of *Phox2B*'s developmental effects. *Phox2B* has been shown to be expressed in both neurons and glia throughout development and into adulthood (17). The presence of a particular haplotype at *Phox2B* could alter the development or function of either of these differentiated cell types. Future studies using a conditional *Sox10* allele (18) will aid in determining the temporal nature of the modifying action of this locus.

The analyses detailed in Chapter IV have shown that a specific haplotype at *Phox2B* can markedly alter the phenotypic presentation of hallmarks of enteric aganglionosis. These studies in mice confirm previous reports of an association between haplotype at *PHOX2B* and presence of HSCR (19,20). Specifically, these studies identified an A→G transition at base pair 1364, within intron 2 of *PHOX2B*, as being significantly associated with HSCR (19,20). A similar SNP exists between the B6 and C3Fe strain backgrounds. The role of this SNP, if any, in modulating the effects of *Phox2B* has yet to be determined; postulated functions include control of splicing or secondary structure in pre-mRNA or recruitment of transcription-inhibitory factors. Future studies are needed to

determine if this SNP is involved in *Phox2B* regulation or if, like in humans, it is simply in LD with the true modifying sequence.

In conclusion, I have shown that strain-specific alleles of *Phox2B* modify *Sox10Dom* aganglionosis. In particular, migration and cell density of ENPs, separate from proliferation, are negatively impacted by the B6 haplotype at *Phox2B*. These studies provide biological evidence that *Phox2B* is a gene underlying the *Sox10m3* modifier interval. In addition, they highlight the role of loci other than the disease-causing gene in determining the final phenotypic presentation in complex diseases such as HSCR.

Materials and Methods

Animals. All animal protocols were approved by the Institutional Animal Care and Use Committee at Vanderbilt University. B6.*Sox10^{Dom}* and C3Fe.*Sox10^{Dom}* congenic lines were established and maintained by backcrosses to C57BL/6J and C3HeB/FeJ stocks, respectively. Both strains have been bred onto their respective inbred strains for >40 generations. The B6D2.*Phox2B^{LacZ}* line was obtained from the laboratory of Dr. Jean-Francois Brunet and maintained by backcrosses to C57BL/6J X DBA/J F₁ stocks.

Fetal mouse dissections. Timed matings of congenic *Sox10^{Dom}* males and *Phox2B^{LacZ}* females were set up to obtain staged mouse fetuses, designating the morning of plug formation as 0.5 days post coitus (dpc). Fetal gastrointestinal tracts (stomach to anus) were sub-dissected for analysis.

Genotyping. Genomic DNA was isolated from limb buds by incubation in tail digest buffer (10mM Tris pH8.0, 100mM NaCl, 10mM EDTA, 0.5% SDS) with proteinase K at 55°C overnight, followed by phenol-chloroform extraction, ethanol precipitation, and resuspension in TE pH7.5. Genotype at the *Sox10* locus was determined using PCR-based methodology with the following primers: dcgs10 Bh2MidFa, CGGATGCAGCACAAAAAGGACC; and dcgs10 Bh2MidRB, GGCCAGGTGGGCACTCTTGTA (15). Genotype at the *Phox2B* locus was determined using PCR-based methodology with the following primers: LacZ 1,

GATCCGCGCTGGCTACCGGC; LacZ 2, GGATACTGACGAAACGCCTGCC; RapSyn Sense, AGGACTGGGTGGCTTCCAACCTCCAGACAC; and RapSyn Antisense, AGCTTCTCATTGGTGCGCGCCAGGTTTCAGG. PCR products were run on a non-denaturing polyacrylamide gel.

Analysis of migration. 12.5dpc fetal guts were dissected, and guts were fixed for 1-2 hours in ice-cold Neutral Buffered Formalin (NBF; Sigma, HT501128) with 0.5% Triton X-100. After fixation, guts were washed twice for a minimum of 10 minutes per wash in ice-cold PBS with 0.1% Triton X-100. Guts were then placed in blocking solution composed of PBS with 0.1% Triton X-100, 1% Bovine Serum Albumin-Fraction V (BSA; Sigma, A-4503), and 5% Normal Donkey Serum (NDS; Jackson ImmunoResearch, 017-000-121) for one hour at room temperature.

All antibodies were diluted in blocking solution. Guts were incubated in polyclonal rabbit anti-mouse Phox2B antibody (5) (1:750) overnight at 4°C, then washed three times for a minimum of five minutes per wash in PBS with 0.1% Triton X-100. Guts were incubated in donkey anti-rabbit Cy3-conjugated secondary antibody (Jackson ImmunoResearch, 711-165-152, 1:1000) for 1 hour at room temperature. Guts were washed for a minimum of ten minutes in PBS with Triton X-100, then washed twice for a minimum of ten minutes in PBS. Guts were transferred to fresh PBS and allowed to sit at 4°C overnight to fully wash out secondary antibody.

Stained guts were flat-mounted in Aqua Poly/Mount (PolySciences, Inc, 18606) on glass slides and cover-slipped for imaging. Clear nail polish was used to seal the edges of the coverslip to prevent mounting media from drying out. Confocal microscopy was performed on a Zeiss Scanning Microscope LSM510 with a rhodamine (Cy3, Texas Red) band-pass filter at 200X and 400X magnifications to visualize ENPs expressing endogenous Phox2B in fetal guts. The HeNe1 laser, at a wavelength of 543nm, was set to 40% power. The pinhole was set to 79, with an optical slice less than 2.4um. For z-stacks, the optimal interval of 6.43um was used.

Tiled confocal images of whole-mount fetal guts were divided into eight equal sections encompassing the mid-small intestine, caecum, and hindgut, with the caecum designated as section four. The density of Phox2B⁺ cells was qualitatively scored on a whole-number four-point scale, with zero being a lack of Phox2B⁺ cells and four being numerous Phox2B⁺ cells, for each individual section. Scoring was completed in a strain- and genotype-blinded fashion (21). Scores for each individual section of the gut were averaged across strain- and genotype-matched embryos, with six to nine embryos from three to four separate litters per genotypic class.

Analysis of proliferation. Fibronectin (1mg vial, Biomedical Technologies, BT-225) was reconstituted the night before analysis using the following protocol: addition of 0.5mL Biowhittaker water (Fisher Scientific, BW17-742Q), incubation at 37°C, 5% CO₂ for 1 hour, addition of 5.5mL Dulbecco's Phosphate Buffered

Saline (DPBS; Gibco, 14040-182), and incubation at 37°C, 5% CO₂ overnight. 24-well plastic tissue culture plates (Falcon, 353047) were prepared using the following protocol: coating with Poly-D-Lysine (PDL, 150ug/mL; Biomedical Technologies, BT-227), removal of PDL, drying of wells by air in the tissue culture hood, rinsing with Biowhittaker water, removal of Biowhittaker water, and drying of wells by air in the tissue culture hood. Opti-MEM medium (Gibco, 31985070) was added to the wells, and the plates were incubated at 37°C, 5% CO₂ to allow the medium to equilibrate. In addition, L15 solution was prepared by combining Leibovitz's L-15 medium with 1mg/mL BSA (Sigma, A-3912), 10mM HEPES pH7.4 (Fisher Scientific, BW17-737E), 1% penicillin/streptomycin (PS; Gibco, 15140-122), and 10% Biowhittaker water.

12.5dpc fetal guts from B6D2.*Phox2B*^{LacZ/+} X B6.*Sox10*^{Dom/+} crosses were dissected and then partitioned into segments comprised of the foregut (mid-small intestine, approximately equal in size to caecal), caecal, and hindgut (entire) regions. Individual gut segments were transferred to polypropylene tubes (Falcon, 353063) containing 3mL of Hanks' Balanced Salt Solution without calcium or magnesium (HBSS; Gibco, 14185-052). Tubes were spun softly (1100rpm for five minutes at 4°C) in a pre-chilled swinging-bucket rotor (Sorvall RTH-750) to pellet the gut sections. While tubes were spinning, dissociation solution comprised of 0.5mg/mL Dispase (Gibco, 17105-041) in HBSS was made. The supernatant was aspirated off of the pelleted gut sections until approximately 100uL remained. 0.5mL of dissociation solution was added to each gut section. Tubes were incubated in a 37°C water bath for 10 minutes,

and tubes were banged against the side of the water bath during the last two minutes of incubation.

Tubes were immediately transferred to ice, and 1mL of quench solution (L15 solution with 37.5ug/mL DnaseI [Sigma, D-4527]) was added. The solution was triturated six times and passed through a 45 micron nylon mesh membrane (Sefar America, 3-38/22) into a clean polypropylene tube. The old tube was washed with 1mL of dilute quench solution (L15 solution with 7.5ug/mL DnaseI), which was also filtered into the new tube. Cells were pelleted as before. The supernatant was aspirated off until approximately 100uL remained. The cell pellet was resuspended in 1mL dilute quench solution by triturating five times. The cell solution was passed through a membrane as above into a clean polypropylene tube. The old tube was washed with 1mL dilute quench solution, which was also filtered into the new tube. The top was topped off with dilute quench solution, and cells were pelleted as before. The supernatant was aspirated off until approximately 200uL remained. The solution was triturated ten times, and 50uL of dissociated cells were plated (approximately ~1/4 gut segment) per well in the 24-well plates.

Plates were incubated at 37°C, 5% CO₂ for 1 hour to allow cells to adhere to the plate surface and then fixed on ice in NBF with 0.5% Triton X-100. Cells were washed twice in wash buffer (PBS with 0.1% Triton X-100 and 0.5% BSA). Blocking solution was added, and cells were incubated at room temperature for 25 minutes. All antibodies were diluted in blocking solution. Cells were incubated in polyclonal rabbit anti-mouse Sox10 (22) (1:100) at room

temperature for two hours, then washed twice in wash buffer. Cells were incubated in monoclonal mouse anti-mouse Phospho-Histone H3 (pH3, Abcam, ab14955, 1:2000) at 4°C overnight, then washed three times in wash buffer. Cells were incubated in donkey anti-rabbit Cy3-conjugated secondary antibody (1:500) at room temperature for 30 minutes, then washed twice in wash buffer. Cells were incubated in donkey anti-mouse Cy2-conjugated secondary antibody (Jackson ImmunoResearch, 715-225-150, 1:500) at room temperature for 30 minutes, then washed in wash buffer. Cells were washed in DAPI solution (Invitrogen, D1306, 1:50,000) and washed in wash buffer. The wash buffer was replaced, and the plates were stored at 4°C overnight before imaging.

Cells were imaged and counted using a DMI6000B microscope (Leica). A total count of Sox10⁺ and Sox10⁺/pH3⁺ cell numbers in each well was determined for each gut region. The ratio of double-positive (Sox10⁺/pH3⁺) cells relative to the total of all Sox10⁺ cells was calculated to determine the proliferative frequency of ENPs in each gut region. Ratios were averaged across genotype-matched embryos, with four to six embryos from three litters per class. Averages and standard deviations were compared by Welch's t test. Statistics were performed using the GraphPad QuickCalcs web interface (<http://www.graphpad.com/quickcalcs/index.cfm>).

Analysis of *in vivo* neurogenesis. 13.5dpc embryonic guts were dissected and fixed on ice for one hour in NBF with 0.5% Triton X-100. Guts were washed twice for a minimum of ten minutes on ice in PBS with 0.1% Triton X-100. All

washes were done in PBS with 0.1% Triton X-100 unless otherwise stated. Guts were incubated in blocking solution (as described in the analysis of migration section) for one hour. All antibody dilutions were made with blocking solution. Guts were incubated in polyclonal rabbit anti-mouse Phox2B antibody (5) (1:750) for three hours and then washed four times for a minimum of 15 minutes. Guts were incubated in polyclonal human anti-human Hu antibody (9) (1:800; cross-reactive with murine protein) at 4°C overnight. Guts were washed four times for a minimum of five minutes. Guts were incubated in donkey anti-rabbit Cy2-conjugated secondary antibody (Jackson ImmunoResearch, 715-225-152, 1:500) for 1 hour and then washed three times for a minimum of five minutes. Guts were incubated in donkey anti-human Texas Red-conjugated secondary antibody (Jackson Immuno Research, 709-075-149, 1:100) and then washed for a minimum of ten minutes. Guts were washed twice in PBS for a minimum of ten minutes and then placed in fresh PBS at 4°C overnight to allow antibodies to completely wash out.

Embryonic guts were mounted for imaging as described in the analysis of migration section. Confocal microscopy was performed on a Zeiss Scanning Microscope LSM510 using rhodamine (Cy3, Texas Red) and FITC (GFP, Cy2, Alexa 488) band-pass filters. The HeNe1 laser, at a wavelength of 543nm, was set to 25% power. The Argon/2 laser, as a wavelength of 488nm, was set to 5% power. The pinhole was set to 440, with an optical slice less than 5.5um. For z-stacks, the optimal interval of 2.72um was used. Foreguts from two to seven embryos from three separate litters per class were imaged.

References

1. Nadeau, J.H. (2001) Modifier genes in mice and humans. *Nat. Rev. Genet.*, **2**, 165-174.
2. Cantrell, V.A., Owens, S.E., Chandler, R.L., *et al.* (2004) Interactions between Sox10 and EdnrB modulate penetrance and severity of aganglionosis in the Sox10Dom mouse model of Hirschsprung disease. *Hum. Mol. Genet.*, **13**, 2289-2301.
3. Lane, P.W. (1966) Association of megacolon with two recessive spotting genes in the mouse. *J. Hered.*, **57**, 29-31.
4. Owens, S.E., Broman, K.W., Wiltshire, T., *et al.* (2005) Genome-wide linkage identifies novel modifier loci of aganglionosis in the Sox10Dom model of Hirschsprung disease. *Hum. Mol. Genet.*, **14**, 1549-1558.
5. Pattyn, A., Morin, X., Cremer, H., *et al.* (1999) The homeobox gene Phox2b is essential for the development of autonomic neural crest derivatives. *Nature*, **399**, 366-370.
6. Flint, J., Mott, R. (2001) Finding the molecular basis of quantitative traits: successes and pitfalls. *Nat. Rev. Genet.*, **2**, 437-445.
7. Walters, L.C., Cantrell, V.A., Weller, K.P., *et al.* (2010) Genetic background impacts developmental potential of enteric neural crest-derived progenitors in the Sox10Dom model of Hirschsprung disease. *Hum. Mol. Genet.*.
8. Young, H.M., Hearn, C.J., Ciampoli, D., *et al.* (1998) A single rostrocaudal colonization of the rodent intestine by enteric neuron precursors is revealed by the expression of Phox2b, Ret, and p75 and by explants grown under the kidney capsule or in organ culture. *Dev. Biol.*, **202**, 67-84.
9. Fairman, C.L., Clagett-Dame, M., Lennon, V.A., *et al.* (1995) Appearance of neurons in the developing chick gut. *Dev. Dyn.*, **204**, 192-201.
10. McCallion, A.S., Stames, E., Conlon, R.A., *et al.* (2003) Phenotype variation in two-locus mouse models of Hirschsprung disease: tissue-specific interaction between Ret and EdnrB. *Proc. Natl. Acad. Sci. U. S. A.*, **100**, 1826-1831.
11. Stanchina, L., Baral, V., Robert, F., *et al.* (2006) Interactions between Sox10, Edn3 and EdnrB during enteric nervous system and melanocyte development. *Dev. Biol.*, **295**, 232-249.

12. Maka,M., Stolt,C.C., Wegner,M. (2005) Identification of Sox8 as a modifier gene in a mouse model of Hirschsprung disease reveals underlying molecular defect. *Dev. Biol.*, **277**, 155-169.
13. Stanchina,L., Van de Putte,T., Goossens,M., *et al.* (2010) Genetic interaction between Sox10 and Zfhx1b during enteric nervous system development. *Dev. Biol.*, **341**, 416-428.
14. Kapur,R.P., Livingston,R., Doggett,B., *et al.* (1996) Abnormal microenvironmental signals underlie intestinal aganglionosis in Dominant megacolon mutant mice. *Dev. Biol.*, **174**, 360-369.
15. Southard-Smith,E.M., Kos,L., Pavan,W.J. (1998) Sox10 mutation disrupts neural crest development in Dom Hirschsprung mouse model. *Nat. Genet.*, **18**, 60-64.
16. Newgreen,D., Young,H.M. (2002) Enteric nervous system: development and developmental disturbances--part 2. *Pediatr. Dev. Pathol.*, **5**, 329-349.
17. Corpening,J.C., Cantrell,V.A., Deal,K.K., *et al.* (2008) A Histone2BCerulean BAC transgene identifies differential expression of Phox2b in migrating enteric neural crest derivatives and enteric glia. *Dev. Dyn.*, **237**, 1119-1132.
18. Finzsch,M., Schreiner,S., Kichko,T., *et al.* (2010) Sox10 is required for Schwann cell identity and progression beyond the immature Schwann cell stage. *J. Cell Biol.*, **189**, 701-712.
19. Garcia-Barcelo,M., Sham,M.H., Lui,V.C., *et al.* (2003) Association study of PHOX2B as a candidate gene for Hirschsprung's disease. *Gut*, **52**, 563-567.
20. Liu,C.P., Li,X.G., Lou,J.T., *et al.* (2009) Association analysis of the PHOX2B gene with Hirschsprung disease in the Han Chinese population of Southeastern China. *J. Pediatr. Surg.*, **44**, 1805-1811.
21. Tsai,Y.H., Gariepy,C.E. (2005) Dynamic changes in the proximal gut neural crest stem cell population are associated with successful development of the distal enteric nervous system in rats. *Pediatr. Res.*, **58**, 636-643.
22. Mollaaghababa,R., Pavan,W.J. (2003) The importance of having your SOX on: role of SOX10 in the development of neural crest-derived melanocytes and glia. *Oncogene*, **22**, 3024-3034.

CHAPTER VI

CONCLUSIONS AND FUTURE DIRECTIONS

Conclusions

HSCR is a complex disease with multigenic effects, incomplete penetrance, and variable expressivity (1). The use of mouse models has greatly increased our knowledge of the genes and mechanisms involved in the pathogenesis of this disease [reviewed in Burzynski et al. 2009 (2)]. In particular, the *Sox10^{Dom}* model has illuminated multiple aspects of the complex interactions between genes (3,4). However, the exact nature of the differences between the *Sox10^{Dom}* congenic lines, both developmentally and genetically, remained unclear.

This study sheds light on the differences that genetic background imposes on the *Sox10^{Dom}* aganglionic phenotype. Genetic background plays a substantial role in the developmental processes that ENPs use to form the ENS. One gene that underlies some of the differences caused by strain background is *Phox2B*. The B6 and C3Fe strains may have differential expression of *Phox2B*, most likely due to the sequence variation in putative regulatory regions of this locus. The effects of this possible difference in expression, as well as composition, of *Phox2B* can be seen during development by utilizing the *Phox2B^{LacZ}* line of mice. The strain-based origin of *Phox2B* explains some of the variability in ENP development between B6 and C3Fe *Sox10^{Dom/+}* mice.

Previous studies detailing the differences between the B6 and C3Fe *Sox10^{Dom}* congenic lines had focused on postnatal phenotype (3). It was hypothesized that postnatal differences in penetrance and severity of aganglionosis were due to differences in the development of ENPs during ENS ontogeny. Three major processes are involved in the formation of the ENS: migration, proliferation, and differentiation of progenitors into multiple cell types. The effect of genetic background seen postnatally could impact one or all of these processes.

ENP migration was affected by both the *Sox10^{Dom}* mutation and strain background. The *Sox10^{Dom}* mutation caused a decrease in both extent of migration and ENP density in both the B6 and C3Fe strains. However, the deficits were more severe in the B6 strain, mirroring the increased aganglionosis seen postnatally. In contrast, neither the *Sox10^{Dom}* mutation nor strain background had an effect on ENP proliferation. Regardless of the region of the gut examined, the proportion of ENPs that was undergoing mitosis remained approximately equal between wild-type and *Sox10^{Dom/+}* embryos of both B6 and C3Fe origin.

The differentiation process was assayed in multiple ways. *In vitro* analysis of the developmental potential of enteric neural crest-derived stem cells demonstrated that a large amount of variation exists between wild-type cells of different genetic backgrounds. In addition, a differential effect of the *Sox10^{Dom}* mutation was seen between B6 and C3Fe samples; the *Sox10^{Dom}* mutation caused a greater shift in proportions of cell types in the B6 strain. The

“protective” C3Fe background had greater buffering capacity to absorb the effects of the *Sox10^{Dom}* mutation.

In vivo analysis of neurogenesis also demonstrated separate effects of the *Sox10^{Dom}* mutation and strain background. While *Sox10^{Dom/+}* embryos consistently showed a decrease in cell density, the different strain backgrounds led to different types of abnormal patterning. Alterations in patterning of the ganglion network were also visible in postnatal samples. The B6 background demonstrated more severe deviations from the normal composition of gut muscle strips from *Sox10^{Dom/+}* animals.

In total, these analyses demonstrate that strain background plays a large role in numerous aspects of ENS development. While the *Sox10^{Dom}* mutation imparts specific defects, the ability of the genetic background to compensate for those deficits varies significantly. The C3Fe genetic background consistently results in an attenuated phenotype for *Sox10^{Dom/+}* mutants. The large amount of variation in phenotype seen in HSCR patients is most likely caused by effects such as those documented in this study. Aspects of the genetic landscape other than the primary mutation clearly contribute to the overall phenotypic presentation.

The search for modifiers of the *Sox10^{Dom}* aganglionic phenotype resulted in a genome-wide linkage scan using a large B6XC3Fe.*Sox10^{Dom}* F₂ population. Five chromosomes were identified as having significant linkage to severity of aganglionosis (4). A peak on chr.14 confirmed an earlier study documenting an interaction between *Sox10* and *EdnrB* (3). Of the remaining linkage hits, chr.5

(*Sox10m3*) was chosen for further study as it had the most significant results. After narrowing the modifier interval through additional genotyping and using bioinformatics to identify potential candidates, *Phox2B* was distinguished as the most logical contender (4).

Phox2B is a neural crest transcription factor that is vital for development of the autonomic nervous system (5). Apart from its known role in ENS ontogeny, several lines of evidence support the hypothesis that *Phox2B* plays a role in modulating HSCR-related phenotypes. Mutations in *PHOX2B* are responsible for CCHS, a disorder of the autonomic nervous system that is occasionally comorbid with HSCR (6,7). Different classes of *Phox2B* mutations are found in patients with CCHS alone and those with CCHS and HSCR (8). Multiple studies have detected an association between *PHOX2B* and HSCR (9,10). Thus, there is strong evidence from human studies that *Phox2B* is the gene underlying the *Sox10m3* modifier interval.

Nonetheless, certain criteria, as put forth by leaders in the field, must be met for a gene to be classified as a modifier. As noted in the 2003 white paper, the members of the Complex Trait Consortium describe a QTL (quantitative trait locus, of which a modifier is a sub-classification) as a gene that has: a biological function in line with the trait being studied; polymorphisms in coding or regulatory regions; an effect, either *in vitro* or *in vivo*, on the trait being studied when different alleles are compared; and a human homolog that has been associated with the trait of interest (11). The first and last qualifications have been met, as

described above. The differences, both in sequence and in effect, between B6 and C3Fe alleles at *Phox2B* were left to be determined.

The first avenue of study was expression analyses. It was hypothesized that the differences in aganglionic severity between the B6 and C3Fe strains due to the *Sox10^{m3}* modifier were caused by different levels of expression of *Phox2B*. A variety of methods were used to determine both the level of overall expression and the composition of *Phox2B* transcripts. Allele-specific expression studies in C3FeXB6.*Sox10^{Dom}* F₁ embryos detected irregularities in the 3' UTR. Differences in allelic expression of *Phox2B* were apparent, but results were inconsistent across the 3' UTR, indicating that the composition of this part of the transcript may vary between strains. Staggered primer reverse-transcriptase PCR across the *Phox2B* 3' UTR unfortunately did not uncover any evidence of alternative splicing between strain backgrounds, possibly due to secondary structure.

Overall *Phox2B* expression was assayed by Northern analysis and real-time PCR. The results from these two types of analysis were inconsistent with each other in terms of which strain displayed higher expression. The Northern analysis was hindered by the use of only one set of pooled embryonic RNA samples, as we have shown that the *Sox10^{Dom}* aganglionic phenotype is prone to extreme biological variation. Analysis by this methodology failed to reach significance. However, real-time PCR was performed on five independent sets of pooled RNA and thus comes closer to recapitulating the broad phenotypic spectrum seen in *Sox10^{Dom/+}* animals. Analysis of individual pools suggests that

Phox2B is differentially expressed across strain and genotype classes; however, combined analysis of biological replicates failed to reach significance

Thus, it is clear that strain background plays a role in determining the composition of *Phox2B* transcripts, particularly in the 3' UTR. It remains possible that overall expression levels of *Phox2B* differ between the B6 and C3Fe genetic backgrounds; however, additional analyses are needed to conclusively demonstrate this hypothesis. The postulated higher level of expression of this locus in the C3Fe strain, as suggested by real-time PCR, provides biological support for the results of *in vitro* studies of developmental potential of enteric neural crest-derived stem cells. *Phox2B* promotes neuronal differentiation (12), and a greater number of neuronal derivatives are seen in the C3Fe strain. A correlation between molecular mechanisms and biological outcomes adds weight to the argument that *Phox2B* modulates *Sox10*^{Dom} aganglionosis.

The most obvious cause of the potential differences in expression is sequence variation at *Phox2B*. However, the knowledge base of genetic variants between B6 and C3Fe in this region of the mouse genome was lacking. To gain a clear picture of the amount of variation between these two strains, BACs carrying portions of the C3H genome around the *Phox2B* locus were sequenced. Close to 800 new SNPs were discovered in this analysis, demonstrating that the possibility of finding a functional variant was high.

The odds of a genetic variation imparting a functional difference would be improved if the variant was found to be associated with phenotype across multiple strains. As with the C3Fe strain, most inbred strains do not have a

substantial amount of sequence data in this region. To rectify this situation, 158 inbred strains of mice were genotyped using a 1536 SNP panel. The genetic diversity across the *Sox10m3* interval was striking, even when compared among the 35 commonly used strains that had been phenotyped for susceptibility to aganglionosis.

Preliminary analysis of association between haplotype at each of the original candidate genes (*Uchl1*, *Atp8a1*, and *Phox2B*) and phenotype gave significant results for *Phox2B*. Both the B6 (risk) and C3Fe (protection) haplotypes were associated with aganglionic severity. However, as no coding variants exist between these two strains, the association analysis was extended to include regulatory regions.

Sliding window haplotype analysis was used to pinpoint the location of the genetic variation underlying the association with aganglionic severity. A 10-SNP haplotype was very significantly associated with phenotypic severity. This SNP block, found 3' of *Phox2B*, had both risk and protective haplotypes within our study population. Its association across disparate strains of mice demonstrates that the *Sox10m3* modifier is an important determinant of aganglionic phenotype in strains other than the two that were originally used for its identification.

Extensive sequence and genotype analysis has demonstrated that there is a large amount of variation at the *Phox2B* locus, including but not limited to the B6 and C3Fe strains. While no coding variants were found, the sheer number of SNPs located 3' of the gene, in a genomic region postulated to contain regulatory elements, indicated that functional variation was most likely present. The

association between aganglionic severity and haplotype in a region 3' of *Phox2B* across multiple strains is consistent with the hypothesis that *Phox2B* is a gene underlying the *Sox10^{m3}* modifier interval. The associated region is postulated to contain a regulatory element of *Phox2B*, one that most likely controls expression in the B6 and C3Fe strains. Thus, this study has shown both sequence variation and explored a possible mechanism by which the different alleles at *Phox2B* modify phenotype.

The last remaining criteria for confirming a modifier gene's identity is demonstration of the varying effects of the different alleles of the gene. To this end, the *Phox2B^{LacZ}* line of mice (5) was utilized. Crosses between this line and the *Sox10^{Dom}* lines would allow for analysis of allele-specific effects in double mutants, as the only functional copy of *Phox2B* would come from the *Sox10^{Dom}* parental strain. A simple decrease in the amount of *Phox2B* should not contribute to phenotype, as *Phox2B^{LacZ/+}* mice have no morphological deficiencies. As marked differences were seen between the congenic lines during ENS development, this analysis also studied the effects of different *Phox2B* alleles on the properties of ENPs.

The effects of different alleles of *Phox2B* were seen in multiple aspects of ENP development. Both migration and foregut patterning were differentially affected in *Sox10^{Dom/+};*Phox2B^{LacZ/+}** double mutants depending on strain background. The B6 allele of *Phox2B* severely worsened the deficits in extent of migration and cell density at 12.5dpc when double mutants were compared with *Sox10^{Dom/+};*Phox2B^{+/+}** embryos. In contrast, double and single mutants on the

C3Fe background were roughly comparable in these categories. Interestingly, when foregut patterning at 13.5dpc was analyzed, B6.*Sox10^{Dom/+};Phox2B^{+/+}* embryos were very similar to wild-types. However, when the *Phox2B^{LacZ}* allele was added, a noticeable decrease in cell density became apparent. Cell density was also decreased on the C3Fe background, but this was true for both single and double mutants. Therefore, the B6 allele of *Phox2B* increases the severity of the *Sox10^{Dom}* allele when compared with the effect of the C3Fe allele.

In total, this study demonstrates that the differences in postnatal aganglionic severity between the B6 and C3Fe *Sox10^{Dom}* congenic lines are due to differences in the development of the ENS. One cause of these differences is the *Phox2B* locus, at which these two strains have variation in potential regulatory regions. This genetic variation likely causes a difference in *Phox2B* expression, which becomes apparent in single-allele studies during development. The B6 and C3Fe alleles of *Phox2B* differentially modify the effect of the *Sox10^{Dom}* mutation on aganglionosis.

Potential Impact

The conclusions reached in this body of work will have a significant impact on the fields of ENS biology and HSCR pathophysiology. The studies on the effects of genetic background on ENS development have identified the different processes that can be affected by variation at genomic locations other than the disease-predisposing mutation. In addition, a novel pathogenic mechanism, the disruption of lineage divergence, was discovered.

HSCR is a complex disease, but previous studies in animal models have failed to take genetic background into account. The large amount of variation seen in HSCR patients, both in penetrance and expressivity of aganglionosis, clearly demonstrate that factors other than the primary mutation are at play in determining the final disease presentation. The effects of genetic background on severity and penetrance of postnatal aganglionosis have already been documented (3). However, as HSCR is a disease that first manifests during ENS development, my studies demonstrate the marked impact of genetic background during this key developmental period.

The most important aspect of these initial studies was the identification of a novel pathogenic mechanism: the disruption of lineage divergence by the *Sox10^{Dom}* mutation. This avenue of pathophysiology had not been previously studied at the level of detail utilized here. The shift in proportions of different cell types, whether caused by the *Dom* mutation or simply genetic background, was striking. The highly significant differences in the *in vitro* behavior of “wild-type” progenitors between the B6 and C3Fe strains demonstrated that different genetic

backgrounds have inherent differences in their “buffering capacity” to absorb deleterious mutations such as *Sox10^{Dom}*.

The process of lineage divergence has not been assayed in other mouse models of HSCR. This new pathogenic mechanism must be studied in these other models to determine if it is confined to the *Sox10^{Dom}* mutation or if it is a common feature among HSCR models. As *SOX10* mutations are relatively rare in HSCR patients, demonstrating the disruption of lineage divergence in other models would indicate that this mechanism is common to the pathophysiology of HSCR.

In addition, this work potentially opened up an entirely new field of HSCR study. Current diagnostic technologies rely on staining of ganglia to discern the amount of aganglionosis. However, these methods do not indicate the functionality of ganglia. Differences in proportions of necessary cell types between patients may lead to differences in the functional nature of present ganglia, which in turn could explain the residual dysmotility issues seen in a substantial portion of HSCR patients (13,14). Future studies on the patterning of “normal” gut in these patients may explain the occurrence of GI disturbances post-surgery.

The differences in ENP development in the B6 and C3Fe *Sox10^{Dom}* strains can be attributed in part to the genomic differences at the *Phox2B* locus between these two inbred backgrounds. These studies conclusively demonstrate that *Phox2B* is a gene underlying the *Sox10m3* modifier interval identified in crosses between these two strains (4). However, the more important finding is the

location of association between haplotype at this locus and aganglionic severity across multiple genetic backgrounds. Previous studies in humans have focused strictly on the locus proper (9,10). In contrast, the association studies found in this body of work highlighted a genomic region approximately 12kb 3' of the transcript region. While haplotype at SNPs found within the *Phox2B* transcript region was also significant, this 3' region clearly imparts the majority of the effect of this locus on aganglionic severity. This discovery underscores the need to look outside of the traditional locations in order to understand the effects of genetic variation on HSCR presentation.

In summary, the analyses detailed in this thesis highlight two avenues of study that should have a definite impact on the fields of ENS biology and HSCR pathophysiology. The process of lineage divergence needs to be studied in greater detail in other HSCR mouse models in order to determine if this process is commonly affected by HSCR-predisposing mutations. In addition, the functionality of the remaining enteric ganglia needs to be assayed in HSCR patients to determine if disruption of cell-type balance can explain residual dysmotility issues seen post-surgery. Finally, the effects of genetic variation in putative regulatory regions of genes that may interact with primary HSCR genes need to be determined to truly understand the impact of genetic background on final disease presentation in a complex disorder like HSCR.

Future Directions

While this study made significant strides in understanding the developmental differences between the B6 and C3Fe *Sox10^{Dom}* congenic strains and the role *Phox2B* plays in modulating some of those differences, many questions remain unanswered. Future studies on both the intricacies of the *Sox10-Phox2B* interaction and the ramifications of this study on other models of HSCR will be vital to truly understanding the impact of genetic background on the pathogenesis of HSCR.

The most obvious choice for future experiments would be the study of *in vitro* developmental potential in *Sox10^{Dom/+};Phox2B^{LacZ/+}* double mutants. These studies were attempted, but the sheer lack of progenitor cells in B6 double mutants prohibited data collection. Even at a later developmental time-point (14.5dpc), it was not possible to collect enough cells to generate an experimental replicate. It is possible that super-ovulating B6D2.*Phox2B^{LacZ/+}* females before copulation with *Sox10^{Dom/+}* males will increase the number of viable embryos that can then be used for flow cytometric isolation of enteric neural crest-derived stem cells (15). As the *in vivo* studies of foregut patterning indicated that the B6 allele at *Phox2B* had a significant impact, understanding how the population of stem cells is affected would greatly increase our mechanistic knowledge of this interaction.

A more basic question concerning the relationship between *in vitro* and *in vivo* studies involves the fate of progenitor cells in *Sox10^{Dom/+}* mutants. Flow cytometry demonstrated that the population of these cells is decreased by

approximately 65% in *Sox10^{Dom/+}* embryos compared to wild-types, regardless of strain background. However, this is not accompanied by a loss of multipotency in a culture system. The fate of these “missing” progenitors is unknown. Are they losing their progenitor status and differentiating early? This can be determined by utilizing Cre-lineage tracing systems. Recently developed *Sox10-Cre* lines (Southard-Smith EM, unpublished data) allow the identification of all cells that expressed *Sox10* and their progeny. By crossing these lines to the *Sox10^{Dom}* lines and crossing their progeny to a reporter line (*Rosa^{26R}* or *Rosa^{YFP}*), the fate of neural crest-derived progenitors can be determined.

In addition, a similar breeding strategy can be used with HSCR mouse models other than *Sox10^{Dom}*, such as *EdnrB^{S-I}*. This study has shown that the *Sox10^{Dom}* mouse model differs from others in key components of the pathogenic process, such as ENP proliferation. In combination with *in vitro* developmental potential studies, the analysis of ENS formation in other models can elucidate different pathways involved in producing aganglionosis. While the end-point of these mouse models, aganglionosis in the distal colon, is the same, the molecular mechanisms involved in achieving that end-point most likely differ.

This breeding strategy can also be used to elucidate the cellular identity of the Phox2B⁺ cells with myofibroblast-like morphology seen in postnatal gut muscle strips. This cell type has not been previously described, and initial attempts to determine its origin were unsuccessful (data not shown). Although numerous control experiments confirm the validity of this cell type, confirmation of its neural crest origin will provide the final piece of evidence. This is

particularly important when considering reports of functional intestinal obstruction due to deficiencies in enteric smooth muscle (16). A neural crest contribution to the smooth muscle layers within the gut could also explain the dysmotility issues experienced by many HSCR patients post-resection (13,14).

A different transgenic approach can be used to determine the exact developmental time-point at which the *Sox10^{Dom}* allele affects different ENP processes. At the present time, it is impossible to uncouple the potentially separate effects of the *Sox10^{Dom}* allele on ENP migration and developmental potential. However, a new conditional allele of *Sox10* (17) may alleviate this problem. By combining this line with an inducible Cre system (18), the exact timing of *Sox10* mutation can be controlled. If migration deficits are a secondary phenotype of disturbances in timing of differentiation, it is possible that ENP migration can be promoted by mutating *Sox10* at a later time. However, the conditional *Sox10* allele would not recapitulate all aspects of the *Sox10^{Dom}* system. The conditional allele loses the entire coding sequence upon Cre recombination (17), whereas the *Sox10^{Dom}* allele retains its DNA binding domain. Thus, certain aspects of the *Sox10^{Dom}* phenotype may be due to its dominant-negative action (19) rather than a simple loss of *Sox10* protein. Nonetheless, an inducible system would further the study of the temporal effects of loss of *Sox10*.

A conditional inversion allele of *Sox10* currently under development (Southard-Smith EM, unpublished data) would rectify this issue and illuminate differences in phenotype due to a dominant negative mechanism vs.

haploinsufficiency. Upon Cre recombination, the second and third exons of *Sox10* are inverted, thereby causing a loss of the transactivation domain of the *Sox10* protein, as in the *Sox10^{Dom}* mutant. In addition, cells that have undergone recombination are marked by a fluorescent reporter, allowing their visualization. Thus, the ramifications of the *Sox10^{Dom}* mutation at different time points can be discovered by utilizing this transgenic line.

This study focused primarily on the role of *Phox2B* as a modifier of *Sox10^{Dom}* aganglionosis. However, the original genome-wide linkage scan identified three other as yet unknown modifiers (4). The genomic intervals for these potential modifiers are quite large (20-31 cM) (4); however, additional genotyping in the F₂ samples may be able to narrow these regions to a reasonable size where candidate genes can be selected. *Phox2B* is not the only modifier of *Sox10^{Dom}* aganglionosis, and the role of the other modifying genes should be explored. Novel biology may be discovered, as no known HSCR-related genes map to the interval identified in the linkage scan. This analysis would substantially impact the field of gut neurobiology.

Other additional studies would expand our knowledge of the role of *Phox2B* in modulating aganglionosis in *Sox10^{Dom/+}* animals. The first obvious experiment would be a panel of Northern blots to determine if analysis of multiple sets of pooled embryonic RNA provided the same results as real-time PCR averaged across multiple biological replicates. The issue of phenotypic variance clearly has underpinnings in molecular mechanisms. By averaging as many individuals as possible, a more realistic population mean can be determined. As

Northern analysis remains the gold-standard in expression studies, verification of the real-time PCR results in this fashion would provide incontrovertible evidence that *Phox2B* is differentially expressed between the B6 and C3Fe strains.

To determine if unequal numbers of *Phox2B*⁺ cells are biasing the results of expression studies, real-time PCR should be performed on cells isolated by flow cytometry. Using the techniques discussed in Chapter II, known numbers of enteric NCSC can be obtained and used for RNA isolation. Comparison of *Phox2B* expression levels between strain and genotype classes would then be normalized based on cell number, omitting one known confounding factor in the original expression analyses. These experiments would provide a clearer picture of the effect of both strain background and the *Sox10*^{Dom} mutation on expression of *Phox2B*.

The methods employed to study alternative splicing at the *Phox2B* locus were not effective, possibly due to secondary structure within the 3' UTR. Apart from possible differences in composition in this area of the transcript, a SNP in intron 2 could play a role in splicing of *Phox2B*. An *in vitro* system could be used to assay differential splicing. The pSPL3 vector has been successfully used to isolate exons from genomic DNA (20). This system could be used to determine if alternative splicing is occurring at the *Phox2B* locus between the B6 and C3Fe strains. However, alternative splicing may be cell-type specific; therefore, an enteric cell line must be used. The rat enteroglial cell line [ATCC, CRL-2690; (21)] could be used for this purpose. Nonetheless, this remains an *in vitro* assay and is thus susceptible to results that may not be biologically relevant.

An emerging technology could assay potential splicing *in vivo*, as well as provide another method of studying expression levels: RNA-Seq (22,23). This technique involves reverse transcription of the entire transcriptome followed by high-throughput sequencing. The relative expression of each transcript can be determined by the proportion of sequence reads from that transcript. Studies using both the human and mouse transcriptomes have shown the amount of knowledge to be gained from this technique (24,25).

Sequencing the transcripts produced in enteric neural-crest derived stem cells isolated by flow cytometry would provide an unprecedented look at the composition of *Phox2B* transcripts in different strains and how that composition varies with the introduction of the *Sox10^{Dom}* allele. As the biological input is flow-isolated cells, this system can be controlled for cell number. RNA-Seq has the ability to detect minute levels of alternatively-spliced transcripts which may not be visualized by other techniques. Therefore, we would be able to determine both the overall amount of *Phox2B* expression as well as possible differences in the amounts of alternative transcripts. Nonetheless, this system would still be susceptible to the effects of biological sampling; thus, multiple biological replicates would be needed to confirm any results.

It remains a possibility that no differences in expression or splicing of *Phox2B* will be seen between the B6 and C3Fe genetic backgrounds. While the levels of *Phox2B* mRNA may be similar, differences in post-transcriptional regulation may be occurring between these two strains. The stability of the *Phox2B* transcript may be different between the two alleles. The effects of the

SNPs in the 3' UTR can be assayed using an *in vitro* mRNA stability assay (26). Differences in stability of the *Phox2B* transcript would in turn lead to differences in the amount of Phox2B protein. These potential differences could be assayed using Western blotting techniques, either in whole gut isolates or flow-isolated cell populations. However, as before, these results could be susceptible to biological sampling and would require multiple biological replicates.

However, the knowledge of the amount and composition of the *Phox2B* transcript does not automatically transition to knowledge of the efficacy of the Phox2B protein. It is unknown whether the different alleles of *Phox2B* between the B6 and C3Fe strains have different levels of functionality in promoting transcription of *Phox2B* targets. A method similar to that employed by Bachetti et al. (27) would answer this question. By assaying the ability of the different alleles to activate transcription of reporter genes under the control of known target promoters (such as *Phox2A*) (27), we would be able to determine if the different abilities of the alleles to modulate *Sox10^{Dom}* aganglionosis are due to functional or merely expression level differences.

Even if the differences are confined to expression levels, there are numerous potential regulatory regions yet to be examined. While the sliding window haplotype analysis identified one putative region as being the most significant, the results from that analysis still have more to offer. Even an arbitrary cut-off value of $p = 2 \times 10^{-19}$ for the X^2 analysis leaves four additional SNP blocks around *Phox2B* that are extremely significantly associated with phenotypic severity.

These SNP blocks, as well as the most significant one discussed previously, need to be assessed for regulatory activity to determine if they are the true cause of association or if they are simply in LD with the real associative factor. The C3Fe-Tg^{Phox2B-H2BCFP} transgenic mouse (28) can assist with this goal. The modified BAC that contains the fluorescent reporter can be modified such that these putative regulatory regions are deleted, either separately or in groups. Production of transient transgenic embryos will determine if the deleted regions are required for *Phox2B* expression. This strategy will also pinpoint the location of the deleted regulatory region in C3Fe-Tg^{Phox2B-H2BCFP} Line C. Small staggered deletions of the 5kb region identified by Illumina genotyping will determine the exact region deleted in this founder line, thereby conclusively identifying a *Phox2B* regulatory region.

As much knowledge concerning the sequence variation between B6 and C3Fe as this study has gained, we are still lacking information. The nature of Solexa sequencing combined with the highly repetitive nature of elements surrounding the *Phox2B* locus left “holes” in the assembly of Solexa reads to the B6 reference genome. Large stretches of sequence supposedly do not contain SNPs, but this needs to be confirmed. PCR-based isolation of these genomic regions will allow for them to be cloned and sequenced. This approach will confirm the lack of SNPs seen by Solexa or will identify those that were previously missed.

To return to the analysis of *Sox10*^{Dom/+}; *Phox2B*^{LacZ/+} double mutants, the phenotype of these animals should be further studied. Analysis of postnatal gut

muscle strips from the congenic *Sox10^{Dom}* lines indicated that ganglion patterning was disrupted in *Dom/+* animals. The effect of *Phox2B* on this process should also be studied. As double mutants on the B6 background are severely affected, this analysis may have to be done earlier in development than P15-P17. However, the results of these studies give more insight into the effects of different alleles of *Phox2B* on ENS development.

Finally, the principles applied in this study could be expanded to other strains. A genome-wide linkage scan between two strains of mice identified five potential modifiers (4). The work completed by the Southard-Smith lab to identify susceptible and protective strain backgrounds has shown that the proclivity towards aganglionosis in the *Sox10^{Dom}* model covers a wide spectrum. Multiple cross mapping is a technique that utilizes information from multiple mouse crosses to separate regions linked to the trait of interest from biological noise. Crosses using the strains already phenotyped by the Southard-Smith lab would most likely identify additional modifier regions, thereby increasing our knowledge of the genes involved in ENS development and HSCR pathogenesis.

In summary, this study has examined the developmental differences between the B6 and C3Fe *Sox10^{Dom}* congenic strains and determined that *Phox2B* is one gene that modifies these differences due to potential expression differences based on sequence variation. However, much work is left to be done. Future studies on the activity of different *Phox2B* transcripts and the locations of putative regulatory regions are necessary to truly understand the interaction between *Sox10* and *Phox2B* in this HSCR model. Exploration of

other potential modifiers will increase our knowledge of ENS development and possibly identify novel pathways involved in HSCR pathogenesis. Finally, the presence of modifiers should be further studied in human populations to explain the variation in penetrance and expressivity of aganglionosis in HSCR patients.

References

1. Chakravarti A, Lyonnet S (2006) *The Online Metabolic and Molecular Bases of Inherited Disease*. pp. 6231-6255.
2. Burzynski,G., Shepherd,I.T., Enomoto,H. (2009) Genetic model system studies of the development of the enteric nervous system, gut motility and Hirschsprung's disease. *Neurogastroenterol. Motil.*, **21**, 113-127.
3. Cantrell,V.A., Owens,S.E., Chandler,R.L., *et al.* (2004) Interactions between Sox10 and EdnrB modulate penetrance and severity of aganglionosis in the Sox10Dom mouse model of Hirschsprung disease. *Hum. Mol. Genet.*, **13**, 2289-2301.
4. Owens,S.E., Broman,K.W., Wiltshire,T., *et al.* (2005) Genome-wide linkage identifies novel modifier loci of aganglionosis in the Sox10Dom model of Hirschsprung disease. *Hum. Mol. Genet.*, **14**, 1549-1558.
5. Pattyn,A., Morin,X., Cremer,H., *et al.* (1999) The homeobox gene Phox2b is essential for the development of autonomic neural crest derivatives. *Nature*, **399**, 366-370.
6. Amiel,J., Laudier,B., Attie-Bitach,T., *et al.* (2003) Polyalanine expansion and frameshift mutations of the paired-like homeobox gene PHOX2B in congenital central hypoventilation syndrome. *Nat. Genet.*, **33**, 459-461.
7. Haddad,G.G., Mazza,N.M., Defendini,R., *et al.* (1978) Congenital failure of automatic control of ventilation, gastrointestinal motility and heart rate. *Medicine (Baltimore)*, **57**, 517-526.
8. Berry-Kravis,E.M., Zhou,L., Rand,C.M., *et al.* (2006) Congenital central hypoventilation syndrome: PHOX2B mutations and phenotype. *Am. J. Respir. Crit Care Med.*, **174**, 1139-1144.
9. Garcia-Barcelo,M., Sham,M.H., Lui,V.C., *et al.* (2003) Association study of PHOX2B as a candidate gene for Hirschsprung's disease. *Gut*, **52**, 563-567.
10. Liu,C.P., Li,X.G., Lou,J.T., *et al.* (2009) Association analysis of the PHOX2B gene with Hirschsprung disease in the Han Chinese population of Southeastern China. *J. Pediatr. Surg.*, **44**, 1805-1811.
11. Abiola,O., Angel,J.M., Avner,P., *et al.* (2003) The nature and identification of quantitative trait loci: a community's view. *Nat. Rev. Genet.*, **4**, 911-916.

12. Dubreuil,V., Hirsch,M.R., Jouve,C., *et al.* (2002) The role of Phox2b in synchronizing pan-neuronal and type-specific aspects of neurogenesis. *Development*, **129**, 5241-5253.
13. Faure,C., Ategbo,S., Ferreira,G.C., *et al.* (1994) Duodenal and esophageal manometry in total colonic aganglionosis. *J. Pediatr. Gastroenterol. Nutr.*, **18**, 193-199.
14. Miele,E., Tozzi,A., Staiano,A., *et al.* (2000) Persistence of abnormal gastrointestinal motility after operation for Hirschsprung's disease. *Am. J. Gastroenterol.*, **95**, 1226-1230.
15. Taketo,M., Schroeder,A.C., Mobraaten,L.E., *et al.* (1991) FVB/N: an inbred mouse strain preferable for transgenic analyses. *Proc. Natl. Acad. Sci. U. S. A*, **88**, 2065-2069.
16. Donnell,A.M., Doi,T., Hollwarth,M., *et al.* (2008) Deficient alpha-smooth muscle actin as a cause of functional intestinal obstruction in childhood. *Pediatr. Surg. Int.*, **24**, 1191-1195.
17. Finzsch,M., Schreiner,S., Kichko,T., *et al.* (2010) Sox10 is required for Schwann cell identity and progression beyond the immature Schwann cell stage. *J. Cell Biol.*, **189**, 701-712.
18. Indra,A.K., Warot,X., Brocard,J., *et al.* (1999) Temporally-controlled site-specific mutagenesis in the basal layer of the epidermis: comparison of the recombinase activity of the tamoxifen-inducible Cre-ER(T) and Cre-ER(T2) recombinases. *Nucleic Acids Res.*, **27**, 4324-4327.
19. Inoue,K., Khajavi,M., Ohyama,T., *et al.* (2004) Molecular mechanism for distinct neurological phenotypes conveyed by allelic truncating mutations. *Nat. Genet.*, **36**, 361-369.
20. Buckler,A.J., Chang,D.D., Graw,S.L., *et al.* (1991) Exon amplification: a strategy to isolate mammalian genes based on RNA splicing. *Proc. Natl. Acad. Sci. U. S. A*, **88**, 4005-4009.
21. Ruhl,A., Trotter,J., Stremmel,W. (2001) Isolation of enteric glia and establishment of transformed enteroglia cell lines from the myenteric plexus of adult rat. *Neurogastroenterol. Motil.*, **13**, 95-106.
22. Marioni,J.C., Mason,C.E., Mane,S.M., *et al.* (2008) RNA-seq: an assessment of technical reproducibility and comparison with gene expression arrays. *Genome Res.*, **18**, 1509-1517.
23. Wang,Z., Gerstein,M., Snyder,M. (2009) RNA-Seq: a revolutionary tool for transcriptomics. *Nat. Rev. Genet.*, **10**, 57-63.

24. Pan,Q., Shai,O., Lee,L.J., *et al.* (2008) Deep surveying of alternative splicing complexity in the human transcriptome by high-throughput sequencing. *Nat. Genet.*, **40**, 1413-1415.
25. Mortazavi,A., Williams,B.A., McCue,K., *et al.* (2008) Mapping and quantifying mammalian transcriptomes by RNA-Seq. *Nat. Methods*, **5**, 621-628.
26. Fritz,D.T., Ford,L.P., Wilusz,J. (2000) An in vitro assay to study regulated mRNA stability. *Sci. STKE.*, **2000**, I1.
27. Bachetti,T., Matera,I., Borghini,S., *et al.* (2005) Distinct pathogenetic mechanisms for PHOX2B associated polyalanine expansions and frameshift mutations in congenital central hypoventilation syndrome. *Hum. Mol. Genet.*, **14**, 1815-1824.
28. Corpening,J.C., Cantrell,V.A., Deal,K.K., *et al.* (2008) A Histone2BCerulean BAC transgene identifies differential expression of Phox2b in migrating enteric neural crest derivatives and enteric glia. *Dev. Dyn.*, **237**, 1119-1132.